Kent Academic Repository

Janco, Miroslav (2013) *Characterisation of tropomyosin heterodimers carrying single cardiomyopathy mutations.* **Doctor of Philosophy (PhD) thesis, University of Kent.**

CHARACTERISATION OF TROPOMYOSIN HETERODIMERS CARRYING SINGLE CARDIOMYOPATHY MUTATIONS

by Miro Janco

A thesis submitted to the University of Kent for the degree of

Doctor of Philosophy in Biochemistry

School of Biosciences

Faculty of Science, Technology and Medical Studies

2013

Declaration

The investigation of flexibility and calcium regulation of myofibril force (Chapter 4) were made by collaborating groups lead by Prof William Lehman (USA, Boston), and Prof Corrado Poggesi and Prof Ciara Tesi (Italy, Florence), respectively. The experimental data of the apparent persistence length as a measure of Tm flexibility were performed by Dr Worawit Suphamungmee and Dr Xiouchan Li under supervision of Prof William Lehman, all from Boston University, USA. The experiments for the assessment of the thin filaments calcium sensitivity in rabbit psoas myofibrils containing replaced hcTn·Tm complex were performed by Dr Beatrice Scellini under supervision of Prof Chiara Tesi and Prof Corrado Poggesi, all from University of Florence, Italy. All protein samples presented in this study were generated by me, unless stated otherwise in the text.

No part of this thesis has been submitted in support of an application for any degree qualification of the University of Kent or any other University or Institute of learning.

Miro Janco

August 2013

"Somewhere, something incredible is waiting to be known."

Carl Sagan

To the love of my life Martina

Acknowledgements

Abstract

It is known that different point mutations in α-tropomyosin (Tm) can cause either hypertrophic (HCM) or dilated (DCM) cardiomyopathy. Both of these serious pathologies have a distinct phenotype with unknown mechanisms of development. Biochemical *in vitro* studies provide valuable information for exploring the downstream consequences of cardiomyopathy mutations in sarcomeric proteins leading to the cardiac remodelling and consequent heart failure.

Tm is a linear α-helical coil-coiled dimer involved in the calcium dependent regulation of muscle contraction. Prior to the work, the effects of the mutations in Tm on the regulation of muscle contraction have been made exclusively with Tm mutant homodimers. However, individuals with a heterozygous background may express the mutant and WT proteins in a 1 : 1 ratio which can assembly into a mixture of αα, αα* and α*α* Tm dimers. We found that presence of mutation has little effect on dimer formation between the mutant and the WT monomers, therefore theoretical ratio of the Tm dimers *in vivo* may be 1 : 2 : 1, respectively. This assumption would make the heterodimer predominant

The properties of *in vitro* assembled Tm heterodimers carrying HCM (WT-D175N and WT-E180G) and DCM (WT-E40K, WT-E54K, and WT-D230N) causing mutations were examined including thermal stability, flexibility, actin affinity, calcium regulation of S1 biding, and calcium regulation of myofibril force. We showed that the various properties of the heterodimers can be similar to those of the wild-type (thermal stability of reduced WT-D175N; actin affinity of WT-E40K, and WT-D175N; ΔpCa of WT-E40K, WT-E54K, WT-E180G, WT-D230N), similar of those to the mutant homodimer (ΔpCa of WT-D175N, flexibility of WT-D175N and WT-E180G), intermediate between the two (actin affinity of WT-E180G), or different from both (thermal stability of reduced WT-E40K, WT-E54K, WT-E180G, and WT-D230N; actin affinity of WT-E40, WT-E54K, and WT-D230N; ΔpCa of D175N).

The results demonstrate that the properties of Tm heterodimers cannot be predicted from the interpolation of the WT and mutant homodimer data. The distinct properties of the heterodimer establish that it will be important to define if the pathogenic agent is the homodimer, the heterodimer or both for each known cardiomyopathy mutation in Tm.

Abbreviations

αα*	heterodimer of αTm in which one chain carries the mutation
Ala	Alanine
Amp	Ampicillin
APS	Ammonioum persulphate
ATP	Adenosine triphosphate
CD	Circular Dichroism
D	Aspartic acid
DCM	Dilated cardiomyopathy
DNA	Deoxiribonucleic acid
DTT	Dithiotreitol
EGTA	Ethylene glycol tetraacetic acid
F-actin	Filamentous actin
G	Glutamine
G-actin	Globular actin
His-Tm	Wild type α-tropomyosin homodimer with a histidine tag
HCM	Hypertrophic cardiomyopathy
hcTn	Human cardiac troponin
HMM	Heavy meromyosin
HMW	High molecular weight
IVM	In vitro motility
IPTG	Isopropyl β-D-1-thiogalactopyranoside
K	Lysine
k_{obs}	Observed rate constant
K_B	Equilibrium constant between blocked and closed states

K_t	Equilibrium constant between closed and open states
LB	Luria-Bretani
LMW	Light molecular weight
MHC	Myosin heavy chain
MOPS	3-(N-morpholino)propanesulfonic acid
N	Asparagine
NMR	Nuclear magnetic resonance
PCR	Polymerase chain reaction
Pi	Inorganic phosphate
PL_a	Apparent persistence lenght
PMSF	Phenylmethanesulfonyl fluoride
ppA	Pyrene labelled, phalloidin stabilised F-actin
Pyrene	N-(1-pyrenyl)iodoacetamide
RLC	Regulatory light chain
S1	Myosin subfragment 1
SDS	Sodium dodecyl sulphate
Ser	Serine
TEMED	N, N, N', N'-tetramethylethylenediamine
Tm	Tropomyosin
WT	Wild type

Table of contents

Chapter 3: Optimisation of the method for in vitro formation of the striated muscle α-Tm heterodimers carrying cardiomyopathy mutations   89

Chapter 4: Characterisation of the striated muscle α-Tm heterodimers carrying one copy of the HCM mutations D175N or E180G   102

List of figures

List of tables

Chapter 1

Introduction

Muscle is a remarkable and highly specialised contractile tissue that performs a broad variety of specific functions. Functional diversity of muscles ranges from general motion or locomotion, maintenance of posture and heat production, to more specialised functions such as cardiac contraction or regulation of blood pressure.

The major components of muscle are the molecular motor myosin and the thin filament proteins actin, tropomyosin (Tm) and troponin (Tn). Tm and Tn are involved in calcium dependent regulation of myosin and filamentous actin (F-actin) which is a central feature of contractile events in muscle cells (Gordon et al., 2001; Tobacman, 1996). The role of Tm in regulation of the muscle contraction has been extensively investigated and is well characterised for all muscle types (Lehman and Craig, 2008; Marston and El-Mezgueldi, 2008). However, there are some remaining questions concerning the extent and functional consequences of Tm heterogeneity in the regulation of muscle contraction including healthy and diseased muscle cells. Tm is expressed from four different genes which can be alternatively spliced to produce over 40 individual isoforms in mammals (Gunning et al., 2005). Since Tm is a dimer of two chains, expression of various isoforms can result in mixed populations of homo- and heterodimers. Additionally Tm can carry point mutations which are, in a heterozygous background, expressed in one allele while the second allele expresses unaffected wild-type (WT) protein. Tm carrying mutation can dimerise with WT or different Tm isoform increasing the number of possible Tm dimers.

Therefore the characterisation of individual Tm dimers would be, due to their large numbers, a challenging task however it will have implications in understanding of muscle function in health and disease.

The project investigates the effects of Tm heterodimer mutations associated with cardiomyopathies on the regulation of muscle contraction, therefore general information is given for the role of Tm in hypertrophic cardiomyopathy (HCM), dilated cardiomyopathy (DCM). In this chapter a literature review on the structural and functional features of Tm is presented. The chapter starts with the general biochemical and biophysical characteristics of Tm. It is followed by functional characteristics of Tm, including mechanism of striated muscle contraction and its regulation together with background information for other sarcomeric proteins.

1.1 General biochemical and biophysical characteristics of tropomyosin

In eukaryotes Tm is a ubiquitous α-helical coiled-coil dimer which consist of two right-handed amphipathic chains (Crick, 1953) with characteristic heptad repeat of seven residues denoted *a* to *g* (Sodek et al., 1972). Tm was originally discovered by Bailey as a structural component of the skeletal muscle (Bailey, 1946) and was believed to be a precursor of myosin. Tm's involvement in calcium dependent regulation of the muscle contraction was described later (Hanson and Lowy, 1964; Huxley, 1972; Parry and Squire, 1973; Spudich and Watt, 1971). The functional diversity of Tm was extended after the discovery of non-muscle contractile proteins (Lazarides, 1975).

The key properties of Tm are the association with F-actin, stabilisation of actin filaments and calcium dependent regulation of myosin binding to F-actin together with Tn. Non-muscle Tms are important for various actin cytoskeletal functions such as cell motility, intracellular vesicle movement, cytokinesis, cell proliferation, apoptosis and others.

1.1.1   Gene structure

Tropomyosins (Tm) form a large family of highly conserved α-helical dimers. Over 40 mammalian isoforms are expressed from four different genes denoted either as α-, β-, γ-

and δ-Tm or as TPM1, TPM2, TPM3 and TPM4 in humans, respectively (Schevzov et al., 2011; Vrhovski et al., 2008). Interestingly each of the human Tm genes is found in different chromosomes. The TPM1 is located on the long (q) arm of chromosome 15 at position 22.1 (Eyre et al., 1995), TPM2 location is on the short (p) arm of chromosome 9 at position 13 (Hunt et al., 1995), TPM3 is on the long (q) arm of chromosome 1 at position 21.2 (Gregory et al., 2006) and TPM4 is localised to chromosome 19p13.1 (Wilton et al., 1996). Human Tm genes can generate at least 21 different isoforms through the use of different promoters, alternatively spliced exons and different poly(A) additional signals (Lin et al., 2008).

The use of alternative promoters results in expression of Tm isoforms with different molecular weight. A distal promoter generates high molecular weight (HMW) Tm isoforms containing 284 – 285 amino acids (with exception of hTm1 – 1) that include exon 1a and exons 2a or 2b. Low molecular weight (LMW) Tm isoforms are formed by an internal promoter and contain 245 – 248 amino acids, starting from exon 1b and missing exons 1a, 2a and 2b.

Alternative splicing of primary gene transcripts can occur at the N-terminal (exon 2), the middle part of Tm (exon 6) or the C-terminal region (exon 9). Utilisation of an alternative exon splicing in a single gene can result in expression of up to 11 different Tm isoforms in humans (TPM1 gene). Regulation of alternative exon splicing involves a large number of factors and is tissue specific. As example the TPM1 gene can express smooth or striated muscle α-Tm isoforms using the set of two different exons 2a and 9d or 2b and 9b, respectively (Gooding and Smith, 2008).
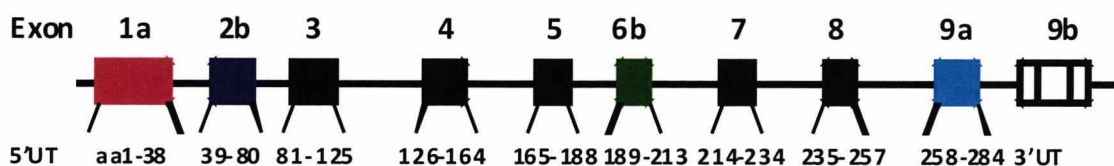
Figure 1.1.1 Exon organisation of striated α-fast Tm (Tmskα1). The gene is shown in 5' to 3' orientation with an individual exon encoding amino acid sequences. The gene is not drawn to scale and the colour coding, indicating alternatively spliced exons, has been adapted from Schevzov et al., 2011.
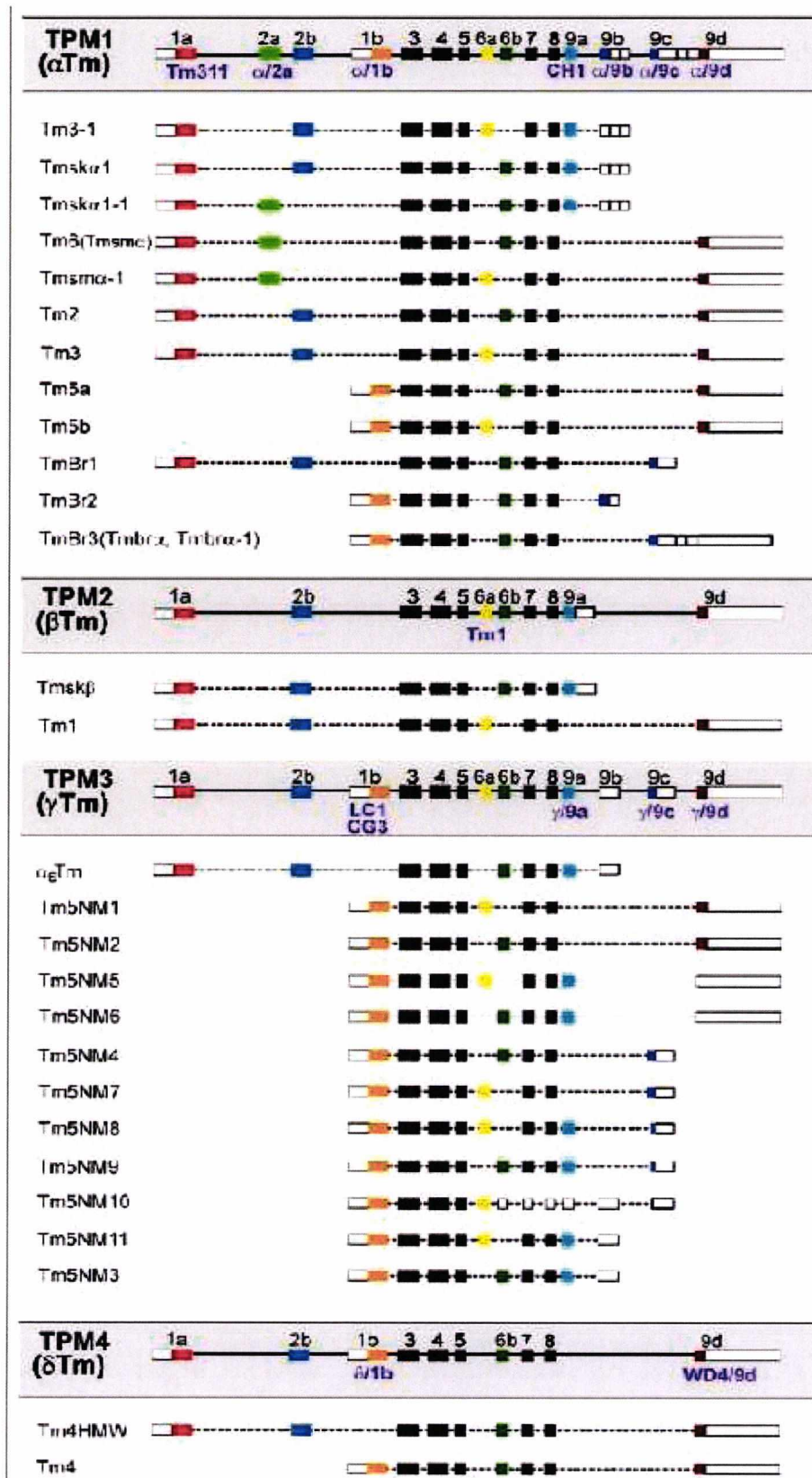
Figure 1.1.2 Organisation of Tm genes in mammals. Tm isoforms are generated by using four different genes, two different promoters and alternative splicing of exons 2, 6 and 9. Different Tm antibodies (denoted purple) are listed below the exon containing the epitope (Schevzov et al., 2011).

The human TPM1 gene spans about 29 kb and comprises of 15 exons. The TPM1 gene expresses the principal isoform used in this study α-fast Tm (Tmskα1) which is typically found in striated muscles. Figure 1.1.1 shows schematic diagram of Tmskα1 gene with an individual exon encoding amino acid sequences. The sequence of Tmskα1 and corresponding exons are shown in Table 1.1. Schematic organisation of mammalian Tm genes and individual Tm isoforms are shown in Figure 1.1.2.

Human TPM1 striated muscle isoform Tmskα1 sequence	Exon
mdaikkkmqmlkldkenaldraeqaeadkkaaedrskq	1a
ledelvslqkklkgtedeldkysealkdaqeklelaekkatd	2b
aeadvaslnrriqlveeeldraqerlatalqkleeaekaadeser	3
gmkviesraqkdeekmeiqeiqlkeakhiaedadrkyee	4
varklviiesdleraeeraelseg	5
kcaeleeelktvtnnlksleaqaek	6b
ysqkedryeeeikvlsdklke	7
aetraefaersvtkleksiddle	8
delyaqklkykaiseeldhalndmtsi	**9a**

Table 1.1 Skeletal human αTm sequence.

1.1.2 Nomenclature of tropomyosin isoforms

The large number of mammalian Tm isoforms is derived from the use of four genes, two transcriptional promoters and alternative exon splicing as discussed in the previous section. However the nomenclature of the Tm genes and isoforms has not been unified. The human Tm genes have been named TPM1 – 4 but are often referred to as α – δTm and inconsistent use of numerous alternative names of Tm isoforms in literature is confusing. Therefore there is a need for general consensus especially in Tm isoforms nomenclature. Alternative Tm genes and isoforms names are shown in Table 1.2.

The protein nomenclature of Gunning is used in this introduction chapter; α striated Tm is referred to as Tmskα1, heart-specific κ isoform as Tmskα1-1, β striated Tm as Tmskβ and γ skeletal Tm as Tmskα2. Following chapters describe mainly one isoform striated α Tm, therefore the traditional protein name α-Tm has been used.

Gene Name	Gene alternative names	Tm isoforms	Isoform alternative names
TPM1	αTm	Tm3-1	-
		αf-Tm	αTm_{fast}, $Tm_{sk\alpha}$, hTmskα1, skα-Tm
		hTmskα1-1	TPM1κ
		hTmsmα	Tmsmα, Tm6
		hTmsmα-1	-
		Tm2	-
		Tm3	-
		Tm5a	-
		Tm5b	-
		TmBr1	-
		TmBr2	-
		TmBr3	hTmbrα-1, hTmbrα
TPM2	βTm	β-Tm	Tmskβ, hTmskβ, skβ-Tm
		Tm1	Smooth muscle Tm1-Fibroblast
		hTm1-1	-
TPM3	γTm, $hTm_{30\,nm}$, hTm_{nm}, Tm-5	αs-Tm	αTm_{slow}, $\alpha_s Tm$, hTmskα2
		Tm5NM1	hTm5, Tm5, Tm30, fibroblast Tm30 nm
		Tm5NM2	-
		Tm5NM6	-
		Tm5NM7	hTm5-1, TC22
		Tm5NM4	hTmbrγ
		Tm5NM8	-
		Tm5NM9	-
		Tm5NM10	-
		Tm5NM11	hTm5-2
		Tm5NM3	-
TPM4	δTm, hTm30pl, hTmpl, Tm-4	hTm4HMW	-
		Tm4	-

Table 1.2 Alternative names of mammalian Tm genes and isoforms (Schevzov et al., 2011).

1.1.3 Tropomyosin genes expression and isoforms distribution

Tissue and cell specific expression of Tm is associated with the morphological changes occurring during development and cell differentiation (Clayton and Johnson, 1998; Muthuchamy et al., 1993).

Mammalian Tm isoforms are classified into two major groups, HMW and LWM, based on their molecular weight. HMW Tm variants are further classified according to their expression in specific tissues as follows: striated muscle isoforms (hTmskα1, hTmskα1-1, hTmskβ); smooth muscle isoforms (hTmsmα, hTmsmα-1, Tm1) including subgroup of brain specific isoforms (TmBr1, TmBr2, TmBr3); and Tms associated with early development/proliferation (Tm1, Tm2, Tm3) (Schevzov and O'Neill, 2008).

LWM Tm isoforms such as Tm5a and Tm5b encoded by the αTm gene, Tm5NM1 – 11 encoded by the γTm gene and Tm4 from the δTm gene are typically expressed in nonmuscle cells (Gunning et al., 2008; Gunning et al., 2005).

The expression of Tm isoforms in striated muscles is associated with the type of muscle, location within the body, developmental stage (Muthuchamy et al., 1993; Wolska and Wieczorek, 2003) and presence of pathological muscle impairments such as cancer (Gunning et al., 2008) or heart failure (Rajan et al., 2010). Fast-twitch skeletal muscles (rabbit psoas) express Tmskα1 and Tmskβ in a 60 : 40% ratio whereas slow-twitch skeletal muscles (rabbit musculus semimembranosus) contains the product of γTm gene, Tmskα2 isoform, in a 45 : 50 : 5 % ratio for Tmskα1, Tmskβ and Tmskα2 respectively (Kopylova et al., 2013; Marston et al., 2013).

Adult hearts of small animals such as rat, mouse, rabbit, dog and guinea pig contain almost exclusively Tmskα1 isoform (Leger et al., 1976; Ookubo et al., 1975; Peng et al., 2013a). The slower beating hearts of larger mammals (human, bovine, ovine, porcine) contain a majority of the Tmskα1 isoform and up to 20 % of Tmskβ isoform present as αβ-Tm heterodimer (Bronson and Schachat, 1982; Brown and Schachat, 1985). However other studies using immunoblotting of tropomyosin extracted from human ventricle identified presence of exclusively Tmskα1 isoform (Marston et al., 2013; Peng et al., 2013b; Purcell et al., 1999). Recently another cardiac isoform Tmskα1-1, also known as TPM1κ, was identified

and accounts for up to 5 % of heart tropomyosin. (Rajan et al., 2010). This isoform is identical with Tmskα1, except for the substitution of exon 2b for exon 2a, found in smooth muscle αTm. Interestingly, the latest studies did not identify presence of Tmskα1-1 isoform in human heart (Marston et al., 2013; Peng et al., 2013b).

Smooth muscle HMW isoforms Tmsmα and Tmsmβ in chicken gizzard are expressed at 1 : 1 ratio and form sm αβ-Tm heterodimers (Fatigati and Murphy, 1984; Ishii and Lehrer, 1990; Xie et al., 1991). However smooth muscle and nonmuscle cells in various stages of development/proliferation can express more than two Tm isoforms. Examples are studies including human fibroblasts (Novy et al., 1993) and mammalian vascular smooth muscle cells (Gallant et al., 2011) that showed expression of a multiple (in latter at least five LMW and HMW) Tm isoforms. Moreover mammalian developing brain cells express numerous isoforms TmBr1 (astrocytes), TmBr2 (oligodendrocytes and astrocytes), TmBr3 (mature neurons specific), Tm4 (all neuronal cells) and multiple products of γTm gene. The levels of these isoforms during the differentiation and maturation decrease (Tm1, Tm4, Tm5a), increase (TmBr2) or remain unchanged (Tm2, TmBr1) (Had et al., 1993).

1.1.4 Tropomyosin structure and unique features

Tm is an elongated molecule which consists of two parallel amphipathic right-handed alpha-helical chains wrapped around each other in a left handed supercoil (Crick, 1953). The amino acid sequence contains characteristic seven-residue repeat pattern (heptad) denoted *a, b, c, d, e, f* and *g* (McLachlan and Stewart, 1975). Mainly small and non-polar residues at positions *a* and *d* form hydrophobic core of Tm molecule (Sodek et al., 1972). The specific interactions of hydrophobic core between two Tm chains, which interlock with each other in a knobs-into-holes fashion, drive the formation and stability of the coiled-coil. Positions *e* and *g* are often occupied by charged amino acid residues which form salt bridges between two chains and further stabilise the coiled-coil structure. The *b*, *c* and *f* positions are usually polar or charged residues and face the surrounding aqueous environment and interacting with partner proteins (Brown et al., 2001). Schematic representation of Tm heptad

organisation and inter-coiled interactions are shown in Figure 1.1.3.A. Intra-helical interactions in the α-Tm helix are illustrated in Figure 1.1.3.B

A   **B**
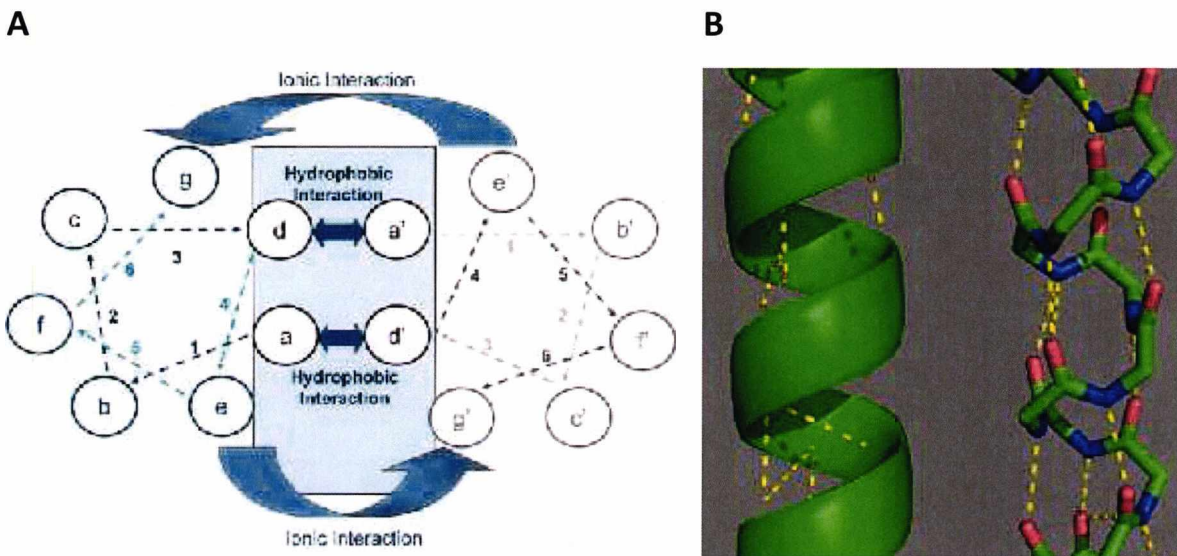
Figure 1.1.3 Schematic representation of Tm inter-(A) and intrahelical (B) interactions. Arrows in (A) illustrate the hydrophobic and ionic interactions between amino acids occupying their respective positions in the heptad (Wolska and Wieczorek, 2003).(B) The yellow dashed lines represent the polar interactions within tropomyosin helix, which stabilise the structure (http://proteopedia.org/wiki/index.php/Tropomyosin).

Human Tmskα1 contains 284 amino acids with molecular length 40 nm and 2 nm in diameter. There are approximately three full turns of the α-helix per molecule (Figure 1.1.4). Depending on the length of Tm isoforms, each dimer can span a certain number of actin monomers i. e. HMW Tms span the length of seven actin monomers, LMW Tms span six actin monomers (Gunning et al., 2008; Wang and Coluccio, 2010). Interestingly, *Saccharomyces cerevisiae* isoforms Tpm1 and Tpm2 contain only 199 and 161 residues and span the length of five and four actin monomers respectively (Drees et al., 1995).
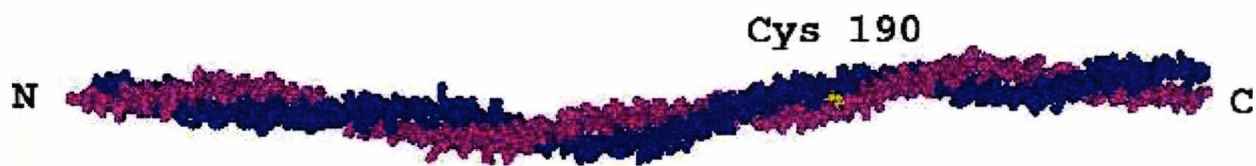
Figure 1.1.4 Crystal structure of porcine α-Tm at 7 Å resolution (Madej et al., 2012; Whitby and Phillips, 2000). Potential site of disulfide cross-link Cys 190 is indicated in yellow.

The hydrophobic core of Tm coiled-coil together with intra- and interhelical interactions between residues *e* and *g* provide stability to the dimer. However, there are perturbations in the coiled-coil structure uniformity which cause destabilisation required for binding to actin (Singh and Hitchcock-DeGregori, 2003; Singh and Hitchcock-DeGregori, 2006; Singh and Hitchcock-Degregori, 2009). Interruptions of the canonical interface are caused by either alanine (Ala) clusters or the "broken" core regions (Brown, 2006; Brown et al., 2001; Minakata et al., 2008).

The Ala clusters are short regions with the high Ala content at the core of the coiled-coil at positions *a* and *d* of the heptad repeat (Figure 1.1.5). The distance between two Tm chains at the Ala cluster is ≈2 Å shorter than in the other regions, and the interface is less well-packed than in a canonical coiled-coil (Brown et al., 2001).
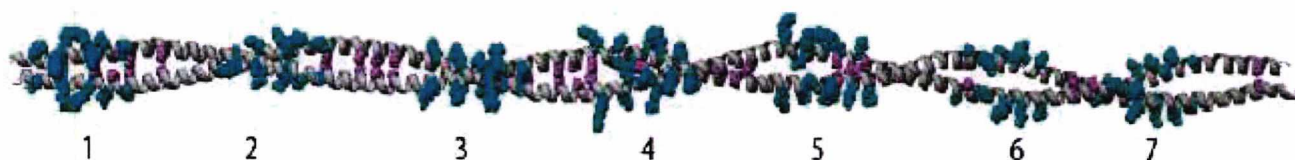
Figure 1.1.5 The alanine clusters (magenta) and consensus residues of proposed actin binding sites (cyan) (Phillips, 1986) on the striated muscle α-Tm (Whitby and Phillips, 2000). The numbers corresponds to the seven periodic repeats. Modified from (Singh and Hitchcock-DeGregori, 2006).

Additionally the Ala rich core regions appear axially out of register (axially staggered) by ≈1Å and narrowed by ≈2 Å. The joining of an axially staggered segment containing Ala

cluster with a canonical in-register segment, gives rise to specific bends (up to 6°) in the molecular axis (see Figure 1.1.6) (Brown et al., 2001; Brown et al., 2005). These bends along the Tm coiled-coil promote the shape complementarity to the surface of the F-actin which is crucial for specificity of Tm binding to actin filaments (Holmes and Lehman, 2008). The importance of local destabilisation has been shown in mutagenesis studies where replacement of Ala clusters in period 2 or period 5 with canonical hydrophobic residues (Val, Leu) results in loss of measurable actin affinity (Singh and Hitchcock-DeGregori, 2003; Singh and Hitchcock-DeGregori, 2006).
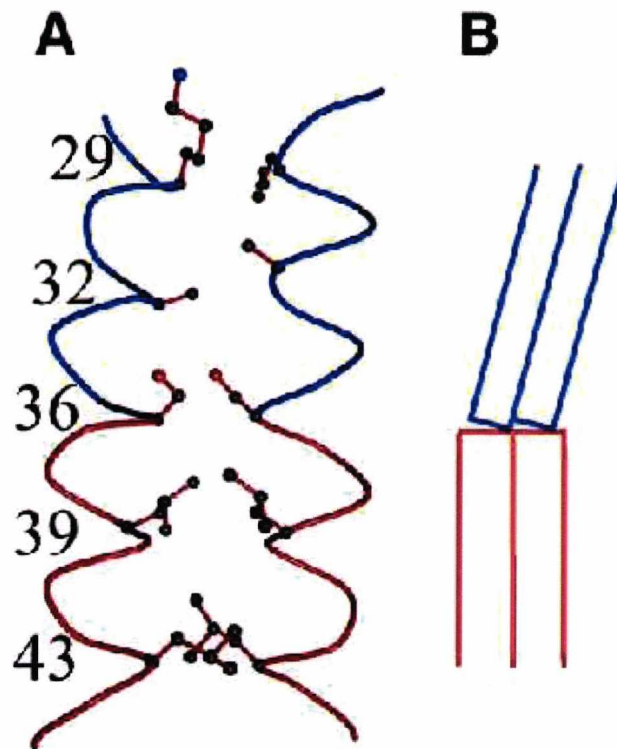
Figure 1.1.6 Axial staggering of Tm coiled-coil segment caused by alanine cluster. (A) An axially staggered alanine rich segment (residues 28 – 36; blue) joined to the leucine rich unstaggered segment (residues 35 – 45; red) produces a bend in the coiled-coil. (B) Simplified schematic of the axial staggering (Brown et al., 2001).

The second important feature that contributes to the bending of Tm coiled-coil is the poorly packed or broken core regions. The broken core regions are formed when instead of

hydrophobic residues typically present in canonical interface of the coiled-coil other residue (Asp137, Glu218, Gln263) is positioned. These residues are associated with an increased spacing between two Tm chains, forming the hole in the middle of the core, destabilising the coiled-coil and subsequently forming bends (Minakata et al., 2008). The gap volume correlates with the magnitude of the bend and the direction of bending (preference to "out of plane" bending) (Brown, 2010).

Local destabilisation of the coiled-coil hydrophobic interface by the Ala clusters and broken core regions, as described above, are required for an optimal shape complementarity and therefore crucial for actin binding. Additionally there is also sequence complementarity between Tm and actin filaments (McLachlan and Stewart, 1976; McLachlan et al., 1975; Parry, 1975). Analysis of Tm's sequence revealed a 7-fold periodic repeat of ≈40 charged or hydrophobic residues that represent a potential actin binding sites (see Figure 1.5) (Phillips, 1986). The relation of periodic repeats to actin was evaluated in experiments where replacement of specific repeats by Leu zippers showed that period 5 is essential for cooperative binding to actin (Singh and Hitchcock-DeGregori, 2006). Additionally the experiments where the actin binding site on period 5 was replaced by equivalent actin binding sites from period 1 or period 2 showed similar actin affinity suggesting that the actin binding sites amongst the seven periods of Tm are quasi-equivalent (Hitchcock-DeGregori, 2008; Singh and Hitchcock-DeGregori, 2007).

The surface of a Tm coiled-coil (positions *b, c* and *f* of the heptad) in the proposed actin binding repeats is rich in charged residues that can form electrostatic interactions with charged residues on actin. However the binding strength of individual Tm molecules to F-actin is weak (Wegner, 1980) and should not be considered of a lock-and-key type, despite the shape complementarity between the two proteins. The atomic models of the actin-Tm complex or the actin-Tm-Tn complex indicate that Tm lies over the F-actin surface at a radius of ≈40 Å (Lorenz et al., 1995; Poole et al., 2006). This estimated distance of Tm is too far away from actin filaments to allow short electrostatic interactions.

Recently a complete molecular model of actin-Tm complex based on computational chemistry and electron microscopy (EM) reconstruction revealed that the successive quasi-repeating units of tropomyosin interact primarily with the basic amino acid clusters (Arg147, Lys326 and Lys328) on actin subdomains 1 and 3 (Li et al., 2011). Additionally negatively

charged Asp25 and non-polar Pro333 residues on actin likely contribute to the binding strength (see Figure 1.1.7 and Table 1.3).
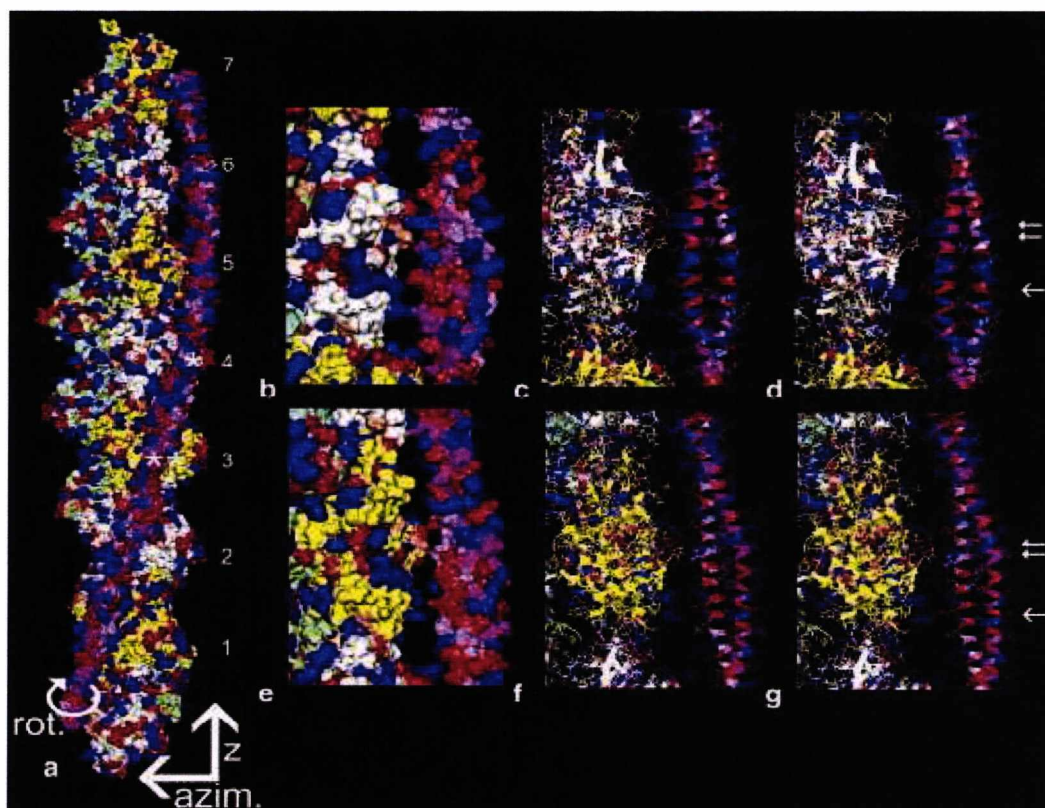
Figure 1.1.7 Electrostatic interactions between F-actin and Tm. (*a*) surface view of electrostatic interactions between Tm and F-actin. Actin subunits are numbered as in Table 1.2. *represents Tm quasi-repeat 4, and **represents Tm quasi-repeat 5; (*b* and *e*) enlarged and rotated segments of the F-actin – Tm model highlighting potential interactions of Tm quasi-repeat 4 (*b*)and Tm quasi-repeat 5 (*e*); (*c* and *f*) the same as *b* and *e* but in wire/ribbon format; (*d* and *g*) the same as *c* and *f* but fitted into the F-actin – Tm reconstruction. The single arrows in *d* and *g* point at Tm residues Glu-139 and Glu-181, respectively. The double arrow in *d* points at actin residue Pro-333 approaching Ser-132 on Tm and actin residues Asp-25, Arg 28 close to Tm residues Asp 121, Arg-125 and Lys-128. The double arrow in *g* points at actin residue Pro-333 close to Val-170 on Tm and actin residues Asp-25, Arg 28 approaching Glu-163 and Arg-167 on Tm. Acidic Tm amino acids are showed in red, basic amino acid in blue and proline is coral (Li et al., 2011).

The largest number of favorable electrostatic interactions is found on period 4 and 5 which have been shown to contribute most strongly to actin binding (Brown and Cohen,

2005; Hitchcock-DeGregori, 2008). The weak electrostatic interactions between actin and Tm facilitate free and rapid movement of Tm over the actin surface crucial for the regulation of the muscle contraction at low energy cost.

Actin subunit	Tm periodic repeat	Residue pairs in close contact		Distance between residues (Å)		
					MD simulation	
		Actin	Tropomyosin	Electrostatic search	Initial values (at 100 ps)	Average values (over 30 ns)
1	7	Arg-147	Asp-258	6.0	4.2	4.3
		Lys-328	Asp-258	-	6.6	-
		Asp-25	Arg-244	1.8	2.3	3.3
2	6	Lys-326	Glu-223	3.1	2.7	4.5
		Arg-147	Asp-219	-	-	6.6
		Lys-328	Glu-223	-	-	3.3
		Lys-328	Asp-219	-	-	3.7
		Pro-333	Ala-209	6.8	6.3	-
		Asp-25	Lys-205	3.1	3.0	-
3	5	Lys-326	Glu-181	5.6	3.0	6.5
		Arg-147	Glu-181	4.3	-	5.4
		Lys-328	Glu-181	5.0	3.4	4.2
		Lys-328	Glu-184	-	-	4.3
		Pro-333	Val-170	5.4	4.0	4.8
		Asp-25	Arg-167	3.2	6.7	5.3
		Arg-28	Glu-163	6.4	5.7	-
4	4	Lys-326	Glu-142	-	-	3.1
		Arg-147	Glu-139	4.1	6.0	2.0
		Lys-328	Glu-139	4.2	3.0	4.9
		Pro-333	Ser-132	5.6	6.3	3.7
		Glu-334	Lys-128	5.2	4.8	5.0
		Asp-25	Lys-128	6.2	5.3	-
		Asp-25	Arg-125	1.8	2.5	4.0
		Arg-28	Asp-121	5.1	5.9	-
5	3	Lys-326	Glu-104	4.3	3.8	3.5
		Lys-328	Glu-104	-	-	3.9
		Lys-328	Asp-100	-	-	4.2
		Arg-147	Glu-97	4.1	1.6	2.0
		Asp-28	Arg-90	-	-	3.0
		Arg-28	Glu-82	-	6.3	-
6	2	Arg-147	Glu-62	5.4	5.0	2.3
		Arg-147	Asp-58	-	-	6.7
		Lys-328	Asp-58	-	-	5.3
		Lys-328	Glu-62	-	-	6.0
		Asp-25	Lys-48	-	-	5.7
		Arg-28	Asp-41	4.6	3.1	5.1
7	1	Lys-326	Asp-20	-	4.3	-
		Arg-147	Asp-20	6.2	4.7	6.3
		Arg-147	Glu-16	6.6	3.7	-
		Lys-328	Asp-20	6.9	3.7	-
		Asp-25	Lys-6	4.6	1.8	-
		Asp-25	Gln-9	-	-	4.6

Table 1.3 F-actin and Tm residues that closely contact each other estimated by molecular dynamics.

Distances measured between the carboxyl and amino ends of closely spaced residues after the electrostatic grid search, at the beginning of a MD simulation at 100 ps, and for the same distances averaged over a 30 ns MD run. Distances ≤ 7 are noted (Li et al., 2011).

Weak binding of individual Tm molecules to actin filament lead to the proposal of a novel mechanism for the Tm-actin association called "Gestalt-binding" (Holmes and Lehman, 2008). The Gestalt-binding model (Figure 1.1.8) emphasises the importance of the shape complementarity of Tm and actin filaments, and end-to-end interactions between Tm dimers.
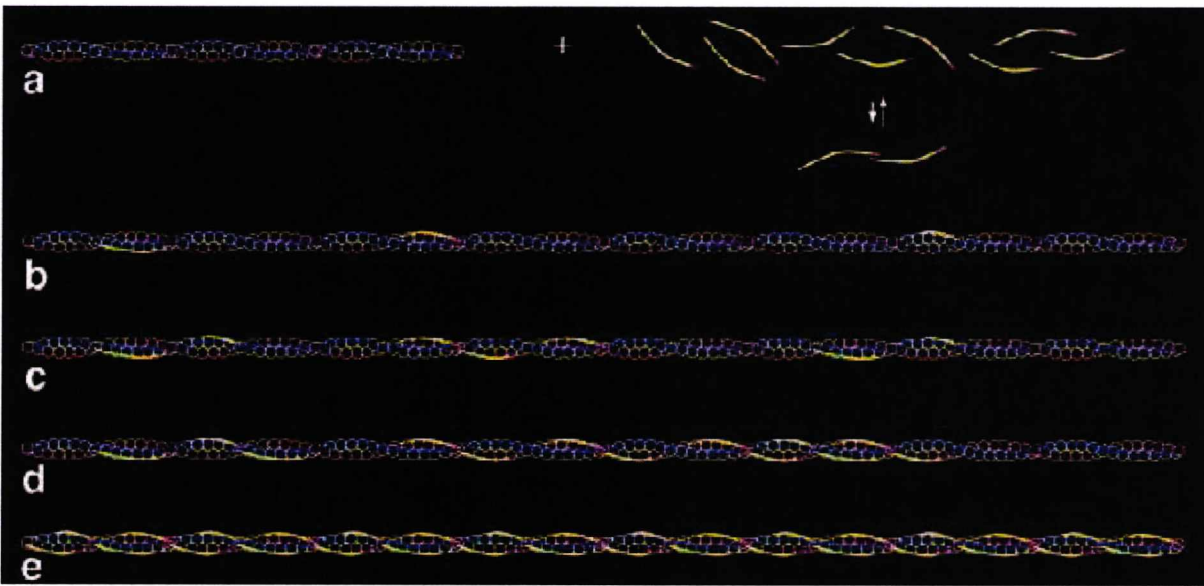
Figure 1.1.8 Schematic representation of Tm polymerisation on actin filament via Gestalt binding mechanism. a) Initial mixture of actin filaments (double chain of beads) and Tm molecules (multicoloured curved rods); b) weak binding of Tm molecules with correct shape to actin; c) initiation of Tm polymerisation by the formation of end – to – end bonds between neighbouring Tms on actin filaments; d) sorting process between long and short Tm; e) full saturation of Tm on F-actin (Holmes and Lehman, 2008).

Initial step of Tm polymerisation on actin is the formation of weak electrostatic interactions between individual Tm molecules and actin. These associations are possible only because of the structural complementarity of Tm and F-actin. When Tms with correct shape reach a critical concentration neighbouring Tm molecules will start to form end-to-

end interactions. As Tm polymers with various lengths start to populate actin filament, there will be a sorting process that favours the long over the short Tm oligomers. This mechanism will eventually lead to the full saturation of Tm on actin filament. Note that occurrence of the initiation likely affects the speed of elongation. If initiation is rare (few initiation per filament) then elongation will be fast as a sorting process for non-matching Tm polymers shortens.

Important question regarding the shape of Tm is whether it is controlled primarily by its amino acid sequence i. e. it is pre-shaped (sequence complementarity as proposed in Gestalt binding mechanism) or whether the Tm molecule is generally flexible and readily adjusts to its environment as suggested previously (Nitanai et al., 2007; Singh and Hitchcock-DeGregori, 2006).

A recent study using the EM and molecular dynamics (MD) simulations confirmed that Tm molecule has an average curved conformation (see Figure 1.1.9) shaped to match F-actin (Li et al., 2010). Single Tm molecules showed smooth curved profiles with no obvious kinks or joints. Additionally the measured persistence length indicates that isolated Tm is stiffer and less flexible than previously estimated for Tm straight rods (Swenson and Stellwagen, 1989; Wolgemuth and Sun, 2006). Tm has therefore a pre-shaped semi-rigid architecture with even more increased rigidity when polymerised on F-actin. Higher Tm rigidity is required in order to provide stability for actin and for the cooperative switching on actin filament.
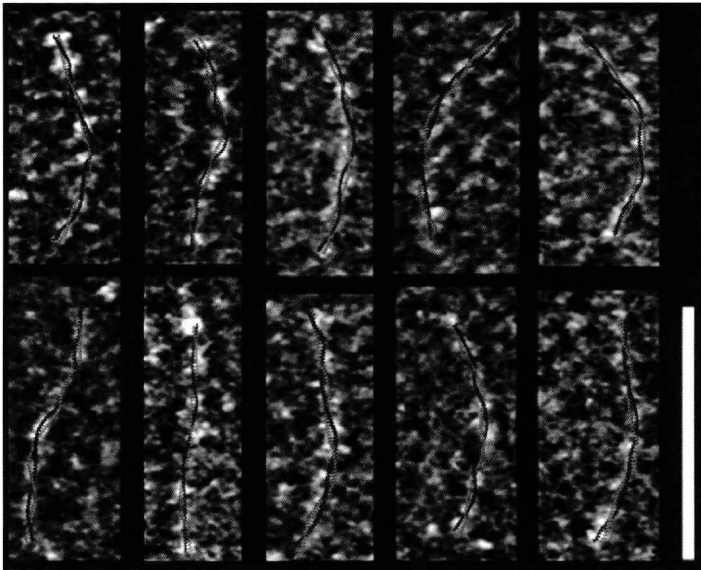
Figure 1.1.9 EM of isolated Tm molecules. Negatively stained bovine cardiac Tm molecules superposed with conformations from MD. Tm molecules showed on average gently curved features. The scale bar represents length of 40 nm (Li et al., 2010).

However, too rigid Tm would not be able to cope with the strain produced during Tm filament movement, especially at the joints between adjacent Tms. Therefore some degree of flexibility is required for the movement. This flexibility is partially provided by the variations in the supercoil pitch and between coiled-coils as discussed above (Brown and Cohen, 2005; Brown et al., 2001; Minakata et al., 2008; Nitanai et al., 2007; Whitby and Phillips, 2000) but most importantly by the conformational flexibility in the intermolecular junctions between Tm molecules (Greenfield et al., 2006). Determination of the structure of the striated α-Tm end-to-end complex by NMR showed that C-terminus splays apart to form a cleft where N-terminus binds and forms 11 residues overlap (Figure 1.1.10). Crystal structure of the cardiac α-Tm end-to-end complex has been also solved and showed the same 11 residues overlap (Murakami et al., 2008). C-terminal residues Q263, Y267 and I270 are poorly packed and conformationally flexible thus allow the ends to splay apart to bind N-terminus forming dynamic complex. The essential role of the C-terminal conformational dynamics has been shown when replacement of Q263 residue for the canonical interface residue (Leu) increased the stability of the C-terminus and abolished binding to the N-terminus and forming a complex with troponin T (Greenfield et al., 2002). The overlap region of chicken smooth muscle Tm resolved by X-ray crystallography (Frye et al., 2010) showed a significant curvature similar to the rat striated structure resolved by the NMR (Greenfield et al., 2006). The smooth muscle overlap region comprises of ~15 amino acid

zone differs between different Tm isoforms as there is a sequence variability between C-terminal exons 1 and 2, and N-terminal exon 9 (Schevzov et al., 2011).

The "head-to-tail" arrangement explains the reduction in the length of Tm in the filament (400 Å) as compared to that of non-polymerised Tm (416 Å) (Greenfield et al., 2006). There are two factors that enhance the head-to-tail polymerisation of skeletal Tm; the N-terminal acetylation of Tm and the interaction of the Tm overlap region with TnT1 (Monteiro et al., 1994; Schaertl et al., 1995).
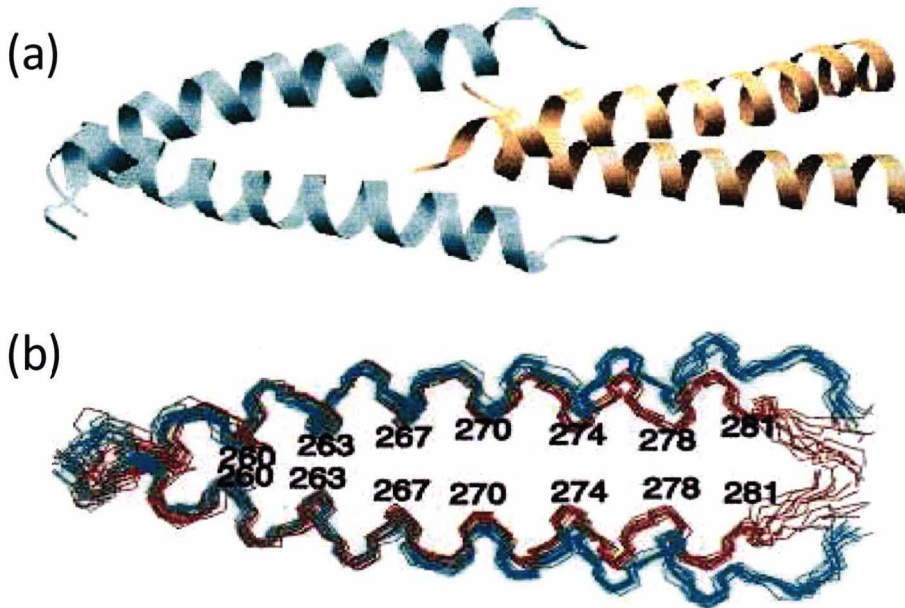
Figure 1.1.10 Structure of the striated α-Tm junctional complex. (a) NMR structure of the Tm complex between C-terminal (cyan) and N-terminal (brown) domains. (b) The conformation of the C-terminal domain in complex with N-terminal domain (cyan), compared to the conformation of the unbound C-terminal domain (brown) (Greenfield et al., 2006).

The native Tm is acetylated and binds to the F-actin initially by weak electrostatic interactions and shape complementarity as described previously (Holmes and Lehman, 2008; Li et al., 2010; Wegner, 1980). Bacterially expressed Tm is unacetylated due to the lack of the post-translational modification and therefore cannot bind actin. There are structural differences in the N-terminal region of acetylated and unacetylated Tms that are responsible for the binding to actin shown in Figure 1.1.11. The N-terminal region of unacetylated Tm is splayed and fails to overlap with the C-terminal end of the neighbouring Tm preventing polymerisation on actin filament. It has been shown that the Ala-Ser

extension used in bacterially expressed Tm can mimic the essential N-terminal acetylation (Monteiro et al., 1994). However, comparison of native α-Tm and AS-α-Tm showed a lowered cooperative unit size of AS-α-Tm (6.5) compared to the native α-Tm (10) suggesting lowered cooperativity of the Tm construct (Mirza et al., 2007).
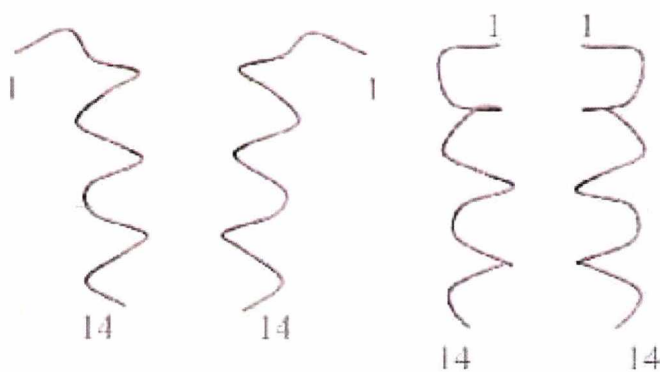
Figure 1.1.11 Structural differences between unacetylated and acetylated Tm. The N-terminal region of unacetylated Tm (left) is splayed and unable to overlap with the C-terminal end of the neighbouring Tm, thus unable to bind F-actin (Brown et al., 2001).

1.1.5 Dimerisation of tropomyosin

The driving force for dimer formation comes from the specific interactions between *a* and *g* Tm heptad residues that form the hydrophobic close packed core of the dimer. This core is further stabilised by electrostatic interactions between residues *g* and *e*, (McLachlan and Stewart, 1975; Perry, 2001; Stewart, 2001; Wolska and Wieczorek, 2003). There are also other requirements for coiled-coil formation such as a strong thermodynamic selection for coiled-coils assembled from polypeptides of equal length. This will maximise the degree of interaction between the two polypeptide chains. It has been shown that coiled-coil dimers also have distinct sites within the heptad-repeat amino acid sequences necessary for mediation of coiled-coil formation (Kammerer et al., 1998). These short autonomous folding units are called trigger sequences or trigger motifs. Trigger sequences were initially identified in the *Dictyostelium discoideum* actin-bundling protein cortexillin I (Steinmetz et al., 1998) and the yeast transcriptional activator GCN4 (Kammerer et al., 1998). The consensus trigger sequence from these studies was aligned with the other two-stranded coil-coiled sequences and revealed putative trigger motifs in chicken gizzard smooth muscle myosin II, human kinesin, nucleoprotein TPR, kinesin, β-tropomyosin (Tmskβ) and others. As

Tm is a major subject of this thesis, the consensus trigger sequence together with corresponding putative trigger sequences of human tropomyosins from TPM1, TPM2, TPM3 and TPM4 genes were aligned for comparison in Figure 1.1.12.

Gene	Heptad position / Tm Isoform	b	c	d	e	f	g	a	b	c	d	e	f	g	
TPM1	Tmskα1; Tmskα1-1	K	V	L	S	D	K	L	K	E	A	E	T	R	- 238
TPM2	Tmskβ	K	L	L	E	E	K	L	K	E	A	E	T	R	- 238
TPM3	Tmskα2	K	I	L	T	D	K	L	K	E	A	E	T	R	- 238
TPM4	Tm4HMW	K	L	L	S	D	K	L	K	E	A	E	T	R	- 238
	Consensus sequence	x	x	L	E	x	c	h	x	c	x	c	c	x	

Figure 1.1.12 Sequence alignment of the putative trigger motifs of human TPM1, TPM2, TPM3 and TPM4 genes. Lower case letters (a – g) indicate heptad position; amino acid residues matching consensus sequence are in bold; x, any residue; c, charged residue; h, hydrophobic residue (image from Janco et al., 2013).

This putative trigger sequence is in exons 7 and 8 which is constitutive in all Tm isoforms expressed from each of the four Tm genes. Sequences of all selected Tm isoforms diverge from the consensus sequence at position 237 with Thr in place of a charged residue. Additionally isoforms Tmsk1, Tmsk1-1 and Tm4HMW have Ser or Thr in place of E229. However, the precise trigger sequence is not essential to coiled-coil formation if a critical threshold stability value is exceeded by the intra- and inter-helical stabilising effects (Kirwan and Hodges, 2010; Steinmetz et al., 2007). Additionally from the evolution point of view it would be beneficial if the trigger sequences of the protein with 21 isoforms in human (Lin et al., 2008; Rajan et al., 2010) were located in highly conserved part of the sequence. As amino acids 266 – 238 are localised in exon 7 (214 – 234) and exon 8 (235 – 258) (Hodges et al., 2009) present in all human Tm isoforms, the requirement for trigger motifs of this part of Tm molecule is fulfilled.

Although the above described 226 – 228 trigger sequence in high molecular weight (HMW) tropomyosins may play important role in the Tm folding, it is not critical for this process in terms of the whole Tm molecule. A recent study (Hodges et al., 2009) showed

20

that deletion of various N- and C- fragments do not affect folding of Tm but dramatically (16 °C) decrease thermal stability of Tm. This study led to the identification of a stability control region (97 – 118) which does not mediate folding but is crucial for the final protein stability. Additionally the N- and C- terminal deletion fragments were fully folded which suggests the existence of more trigger sites within Tm molecule or simply a unique short amino acid sequences able to form hydrogen-bonding network that stabilises Tm α-helices and promote hydrophobic core residue interactions for the formation of coiled-coil (Hodges et al., 2009; Kirwan and Hodges, 2010; Steinmetz et al., 2007).

The other important function of trigger sequences was shown in an earlier study (Araya et al., 2002) involving low molecular weight fibroblast tropomyosins TM-4 and TM-5(NM-1). The TM-4 and TM-5(NM-1) Tm isoforms are normally able to form heterodimers as well as homodimers (Gimona et al., 1995; Temm-Grove et al., 1996). These 248 amino acids long Tm isoforms were found to contain the trigger sequence located at amino acids 190 – 202 derived from previously described trigger motif of the GCN4 leucine zipper (Kammerer et al., 1998). The 190 - 202 trigger sequence was shown to be required for the formation of TM-4 homodimers but not for the formation of heterodimers between TM-4 and TM-5(NM-1). Involvement of the trigger sequence in LMW tropomyosins dimerisation is important as the dimerisation of various Tm isoforms might be critical for their cellular function.

It is well established that the information for the homo- vs heterodimerisation of HMW tropomyosins is largely contained within the Tm molecule itself by the alternatively spliced exons (Araya et al., 2002; Gimona, 2008; Gimona et al., 1995). However the role of trigger sequences in HMW tropomyosin dimerisation remains to be confirmed.

1.2 Functional characteristics of tropomyosin in muscle and nonmuscle cells

The structural appearance of a uniform Tm coiled-coil dimer at first glance might give the impression of simplicity but there are perturbations specifically tailored to fulfil Tm's diverse functional roles within muscle and non-muscle cells as described in previous sections.

Tm is primarily associated with its function in the muscle contraction mechanism which is a fundamental physiological process responsible for movement. This section describes the functional characteristics of muscle contraction and the regulation of muscle contraction. It is followed by general characteristics of striated and cardiac muscle including description of individual sarcomeric proteins involved in the muscle contraction. In conclusion of the section 1.2 a brief description of Tm function in smooth and non-muscle cells is provided.

1.2.1 Mechanism of striated muscle contraction

According to their morphology and function, muscles are divided into three distinct classes: skeletal muscle, responsible for voluntary movements with characteristic patterns of cross-striation; striated but involuntary cardiac muscle and involuntary smooth muscle without a striation pattern. Current understanding of muscle contraction is largely based on characterisation of the striated muscle structures at the molecular level.

A striated muscle cell, known as a muscle fiber (in skeletal muscle), is elongated, cylindrical shaped, multi-nucleated and relatively large cell with diameter from 10 to 100 μm and length up to several centimeters. The cytoplasm of striated muscle, known as the sarcoplasm, predominantly consists of myofibrils. Myofibrils are cylindrical bundles containing thick filaments of myosin and thin actin filaments with an average diameter 15 nm and 7 nm respectively. Myofibrils are organised as a chain of basic functional or contractile units called sarcomeres (Figure 1.2.1). The arrangement of the contractile muscle proteins in the myofibrils is responsible for the striated appearance of skeletal and cardiac muscle. Within each sarcomere thick myosin containing filaments: appearing under the microscope as a dark bands, also called A bands, alternate with thin actin containing filaments: appearing under the microscope as light bands or I bands. Thick and thin sarcomeric filaments overlap in peripheral regions of the A band however a middle region called H zone contains only thick myosin filaments. Actin filaments are anchored into a protein disc known as the Z-line which defines the end of sarcomere. Myosin filaments are anchored into a band called M line located in the middle of H zone (Clark et al., 2002).

22
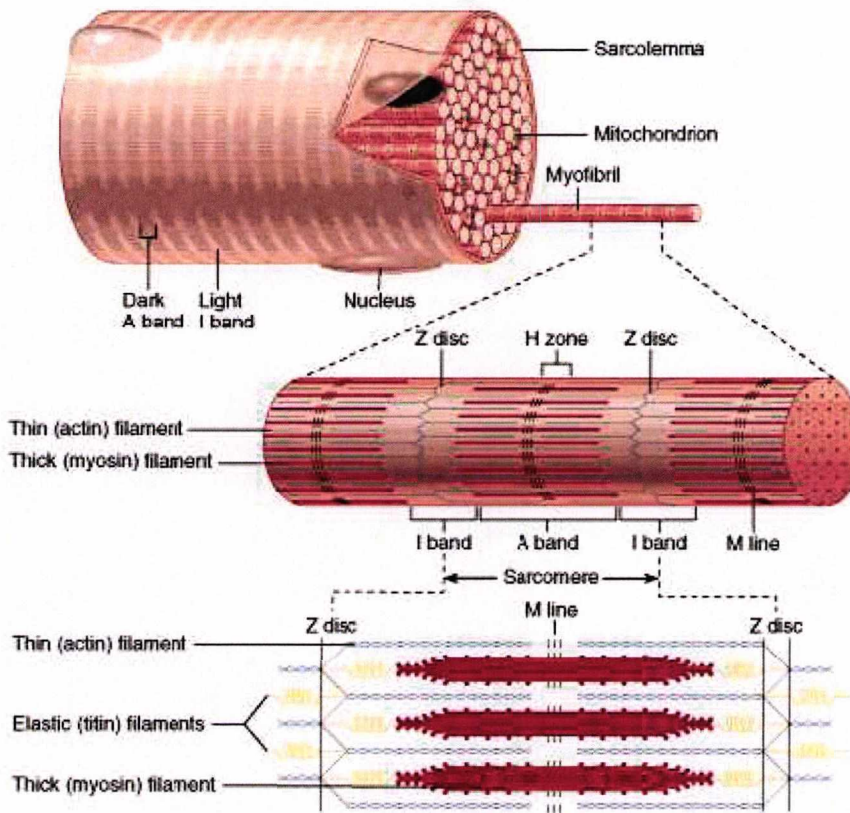
Figure 1.2.1 Structure and organisation of a skeletal muscle fibre. Section of skeletal muscle fibre shows high numbers of myofibrils in the sarcoplasm, multiple mitochondria and peripheral nuclei. The sarcomere as a basic contractile unit of skeletal muscle with location and organisation of actin and myosin filaments is also shown (image from http://faculty.etsu.edu/forsman/Histologyofmuscleforweb.htm).

Muscle contraction is based on sliding filament model, first proposed in 1954 by two independent studies (Huxley and Niedergerke, 1954; Huxley and Hanson, 1954). During muscle contraction sarcomeric thin and thick filaments slides along each other and bring the Z discs closer together. During this process the overlap area of thin and thick filaments increases, the I bands become very narrow and H zone almost completely disappears but the width of the A band stays unchanged (Figure 1.2.2).
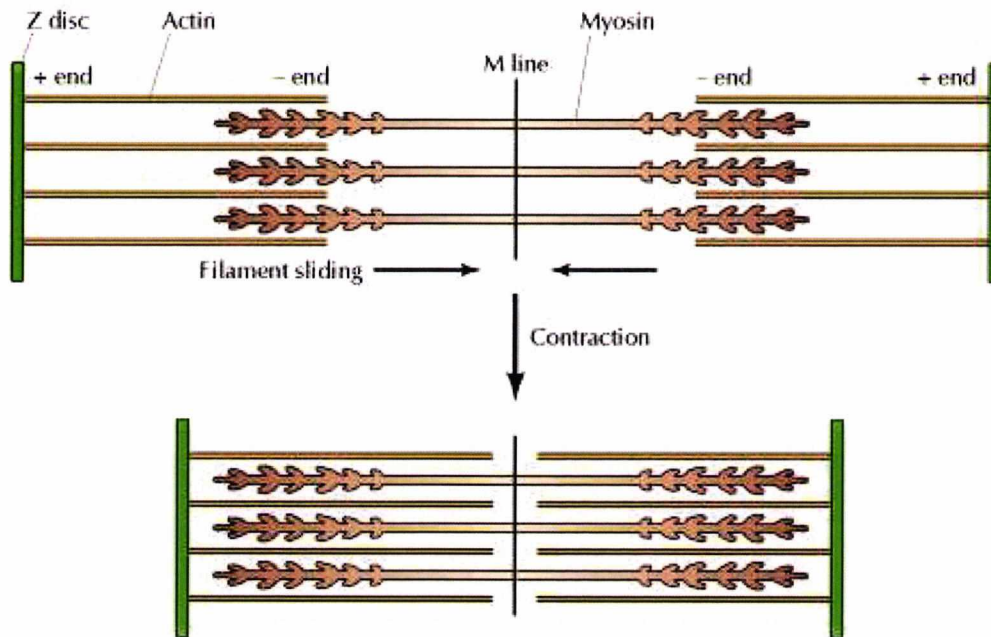
Figure 1.2.2 The sliding filament mechanism of a skeletal muscle. Actin filaments slide along myosin filaments into the A bands and H zone without change in the length of individual thin or thick filaments. Energy for the movement is provided by ATP hydrolysis and actomyosin binding is regulated by presence or absence of Ca^{2+} (Image from https://www.boundless.com/image/the-sliding-filament-model/).

The sliding filament mechanism is based on interactions between the actin thin filament and the myosin globular head also known as subfragment 1 (S1) or cross-bridge. Actin filaments form a complex with regulatory proteins Tm and Tn which inhibits acto-myosin binding by steric hindrance of cross-bridge in the absence of Ca^{2+}. Moreover cross-bridges are ATPases in which ATP hydrolysis provides energy for conformational changes in myosin S1 resulting in mechanical movement responsible for the sarcomere shortening. The muscle contraction mechanism therefore depends on alteration of Ca^{2+} concentration and ATP hydrolysis.

ATTACHED   DETACHED

weak/strong   weak

top-of-power-stroke   pre-power stroke

4   switch 1 open   switch 1 closed   **3**
         switch 2 closed   switch 2 closed
         actin-cleft closed   actin-cleft half closed
         β-sheet strained   β-sheet untwisted

                power   recovery

strong   weak

rigor-like   post-rigor

1   switch 1 open   switch 1 closed   **2**
         switch 2 closed   switch 2 open
         actin-cleft closed   actin-cleft open
         β-sheet twisted   β-sheet untwisted

Figure 1.2.3 The cross-bridge cycle. The cycle starts with myosin cross-bridge tightly bound to the actin in the absence of nucleotide forming the rigor complex (state 1). The binding of ATP results in the post-rigor conformation (state 2). ATP is then hydrolysed by myosin. This stage is called the pre-power stroke (state 3) where the lever arm is repriming. The cross-bridge reattaches to a neighbouring actin binding site (top-of-power-stroke conformation, state 4). (Geeves, Holmes, 2005).

The production of the force by myosin molecules is made in the progressive biochemical reaction of ATP hydrolysis. The first biochemical model of the cross-bridge cycle was proposed by Lymn and Taylor in 1971, describing the role of the ATP hydrolysis in the muscle contraction mechanism. The substrate of the cross-bridge cycle is MgATP and the product is MgADP + Pi. The Lymn-Taylor cycle (Figure 1.2.3) has four steps beginning with myosin cross-bridge tightly bound to the actin in the absence of nucleotide forming the rigor

complex (state 1). The binding of ATP results in the post-rigor conformation (state 2) where rapid dissociation of the actomyosin complex (AM) occurs. ATP is then hydrolysed by myosin into a stable myosin-products complex (M·ADP·Pi). This stage of cross-bridge cycle refers to as pre-power stroke (state 3) where the lever arm is reprimed. The cross-bridge reattaches to a neighbouring actin binding site (top-of-power-stroke conformation, state 4). Binding to actin causes conformational change of myosin head and triggers the power stroke which executes mechanical movement of the actin by approximately 10 nm. Additionally reattachment to the actin enables the release of the phosphate and ADP (Geeves, Holmes, 2005).

The changes leading to the mechanical movement of muscle filaments described above are quite complex. Therefore, structural description of individual proteins involved in cross-bridge cycle is provided in section 1.2.3. The same section additionally contains details of conformational changes in myosin head during the cross-bridge cycle.

1.2.2 Differences between skeletal and cardiac muscle tissue

The sliding filament theory described above is based on a description of skeletal muscle whose structural and functional characteristics differ in comparison with cardiac muscle. Both skeletal and cardiac muscle (Figure 1.2.4 A and B respectively) are categorised as striated muscles. However cardiac cells are significantly smaller (~20 µm width and ~100 µm length) in comparison to skeletal muscle (~100 µm width and 1 - 30 cm length). Myocytes have typically 1 - 2 centrally placed nuclei, while striated muscle cells contain multiple peripherally placed nuclei. Additionally cardiac muscle cells are almost entirely dependent on aerobic metabolism whereas striated muscle cells are able to function under aerobic and anaerobic conditions. Due to the dependency on cellular respiration, mitochondria make up to 30 % of the sarcoplasmic volume of cardiac myocyte, however mitochondria in anaerobic skeletal muscle fibre form approximately 2 % of the cytoplasmic volume.
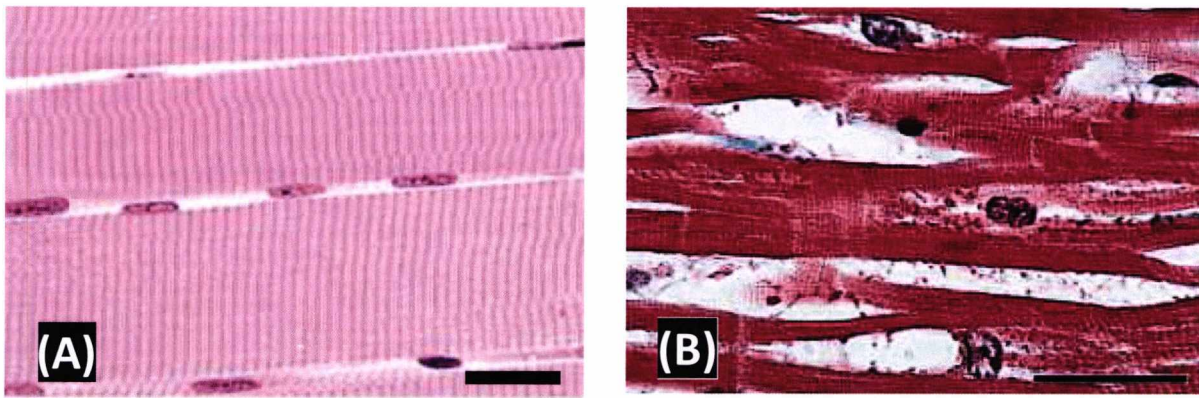
Figure 1.2.4 Structural characteristics of striated (A) and cardiac (B) muscle cells. Multiple peripherally placed nuclei, visible alterations of dark and light bands, and linear organisation of striated muscle fibres (A). Branched cells with centrally placed nucleus and indicated intercellular junction called intercalated disc of cardiac muscle tissue. Scale bar represents 50 μm. (Figure 1.2.4 A from http://bio1152.nicerweb.com/Locked/media/ch40/40_05Muscle-skeletal.jpg; Figure 1.2.4 B from http://www.kumc.edu/instruction/medicine/anatomy/histoweb/muscular/muscle16.htm)

Characteristic structural features of cardiac muscle cells are intercellular adhesive junctions called intercalated discs and a network of branching fibres formed by individual cells. Moreover the endomysium of cardiac muscle cells, which is the electrically insulating sheath between individual cells, is denser in comparison with skeletal endomysium. Fundamental functional differences between cardiac and skeletal muscle cells are based on involuntary and voluntary muscle control respectively. Plasma membrane of both types contains invaginations called the transverse or T tubules that are the pathways for activation and electrical stimulation. Cardiac cells contain fewer and wider T tubules for better signal and activation of the muscle. The arrangement of T tubules in skeletal muscle is organised more regularly. They can be found at the A/I junction in contrast with cardiac muscle T tubules found in the Z line.

1.2.3 Functional components of striated muscle

Detailed description of the structural features of proteins involved in the cross-bridge cycle provided in following sub-sections serve as a background for the calcium dependent

regulation of muscle contraction described in section 1.2.4. Additionally section 1.2.3.1 describing myosin structure contains detailed description of the conformational changes in this molecule during the cross-bridge cycle.

1.2.3.1 Molecular motor myosin

Myosin is a major component of cardiac and skeletal muscle which plays a key role in muscle contraction. Myosins are a large family of molecular motor proteins divided into 35 classes, with individual structural diversity between each class (Odronitz and Kollmar, 2007). Myosin participates in a wide range of biological processes such as regulation of cell shape, skeletal and cardiac muscle contraction (Gordon et al., 2001), regulation of heart rate, adult heart development, visual perception, ultrafast sound vibrations detection (Fettiplace and Hackney, 2006), intracellular trafficking, Golgi organisation, cytokinesis (Ross et al., 2008) and many others.

The muscle contraction in skeletal and cardiac muscle is facilitated by myosin II molecules. The myosin II is a heterohexamer composed of two myosin heavy chains (MyHC) and two pairs of nonidentical, calmodulin-like myosin light chains (MyLC) called the regulatory light chain and the essential light chain. Myosin II also contains the large globular myosin head also called subfragment 1 (S1) subdivided into a motor domain and alpha helical neck domain known as a lever arm containing two IQ domains where the regulatory and essential MyLC are bound. These structures are followed by a coiled coil tail domain and the targeting region, which binds the myosin to the M line of the sarcomere (Sweeney and Houdusse, 2010).

The myosin II molecule is insoluble at physiological salt conditions (~90 mM *in vivo*) due to its ability to form the thick filaments by dimerisation via side-by-side associations. Muscle myosins can be solubilised in high salt concentration (≤500 mM KCl) however high densities of solution, higher content of fluorescent tryptophan and difficulties with purification of whole fibrous myosin molecule are reasons why for experimental purposes only S1 is used. The myosin head domain is soluble at physiological salt conditions and contains both the actin binding site and the nucleotide binding site required for complete

performance of the actomyosin ATPase cycle. The S1 containing only the essential light chain or both essential and regulatory light chains can be obtain by chymotrypsin and papain proteolytic digestion respectively. Further limited digestion separates the S1 into three fragments named after their apparent molecular weights: the N terminal 25K, the middle 50K and the C terminal 20K domains (Geeves and Holmes, 1999).

The first high resolution structure of a myosin motor domain was solved in 1993 by Rayment et al., specifically structure of chicken skeletal S1 (Figure 1.2.5) at the post-rigor state (Rayment et al., 1993).
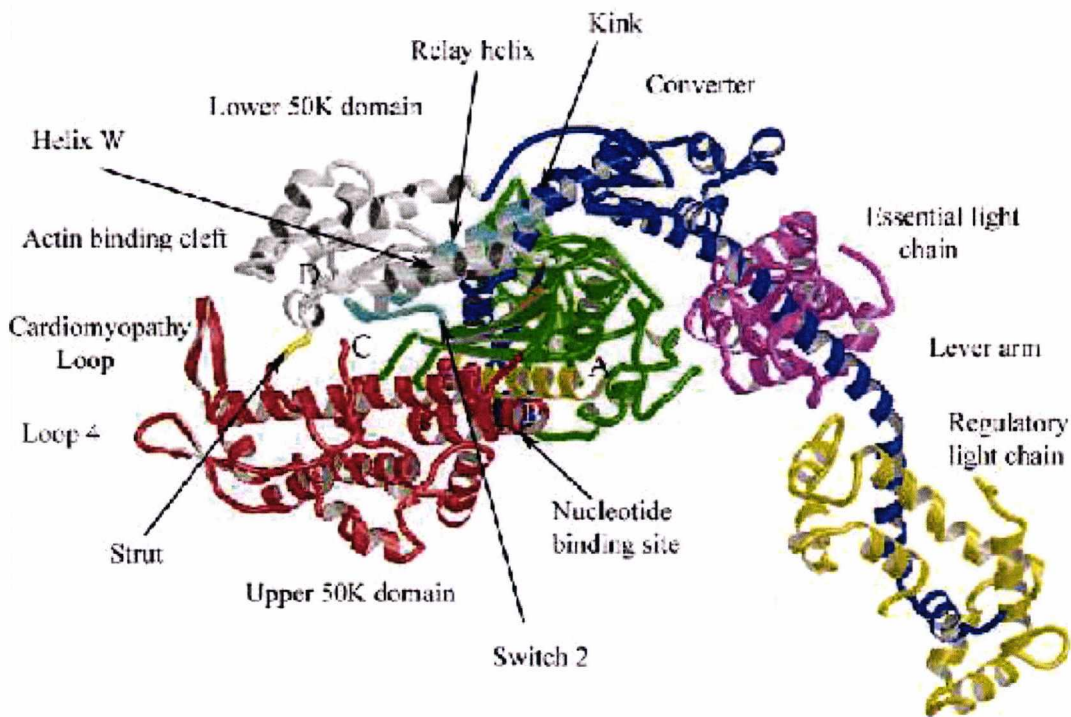
Figure 1.2.5 The myosin motor domain crystal structure of the chicken skeletal muscle at the post-rigor state. Individual structural segments of the cross bridge are colour coded. The N-terminus is shown green; the nucleotide binding P-loop and adjoining helix are yellow; the upper 50K domain is red; lower 50K domain is grey; the proximal end of relay helix (in rigor state with the kink) is shown light blue however it is part of the lower 50K domain; the C-terminal long helix, the converter and the distal end of relay helix (beyond the kink) are dark blue; the essential light chain is purple and the regulatory light chain is yellow. Important structural feature is a large cleft which separates the upper 50K domain and the lower 50K domain. The entrance to the cleft is the primary actin-binding site (Geeves and Holmes, 2005).

Crystallographic representation of elongated myosin head revealed following structural details. A seven-stranded β-sheet and associated α-helices form a deep cleft and previously mentioned the upper 50K and the lower 50K domains separate the cleft. Both the upper 50K and the lower 50K domains are involved in strong actin-binding (Guo and Guilford, 2006). The P loop nucleotide binding site is flanked by switch 1 and switch 2 segments where latter connects with the relay helix. The relay helix is firmly attached to the converter domain in which the C-terminal region of the cross-bridge or lever arm is anchored. The lever arm is a long α-helical structure where the regulatory and essential MyLC are bound, stabilising the α-helix and making it stiff (Geeves and Holmes, 2005). Both light chains share sequence and structural homology with protein calmodulin. However, unlike calmodulin which contains four Ca^{2+}-binding motifs, regulatory MyLC contains only one and essential MyLC no Ca^{2+}-binding sites.

As described above myosin is a complex molecule and during the cross-bridge cycle (section 1.2.1) undergoes conformational changes which are critical for the muscle contraction. These conformational changes of myosin head are strongly linked and involve structural elements including the actin binding cleft, switch 1 (SW1), switch 2 (SW2), P-loop, β-sheet, relay helix, converter domain and lever arm. In the absence of nucleotide when myosin and actin form a rigor complex, both SW1 and SW2 are open and the 50K cleft is closed. The process of ATP binding to myosin, causing the shift from rigor to post-rigor conformation, occurs in two consecutive steps. Firstly, ATP forms a weak complex with myosin strongly bound to actin (A·M-ATP) and then interaction between actin and myosin weakens (A-M·ATP). The transition between these two steps results in simultaneous opening of the 50K cleft and closing of SW1 which cause a rapid release of actin from myosin. The binding of ATP also moves SW2 from the open to closed position (repriming step; away from the nucleotide pocket) which causes a series of following events leading to the pre-power stroke conformation. The inward rotational movement of the lower 50K domain towards the β-sheet, caused by SW2 opening, also moves the relay helix against the β-sheet forming a small kink in the helix. Distortion of the relay helix causes a 60° rotation of the converter arm and the leaver arm. In this stage the SW2 moves back to the closed position (close to the nucleotide binding site). The movement of SW2 into the close position also causes the conformational change that closes the inner part of the actin binding cleft.

Additionally the bound nucleotide restrains the β-sheet in the un-twisted conformation and holds the P-loop in the "down" position. The described events result in the closed position of both SW1 and SW2 with the nucleotide completely enclosed in the nucleotide binding pocket which triggers hydrolysis of ATP into ADP and Pi. Hydrolysis of ATP causes the rebinding of myosin to actin, thus entering the top-of-power-stroke conformation. Binding to actin causes β-sheet to twist and subsequent rotation of the converter domain releases the pressure and removes the kink from the relay helix. The P-loop moves in the "up" position, SW1 opens and the 50K cleft closes causing an increase in the myosin affinity for actin. The binding of Pi is weakened and it's released. The release of Pi opens SW2 and drives the power stroke. Reaching the post-power stroke conformation (rigor-state) the ADP is also released and the cycle starts again (Geeves and Holmes, 1999; Geeves and Holmes, 2005; Holmes and Geeves, 2000).

1.2.3.2 Actin thin filaments

Actin is highly conserved and one of the most abundant of all eukaryotic proteins. Its involved in a very wide spectrum of biological functions including cell division, locomotion, cytoplasmic cargo transport, cell adhesion, vesicle formation, transcription, tension, contraction, nuclear architecture and others (Schoenenberger et al., 2011). However there are only six actin genes in mammals and each encodes a single isoform (Perrin and Ervasti, 2010). These are the α-skeletal, α-smooth, α-cardiac, β-cytoplasmic, γ-cytoplasmic and γ-enteric actin isoforms. The major constituents of the striated muscle thin filaments are the α-skeletal and α-cardiac isoforms (accession numbers P68133 and P68032 respectively in http://www.uniprot.org), both 377 residues long with remarkable similarity of 98.9% (Laing et al., 2009).

Globular or G-actin monomer (42kDa) under physiological conditions spontaneously polymerises into a filamentous or F-actin, forming the backbone of the thin filament (Gordon et al., 2000). F-actin is an extended linear polymer consisting of 13 actin monomer repeats for every 6 left-handed turns and occupy 36 nm (Egelman, 1985; Holmes et al., 1990). Actin monomers are composed of two domains known as large and small. Each

domain is further subdivided into two subdomains, referred to as subdomain 1, 2, 3 and 4. Structural representation of the native G-actin monomer and its filamentous form (single molecule and as a filament) are shown in Figure 1.2.6.

Native G-actin

A

F-actin (2ZWH)

D-loop

B

Actin filament   C
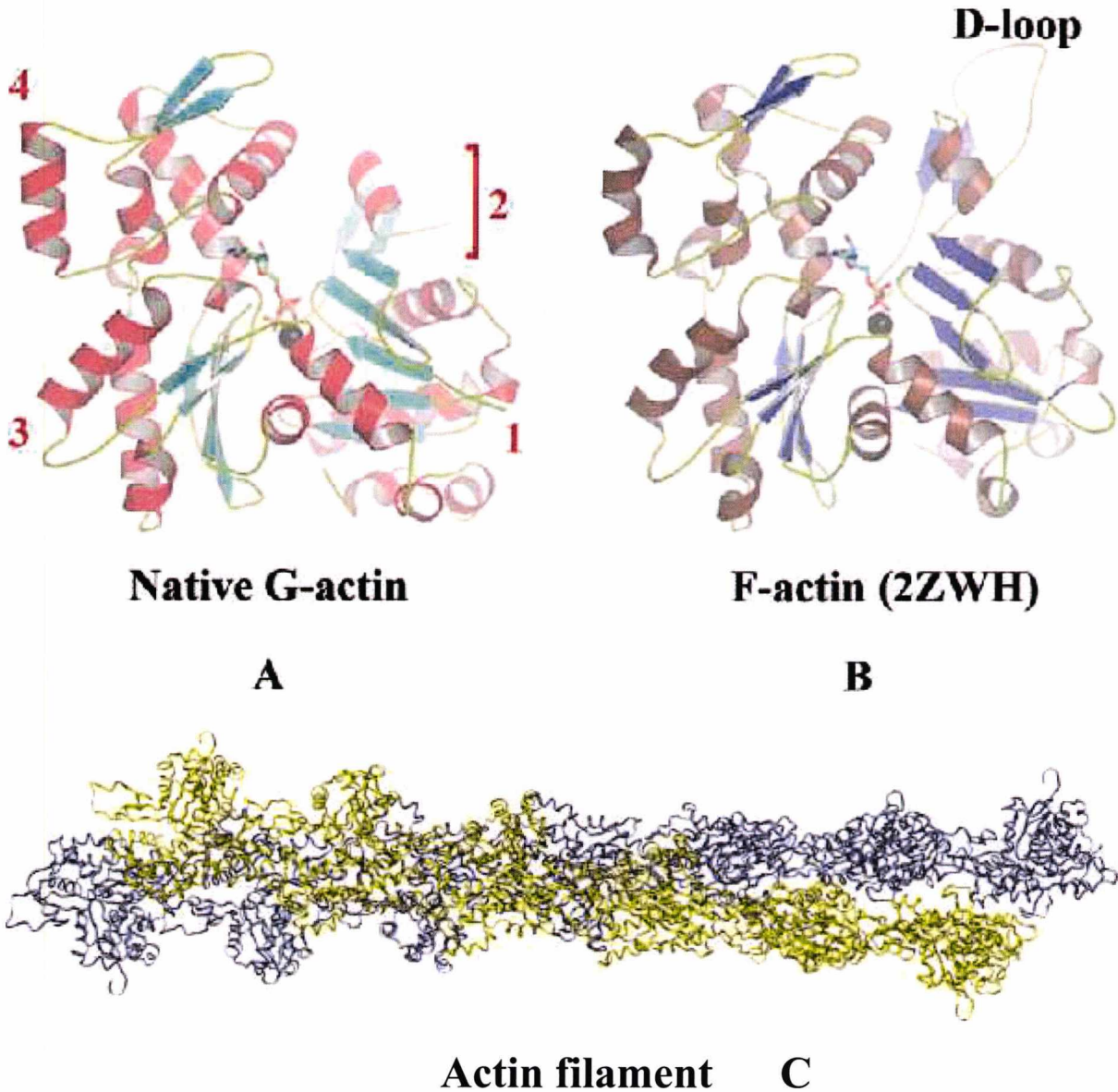
Figure 1.2.6 The actin structures. (A) Native G-actin structure with one ATP molecule and one Ca^{2+} ion located in the nucleotide cleft, which is in the closed state. The actin subdomains are labelled 1-4. (B) F-actin (PDB ID 2ZWH) with one ADP molecule and Ca^{2+} ion. The major differences between G-actin and F-actin structures are: the D-loop conformation in F-actin is extended (open loop) while the same region in G-actin is disordered; the twisted arrangement of G-actin domain, consisting of subdomains 1 and 2, relative to the other domain compared to the flattened conformation in an F-

actin. Rabbit skeletal muscle was used in both crystal structures (Wang, *et al.,* 2010). (C) Ribbon structure of the actin filament (Image from http://www.psc.edu/science/2010/cellularbones)

Subdomains 1 and 2 form the small domain which is oriented on the outside of F-actin. The subdomains 3 and 4 form a large domain facing the inside of F-actin, where they interact with the subdomains 3 and 4 from neighbouring monomers. Both domains are divided by a deep cleft containing nucleotide and Ca^{2+} or Mg^{2+} ion bound to a high-affinity divalent cation binding site. Subdomains 1 and 3 contain five-stranded antiparallel β-sheets and associated short α-helices. Both N and C termini are located in subdomain 1 which contains also the primary binding site for myosin during the cross-bridge cycle. Subdomain 2 contains the DNase I binding loop (D-loop), which is a key structural element of actin, involved in the actin polymerisation, actin-myosin interactions of myosin II (modulation of the force generation) and myosin V (modulation of the processivity) (Kubota et al., 2009). Moreover subdomain 2 can make multiple contacts with C terminus of the actin subunit above and therefore it controls the connectivity between F-actin strands (Galkin et al., 2010).

Polymerisation of G-actin leads to formation of a structural filament (F-actin) in the form of a two-stranded-helix. Polymerisation is essentially a condensation reaction which occurs in three distinct stages: activation, nucleation and elongation. The main features of polymerisation are a slow initial association to unstable dimer, formation of a stable trimer and rapid elongation phase (dos Remedios et al., 2003). Polymerisation and other actin activities are regulated by over 150 actin binding proteins, including the conformation modulators (profilin, gelsolin, cofilin, thymosin β4, capping protein); nucleation factors and elongation factors (formin, Arp2/3 complex); motors (myosins); membrane anchors (talin, vinculin, ezrin/radixin/moesin); organisers of supramolecular structure (Tm, α-actinin, filamin, fascin, villin) and others (Chesarone and Goode, 2009; Schoenenberger et al., 2011).

The transition from the G-actin to F-actin involves two major structural modifications of actin molecule which lead to the ATP activation. The first structural change is at 20° rotation of the outer domain (subdomains 1 and 2) with respect to the inner domain (subdomains 3 and 4). This rotation leads to a flat conformation in which the position of the

residue Gln137, involved in ATP hydrolysis, is in closer proximity with the γ-P of an ATP molecule sitting in a closed cleft. Second structural change is an extension of the D-loop shown in Figure 1.2.6 (Oda et al., 2009).

1.2.3.3 Troponin complex

Troponin (Tn) is a heterotrimer complex consisting of troponin C (Ca^{2+} binding subunit), troponin I (inhibitory subunit) and troponin T (Tm binding subunit). The crystal structure of human cardiac Tn core domain is shown in Figure 1.2.7 (Takeda et al., 2003). Tn bind to actin in the presence of Tm in the stoichiometry 7 : 1 : 1 for actin Tm and Tn, respectively. Tn is an integral part of the calcium dependent regulation of muscle contraction in skeletal and cardiac muscle, but not in smooth muscle. Additionally the presence of free Tn subunits TnI and TnC are important indicators of myocardial damage (Ammann et al., 2004; Antman et al., 1996; Tsai et al., 2008).
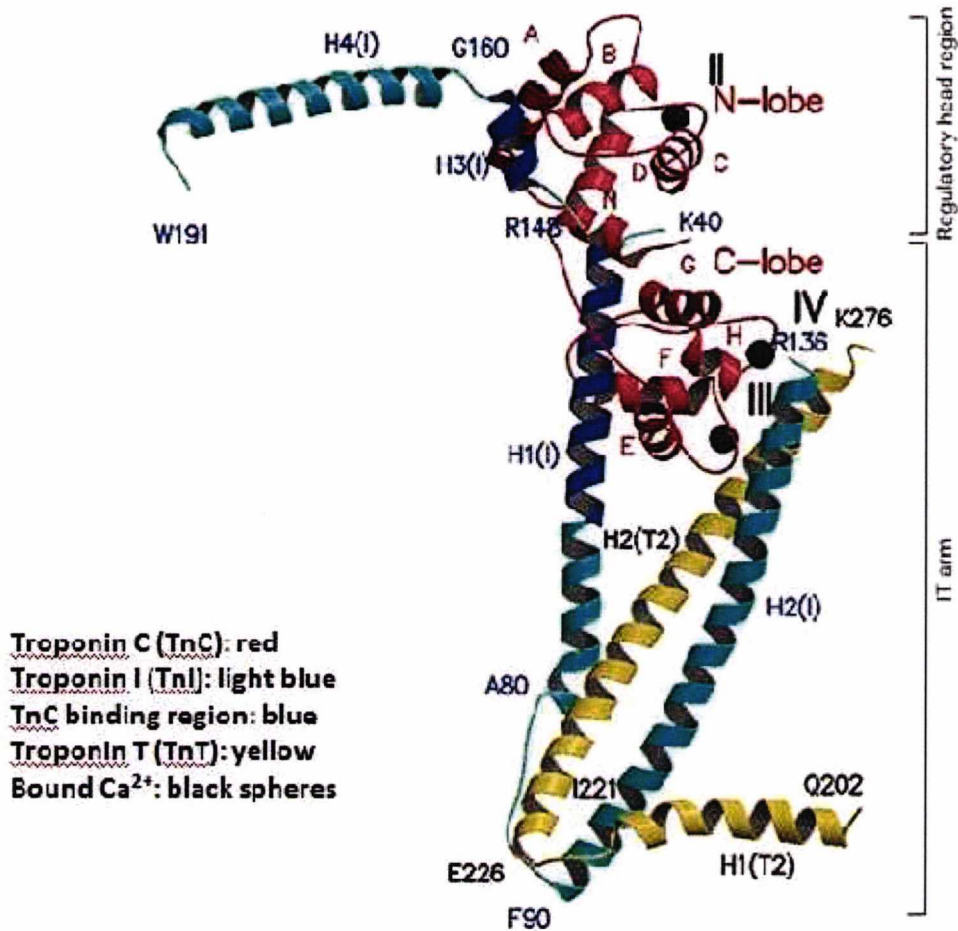
Figure 1.2.7 Crystal structure of the human cardiac troponin complex in the Ca^{2+} saturated form. Individual subunits are colour coded. The three calcium ions, represented by black spheres, are bound to the Ca^{2+} binding sites II-IV. The helices within TnI and TnT are indicated by the helix number, whereas each helix of TnC is indicated by a capital letters N and A-H (Takeda et al., 2003).

Troponin C (TnC) primary function is to bind calcium to produce a conformational change on TnI. There are two tissue specific types of TnC - cardiac and slow skeletal TnC (cTnC) which is encoded by TNNC1 gene containing 161 amino acid residues and mass of 18,403 Da in humans (UniProt ID P63316). The second type is fast skeletal muscle Tn (sTnC) encoded by TNNC2 gene containing 160 amino acid residues and mass 18,122 Da (UniProt ID P02585). The human cTnC contains a helix-loop-helix structural domains called the EF hand motifs found in calcium-binding proteins such as calmodulins. The EF hand motifs are calcium binding sites. The cTnC has two EF hand motifs at the C- and only one EF hand motif at the N-terminus however sTnC has two EF hand motifs at the N-terminal region. The C-terminal EF hand motifs are known as structural binding sites because they can bind Ca^{2+} or

Mg^2 ions and following conformational interactions between TnC and TnI promotes stability of the Tn complex. The affinity for calcium is higher (10^7 M^{-1}) than for magnesium (10^3 M^{-1}) therefore after Ca^{2+} influx from the sarcoplasmic reticulum all TnC binding sites are occupied by calcium (Potter and Gergely, 1975). In the relaxed muscle where Ca^{2+} concentration is low, Mg^{2+} ions can bind the the C-terminal binding sites. Although the N-terminal EF hand motifs have lower Ca^{2+} affinity (10^5 M^{-1}) than C-terminal EF hand motifs, these sites bind exclusively Ca^{2+} due to the higher specificity (Filatov et al., 1999). The trigger for muscle contraction is sequential binding of Ca^{2+} at the two N-terminal sites of sTnC (Li et al., 1995).

Troponin I (TnI) is the inhibitory subunit which is involved in calcium dependent steric inhibition of myosin ATPase on actin together with Tm at diastolic level of intracellular Ca^{2+} (Galinska-Rakoczy et al., 2008). There are three independent genes which encode TnI in humans and each express only one isoform. The gene TNNI1 (UniProt ID P19237) encodes 180 amino acid residues of slow skeletal muscle TnI (ssTnI) and mass of 21,692 Da; TNNI2 gene (UniProt ID P48788) encodes 182 amino acid residues of fast skeletal muscle TnI isoform (fsTnI) and mass of 21,339 Da; and finally TNNI3 gene (UniProt ID P19429) encodes 210 amino acid residues of cardiac muscle isoform (cTnI) and mass of 24,008 Da.

Additionally to the cTnI role in Ca^{2+} dependent regulation of muscle contraction, it has been shown that the phosphorylation of specific serine (Ser) or threonine (Thr) residues by protein kinases A and C plays an important physiological mechanism in alteration of myofilament properties (Metzger and Westfall, 2004). PKA-mediated phosphorylation of several proteins, including cTnI, myosin binding protein C (MyBP-C), phospholamban, sarcoplasmic reticulum ryanodine receptor channels and sarcolemmal L – type Ca^{2+} channels, is induced by the β-adrenergic stimulation in heart (Layland et al., 2005). The PKA-mediated cTnI phosphorylation is cAMP-dependent and reduces the affinity of TnI for TnC (al-Hillawi et al., 1995; Reiffert et al., 1998), and the affinity of TnC for Ca^{2+} (Chandra et al., 1997; Robertson et al., 1982), resulting in a decrease of myofilament Ca^{2+} sensitivity and force development (Ray and England, 1976). As described above, the cardiac isoform is larger than ss- and fsTnI isoforms since the N-terminal domain of cTnI contains unique 27 - 33 amino acid residues sequence. This sequence has on positions 22 and 23 in the mouse, and positions 23 and 24 in human serine residues which are involved in PKA

phosphorylation of cTnI. Additionally there has been found other two main sites of phosphorylation at Ser38 and S165 (Ward et al., 2001).

Troponin T (TnT) is the subunit expressed in humans by three genes. TNNT1 (UniProt ID P13805) gene encodes slow skeletal muscle TnT1; TNNT2 gene (UniProt ID P45379) encodes cardiac muscle TnT2; and TNNT3 gene (UniProt ID P45378) encodes fast skeletal TnT3. In contrast with the genes expressing TnC and TnI, all of TnT genes can be alternatively spliced and produce numerous tissue specific isoforms (in humans 3, 11 and 7 isoforms in TNNT1, TNNT2 and TNNT3 respectively).

TnT is an asymmetric protein that consist of an extended α-helical N-terminal domain TnT1 and a globular domain TnT2 at the C-terminus. The two domains can be generated by chymotryptic digestion where TnT1 is a fragment containing residues 1 – 158 and TnT2 is formed by remaining residues 159 – 258.

The role of TnT is to fix the troponin complex to the thin filament via interaction with Tm (Flicker et al., 1982; White et al., 1987). The main interaction site with Tm is located in a highly conserved central region of cTnT1 (residues 98 – 136)(Jin and Chong, 2010). The N-terminal of TnT1 lies antiparallel along the C-terminal of Tm forming a four helix bundle between the end-to-end overlap region of adjacent Tms and cTnT (Murakami et al., 2008). The binding of cTnT1 to the overlap region of Tm influence the flexibility of Tm and enhances its binding affinity to actin filaments (Gordon et al., 2000; Palm et al., 2001). It has been shown that addition of TnT1 and TnT in actin/Tm filaments also increase the cooperative unit size from 6 to 9 for TnT1 and to 12 in the case of TnT (Schaertl et al., 1995)

A second interaction site for Tm lies in the middle part of Tm near Cys 190 comprising amino acid residues 197 – 236 (Jin and Chong, 2010). The beginning of a globular domain TnT2 interact with Tm near Cys 190 in a Ca^{2+} dependent manner (Chong and Hodges, 1982). Ca^{2+} weakens TnT binding to Tm however the molecular mechanism of Tm/Tn binding alteration is not known yet. Additionally a less flexible TnT2 domain binds the other two cTn subunits TnI and TnC (Takeda et al., 2003).

1.2.3.4 Other muscle tissue proteins

In addition to the thick and thin filament proteins, described in previous sections, the sarcomeres contain a plethora of other proteins required for structural integrity and correct function of the muscle cell.

Thick filaments contain the myosin binding proteins C, H and X (MyBP-C, MyBP-H, MyBP-X). The most abundant is MyBP-C (2 % of the total myofibrillar protein) which belongs to a family of accessory proteins of the thick filaments. The two major roles of MyBP-C are contribution to the structural organisation and stabilisation of the thick filament, and modulation of the cross-bridge formation between actin and myosin (Ackermann and Kontrogianni-Konstantopoulos, 2011). The acto-myosin cross-bridge formation is regulated by MyBP-C via dynamic phosphorylation by protein kinase A (PKA), protein kinase C (PKC) and Ca^{2+}-calmodulin activated kinase II (Barefield and Sadayappan, 2010). Three MyBP-C isoforms have been identified; fast skeletal, slow skeletal and cardiac. The core structure of all isoforms consists of three fibronectin type III (Fn-III) domains and seven immunoglobulin (Ig) domains. Cardiac and skeletal isoforms of MyBP-C interact with myosin (S2 region and light meromyosin), F-actin and titin. Additionally the MYBPC3 gene coding MyBP-C and MYH7 gene coding for β-myosin heavy chain are the most common mutated genes (up to 40 % each) resulting in hypertrophic cardiomyopathy (Marston, 2011).

Adenosine monophosphate deaminase (AMPD) encoded by AMPD1 gene is a muscle specific enzyme involved in the regulation of adenosine metabolism. AMPD prevents accumulation of ADP during vigorous muscle contraction which may cause critical drop in ATP concentration and affect energy available for muscle contraction and other cellular processes. ADP excess is removed by the coupled action of adenylate kinase (AK) and AMPD. Initially ADP is converted into AMP via AK and AMP is then irreversibly deaminated to inosine monophosphate (IMP) and NH_3 by AMPD (Hancock et al., 2006).

A central M-line of each sarcomere comprised of thick filaments only contains numerous proteins including M-protein, the cystein protease p94 (a muscle specific Calpain 3), MURF-1, a muscle isoenzyme of creatine kinase (MM-CK) and myomesins (Clark et al., 2002). Myomesins 1 and 2 are titin-associated proteins which together with titin form the sarcomeric cytoskeleton providing scaffold for the thick and thin filaments. Titin, also called

connectin, is 3 - 4 MDa (depending on the isoform) protein spanning half the sarcomere, anchoring its C- and N-termini in the M-band and Z-disc, respectively. In addition to its role as a molecular scaffold titin is responsible for the elasticity of relaxed muscle (Tskhovrebova et al., 1997); coordinates the assembly the structural, regulatory and contractile saromeric proteins, and may be involved in signal transduction between the myofibrils to the other compartments of the myoplasm (Kontrogianni-Konstantopoulos et al., 2009). Other large proteins of the sarcomere are nebulin (600 – 800 kDa) and obscurin (720 – 900 kDa). Nebulin is involved in the regulation of the thin filament length and assembly in striated muscle (McElhinny et al., 2005). C-terminus of nebulin is partially inserted into the Z-disc, whereas N-terminal region extends to the pointed ends of thin filaments, where it interacts with the capping Tmod. Obscurin is not an integral component of sarcomere such as titin and nebulin but closely surrounds sacomeres, primarily at the level of the M-band and Z-disc. It interacts with diverse protein partners such as slow MyBP-C, sarcomeric myosin, titin and small ankyrin 1. It has been proposed that obscurin is involved in the assembly and organisation of the sarcoplasmic reticulum (SR) and myofibrillar elements in the middle of the sarcomere (Kontrogianni-Konstantopoulos et al., 2006).

The lateral borders of the sarcomere are defined by the sarcomeric Z-disc which contains proteins including filamin, T-cap/telethonin, myotillin, nebulette, MURF-3, α-actinin, actinin-associated LIM protein (ALP), the enigma family and the FATZ family of proteins. Filament systems found in the muscle cells include microtubules, which may play role in the myofibrilogenesis, microfilaments, and intermediate filaments found mainly in the extra-sarcomeric cytoskeleton of myoblasts. Intermediate filaments proteins include desmin, syncoilin, synemin, vimentin, nestin, desmulin, paranemin and lamins. Another group of proteins such as integrins, spectrin and dystroglycan complex connect the sarcomere to the sarcolema (Clark et al., 2002; Fatkin and Graham, 2002).

1.2.4 Calcium regulation of the muscle contraction

The thin filament proteins form the interconnected complex where interactions between individual proteins and their subunits differ with Ca^{2+} binding. In the absence of

Ca^{2+}, TnC is bound to TnI and the C terminus of TnT. TnI additionally interacts with the C terminus of TnT and forms strong binding with the N-terminal region of F-actin molecules, inhibiting the acto-myosin interactions.
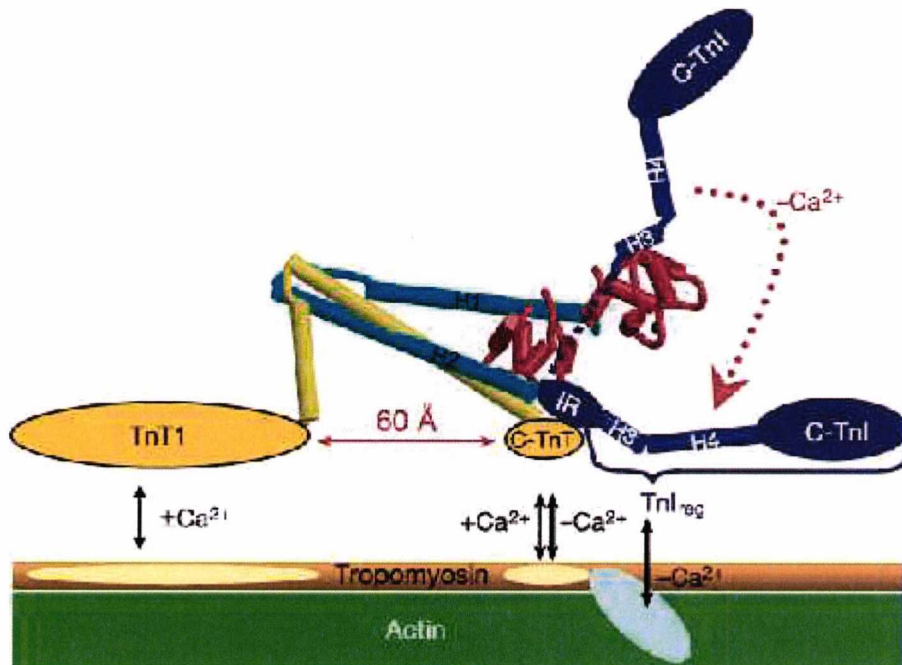
Figure 1.2.8 Schematic representation of the thin filament protein interactions in the presence and absence of Ca^{2+}. Individual structural segments of the thin filament are colour coded: TnT – yellow, TnC – red, TnI - blue, Tm – brown, actin – green. The amphiphilic segment of TnI that undergoes major conformational changes upon binding of Ca^{2+} in the N-lobe of TnC is indicated in dark blue colour. The black arrows represent the interactions between Tn and Tm-actin complex (Takeda et al., 2003).

The N-terminus of TnT forms one strong and one weaker bond with Tm C and N-termini respectively in the head-to-tail overlap region. In presence of Ca^{2+}, TnC binds one (in cardiac TnC) or two (in skeletal TnC) Ca^{2+} ions in the N-terminus and forms strong specific interactions with TnI (Gordon et al., 2000). Schematic representation of the actin-Tm-Tn interactions in the presence and absence of Ca^{2+} is shown in Figure 1.2.8.

The mechanism of the actomyosin ATP-ase regulation by the Tn·Tm complex has been extensively investigated. The calcium regulation of muscle contraction is complex process and its best and widely accepted description was proposed by McKillop and Geeves as a three-state model of regulation (McKillop and Geeves, 1993). This model shows that the full activation of muscle contraction is not dependent only on calcium binding to Tn (two-step

steric model), but the rigor binding of myosin heads to actin are also required. The three-state model predicts that the thin filament exists in a dynamic equilibrium between three myosin binding states. These are blocked (B-state), closed (C-state or Ca^{2+}-induced state) and open (M-state or myosin-induced state) states (Figure 1.2.9).
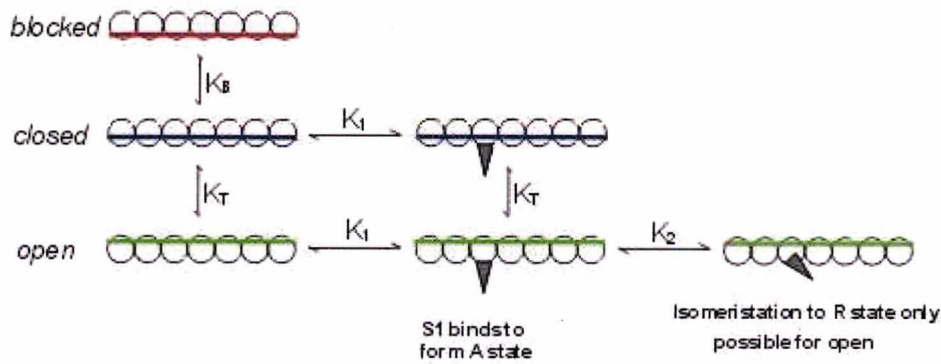
Figure 1.2.9 Three-state model of the thin filament regulation. Three states of the thin filament (blocked, closed and open) exist in the dynamic equilibrium and depend on the position of Tm on the filament. K_B is the equilibrium constant between the blocked and closed states, and K_T is the equilibrium constant between the closed and open states. K_1 and K_2 are the equilibrium constants of S1 binding to form an A-state (weak binding) and R-state (strong binding), respectively (http://www.kent.ac.uk/bio/profiles/staff/geeves.html).

In the absence of calcium, the thin filament is mostly in the B-state as Tm sterically blocks the actin binding sites preventing the formation of the acto-myosin complex. When calcium binds to TnC, Tm shifts away towards the inner region of actin, partially exposing actin binding sites and allowing weak interactions of myosin heads with actin (C-state). Further binding of myosin heads shifts the position of Tm further, exposing all actin binding sites and switching the equilibrium into the M-state. In the M-state myosin isomerises from weakly (A-state) to strongly-bound (rigor or R-state) state. The full activation of the muscle contraction is achieved only in the M-state as the Pi from ATP hydrolysis is released during the isomerisation from A- to R-state. Transitions from the B to the C-state and from the C to the M-state are defined by the equilibrium constants K_B and K_T, respectively. K_B is calcium dependent while the presence of calcium has lower effect on K_T, as the transition to the M

state is promoted by the strong binding of myosin heads. The equilibrium constants K_1 and K_2 define the transition to the A-state and to the R-state, respectively.

According to the three-state model, myosin can bind to the thin filaments only in the C-state and the M-state. It has been shown that the thin filament transition from the C- to M-state is the cooperative process as the association/dissociation experiments of myosin with actin·Tm or actin·Tm·Tn filaments show a sigmoidal curves, typical for cooperative binding (Geeves and Lehrer, 1994). Myosin binds cooperatively to the thin filaments only in the presence of Tm, therefore the cooperativity phenomenon is considered as a Tm filament property (Lehrer and Geeves, 1998).

The original study proposing the three-state model (McKillop and Geeves, 1993) based on biochemical evidence from kinetic and equilibrium binding methods were later supported by structural evidence (Figure 1.2.10) using electron microscopy reconstructions (Craig and Lehman, 2001; Holmes et al., 2003; Narita et al., 2001; Pirani et al., 2005; Poole et al., 2006; Vibert et al., 1997).
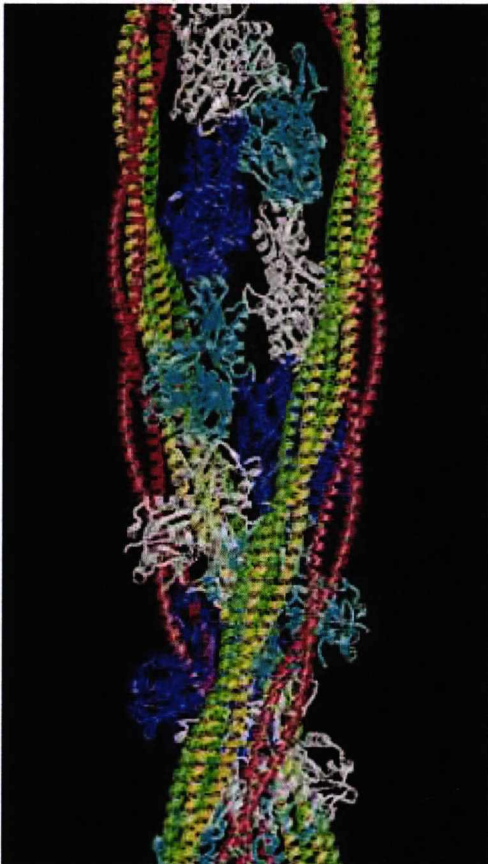
Figure 1.2.10 Three positions of Tm on F-actin. The B-state (red), the C-state (yellow), and the M-state (green) of the thin filament derived from electron microscopy reconstructions. Tm in the B-state fully inhibits myosin binding whereas in the C-state Tm moves 25° away from blocking position and permits weak myosin biding. Further shift of Tm by 10° (green) allows strong myosin binding (Poole et al., 2006).

1.3 Tropomyosin in human cardiomyopathies

1.3.1 Human heart

The human heart is a roughly cone-shaped, hollow muscle comprised of two thin-walled atria and two ventricles. The left and right atria function as reservoirs for returning blood from the systemic and pulmonary circulations, respectively. The left ventricle pumps oxygenated blood into body and the right ventricle pumps deoxygenated blood into lungs.

Contraction or systole and relaxation also called diastole of the heart represent two phases of the cardiac cycle. Systole is initiated by electrical depolarization of the ventricles. The process in which electrical impulses are translated into mechanical movement of the muscle is called excitation-contraction coupling and involves Ca^{2+} signalling events.

Although heart seems to have a simple design, considering its importance within the body, cardiovascular diseases are the leading cause of human death in the world. Cardiac dysfunction can be caused by many factors including ischemia, myocardial infarction, amyloidosis, genetic diseases and hypertension. These stress factors can cause chronic alterations in loading conditions resulting in the structural changes of the heart called remodelling. Pathologic remodelling is associated with cardiomyopathies which are known to result primarily from heritable gene mutations. The mutations affect contractile proteins including Tm which is the major subject of this study. Therefore, two of the most common types, hypertrophic and dilated cardiomyopathy, are described in following sections.

1.3.2 Hypertrophic cardiomyopathies (HCM)

HCM is a disorder of cardiac myocytes, defined as increased muscle mass. It is the most common cause of sudden death in young people, under 30 years, with estimated incidence 1 in 500 individuals (Maron et al., 1995).

43

The predominant site of HCM is interventricular septum (Figure 1.3.1), in approximately two-third of the cases. Clinical symptoms of the HCM are variable such as shortness of breath (dysphnea), angina, chest pain and syncope (loss of consciousness). However most of the patients are asymptomatic or show mild symptoms.

HCM is a familial disease with autosomal pattern of inheritance in ~50 % of the cases. Mutations causing HCM are found in almost any of the sarcomeric proteins but the most affected are β-myosin heavy chain (MYH7) and myosin binding protein C (MYBPC3), together they make up to 80 % of all HCM mutations. The effect of cardiomyopathy mutations on α-Tm (TPM1) is of particular interest of this thesis and the prevalence of α-Tm gene mutations causing HCM is approximately 2 – 5 % (Marian, 2008). The α Tm HCM mutations include the Glu180Gly (Thierfelder et al., 1994), Ala63Val, Asp175Asn (Nakajima-Taniguchi et al., 1995), Lys70Thr (Yamauchi-Takihara et al., 1996), Glu180Val (Regitz-Zagrosek, *et al*., 2000), Val95Ala (Karibe, *et al.,* 2001) and Glu62Gln (Jongbloed, *et al.,* 2003). The full list of to date identified Tm HCM causing mutations (11) could be find in the Leiden Open Variation Database (LOVD) at:

(http://www.genomed.org/lovd2/variants.php?select_db=TPM1&action=search_all&search _Variant%2FType=Substitution).
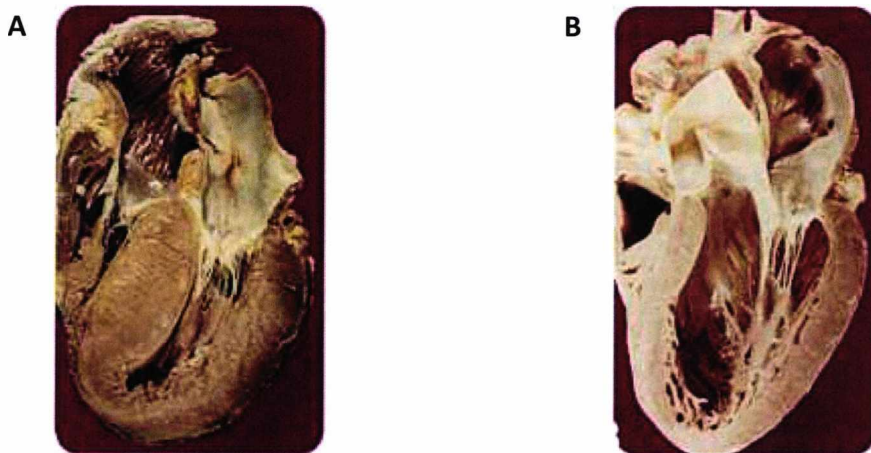
Figure 1.3.1 Thickened ventricular wall and decreased chamber volume (A), characteristic for HCM in comparison to the healthy human heart (B)(Images from Seidman, Seidman, 2001).

44

1.3.3 Dilated cardiomyopathies (DCM)

DCM (Figure 1.3.2) is a common and largely irreversible disease characterised by cardiac dilation and systolic dysfunction leading to heart failure (Marian, 2008). An estimated prevalence of DCM is 1 in 2500 and it is a third most common cause of heart failure (Maron, *et* al., 2006). DCM is familial in 50 % of the patients with largely the autosomal dominant mode of inheritance. The pathogenesis of DCM is not fully understood but mutations is sarcomeric proteins are likely to impair proper mechanical coupling during muscle contraction.

It has been shown that mutations in Tn and α-Tm causing HCM increase the Ca^{2+} sensitivity and mutations causing DCM decrease the Ca^{2+} sensitivity of the cardiac thin filaments (Robinson et al., 2007; Robinson et al., 2002). There have been 7 αTm DCM causing mutations identified to date. These are listed in LOVD database (http://www.genomed.org/lovd2/variants.php?select_db=TPM1&action=search_all&search _Variant%2FType=Substitution) and include Gly40Lys, Glu54Lys (Olson, *et al.*, 2001) and Asp230Asn (Lakdawala, *et al.*, 2010) used in our study.
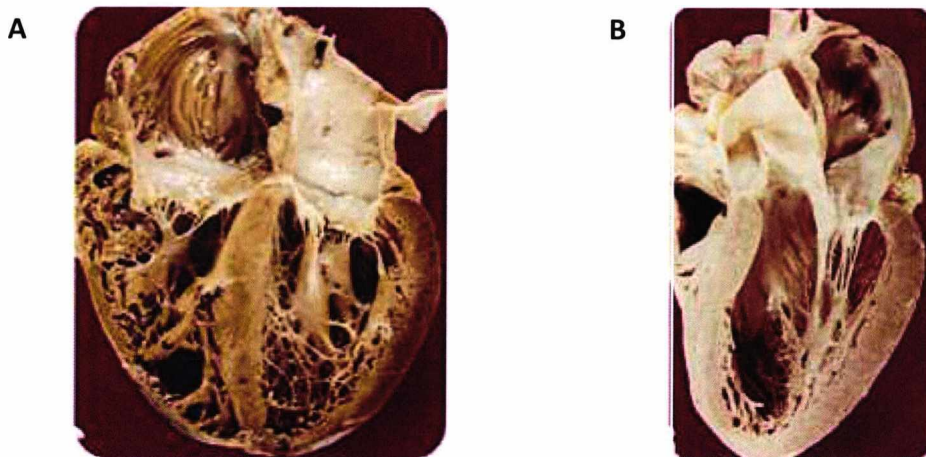
Figure 1.3.2 Histopathology of DCM (A) showing increased cardiac chamber volume and dilation of the left ventricle; (B) healthy human heart (Seidman and Seidman, 2001).

In general, both HCM and DCM mutations may affect the protein's structure and function. It has been shown that truncated forms of MyBP-C (causing HCM in humans)

produced hypertrophy in heterozygous but dilation in homozygous transgenic mice (McConnell et al., 1999). This result might suggest that the resultant phenotype is determined by quantitative, rather than qualitative nature of the defect. However, the underlying histology of HCM (myocyte disarray) is different from those of DCM (Kamisago et al., 2000). There is high frequency of early-onset ventricular dilation and congestive heart failure in DCM cases suggesting that the dilation is a primary manifestation of the disease. Whereas hypertrophic response is considered as a secondary manifestation which develops progressively as a compensation of the sarcomere dysfunction (affected force production caused by lower or higher Ca^{2+} sensitivity, a lower Ca^{2+} affinity for TnC, a lower rate of crossbridge turnover, lower cooperativity and phosphorylation status of Tn) (Marston, 2011).

There have been suggested two models of how a single mutation on sarcomeric proteins leads to the cardiomyopathy phenotype. The first one is based on the expression of the mutant protein in the heart which may be expressed at levels less or at most equal than 50 % of the total protein (dominant negative). Therefore, both WT and mutant proteins are expressed but the mutant protein functions as a "poison peptide" that can be incorporated into the sarcomere and impair normal cell function. The second model is the haploinsufficiency. This is characterised by the phenotype resulting from the absence of one allele (null allele) which may lead to the low (up to 50 %) levels of the corresponding protein in heterozygous patients. Haploinsufficiency occurs when the mutation causes lower expression of the protein or prevents the full-length expression, leading to non-functional protein. An example of the gene affected by haploinsufficiency is MYBPC3 where many mutations involve premature chain termination (Marston et al., 2012). On the other hand majority of HCM and DCM-causing mutations are expressed in a negative dominant manner. The evidence of Tm mutant protein expression in a negative dominant manner was shown by Botinelli et al., where the level of D175N Tm mutant *in vivo* was 47 – 53 % (Bottinelli et al., 1998).

The primary signal for the hypertrophy phenotype development may include increased calcium sensitivity of the myofibril, activation of mRNA transcription controlled by Cdk9 (Kulkarni et al., 2004) or impaired energy metabolism (Ashrafian et al., 2003; Crilley et al., 2003). Decades of an intensive research on the mechanism of how the contractile

protein mutations cause the phenotype showed that HCM mutations cause a higher Ca^{2+} sensitivity, a faster crossbridge turnover rate and incomplete relaxation at low Ca^{2+} due to the slower release of Ca^{2+} (Marston, 2011). The situation in the case of DCM mutations is not as clear as in HCM mutations. Studies on DCM mutants showed decreased (Lakdawala et al., 2010; Mirza et al., 2005; Robinson et al., 2002) but also increased (Memo et al., 2013; Robinson et al., 2007) Ca^{2+} sensitivity, depending on the experimental conditions. On the other hand, the uncoupling of TnI phosphorylation from changes in myofibrillar Ca^{2+} sensitivity has been shown as key factor for determination of the DCM phenotype (Marston, 2011; Memo et al., 2013; Tardiff, 2011)

1.4 Aim of the project

The aim of this study is the investigation of the effects of αTm heterodimers carrying cardiomyopathy mutations in only one chain of the dimer on the regulation of the muscle contraction. We aim to define the changes that can arise from cardiomyopathy mutations and identify possible implications for the modification of myocardial phenotype. To date, *in vitro* studies of Tm carrying cardiomyopathy mutations were carried out exclusively with homodimers due to the lack of reliable method for production of defined skeletal Tm heterodimers.

In vitro biochemical studies of the smooth muscle α and βTm isoforms showed preferential formation of thermodynamically more stable αβTm heterodimers (Lehrer and Qian, 1990; Lehrer and Stafford, 1991). Additionally *in vivo* study, using rat embryo fibroblasts, shown that also skeletal α and βTm isoforms, when combined, form preferentially heterodimers (Gimona et al., 1995). The same study also demonstrated that HMW nonmuscle isoforms Tm1, Tm2, and Tm3 formed preferentially heterodimers with smooth and striated muscle α and βTm isoforms. On the other hand LMW nonmuscle isoforms Tm4, Tm5a and Tm5b failed to form heterodimers with HMW smooth muscle αTm, skeletal muscle βTm and nonmuscle Tm2 (Gimona, 2008; Gimona et al., 1995). These studies strongly suggest that Tm heterodimers could be formed *in vivo*.

Recently a novel method for the formation and purification of recombinant skeletal αβ-Tm heterodimers was developed (Kalyva et al., 2012). We aim to optimise this method for the α-Tm heterodimers carrying cardiomyopathy mutations in only one chain of the dimer. We predict that Tm cardiomyopathy heterodimers may exist in cardiac cells of affected individuals with heterozygous background. Our predictions are supported by thermodynamical preferences for the formation of heterodimers described above and the manner of the cardiomyopathy mutant protein expression (negative dominant) showed by Botinelli et al., where the D175N Tm mutant showed ~50 % expression *in vivo* (Bottinelli et al., 1998). The mutant expressed at this level may potentially form dimer with WT Tm monomer.

Additionally our preliminary assays did not show any preferences in dimer formation for the WT and HCM mutants Tm *in vitro* (see Chapter 3; Figure 3.2.3 C). We mixed His tagged WT-Tm together with various non-tagged Tm constructs including WT, D175N and E180G. These mixtures were then heated in reducing conditions in order to get Tm monomers and then dimerised again by chemical oxidation. Tm dimers formed by this process showed 1 : 2 : 1 ratio of doubly tagged Tm, one tag containing heterodimer, and non-tagged Tm homodimer respectively. This lack of preferential binding between Tm monomers *in vitro* may suggest a similar scenario in affected cells. The predicted ratio of Tm dimers formed in the cell with heterozygous background expressing equal amounts of each isoform would be close to 50 % for the heterodimers and 25 % for each WT and mutant homodimers. Therefore, Tm heterodimers may be potentially predominant dimeric species within the cell and if their properties differ from those of homodimers then it is important to identify the differences.

We aim to produce cardiomyopathy Tm heterodimers in sufficient amounts and purity, and then use various biochemical and biophysical assays to characterise properties of Tm heterodimers. Characterisation of Tm heterodimers with DCM and HCM mutations is the main objective of our study as they may provide an insight into the molecular mechanism of functional impairment of the muscle contraction leading to the cardiomyopathy.

Cardiomyopathy mutations change the surface charge residues which may alter the stability of inter- and intrachain interactions of the dimer. Therefore we will measure thermal stability of Tm heterodimer constructs by circular dichroism as the possible changes in unfolding of the dimer, initiated by an increased temperature, may affect other properties of the molecule and the overall function. Thermal stability of Tm dimer may be directly related to the stiffness or flexibility which is widely recognised as an important parameter defining Tm function will be also assessed. Impaired stability and flexibility of Tm heterodimers may alter the interaction with actin or with troponin and hence alter calcium sensitivity. Actin affinity will be assessed by co-sedimentation and calcium sensitivity will be measured in solution using either reconstituted thin filaments (transient kinetics approach by stopped flow) or myofibrils containing replaced Tm·Tn complex (mechanical measurements of force development).

Chapter 2

Materials and methods

2.1 Protein biochemistry materials and methods

2.1.1 Chemicals

Unless otherwise stated, all the chemicals used in the preparations were purchased from Sigma-Aldrich®, Fisher Scientific, Life technologies™ or Melford Laboratories Ltd.

2.1.2 SDS-PAGE

Purity, size, ratios and affinity of various proteins were examined by Sodium Dodecyl Sulphate Polyacrylamide gel electrophoresis (SDS-PAGE).

10% SDS gels were prepared firstly by mixing 3.6 ml dH$_2$O, 0.8 ml of 30 % w/v acrylamide (680 mM), 0.5 ml of 1 M stacking buffer (100 µM; see section below), 50 µl of 10 % w/v SDS (3.5 mM), 10 µl of TEMED (N,N,N',N'-Tetramethylethylenediamine; ~0.2 % v/v) and 34 µl of 10 % w/v APS (ammonium persulfate; 3 mM) for 4.8 % stacking gel. Secondly, a 10 % resolving gel was prepared by mixing 6.8 ml of dH$_2$O, 5 ml of 30 % v/w acrylamide (1.4 M), 3 ml of 1M resolving buffer (200 µM; see section below), 150 µl of 10 % v/w SDS (3.5 mM), 10 µl of TEMED (~0.1 % v/v) and 100 µl of 10 % v/w APS (4.4 mM). 10 % SDS gels were used mainly for the co-sedimentation assays as they clearly resolve the WT Tm bands from the HCM mutants.

Pre-cast polyacrylamide gels NuPAGE® Novex® 4-12% Bis-Tris Gels (1.0 - mm thick, 12 - well) were used to check protein purity after purification as the resolution of all proteins (including impurities) is higher compared to the gels prepared manually.

Sample buffer (5x) containing 2-mercaptoethanol (BME) was added into the samples run under reducing conditions and heated at 95 °C for 8 min before loading. Sample buffer for the non-reducing electrophoresis runs did not contain BME and heating was omitted. 10 % SDS gels were run in the Tris – running buffer (see section below) at 38 V for 50 min (one gel) and 78 V for 50 min (two gels). Pre – cast gels (4 – 12 %) were run in the MOPS – running buffer (see section below) at 300 mA for 50 min. The gels were incubated in the staining solution for 25 min. The destaining solution (for both staining and destaining solution see section below) was added and gels were stirred until most of the background staining was removed. Proteins of interest were identified by comparison with PageRuler™ unstained protein ladder ranging from 200 to 10 kDa (#SM0661 from Fermentas Life Sciences).

SDS-PAGE standard buffers and solutions

Resolving gel buffer	23 g Tris / HCl pH 8.8 in 100 ml total volume
Stacking gel buffer	7.56 g Tris / HCl pH 6.8 in 50 ml total volume
Sample buffer	2.5 ml stacking gel buffer, 1 g SDS, 2.5 ml BME, 5.8 ml glycerol, 5 mg bromophenol blue, dH$_2$O added up to a final volume of 50 ml
Tris - running buffer	7.2 g glycine, 1.52 g TRIS, 0.5 g SDS for 1 l
MOPS - running buffer	50 ml of NuPage® MOPS SDS running buffer (20 x) (Life Technologies) mixed with 950 ml of dH$_2$O
Staining solution	1 g of Coomassie brilliant blue was dissolved in 1 l of following solution: 50 % (v/v) methanol 10 % (v/v) glacial acetic acid 40 % dH$_2$O
Destaining solution	7 % (v/v) glacial acetic acid 25 % (v/v) methanol 68 % dH$_2$O

2.1.3 Determination of protein concentration

All protein concentrations were estimated by UV spectroscopy at 280 nm using the Beer-Lambert law ($A = \varepsilon . c . l$) where A is the solution absorbance, ε is the molar extinction coefficient ($l\ mol^{-1}\ cm^{-1}$), l is the length of the light path in cm and c is the protein molar concentration.

2.1.4 Native muscle protein preparations

Muscle was dissected from the backs and legs of two rabbits. Protein preparations were carried out at 4 °C and their purity was verified by SDS electrophoresis. Tm·Tn complex, actin, myosin and S1 preparations were regularly carried out by our technician Ms Samantha Lynn.

Briefly, all ligaments and connective tissue were removed from two medium sized rabbits. Muscle tissue (800 – 1200 g) was chopped up to a fine mince, mixed with 3 l of Guba-Straub buffer (0.3 M KCl, 0.1 M KH_2PO_4, 0.05 M K_2HPO_4, pH 6.6), homogenised and stirred on ice for 30 min. The mixture was spinned for 30 min at 6000 rpm at 4 °C. The pellet containing the thin filaments was used for actin and Tm·Tn complex preparations (Spudich and Watt, 1971), whereas the supernatant was used for myosin and S1 preparations (Margossian and Lowey, 1982).

2.1.4.1 Acetone powder preparation

Production of the acetone powder is the first step in F-actin preparation (described in following section). However it has been used for the preparation of native Tm·Tn complex.

The pellet from rabbit muscle mixture obtained after centrifugation for the separation of myosin (described above) was dialysed in 5 l of extraction buffer (4% $NaHCO_3$, 0.1 mM $CaCl_2$) and stirred for 30 minutes. The pellet was then filtered through a double layer of muslin and dialysed in 1 l of buffer containing 10 mM $NaHCO_3$, 10 mM Na_2CO_3 and 0.1 mM

$CaCl_2$. 10 l of distilled water (20 °C) were added, and the mixture was filtered again through a double layer of muslin. The solid residue was washed in 2.5 l acetone, incubated for 20 minutes, and filtered through a double layer of muslin. The wash with acetone was repeated three times. The residue was then sandwiched between blotting paper and left to air-dry in a fume cupboard for 2 days. The dried acetone powder was sieved through a mesh to remove unwanted connective residues. The acetone powder was stored at -20 °C.

2.1.4.2 F-actin preparation

The preparation of F-actin is based on a method described previously by Spudich and Watt (Spudich and Watt, 1971). The dried acetone powder (1 – 1.5 g) was dissolved in pre-chilled (1 °C) 200 ml beaker containing 10 mM TRIS, 0.5 mM ATP, 0.2 mM $CaCl_2$, 1 mM DTT, pH 8.0 depolymerisation buffer. The mix was stirred for 30 min and then filtered through a double layer of cheesecloth. This resulted in separation of G-actin (in filtrate) and the Tm·Tn complex (solid residue; preparation is described in section 2.1.4.6).

The filtrate was then centrifuged at 30,000 rpm (Beckman, 70 Ti-rotor) for 1 hour at 4 °C. The supernatant containing G-actin was polymerised by addition of 3 M KCl (up to a final concentration of 100 mM) and 1 M $MgCl_2$ (final concentration of 2 mM) into the buffer and stirring for 1 h at room temperature. The viscous polymerised F-actin was centrifuged at 30,000 rpm for 3 h at 4 °C. The supernatant was discarded and the pellet was resuspended in ~25 – 50 ml of depolymerising buffer (5 mM TRIS, 0.2 mM $CaCl_2$, 1 mM NaN_3, pH 7.5) and dialysed in 4.5 l of depolymerisation buffer overnight. Dialysis residue was centrifuged at 30,000 rpm for 1 h at 4 °C and G-actin was collected in supernatants. Concentration of the sample was measured by UV spectroscopy (section 2.1.3) and G-actin was diluted to 1 mg/ml with depolymerisation buffer. The solution was polymerised again by addition of 3 M KCl, 1 M Mg Cl_2 and 100 mM ATP to final concentrations of 100 mM KCl, 2 mM Mg Cl_2 and 5 µM ATP stirring in buffer for 1 h at room temperature. The polymerised F-actin was centrifuged at 30,000 rpm for 3 h at 4 °C and the pellet containing F-actin was then resuspended and dialysed in buffer (50 mM KCl, 20 mM MOPS, 5 mM $MgCl_2$, 1 mM NaN_3, pH 7) overnight. The concentration of unlabelled F-actin determined by UV-spectroscopy was typically between 100 – 200 µM and the final volume was ~8 ml (extinction coefficient

of actin at 280 nm $\varepsilon^{1\%}$ = 11.04 cm^{-1} and molecular weight of 42kDa). Actin was stored up to three weeks at 4 °C.

2.1.4.3 Purification of unlabelled F-actin for cosedimentation assays

F-actin used in cosedimentation assays with recombinantly expressed Tms was further purified from the native Tm and Tn contaminants. The unlabelled F-actin was treated with high salt buffer by adding KCl (3 M stock) to a final concentration of 0.6 M and the solution was incubated overnight at 4 °C. The clean F-actin was then pelleted by centrifugation at 100,000 rpm for 20 min at 4 °C and resuspended by homogeniser in 3 ml of experimental buffer (100 mM KCl, 20 mM MOPS, 5 mM MgCl$_2$, 1 mM NaN$_3$, pH 7). Sample was then dialysed in 3 l of experimental buffer overnight and the concentration was measured by UV-spectroscopy (section 2.1.3) at 280 using the same extinction coefficient as in 2.1.4.2. Sample was stored at 4 °C and used within three weeks. Purity of F-actin was checked routinely on SDS gels in cosedimentation assays (Figure 2.3.1; lane A).

2.1.4.4 Pyrene labelled F-actin preparation

F-actin was labelled for the stopped flow fluorescence experiments with the N-(1-pyrenyl) iodoacetamide based on a procedure described previously by Criddle et al. (Criddle et al., 1985).

Pyrene iodoacetamide stock (5 mg/ml in DMF) was very slowly added to a stirring 1mg/ml F-actin solution until a final concentration of 0.6 – 1 % w/w (pyrene/actin) was reached. The mixture of pyrene and F-actin was wrapped in foil and left stirring over an 18 h period at room temperature. The mixture was then centrifuged at low speed (8,000 rpm) for 1 h at 4 °C to precipitate any unbound pyrene and denatured protein. The supernatant was then centrifuged at higher speed (30,000 rpm) for 3 h at 4 °C to sediment the pyrene-labelled F-actin. The pellet was resuspended using a glass homogeniser, and then dialysed in experimental buffer (100 mM KCl, 20 mM MOPS, 5 mM MgCl$_2$, 1 mM NaN$_3$, pH 7) overnight.

The actin solution was assayed by determination of actin and pyrene content using UV-spectroscopy (extinction coefficient of pyrene at 280 nm $\varepsilon^{1\%}$ = 0.22; at 344 nm $\varepsilon^{1\%}$ = 0.233). The final concentration of pyrene labelled F-actin was similar to those of unlabelled actin (100 – 200 µM) and the efficiency of labelling was 90 – 100 %.

2.1.4.5 Phalloidin stabilised F-actin preparation

Actin used in experiments at low (0.25 – 2.5 µM) concentrations was stabilised by the fungal toxin phalloidin. Phalloidin (500 mM stock solution) was mixed in a 1 : 1 molar ratio with actin and incubated overnight to keep actin in filamentous form (Cooper, 1987; Kurzawa and Geeves, 1996).

2.1.4.6 The Tm·Tn complex preparation from native rabbit muscle tissue

Native Tm·Tn complex was prepared using the solid residue from the cheesecloth filtration in the F-actin preparation (section 2.1.4.2). This was resuspended in 100 ml of 10 mM TRIS, 2 mM DTT, 1 mM NaN_3 pH 8.0 buffer, stirred for 5 hours at room temperature and then filtered through cheesecloth again. The filtrate was subjected to a 40 % ammonium sulphate cut (by adding 0.24 g/ml of ammonium sulphate slowly into the solution continuously stirred on ice) and then the sample was centrifuged at 9,000 rpm for 30 minutes. The pellet was discarded and the supernatant was subjected to a second ammonium sulphate cut reaching 60 % saturation (0.13 g/ml). The mixture containing precipitated Tm·Tn complex was then centrifuged at 9,000 rpm for 30 min. The pellet was resuspended and dialysed in 5 mM TRIS, 0.5 mM DTT pH 8.0 buffer. The concentration of Tm·Tn complex was measured by UV-VIS spectroscopy (extinction coefficient of the complex at 280 nm is ε = 0.385 mg^{-1} ml cm^{-1} and molecular weight of 136,000 Da). The final concentration was typically between 15 - 30 µM. Proteins were stored at 4 °C and used within two weeks.

2.1.4.7 Purification of Tm and Tn from the native Tm·Tn complex

The native Tm was purified from the Tm·Tn complex that was obtained as described in previous section 2.1.4.6. The native protein complex dialysed overnight against 50 mM KCl, 10 mM TRIS, 0.5 mM DTT buffer at pH 8.0. Concentration of the Tm·Tn complex was then diluted to 1 mg/ml using the same buffer. Tm was then isoelectrically precipitated by slow drop of pH to 4.6 and then stirring the solution for 20 min on ice. Sample was then centrifuged at 12,000 rpm for 20 min at 4 °C separating Tm in pellets and Tn in supernatants.

Pellets were resuspended in 50 mM KCl, 10 mM TRIS, 0.5 mM DTT pH 8.0 buffer using 85 % of starting volume. The pH cut was repeated two more times and Tm pellets were resuspended in the same buffer using 75 % and then 65 % of the starting volume. The final Tm pellet was resuspended in 250 mM KCl, 5 mM TRIS, 0.2 mM EDTA, 0.2 mM DTT pH 7.5 buffer using 45 % of the starting volume. This step was followed by 53 % ammonium sulphate cut to precipitate any remaining Tn in the pellet. The sample was then stirred on ice for 30 min and centrifuged at 12,000 rpm for 20 min. Supernatant containing Tm was heat-percipitated in an 80 °C waterbath for 30 min to irreversibly denature other cellular proteins and solution was then centrifuged at 12,000 rpm for 30 min. The pellet was resuspended and dialysed in 2.5 l of 5 mM Tris, 0.5 mM DTT pH 8 buffer.

The Tn containing supernatants were pooled together and pH was adjusted to 8. Tn was precipitated by 70 % ammonium sulphate cut and the sample was stirred on ice for 30 min. The sample was then centrifuged at 12,000 rpm for 30 min and the pellet was then resuspended and dialysed in 2.5 l of 5 mM Tris, 0.5 mM DTT pH 8 buffer.

Protein concentrations were estimated by UV spectroscopy using extinction coefficient ε for Tm = 0.24 mg^{-1} ml cm^{-1} (MW of Tm dimer = 66 kDa) and ε for Tn = 0.45 mg^{-1} ml cm^{-1} (MW = 70 kDa). Both Tm and Tn were aliquoted and stored at 4 ° C.

2.1.4.8 Myosin preparation

Myosin preparation was based on the method described by Margossian and Lowry (1982). The supernatant from the rabbit muscle mixture (section 4.2.1) was diluted to at least 10-fold with cold dH_2O (in 250 ml tubes) to precipitate myosin. The sample was then centrifuged at 12,000 rpm for 20 min. Myosin was then purified by the following steps which were repeated three times. The myosin pellet was firstly dissolved in 3 ml of 3 M KCl and then cold dH_2O was added up to 250 ml to precipitate myosin. Sample was centrifuged at 12,000 rpm for 20 min. The final myosin pellet was dissolved in 500 ml of 0.5 M KCl, 10 mM KPi, 1 mM DTT pH 6.5 buffer. The concentration of myosin was measured by UV-spectroscopy (the extinction coefficient for myosin $\varepsilon^{1\%}$ = 5.6 cm^{-1} and the molecular weight is 0.45 kDa). The myosin solution was mixed with an equal volume of glycerol (v/v) for long term storage at $-$ 20 °C.

2.1.4.9 Skeletal myosin subfragment 1 preparation

The myosin glycerol stock was mixed with a large volume of dH_2O to precipitate myosin and then centrifuged at 12,000 rpm for 20 min. Pellet containing 10 $-$ 20 g of myosin was dissolved in 1 l of 125 mM KCl, 10 mM KPi, 2 mM EDTA, 4 mM DTT pH 6.5 digestion buffer. Chymotrypsin was added to a final concentration of 0.1 mg ml^{-1} and the mixture was stirred for 10 min exactly at 23 °C. The digestion reaction was stopped by addition of 0.5 mM of PMSF (using 200 mM stock solution in ethanol) and the sample was centrifuged at 10,000 rpm for 30 min. Supernatant was dissolved and dialysed overnight in 5 l of 10 mM KPi pH 6.5 buffer. The undigested myosin was removed by centrifugation at 10,000 rpm for 30 min. The digested S1 was then further purified by ion-exchange chromatography using the DEAE-Sephacel column equilibriated in 50 mM imidazole pH 7 buffer. Elution of S1 was achieved by a 0 - 250 mM KCl gradient. The S1-containing fractions indicated by peaks at absorbance 280 nm were pooled together and dialysed in 5 l of 10 mM KPi pH 7.5 buffer overnight. The concentration of S1 was determined by UV-spectroscopy (the extinction coefficient for S1 $\varepsilon^{1\%}$ = 7.9 cm^{-1} and the molecular weight is 115 kDa). For the long term storage of S1 at -20 or -80 °C an equal amount (w/w) of sucrose was added and the sample was then freeze-dried.

2.2 Molecular biology materials and methods

2.2.1 Chemicals, enzymes and kits

Enzymes used for molecular biology techniques were purchased from Qiagen and Promega unless otherwise stated and all DNA purification kits were from Qiagen. Chemicals used for recombinant expression were purchased from Sigma-Aldrich® and Fisher Scientific.

2.2.2 Bacterial strains

DH5α and BL21 *E. coli* competent cells were used for plasmid DNA amplification and protein expression respectively.

2.2.3 Bacterial growth media recipes

LB broth/agar: 10 g l^{-1} NaCl

10 g l^{-1} bactopeptone

5 g l^{-1} yeast extract

15 g l^{-1} agar (1.5 % w/v) used for solid medium

pH adjusted to 7 by 1 M of NaOH

Media were autoclaved and allowed to cool down to about 50 °C. 1000 µl of 100 mg/ml ampicillin stock was then added to a final concentration of 100 mg l^{-1}. LB/Amp broth was stored at RT and LB/Amp agar plates were stored at 4 °C.

NZY: 10 g l^{-1} NZ amine (casein hydrolysate)

5 g l^{-1} NaCl

5 g l^{-1} yeast extract

pH adjusted to 7 by 1 M of NaOH

Supplements: 12.5 mM $MgCl_2$ (12.5 ml of 1 M $MgCl_2$ stock)

12.5 mM MgSO$_4$ (12.5 ml of 1 M MgSO$_4$ stock)

4 % glucose w/v (20 ml of 20 % w/v glucose stock)

Media containing NZ amine, NaCl and yeast extract was autoclaved. Sterile stocks of MgCl$_2$, MgSO$_4$, glucose and ampicillin (100 mg l^{-1}) were then added under aseptic conditions.

SOC: 20 g bactotryptone

5 g yeast extract

20 mM glucose (20 ml of 1 M glucose stock)

10 mM MgCl$_2$ (10 ml of 1 M MgCl$_2$ stock)

10 mM MgSO$_4$ (10 ml of 1 M MgSO$_4$ stock)

10 mM NaCl (2 ml of 5 M NaCl stock)

2.5 mM KCl (2.5 ml of 1 M KCl stock)

All components were mixed in 900 ml of distilled H$_2$O. Volume was then adjusted to 1 l and mixture was autoclaved. SOC medium was aseptically aliquoted (1 ml) into 1.5 ml sterile eppendorf tubes and stored at -20 °C.

2.2.4 Vectors used for cloning and protein expression

The pGEM-T Easy is an approximately 3 kbp long plasmid vector (Figure 2.2.1). It contains 3' thymine overhangs that provide compatible ends for the ligation of DNA inserts designed to have 5' adenine overhangs. The pGEM-T Easy vector contains T7 and SP6 RNA polymerase promoters flanking a multiple-cloning region within the lacZ gene sequence of the enzyme beta-galactosidase. This means that transformed bacteria containing the insert show no β-galactosidase activity and produce white colour colonies, while cells without the insert can produce β-galactosidase, thus the colonies appear blue. Moreover the vector contains ampicillin resistance gene.
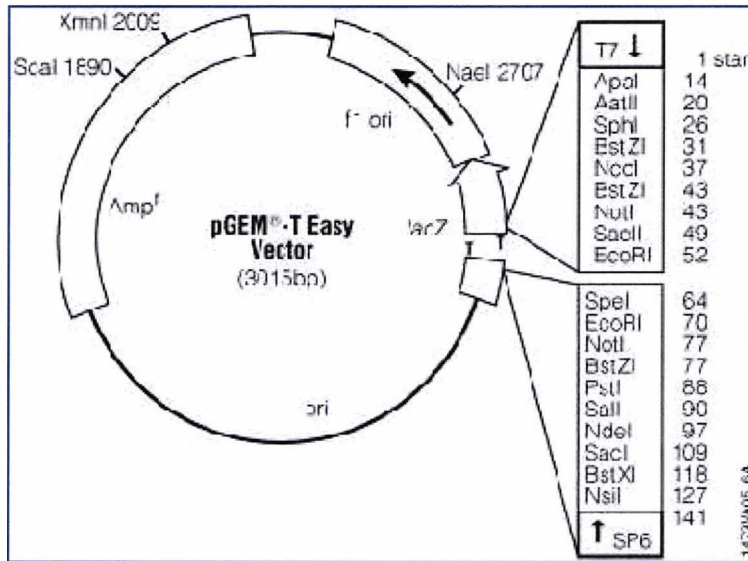
Figure 2.2.1 Schematic representation of pGEM-T easy vector. The multiple-cloning region enclosed by T7 and SP6 RNA polymerase promoters is positioned between the lacZ reporter gene. The vector contains ampicillin resistance gene and the protein expression is induced by IPTG (Image from http://www.promega.com/~/media/Files/Resources/Protocols/Technical%20Manuals/0/pGEM-T%20and%20pGEM-T%20Easy%20Vector%20Systems%20Protocol.pdf).

The pJC20 is a 2.34 kbp long plasmid vector designed for the expression of recombinant proteins in *E. coli* (Clos and Brandau, 1994). It contains a T7 RNA polymerase-dependent promoter region. *E. coli* strain BL21 carries the gene for T7 RNA polymerase therefore pJC20 is suitable for the protein expression in these cells. The expression is controlled by the *lac*UV5 promoter thus can be induced by IPTG. The small size of the pJC20 and a multiple-cloning region containing the restriction sites for the most commonly used enzymes (Figure 2.2.2) makes it an ideal vector system for the cloning of large inserts and the production of high plasmid copy numbers. Additionally pJC20 has an ampicillin resistance gene.
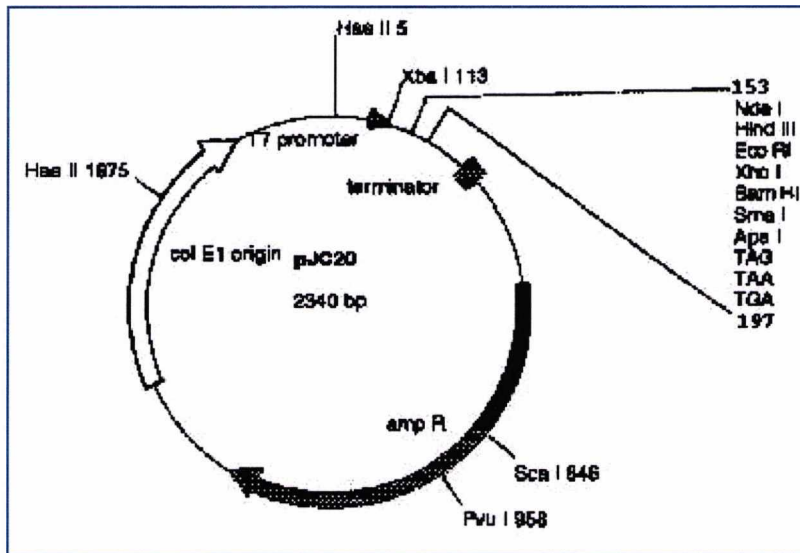
Figure 2.2.2 Schematic representation of pJC20 vector. The vector contains multiple–cloning region and ampicillin resistance gene. Expression is under the control of T7 promoter and can be induced by IPTG (Image from Clos and Brandau, 1994).

The pMW172 is a 2.58 kbp long plasmid vector carrying ampicillin resistance gene used for cloning PCR products for native expression of proteins in *E. coli* (Figure 2.2.3). Similarly to pJC20, pMW172 contains T7 RNA polymerase gene promoter thus the expression is controlled by the *lac*UV5 and induced by IPTG.
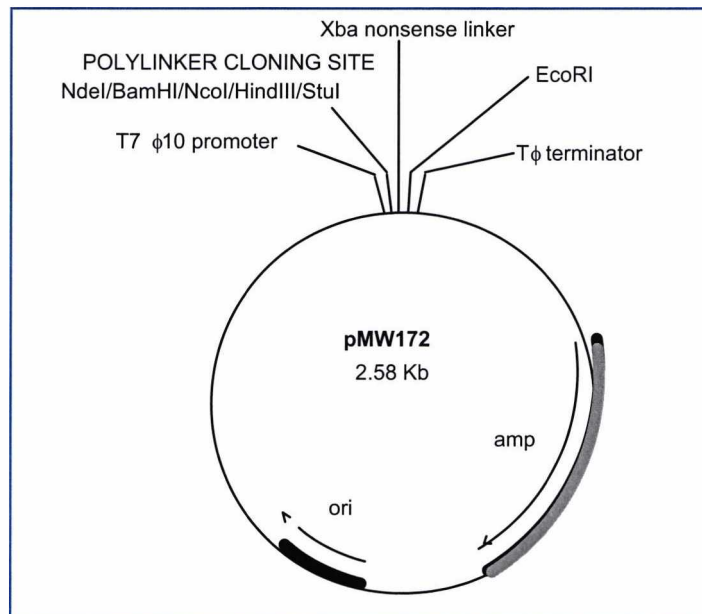
Figure 2.2.3 Schematic representation of pWM172 vector. The vector contains T7 promoter, polylinker cloning site and ampicillin resistance gene (Image from Charles Redwood personal comunication).

61

2.2.5 Oligonucleotide primers

Primers were synthesised by Eurofins MWG Operon. Genes encoding rat striated α-Tm were designed to create an *Nde*I restriction site at the start codon and *Bam*HI restriction site directly downstream of the stop codon, for the cloning of the amplified fragments into the expression vectors. The primers had an Ala-Ser extension at the 5' end as reported previously (Boussouf et al., 2007; Kremneva et al., 2004).

Other set of primers was designed to insert His- or Strep-tag followed by factor Xa protease sequence prior to the Ala-Ser extension at the 5' of α Tm gene as described previously (Janco et al., 2012; Kalyva et al., 2012).

Change of striated rat to human α-Tm sequence was made by site directed mutagenesis using forward and reverse primers listed below. This approach was used as the rat α-Tm protein sequence differs from human at a single site. R220 in human is K220 in rat (P09493, P04692 for human and rat respectively).

Primers for the Ala-Ser extension addition:

Forward AS-αTm primer

5' GG CAT ATG GCG AGC ATG GAC GCC ATC AAG AAG AAG ATG CAG ATG 3'

     Ndel   AS   α-Tm

Reverse AS-αTm primer

5' CC GGA TCC TTA TAT GGA AGT CAT ATC GTT GAG AGC GTG GTC 3'

     BamHI   α-Tm

Primers for Strep- and His-tag addition:

Forward StrepFXaAS Tm primer

5' GG CAT ATG TGG AGC CAC CCG CAG TTC GAA AAA ATC GAA GGG CGC GCG AGC ATG GAC GCC ATC AAG AAG 3'

     Ndel   Strep tag   FactorXa   AS   α-Tm

Forward HisFXaAS α-Tm primer

5' GG CAT ATG AGA GGA TCG CAT CAC CAT CAC CAT CAC ATC GAA GGG CGC GCG AGC ATG GAC GCC ATC AAG AAG 3'

     Ndel   6 His tag   FactorXa   AS   α-Tm

Primers for the change of rat α-Tm to human α-Tm:

Forward human α-Tm primer

GAG AAG TAC TCT CAG AAA GAA GAC AGG TAT GAA GAG GAG ATC AAG

<div align="center">R residue</div>

Reverse human α-Tm primer

CTT GAT CTC CTC TTC ATA CCT GTC TTC TTT CTG AGA GTA CTT CTC

<div align="center">R residue</div>

2.2.6 Agarose gel electrophoresis

Agarose gel electrophoresis was used to visualise plasmid DNA and the products of PCR and restriction digest.

1 % agarose gels were prepared by dissolving 1 g of high melting point agarose (BioRad) in 100 ml of TAE buffer (40 mM TRIS pH 8.0, 20 mM glacial acetic acid, 1 mM EDTA). Agarose was melted in the microwave at the maximum power. The flask containing the agarose was removed from microwave in 30s intervals and mixed until agarose was completely dissolved. Gels were cooled to 65 °C and poured into the 50 ml mould. Ethidium bromide was added to a final concentration of 0.5 μg/ml and the gel was allowed to set at room temperature. 5 - 10 μl of the DNA of interest was mixed typically with 1 μl of BamHI and 1 μl of NdeI restriction enzymes in 4 μl of 5x buffer D (Promega) adjusted to a final volume of 20μl with dH$_2$O. The DNA sample was left in 37 °C for 1 h to digest sequence of interest from plasmid and then mixed with 5 μl of 5x DNA sample buffer before loaded onto 1 % agarose gel. Gels were run in the same TAE buffer as used for the preparation of the gel under constant 55 V. The 1 kb DNA ladder (Promega) was used as a marker for estimation of the size of the DNA samples. The DNA bands on the agarose gel were detected by UV light.

2.2.7 α-Tm subcloning into pJC20 vector

The rat skeletal α-Tm gene cloned into pGEM-T easy vector was subcloned into a pJC20 expression vector as follows.

2.2.7.1 PCR for the amplification of DNA encoding various tropomyosins

The DNA sequences of interest were amplified by polymerase chain reaction (PCR) using the high fidelity Pfu DNA polymerase. Genes encoding for rat skeletal α Tm were modified at their 5' end using specially designed primers, described in section 2.2.5. The forward and the reverse primers contained the NdeI and the BamHI restriction sites, respectively. These sites are required for subcloning of the amplified Tm fragments into pJC20 vector.

The PCR recipe: 1 μl DNA template

       1 μl Pfu DNA polymerase

       5 μl Pfu 10 x buffer

       1 μl Forward Primer (25 pmol/ μl)

       1 μl Reverse Primer (25 pmol/ μl)

       1 μl DNTPs (10 mM)

       40 μl sterile dH$_2$O

The PCR machine was programmed as follows:

       Denaturation at 95 °C for 2 min (1 initial cycle)

       Denaturation at 95 °C for 1 min (35 cycles)

       Annealing at 50 °C for 1 min (35 cycles)

       Elongation at 72 °C for 3.5 min (35 cycles)

The products of PCR reaction were loaded onto 1 % (w/v) agarose gel and the amplified DNA of the correct size (~900 kbp) was purified using the QIAquick gel extraction kit, following the manufacturer's instructions.

2.2.7.2 Restriction enzyme digest of the PCR product

5 µl of the purified PCR product was digested by BamHI and NdeI restriction enzymes (added 1.5 µl of each enzyme) in 4 µl of 10x buffer D (Promega). The mixture was adjusted to a final volume of 40 µl with dH$_2$O and incubated for 1 h at 37 °C. The Tm fragments were run on 1 % (w/v) agarose gel and puirifed using the QIAquick gel extraction kit.

2.2.7.3 Ligation of the target Tm sequence into vectors

The pJC20 vector was firstly digested by BamHI and NdeI restriction enzymes using the same method as described in section 2.2.7.2. The ligation of purified Tm sequence of interest (10 µl) into the pJC20 vector (1 µl) was then catalysed by the T4 DNA ligase enzyme (1µl) in 1.5 µl 10x ligase buffer (Promega). The final volume was adjusted to 15 µl with dH$_2$O and the mixture was incubated at 4 °C overnight.

2.2.7.4 PCR for site directed mutagenesis of DNA encoding His-tagged α-Tm

The rat His-tagged α-Tm used for characterisation of the Tm heterodimers carrying HCM mutations (chapter 4) was changed by using the DpnI-mediated site directed mutagenesis (Fisher and Pei, 1997) to human Hisα-Tm. The human isoform was used for the characterisation of Tm heterodimers carrying DCM mutations (chapter 5). Rat α-Tm protein sequence differs from human at a single site (R220 in human is K220 in rat). Therefore, the change from rat to human Tm via site directed mutagenesis was faster and more effective approach compared to the His-tag insertion to the human α-Tm.

Three single colonies of *E. coli* DH5α containing the rat His-tagged α-Tm (inserted in the pJC20 vector) were incubated overnight in 20 ml of LB/Amp. The cell cultures were then centrifuged and DNA was purified using the QIAprep spin miniprep kit following the product manual. The purified DNA was used in PCR reaction together with the the primers described in section 2.2.5 as follows:

The PCR recipe: 1 µl DNA template

  1 µl Pfu DNA polymerase

  5 µl Pfu 10 x buffer

  1 µl Forward Primer (25 pmol/ µl)

  1 µl Reverse Primer (25 pmol/ µl)

  1 µl DNTPs (10 mM)

  40 µl sterile dH_2O

The PCR machine was programmed as follows:

  Denaturation at 95 °C for 1 min (1 initial cycle)

  Denaturation at 95 °C for 1 min (30 cycles)

  Annealing at 50 °C for 1 min (30 cycles)

  Elongation at 68 °C for 3.5 min (30 cycles)

After the completion of a PCR reaction, the mixture contained the parental methylated DNA plasmids and the PCR amplified unmethylated DNA plasmids. The PCR product was treated with DpnI endonuclease for 1 h at 37 °C to digest the parental plasmids containing methylated DNA in one or both strands. Unmethylated DNA plasmids containing human His α-Tm were sent for sequencing to MWG-operon and then used to transform DH5α competent cells (section 2.2.7.6).

2.2.7.5 Production of competent *E. coli* cells

T-salts   75 mM $CaCl_2$, 6 mM $MgCl_2$, 15 % (v/v) glycerol

$MgCl_2$ 100 mM $MgCl_2$, 15 % (v/v) glycerol

Initially 1 M stock solutions of $CaCl_2$ and $MgCl_2$ were prepared. Stock solutions were then diluted as required (see above) and after glycerol addition and filter sterilisation solutions were stored at -20 °C.

Single colonies of DH5α or BL21 cells were inoculated into 10 ml broth (2 % w/v tryptone, 0.5 % w/v yeast extract, 0.4 % w/v $MgSO_4$, 10 mM KCl, pH 7.6) and left to grow

overnight at 37 °C in flask with aeration. Overnight culture (8 μl) was used to inoculate 28 ml of fresh broth with rapid aeration at 37 °C. This culture typically reached OD_{600} of 0.5 in 4.5 hours. Five minutes before culture reached required OD_{600}, 3.75 ml of sterile warm glycerol was slowly added into the culture while flask was still shaking. Glycerol was heated firstly in microwave and then left in 37 °C water bath. Cells were afterwards chilled on ice for 10 min. The cells were centrifuged at 4 °C for 10 min at 4000 rpm. Supernatant was carefully discarded and pelleted cells were resuspended in an equal volume of ice cold 0.1 M $MgCl_2$ and 15 % v/v glycerol. Cells were then centrifuged at 4 °C for 8 min at 3800 rpm. Pelled cells were resuspended in 6.25 ml of ice cold T-salts and incubated on ice for 20 min with occasional mixing. Cells were again centrifuged at 4 °C for 6 min at 3600 rpm and pellets were resuspended in 1.25 ml of T-salts. Final stock was aliquoted into pre-cooled tubes and immediately stored at − 70 °C. Cells were frozen overnight before use.

2.2.7.6 Transformation into competent cells

Competent DH5α or BL21 cells (section 2.2.7.5) were transformed with the pJC20 or pMW172 vectors containing His-tagged or non-tagged α-Tm gene with or without various HCM and DCM mutations. 50 μl aliquots of the cells were gently thawed on ice and 3 − 5 μl of the ligation mixture was added. The cells were then incubated on ice for 30 min and then heat-shocked at 42 °C for 55 second. This step was followed by immediate incubation of the cells on ice for 2 minutes. SOC medium was added to a final volume of 400 μl and the cells were left to recover at 37 °C for 1 h. The cell culture (200 μl) was streaked onto LB/Amp plates and incubated at 37 °C overnight.

2.2.8 Recombinant proteins expression and purification

2.2.8.1 Recombinant expression of rat and human striated αTm

Expression of Tm proteins was made in BL21 *E. coli* cells. Transformed BL21 *E. coli* with the pJC20 or pMW172 vectors containing TPM1 gene of interest (rat or human skeletal

αTm) were streaked onto LB/Amp agar plate and incubated at 37 °C overnight. Single colonies from this plate were used to inoculate 20 ml of LB/Amp broth in 50 ml falcon tube and the miniculture was left to incubate at 37 °C and 220 rpm overnight. Overnight culture was used for a large scale protein expression (Figure 2.2.4). 0.5 l of LB/Amp broth was inoculated by 1 ml of overnight culture and incubated at 37 °C and 180 rpm until OD_{600} reached values between 0.4 – 0.6. Cultures were then induced by 0.5 ml of 100 mg/ml IPTG stock (final concentration of IPTG was 100mg/l) and left to incubate for 3 hours. The cells were then centrifuged at 7000 rpm for 15 min and collected pellet was stored at -20 °C.
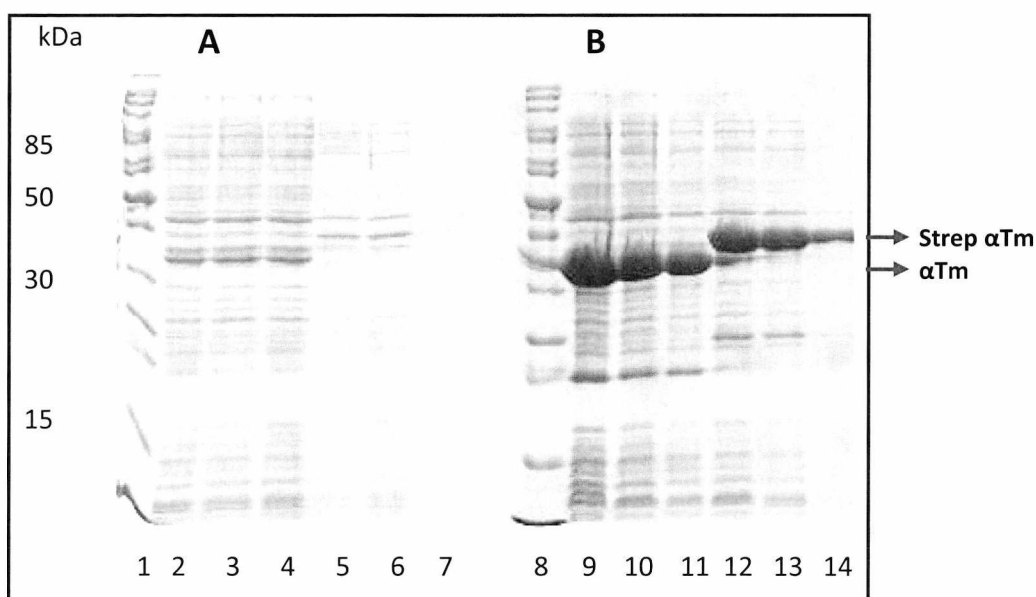
Figure 2.2.4 Recombinant expression of striated WT and Strep-tagged WT αTm. Lanes 1 and 8, molecular mass marker: lanes 2, 3, and 4, WT-αTm after 3, 2, and 1 hours growth respectively; lanes 5, 6, and 7, Strep-αTm after 3, 2, and 1 hours growth respectively; lanes 9, 10, and 11, WT-αTm after 3, 2, and 1 hours of expression induction by IPTG, respectively; lanes 12, 13, and 14, WT-αTm after 3, 2, and 1 hours of expression induction by IPTG, respectively.

2.2.8.2 Recombinant Tm purification

The pellet from a large scale protein expression (section 2.2.8.1) was resuspended in 35 ml of ice-cold lysis buffer (0.3 M NaCl, 20 mM TRIS, 5 mM EGTA, 20 mM DTT pH 7) together with two protease inhibitor tablets and 1 mM PMSF (175 µl of 200 mM PMSF stock). The cells were then lysed on ice by sonication (2 minutes pulse, 1 minute rest and another 2 minutes pulse). After sonication the proteins were kept on ice and each step was

performed as quickly as possible to prevent digestion by cellular proteases; oxidation or other degradation of Tms. The lysate was quickly transferred to 80 °C waterbath for 8 min. The contaminant proteins in this step were irreversibly denatured while heat-stable Tm was refolded after cooling the lysate. The sample was transferred into a pre-cooled centrifugation tube, gently mixed and left at -20 °C for 8 minutes. This quick cooling procedure was followed by centrifugation at 21,500 rpm; 4 °C for 10 min. Supernatant was then precipitated by pH drop to 4.7 and centrifuged at 4600 rpm, 4 °C for 12 min. The pellet was resuspended in a low salt buffer A (0.1 M NaCl, 5 mM $MgCl_2$, 5 mM KPi pH 7) and purified by FPLC.

The purification of non-tagged Tms by FPLC was made by using two serial 5 ml anion exchanger HiTrap Q HP sepharose columns (from Amersham Pharmacia). First 10 ml of Tm sample was loaded on the column at high flow rate (5ml/min). This volume is needed for the sample to reach the column resin. Flow rate was then adjusted to 1.5 ml/min therefore protein can bind to the resin. After a 20 ml wash with a low salt buffer A, the flow rate was increased to 3.5 ml/min until all unbound cellular impurities were washed out from the column. Tm protein was then eluted by linear gradient of 0.1 – 1 M KCl (0 – 100 % controlled by FPLC) using a mixture of low salt buffer A and a high salt buffer B (1 M NaCl, 5 mM $MgCl_2$, 5 mM KPi pH 7). Elution of Tm from the column typically occurred at 40 % of buffer B. Fractions containing purified Tm (Figure 2.2.5) were pooled together, precipitated by pH drop to 4.7, centrifuged at 4600 rpm for 12 min and pellets were resuspended in high salt (0.5 M KCl, 20 mM KPi, 5 mM $MgCl_2$, 1 mM NaN_3 pH 7) or low salt (100 mM KCl, 20 mM MOPS, 5 mM $MgCl_2$, 1 mM NaN_3 pH 7) buffer (depending on further use). Typical yield of Tm purification was 50 – 70 mg per litre of bacterial culture.
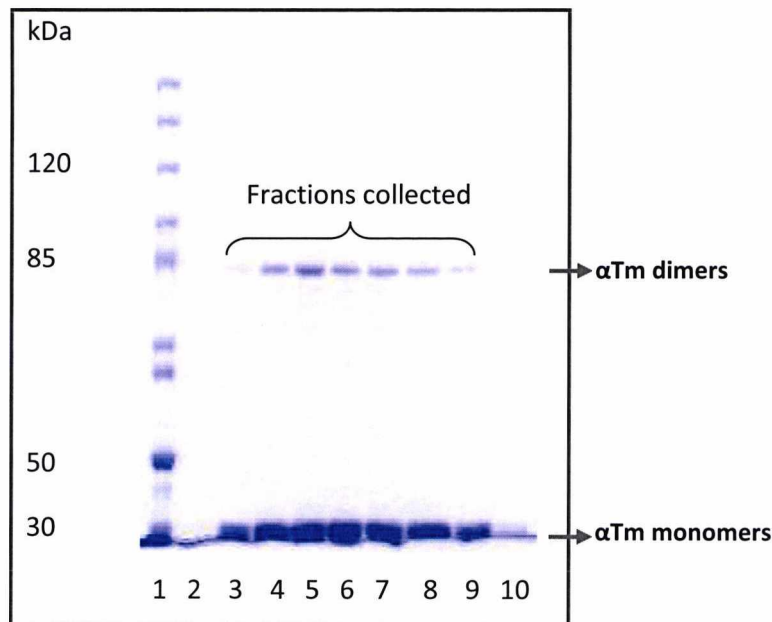
Figure 2.2.5 Elution profile of recombinantly expressed skeletal αTm. Lane 1, molecular mass marker; lane 2, Ctrl WT-Tm under reducing conditions; lanes 3 – 10, WT-Tm homodimers eluted under non-reducing conditions.

2.2.8.3 His-tagged Tm purification

Pellets of BL21 cells expressing rat or human His-tagged α-Tm were resuspended in 30 ml of ice-cold lysis buffer (0.3 M NaCl, 20 mM TRIS, 5 mM EGTA, 20 mM DTT pH 7). The cells were then lysed on ice by sonication similarly as non-tagged Tms (2 minutes pulse, 1 minute rest and another 2 minutes pulse). The lysate was centrifuged at 10,000 rpm for 20 min. Supernatant containing Tm was precipitated by pH drop to 4.7 and centrifuged at 4,600 rpm for 12 min. The Tm pellet was resuspended in buffer A (0.3 M NaCl, 50 mM KPi, 1 mM NaN_3 pH 8) and ultracentrifuged at 100,000 rpm for 20 min. The sample was then applied onto a 2.5 ml gravity NiNTA column and washed by 40 ml of buffer A. Tm protein was eluted by 14 ml of buffer B (0.25 M imidazole, 0.3 M NaCl, 50 mM KPi, 1 mM NaN_3 pH 8). Collected Tm was precipitated by pH drop to 4.7; centrifuged at 4,600 rpm for 12 min and resuspended in high salt buffer (0.5 M KCl, 20 mM KPi, 5 mM $MgCl_2$, 1 mM NaN_3 pH 7). Small aliquots from each step of the purification were run on 10% SDS gel. This monitoring showed that significant amount of His-tagged proteins were present in the flow through indicating insufficient affinity for NiNTA resin (caused probably by the small capacity of the column).

Therefore purification was repeated two times using the flow through. Resin was regenerated by 50 ml of 0.5 M NaOH followed by 50 ml of dH_2O and 50 ml of 20 % ethanol. Typical yield of His-tagged Tm purification was 15 -25 mg of protein per litre of bacterial culture.

2.2.8.4 Strep-tagged Tm purification

Pellets of BL21 cells expressing rat Strep-tagged α-Tm, were resuspended in 30 ml lysis buffer (0.3 M NaCl, 20 mM TRIS, 20 mM DTT, 5 mM EGTA pH 7). The cells were then disrupted by sonication (2 minutes pulse, 1 minute rest and another 2 minutes pulse). The lysate was then centrifuged at 10,000 rpm for 20 min. Supernatant containing Tm was then precipitated by pH drop to 4.7 and centrifuged at 4,600 rpm for 12 min. The Tm pellet was resuspended in buffer A (150 mM NaCl, 100 mM Tris·Cl, 1 mM EDTA, 1 mM NaN_3 pH 8) and ultracentrifuged at 100,000 rpm for 20 min. The supernatant was then applied onto a 2.5 ml gravity Strep-Tactin column and washed with buffer A (6 x 2 ml). Tm heterodimers were then gently eluted by applying 4 times 2.5 ml of buffer B (150 mM NaCl, 100 mM Tris·Cl, 0.1 mM desthiobiotin, 1 mM EDTA, 1 mM NaN_3 pH 8). The final elution of bound Tm was made by applying 3 times 2.5 ml of buffer C (150 mM NaCl, 100 mM Tris·Cl, 2.5 mM desthiobiotin, 1 mM EDTA, 1 mM NaN_3 pH 8). The Strep-Tactin resin was then regenerated by regeneration buffer R (150 mM NaCl, 100 mM Tris·Cl, 1 mM hydroxy azophenyl benzoic acid (HABA), 1 mM EDTA, 1 mM NaN_3 pH 8). Column was then washed by 20 ml of dH_2O followed by another wash by buffer A (20 ml) to remove HABA. Purification was monitored by running the small aliquots from each step on 10 % SDS gel. Typical elution profile of the Strep-WT-E180G Tm purification is shown in the following chapter 3 (Figure 3.2.4). Due to the high content of Tm heterodimers in the flow through and in the fractions from the final elution, purification was repeated up to six times.

2.2.8.5 Recombinant expression of human cardiac troponin

Expression of Tn complex was made in BL21 *E. coli* cells. Transformed BL21 *E. coli* with the pET3c and pSBETc vectors containing human cardiac TnC (hcTnC) isoform 1 expressed by the TNNC1 gene (UniProt P63316; the pET3c vector containing ampicillin resistance gene); human cardiac TnI (hcTnI) isoform 1 expressed by TNNI3 gene (UniProt 19429; the pET3c vector containing ampicillin resistance gene); and human cardiac TnT (hcTnT) isoform 6 which is predominating isoform in normal adult heart encoded by TNNT2 gene (UniProt P45379-6; the pSBET vector containing kanamycin (Knm) resistance gene) were streaked onto LB/Amp or LB/Knm agar plates and incubated at 37 °C overnight. All Tn vectors were kindly provided by Dr. Kornelia Jacquet (University of Bochum, Germany).

Single colonies from individual plates were used to inoculate 20 ml of LB/Amp broth in the case of hcTnI and hcTnC, and LB/Knm broth in the case of hcTnT. The minicultures were left to incubate at 37 °C and 220 rpm overnight and then used for a large scale protein expression. 0.5 l of LB broth, containing appropriate antibiotics, was inoculated by 1 ml of overnight culture and incubated at 37 °C and 180 rpm until OD_{600} reached values between 0.4 – 0.6. Cultures were then induced by 0.5 ml of 100 mg/ml IPTG stock (final concentration of IPTG was 100mg/l) and left to incubate for 3 hours. The cells were then centrifuged at 7000 rpm for 15 min and collected pellet was stored at -20 °C.

2.2.8.6 Purification of human cardiac troponin

The pellets of individual Tn proteins were resuspended in 2 x 35 ml of 6 M urea, 200 mM NaCl, 1 mM EDTA, 25 mM Tris·HCl, 20 % sucrose (w/v), 0.1 % Triton X100 pH 7 buffer. Two protease inhibitor tablets were added into each sample and cell were then sonicated (four times 1 minute pulse with 1 minute rest between each pulse). The lysate was then dialysed in step decreasing buffers.

First step was dialysis in 5 l of 6 M urea, 200 mM NaCl, 1 mM EDTA, 25 mM Tris·HCl, 20 % sucrose (w/v), 0.1 % Triton X100 pH 7 buffer for 6.5 hours. In second step the lysate was transferred into 5 l of 2 M urea, 1 M KCl, 1 mMDTT, 10 mM imidazole, 1 mM NaN_3 pH 7 buffer and dialysed for 5 hours. Third step was dialysis of the lysate in 5 l of 0.75 M KCl, 1

mMDTT, 10 mM imidazole, 1 mM NaN_3 pH 7 overnight. Fourth and the last step was dialysis in 5 l of 0.5 M KCl, 1 mMDTT, 10 mM imidazole, 1 mM NaN_3 pH 7 buffer for 5 hours. The volume of the sample after dialysis was approximately 120 ml. Due to the large decrease in urea and salt concentration the lysate increased significantly in volume during the dialysis. Therefore it was important to leave extra volume in dialysis tubing to prevent its disruption. The lysate was then centrifuged at 14,000 rpm; 4 °C for 10 min. Pellet containing cell debris was discarded and supernatant containing Tn was transferred into a beaker (on ice) and precipitated in two steps by ammonium sulphate $(NH_4)_2SO_4$.

First step was 30 % ammonium sulphate precipitation by its slow addition (20.37 g) into the continuously stirring supernatant. After addition of all ammonium sulphate the sample was stirred for further 20 to 60 minutes and then centrifuged at 9,000 rpm; 4 °C for 30 min. The pellet was discarded and the supernatant was precipitated by 50 % ammonium sulphate in the second step. The sample was centrifuged at 14,000 rpm; 4 °C for 10 min and the pellet was resuspended in 16 ml of 200 mM NaCl, 10 mM imidazole, 1 mM DTT, 100 µM $CaCl_2$, 1 mM NaN_3 pH 7. Tn was dialysed in 5 l of the same buffer overnight and further purified by the size-exclusion chromatography (SEC).

Using the FPLC, 1 ml of the sample was loaded onto the column containing 75 ml Sephacryl resin and slowly (0.2 ml/min) eluted overnight. The elution was monitored by running the small aliquots from selected fractions on 15 % SDS gel. Typical elution profile of the hcTn is shown in Figure 2.2.6.
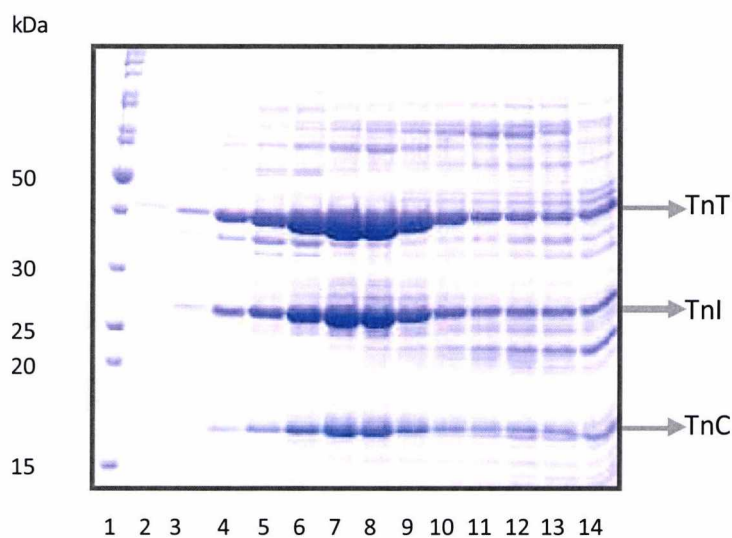
Figure 2.2.6 Elution profile of human cardiac Tn complex. The size-exclusion chromatography resin and FPLC was used for the purification of Tn complex. Aliquots from selected fractions were run in 15 % SDS-PAGE gel under reducing conditions (+BME). Lane 1, molecular mass markers; lanes 2 - 14, correspond to the fractions A14, A15, B15, B14 – B5.

The fractions containing high amounts of relatively pure Tn complex were pooled together and dialysed in 3 l of 100 mM KCl, 20 mM MOPS, 5 mM MgCl$_2$, 1 mM NaN$_3$ pH 7 buffer overnight. Dialysed sample was concentrated by centrifugation for 60 min at 3,150 rpm in a centrifugal filter unit Amicon® Ultra (3,000 MWCO; Millipore™). Concentration was measured as described in section 2.1.3. where $\varepsilon = 0.45$ l mol^{-1} cm^{-1} l and Mw = 78,000 Da. Purification of hc Tn is based on the protocol described by Al-Sarayreh (Al-Sarayreh, 2011).

2.3 Techniques and analytical procedures used for protein characterisation

2.3.1 Thermal stability measurements using circular dichroism, and data analysis

Circular dichroism (CD) is the spectroscopic technique for investigating the secondary structure and function of the proteins in solution and can be used to monitor thermal unfolding of protein domains. In this work, CD was used for the determination of thermal stability of recombinantly expressed Tm homo- and heterodimers carrying HCM or DCM mutations.

The CD data were collected on a Jasco 715-Spectropolarimeter, UK (software: spectra management V1.51.00) in a stoppered 1 mm cuvette (Starna Scientific Ltd.) as described in Janco, et al. (2012). The Tm proteins were dialysed in high salt 0.5M KCl, 20 mM KPi, 5 mM MgCl$_2$, 1 mM NaN$_3$ pH 7 buffer to prevent polymerisation of Tms. Thermal unfolding was recorded at a fixed wavelength of 222 nm that can report for changes in the α-helical content of the proteins. Each scan was performed over a temperature range from 5 °C to 65 °C using a peltier device (Jasco PTC 423S/15) and a heating rate of 1 °C/minute. The final concentration of Tm was 7 µM. The reversibility of the unfolding-refolding process was

assessed by reheating of the Tm sample directly after cooling from the previous scan. The temperature scans were repeated three times without and four times with 1 mM DTT added. Multiple measurements were made to ensure reversibility of the process and a full reduction of Tm dimers in presence of DTT.

The CD data from thermal unfolding experiments were analysed by using MicroCal Origin 8.6 software. Raw data were firstly normalised by following formula: $X-X_{max}/X_{max}-X_{min}$. Where X represents measured raw data; X_{max} is the highest measured value and X_{min} is the lowest measured value. Thus the melting curves of each scan can be compared.

The melting curves were then smoothed by Savitzky-Golay method (50 point window) and differentiated (1st derivative). Differentiated data were plotted (line) and then fitted to multiple Gaussian peaks. The data derived from the best fit to Gaussian peaks included the fractional peak areas (a measure of the free energy change associated with each unfolding "domain"), the width of half peaks (measure of unfolding cooperativity) and the midpoints of unfolding.

Thermal unfolding curves and differentiated data of skeletal α-Tm dimers with HCM and DCM mutations are shown in the result sections of the chapters 4 and 5, respectively.

2.3.2 Measurements of Tm affinity for actin

Co-sedimentation assays were used to determine the affinity of various HCM and DCM Tm dimers to F-actin. The basis of the co-sedimentation experiment is that F-actin can be pelleted down when ultra-centrifuged at 100,000 rpm. Therefore, all Tm that would normally remain in supernatant fraction after centrifugation will be pelleted down when bound to actin.

In the co-sedimentation assays increasing concentrations of Tm dimers (0.2 – 2.4 µM) were added to a fixed concentration of F-actin (7 µM) and then adjusted to a final volume 50 µl with the experimental buffer (100 mM KCl, 20 mM MOPS, 5 mM $MgCl_2$, 1 mM NaN_3 pH 7), as shown in Table 2.1. The samples were then incubated for 1 h at 20 °C and then ultra-centrifuged at 100,000 rpm for 20 min (Beckman, TLA 100.1 rotor). A fixed volume of supernatants (25 µl) was transferred into a fresh tube and the remaining supernatant was carefully removed by pipetting without disrupting the pellet. 50 µl of dH_2O was added into

the pellet samples were resuspended by vortexing at the highest speed. 10 µl and 5 µl of sample buffer were added into the pellet (50 µl) and supernatant (25 µl) samples, respectively. All samples were heated at 95 °C for 9 minutes and then 16 µl of each sample was loaded on 10 % SDS-PAGE gel (Figure 2.3.1).

Tube	Tm final concentration (µM)	Tm volume (µl) (10µM Tm stock)	Actin volume (µl) (14µM actin stock)	Buffer (100mM KCl)
1	0.2	1	25	24
2	0.4	2	25	23
3	0.6	3	25	22
4	0.8	4	25	21
5	1	5	25	20
6	1.2	6	25	19
7	1.4	7	25	18
8	1.6	8	25	17
9	1.8	9	25	16
10	2	10	25	15
11	2.2	11	25	14
12	2.4	12	25	13
13 - Tm Ctrl	1	5	-	45
14 - Actin Ctrl	-	-	25	25

Table 2.1 Volumes and concentrations of F-actin and Tm used in co-sedimentation assays. Both proteins were resuspended in the experimental buffer (100 mM KCl, 20 mM MOPS, 5 mM $MgCl_2$, 1 mM NaN_3 pH 7).
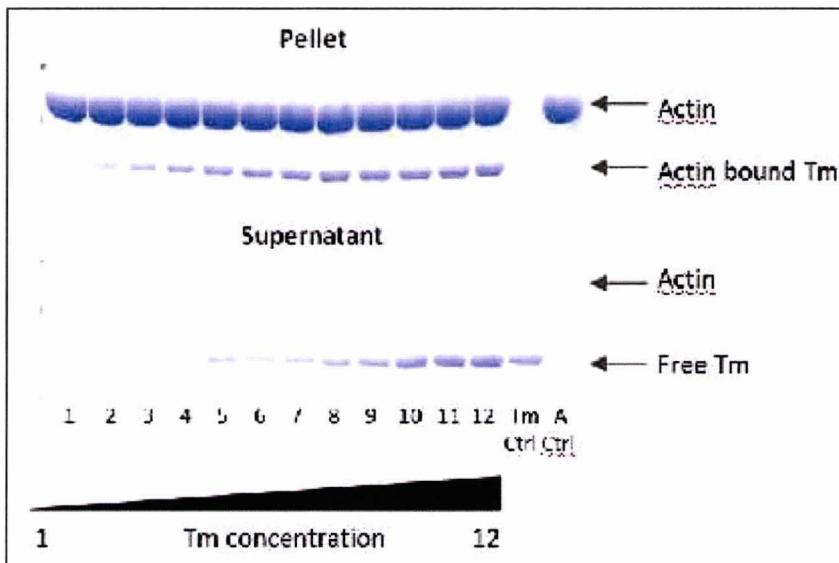
Figure 2.3.1 Co-sedimentation assay gel for determination of Tm affinity for F-actin. Lanes 1 – 12, F-actin (7 µM) incubated with increasing concentrations of Tm dimers (0.2 – 2.4 µM) at 20 °C for 1 h and then centrifuged at 100,000 rpm. SDS gels (10 %) of were used for analysis of Tm and actin in

the pellet and supernatant. The Tm control sample indicated that major fraction of Tm remained in supernatant and the control sample of F-actin was pelleted down.

The control samples of Tm and F-actin were also prepared and loaded onto each gel to check actin sedimentation and the amount of Tm in pellets and supernatants. Any pelleted Tm was used for correcting the calculation of the actin fractional saturation by Tm. After electrophoresis the gels were stained in a standard Coomassie blue stain solution and then destained (section 2.1.2).

2.3.2.1 Densitometry

Co-sedimentation experiments were combined with densitometry analyses in order to transform the protein bands from the gels to digitalised and therefore quantifiable form of the data. The gels were scanned by an Epson Perfection V750 Pro scanner and then the density of each protein band was measured by the ScionImage software (Scion Corp., Frederick, MD). A total Tm band density (addition of Tm density values from pellet and supernatant) was plotted against Tm concentrations. A fitted standard calibration curve from this plot (Figure 2.3.2) was used for the calculation of the bound and free Tm concentrations.
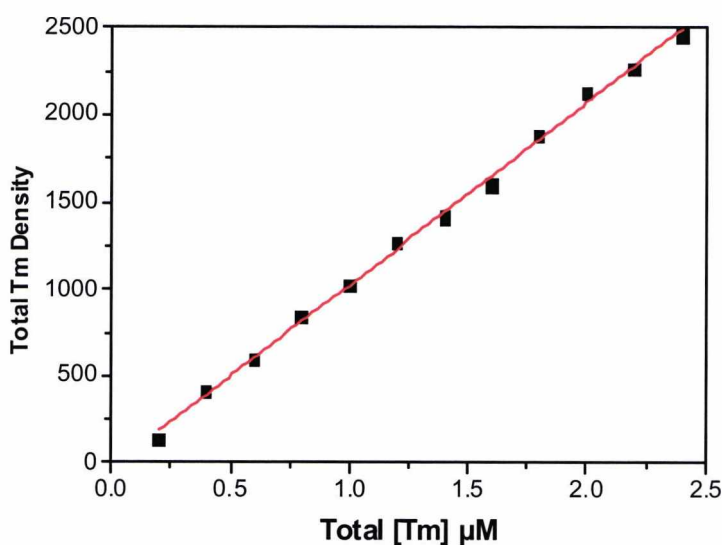
Figure 2.3.2 Tm standard calibration curve. The band density was determined by scanning the gels from co-sedimentation assays and then measuring the density of individual protein bands using the ScionImage software (Scion Corp., Frederick, MD). The total band density was plotted against known Tm concentrations to produce the calibration curve.

The free Tm concentration was plotted against the fractional actin saturation (defined as Pel Tm/Pel Act) and the Hill equation [$y = V_{max} [x]^h/(K_{50\%}^h + [x]^h)$] was used for determination of the midpoint of the fitted curve ($K_{50\%}$) and the Hill coefficient (h). Fitting parameter x in the Hill equation is an independent variable (total Tm concentration) and y is a dependent variable (Tm bound to actin). The fitted data showed a typical sigmoid curve indicating cooperative binding of Tm to F-actin (Figure 2.3.3). In the Hill equation, the Hill coefficient (h) describes the cooperative binding and $K_{50\%}$ is the point where half of the actin becomes saturated ($\theta = \frac{1}{2}$), solving the Hill equation as $K_{50\%}^h = [Tm]^h$. $K_{50\%}$ is ligand concentration producing half occupation (ligand concentration occupying half of actin binding sites) .

Results of the co-sedimentation assays of Tm affinity to F-actin are shown in chapters 4 and 5 for HCM and DCM mutants, respectively.
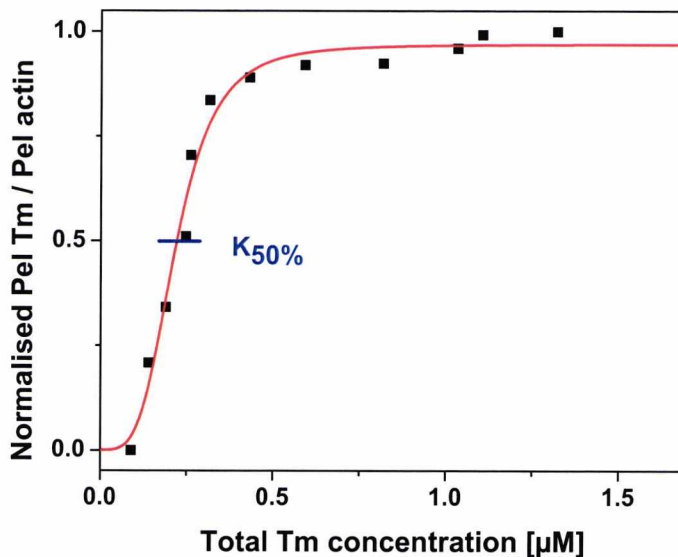
Figure 2.3.3 Binding curve of Tm for F-actin. The plot of the fractional saturation of actin by Tm (Pel Tm/PelAct) as a function of free Tm concentration. The Hill equation was fitted to the data and the best fit (red line) show a typical sigmoid curve indicating cooperative binding of Tm to F-actin. $K_{50\%}$ is indicated by blue line.

2.3.3 Ca^{2+} regulation of myosin S1 binding to a thin filament using stopped-flow

Stopped-flow (SF) is a spectroscopic technique used for the monitoring of fast reactions that occur at the millisecond time scale, such as S1 binding to F-actin. The SF technique is based on use of visible or ultraviolet (UV) detection methods, either by absorption or fluorescence spectroscopy, to measure the association or dissociation rates of protein interactions. The SF relies on rapid mixing of reactants and a suitable detection system that is able to follow the reaction in real time.

2.3.3.1 Stopped flow apparatus and software

The stopped-flow fluorimeter used in the experiments was the SF-61DX2 spectrophotometer (HiTech Scientific). The reactant solutions are loaded into two separate drive syringes and pushed by air-compressed pressure driven syringe pistons through flow tubing to the mixing chamber and on to the observation chamber. The mixed solution in the observation chamber is excited by UV light produced by a xenon/mercury lamp (Hamamatsu 100-W) and the wavelength chosen for the individual experiments is entered via the computer and then selected by a monochromator (Photon Technology International LP S-20). The emitted light is detected by a photomultiplier, which is placed on an axis at 90° from that of the incident light. The incident light passes through the test solution without contaminating the output signal received by the fluorescence detector. However, the detector receives a small portion of the incident light as a result of scattering properties of the solutions themselves or impurities in the solution. A cut-off filter (KV 389 nm) is used to allow the longer wavelength fluorescence emission to be transmitted but blocks the scattered excitation light. The reactant solution pushes the old cell content to the back or stop syringe which acts as a stopping device when filled. When the flow of the solution is stopped by the back syringe, this action simultaneously stops the flow and starts the time resolved fluorescence recording. Acquired data were visualised and analysed by Kinetic Studio software version 2.0.23.23540 (Copyright © TgK Scientific Ltd 2011). The

experiments were carried out at 20 °C. The temperature was maintained by an external water bath.
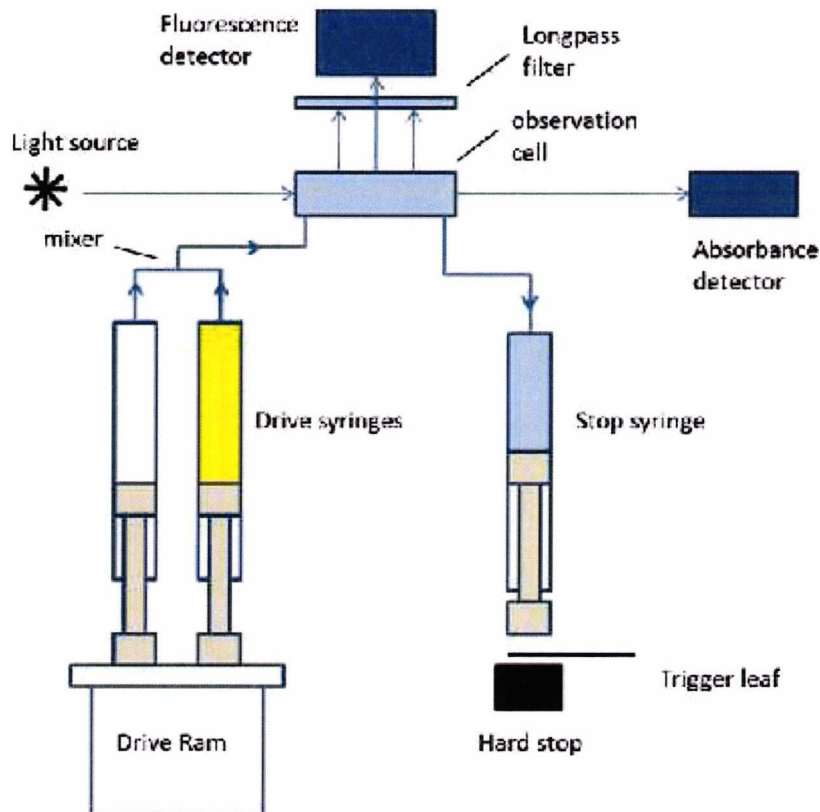
Figure 2.3.4 Schematic representation of a typical stopped-flow machine design. (http://thelab.photophysics.com/stopped-flow).

2.3.3.2 Transient kinetic principles

The reaction between S1 and actin filaments yielding the acto-myosin complex is a second order reaction (two reactants). This type of reaction can be complex and difficult to analyse, however the experimental conditions can be adjusted to make the reaction appear as a first order reaction thus it is called pseudo-first order. The conditions for pseudo-first order reaction are simply when the initial concentration of the first reactant is in large excess over the second reactant, so the concentration of the first reactant remains essentially constant throughout the reaction.

The data acquired from the SF experiments require understanding of the kinetics of first, second and pseudo-first order reactions described by the following equations.

First order reaction: is a reaction in which the rate or velocity is directly proportional to the concentration of the reactant A at time t.

$$A \xrightarrow{\ k\ } B$$
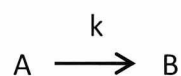
The rate of reactant disappearance or the rate of product appearance is measured in Ms^{-1}. The rate of reaction is described by equation:

$$d[B]_{(t)} / dt \ \ or \ -d[A]_{(t)} / dt = k\,[A]_{(t)}$$

Integration of the equation above yields the following single exponential equation:

$$[A]_{(t)} = [A]_{(0)}\,e^{-kt}$$

where $[A]_{(t)}$ is the concentration at time t, $[A]_{(0)}$ is the initial concentration and k is the first order rate constant of the reaction (s^{-1}).

Second order reaction: there are two types of second order reactions, those that are second order in a single reactant (2A) and those that are first order in each of two reactants (A+B). The rate of second order reaction is directly proportional to the square of the concentration of the reactant A or to the concentration of reactants A and B at time t for both reaction types, respectively.

$$2A \xrightarrow{\ k\ } B \qquad or \qquad A + B \xrightarrow{\ k\ } C$$

The rate of second order reaction (A+B scenario) is described by following equation:

$$d[C]_{(t)} / dt = k\,[A]_{(t)}\,[B]_{(t)}$$

The analysis of the above equation is quite complex therefore the second order reactions are usually studied under pseudo-first order conditions.

Pseudo-first order reaction: defines a second order reaction in which the experimental conditions are adjusted to make it appear as a first order in one of the reactant and zero order in the other. The reaction conditions are set in a way that the initial concentration of one reactant is in a large excess compared to the other reactant so the one in excess remains effectively constant.

$$A + B \xrightarrow{\ k\ } C$$
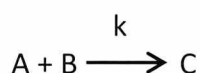
The rate of pseudo-first order reaction is described by following equation:

$$d[C]_{(t)} / dt = k \, [A]_{(t)} \, [B]_{(t)}$$

where k is the second order rate constant of the reaction, $[A]_{(t)}$ is the concentration of the first reactant at time t and $[B]_{(t)}$ is the concentration of the second reactant at time t.

Since [A] is in a large excess to [B] or [A] >> [B], then $[A]_{(t)} \approx [A]_{(0)}$.

This gives rise to a new constant termed the observed rate constant k_{obs}.

$$k_{obs} = k \, [A]_{(0)}$$

Solving of the pseudo-first order reaction in multiple steps yields the following single exponential equation:

$$[B]_{(t)} = [B]_{(0)} \, e^{(-k_{obs} \, t)}$$

where the k_{obs} is a linear function of [A].

2.3.3.3 Kinetic analysis of S1 binding to F-actin

The calcium dependent binding of S1 to reconstituted thin filaments (reaction scheme in shown below) was monitored by the SF at 20 °C. The concentration of either S1 or F-actin with bound regulatory proteins was in 10-fold excess to fulfil the conditions for the pseudo-first order reaction (as described in previous section). Experimental buffer used in all SF experiments was 100 mM KCl, 20 mM MOPS, 5 mM $MgCl_2$, 1 mM NaN_3 pH 7 with addition of 1 mM DTT when Tn was present in the solution.

$$A + S1 \xrightarrow{k} A \cdot S1 \qquad A = actin$$

$$S1 = myosin\ subfragment\ 1$$
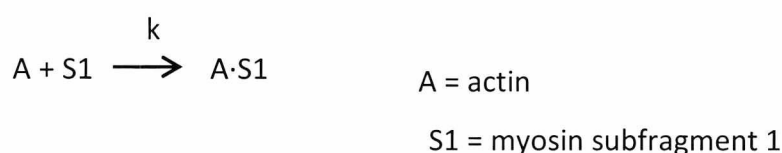
Excess of actin reactions: in these reactions the F-actin concentration remains relatively unchanged. The rate of reaction in the [A] >> [S1] scenario is described by following equation:

$$-d[S1]_{(t)} / dt = k\ [A]_{(t)}\ [S1]_{(t)}$$

Integration of above equation predicts an exponential decrease of S1 concentration as

$$[S1]_{(t)} = [S1]_{(0)}\ e^{(-k_{obs}\ t)}$$

where $k_{obs} = k\ [A]_{(0)}$ indicating a linear relationship with the actin concentration.

Excess of S1 reactions: in case of [S1] >> [A] the rate of reaction is described by the same equation as above. However, integration of the reaction will yield

$$[A]_{(t)} = [A]_{(0)}\ e^{(-k_{obs}\ t)}$$

indicating an exponential decrease of actin concentration. The observed rate constant k_{obs} is a linear function of the S1 concentration, described as $k_{obs} = k \, [A]_{(0)}$.

2.3.3.4 Ca^{2+} dependent binding of S1 to the thin filaments

The binding of S1 to the thin filaments is a calcium dependent reaction. The F-actin excess SF reactions were used to test the quality and activity of the thin filament proteins and to determine the equilibrium constant K_B, as described in results sections of the chapters 4 and 5. The protein concentrations used in SF experiments are all after mixing unless stated otherwise.

The activity of reconstituted thin filaments was assayed by mixing 0.25 µM of S1 in the absence of calcium with a 10-fold excess of F-actin (2.5 µM), WT-Tm at 1 µM and increasing concentrations of cTn (concentrations after mixing). The increasing concentration of cTn reached the saturation at 2.5 µM. This concentration was used in all subsequent measurements with the same batch of cTn. Repeating the reaction in the presence of calcium typically increased k_{obs} 3.5-fold as observed previously (Boussouf et al., 2007; Maytum et al., 2003). The effect of calcium on the observed rate constant of S1 to thin filament is shown in Figure 2.3.5.

The ratio of k_{obs} in the presence (2 µM Ca-EGTA) and absence (2 µM EGTA) of calcium was used to calculate the equilibrium constant K_B. K_B is defined by the three-state model of thin filament regulation as the equilibrium constant between the blocked and closed states of the thin filament (McKillop and Geeves, 1993). The observed rate constant for binding of S1 to the excess of F-actin concentration is defined as

$$k_{obs} = [A] \, k \times K_B/(1+K_B)$$

where $K_B/(1+K_B)$ is the fraction of actin sites in the on state (actin can bind S1) and $[A]k$ is the pseudo-first order rate constant for S1 binding to actin. This experiment was conducted to test the quality and activity of reconstituted thin filament containing recombinantly expressed hcTn and Tm. The effect of Tm cardiomyopathy mutations on calcium dependent binding of S1 to the thin filament could be also estimated as K_B values indicates the

availability of actin binding sites in closed state. Any differences would indicate the gain or loss of the function as an indirect effect caused by the mutation.
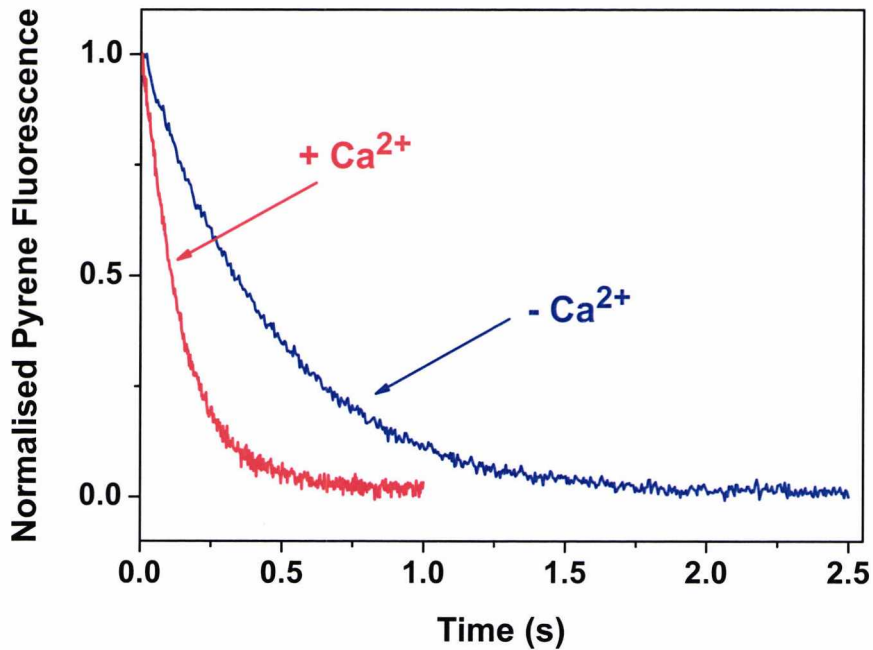
Figure 2.3.5 The effect of Ca^{2+} on the observed rate constant of S1 binding to reconstituted thin filament. Observed transients for excess F-actin (2.5 µM ppA, 1µM sk α-Tm and 1µM hcTn) binding to 0.25 µM S1 in the presence (red line) and absence (blue line) of Ca^{2+}. Experimental conditions: 100 mM KCl, 20 mM MOPS, 5 mM $MgCl_2$, 1 mM DTT, 1 mM NaN_3 pH 7 with addition of 2 mM EGTA or 2 mM Ca-EGTA.

2.3.3.5 The generation of Ca^{2+} sensitivity curves

The kinetics of acto-myosin binding under various calcium concentrations can be used for determination of the Ca^{2+} sensitivity of the system. This type of assay was used to measure the effect of HCM and DCM Tm mutations on calcium sensitivity of the reconstituted thin filaments *in vitro*.

Important requirement of this assay is a precise controlling of the free Ca^{2+} concentration using chelators such as EGTA. The pCa buffers at defined free Ca^{2+} concentrations were prepared by mixing of given volumes of EGTA and Ca-EGTA (µl) as

shown in the Table 2.2. The volumes were calculated by using a specialised software
WEBMAXCLITE v1.15 (http://maxchelator.stanford.edu/webmaxc/webmaxclite115.htm).

[EGTA] (100 mM)	1999.3	1955.7	1630.5	1274.3	822.6	611.4	296.4	124.5	9.5
[Ca-EGTA] (100mM)	0.7	44.3	369.5	725.7	1177.4	1388.6	1703.6	1875.5	1990.5
pCa (2 mM)	9.8	8.0	7.0	6.6	6.2	6.0	5.6	5.2	4.6

Table 2.2 Calculated values of EGTA and Ca-EGTA (in µl) for the formation of defined pCa
concentrations at 2 mM.

Thin filaments were reconstituted by initial mixing of 2.5 µM F-actin, 1 µM Tm and 1
µM hcTn and incubation at 4 °C for 1 hour. These proteins were then diluted 10-fold in
experimental buffer for use in following SF experiments. Calcium sensitivity curves were
obtained by mixing 0.25 µM F-actin, 0.1 µM Tm and 0.1 µM hcTn with a 10-fold excess of S1
(2.5 µM) in the presence of different pCa buffers (Figure 2.3.6). The experiment was
conducted using an excess of S1 binding to the thin filament because of limited yields of
αα*-Tm heterodimers.
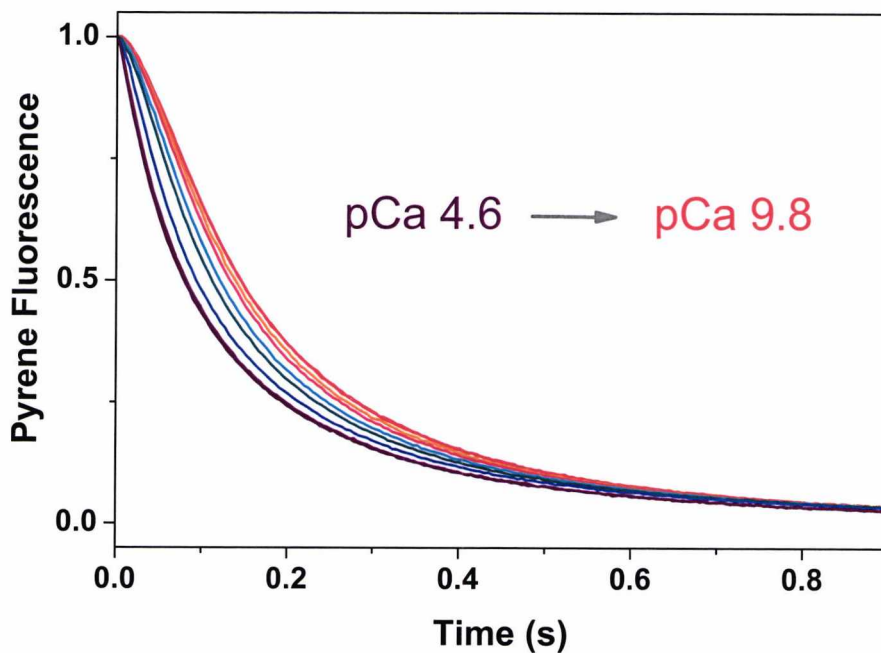
Figure 2.3.6 Normalised transients observed for the reconstituted pyrene-labelled F-actin·Tm·Tn
complex (0.25 µM ppA, 0.1 µM WT-Tm, 0.1 µM hcTn) rapidly mixed with an excess S1 (2.5 µM) at

various Ca^{2+} concentrations at 20 °C. Experimental conditions: 100 mM KCl, 20 mM MOPS, 5 mM $MgCl_2$, 1 mM DTT, 1 mM NaN_3 pH 7 with addition of 2 mM pCa buffers at various concentrations.

The half time of each reaction ($t_{1/2}$) was then plotted against corresponding pCa value as shown in Figure 2.3.7. The Hill equation was fitted to data to obtain the Hill coefficient (h) and the midpoint of the curve. The midpoint of the fitted sigmoid curve ($K_{50\%}$) is an indication of a change in the calcium sensitivity and the Hill coefficient is a measure of the cooperativity of the system (for the measured values of $K_{50\%}$ and h see the result sections of chapters 4 and 5). Statistical differences between the measurements of $K_{50\%}$ were evaluated by two sample T-test using Origin 6.8 software.
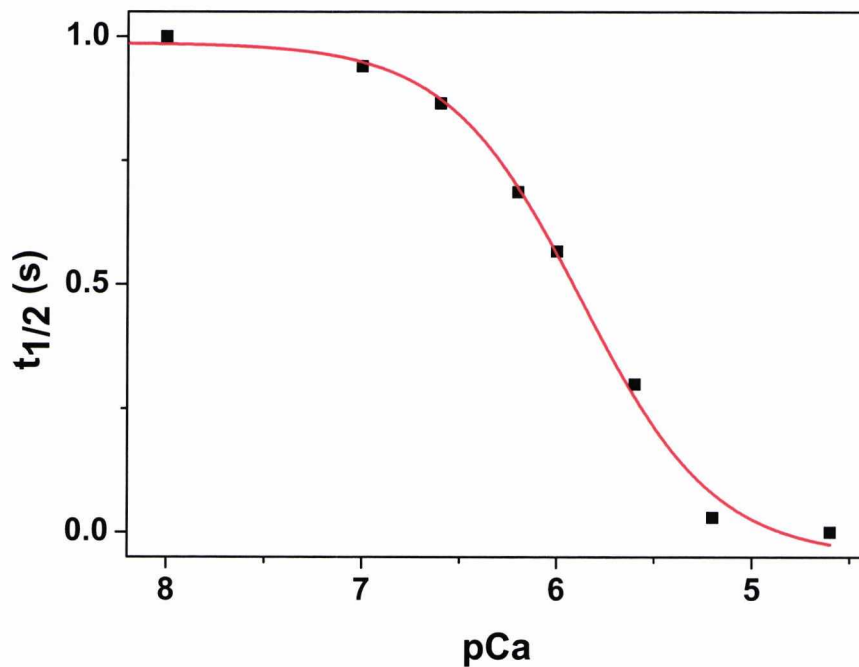
Figure 2.3.7 Dependence of the observed transients of S1 binding to the thin filaments on Ca^{2+} concentrations. The fractional half-time ($t_{1/2}$) is plotted against pCa and the Hill equation was fitted to the data..

The Hill equation has been widely used in biochemistry to analyse the binding equilibria in ligand – receptor interactions. The Hill coefficient derived from this model provides an accurate estimation of the number of binding sites but only under the very specific conditions involving extreme positive cooperativity present between the binding of

the first and subsequent ligand molecules. Note that the Hill equation used to fit the data from Ca^{2+} sensitivity assays is rather rough estimation of a functional effect of Ca^{2+} on the thin filament containing cardiomyopathy mutations. There are multiple binding sites on F-actin and reaction involves multiple proteins therefore The Hill equation does not reflect the reaction scheme. It has been used as a convenient alternative for the model which would describe whole reaction but is rather challenging task (work in progress). On the other hand the Hill coefficient derived from the Hill equation reflects the extent of cooperativity among multiple ligand binding sites (Goutelle et al., 2008; Weiss, 1997).

Chapter 3

Optimisation of the method for *in vitro* formation of the striated muscle α-Tm heterodimers carrying cardiomyopathy mutations

3.1 Introduction

In this chapter an optimised method for the formation and purification of defined α-Tm heterodimer carrying missense mutations associated with HCM and DCM is described using various affinity chromatography techniques. The same method has been used for the formation and purification of Tm heterodimers carrying DCM mutations (used in chapter 5) and can be used for any other Tm missense mutations.

Using controlled conditions of the fast protein liquid chromatography (FPLC) combined with TALON® Metal Affinity matrix (25ml) we were able to improve the protein purity and increased yield over 10-fold in comparison to the previously described method (Kalyva et al., 2012).

3.2 The method for in vitro assembling of striated Tm heterodimers

The novel method for in vitro assembling of striated Tm heterodimers was developed and described by Dr. Athanasia Kalyva in 2009. This method uses bacterially expressed and

purified Tm homodimers as a starting material. *E. coli* BL21 strain was used for the expression of our Tms and affinity chromatography (ion exchange chromatography; sections 2.2.8.2, 2.2.8.3, and 2.2.8.4) was used for their purification.

His or Strep tagged striated wild type α-Tm (N-terminal sequences shown in Figure 3.2.1) and a non-tagged α-Tm (wild type), D175N-Tm and E180G-Tm homodimers were used for the heterodimer formation. Strep and His tagged α-Tm are striated α-fast Tm (Tmskα1) isoforms carrying respective affinity tags in N-terminal region of the Tm molecule (sequence and position of each tag is shown in Figure 3.2.1). These constructs are denoted in the following text as His WT-Tm and Strep WT-Tm. WT-Tm, D175N-Tm and E180G-Tm are the same Tm isoforms without affinity tags which stand for the wild type, and the mutant homodimers carrying D175N and E180G mutations, respectively. WT-D175N- and WT-E180G-Tm indicate the heterodimers carrying respective mutations in only one chain of the dimer. Proteins were expressed with Ala-Ser dipeptide extension which mimics the N-terminal structure of acetylated native Tm and is essential for the binding to actin (Boussouf et al., 2007; Monteiro et al., 1994). Moreover both tagged α-Tms contain an FXa digestion site between the tag and Ala-Ser dipeptide extension.

The method for in vitro assembling of striated Tm heterodimers is outlined in Figure 3.2.2) and includes the following steps.

I.   Thermal denaturation of the mixed tagged and non-tagged Tm homodimers

II.   The chemical cross-linking of formed dimers

III. Purification by affinity chromatography

IV.   Removal of the affinity tag

Factor FXa digestion site	Factor FXa digestion site
↓	↓
W S H P Q F E K - **I E G R** – **A S** - **M D A I K K**	**M R G S H H H H H H** - **I E G R** – **A S** - **M D A I K K**
Strep tag Factor Xa **AS** **α-Tm**	**His tag** Factor Xa **AS** **α-Tm**
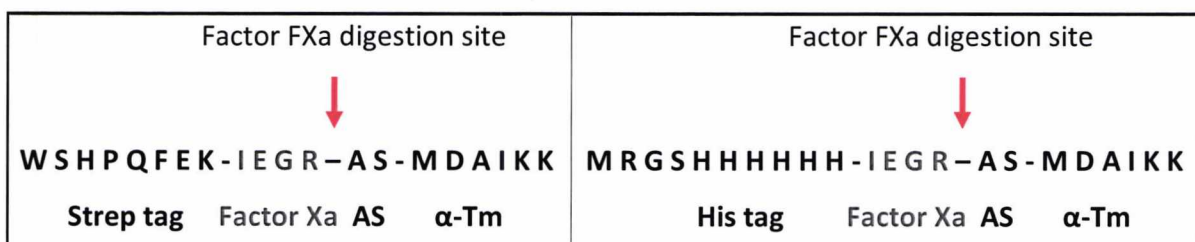
Figure 3.2.1 The N-terminal sequences of Strep- and His-tagged α-Tm constructs. The FXa digestion site is indicated (red arrow).
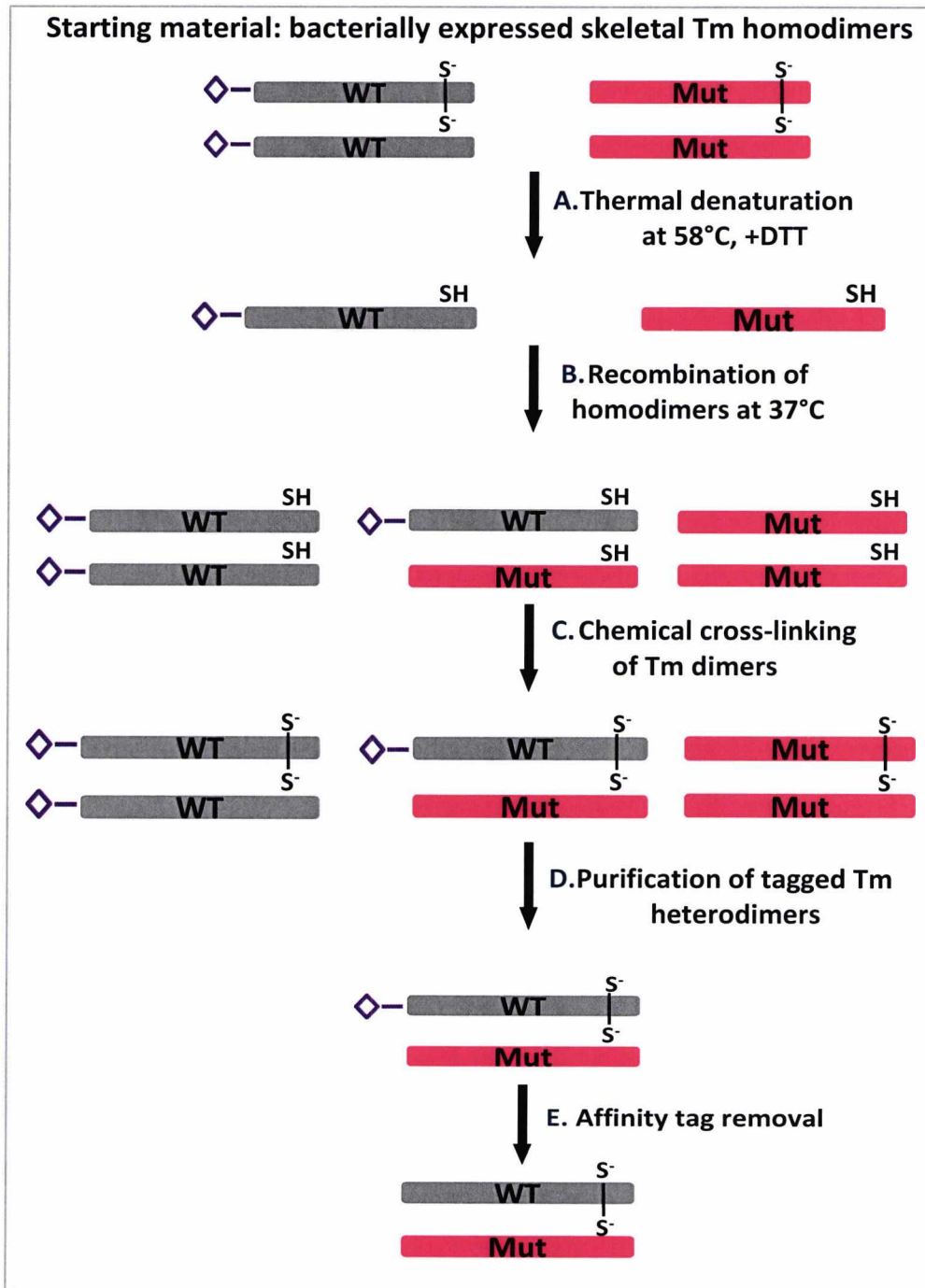
Figure 3.2.2 Schematic representation of the method for *in vitro* assembling of defined skeletal Tm heterodimers. Where ◇ represents His or Strep tag; and ▬ is the factor Xa tag digestion site. Note that step C was ommited in the formation of non-crosslinked DCM constructs.

Bacterially expressed tagged and non-tagged proteins in defined buffer were mixed together in ratio of 1 : 3 respectively. An excess of the non-tagged proteins was chosen in order to increase formation of tagged heterodimers over the tagged homodimers (non-tagged dimers will be eluted). Mixed proteins in high salt buffer (0.5 M KCl, 20 mM KPi, 5 mM MgCl$_2$, 1 mM NaN$_3$ pH 7) additionally contained 20 mM of reducing agent dithiothreitol (DTT) which prevents disulphide cross-linking of the Tm dimers. The sample was heated in water bath at 58 °C for 10 min and then transferred into 37 °C for 45 min. DTT was then removed by the gel filtration using Econo-Pac 10DG desalting columns. After this step the sample containing Tm proteins was added to the oxidation buffer (10 mM K$_3$Fe(CN)$_6$, 2 μM CuSO$_4$, 2 M NaCl, 10 mM MOPS pH 7) in ratio of 2 : 1 respectively and incubated at room temperature overnight. Oxidation of Tm allows formation of the disulphide cross-bridges between two cysteins at position 190 (Figure 3.2.3) and prevents further the chain exchange between the dimers. The oxidation buffer was removed from the sample by dialysis.
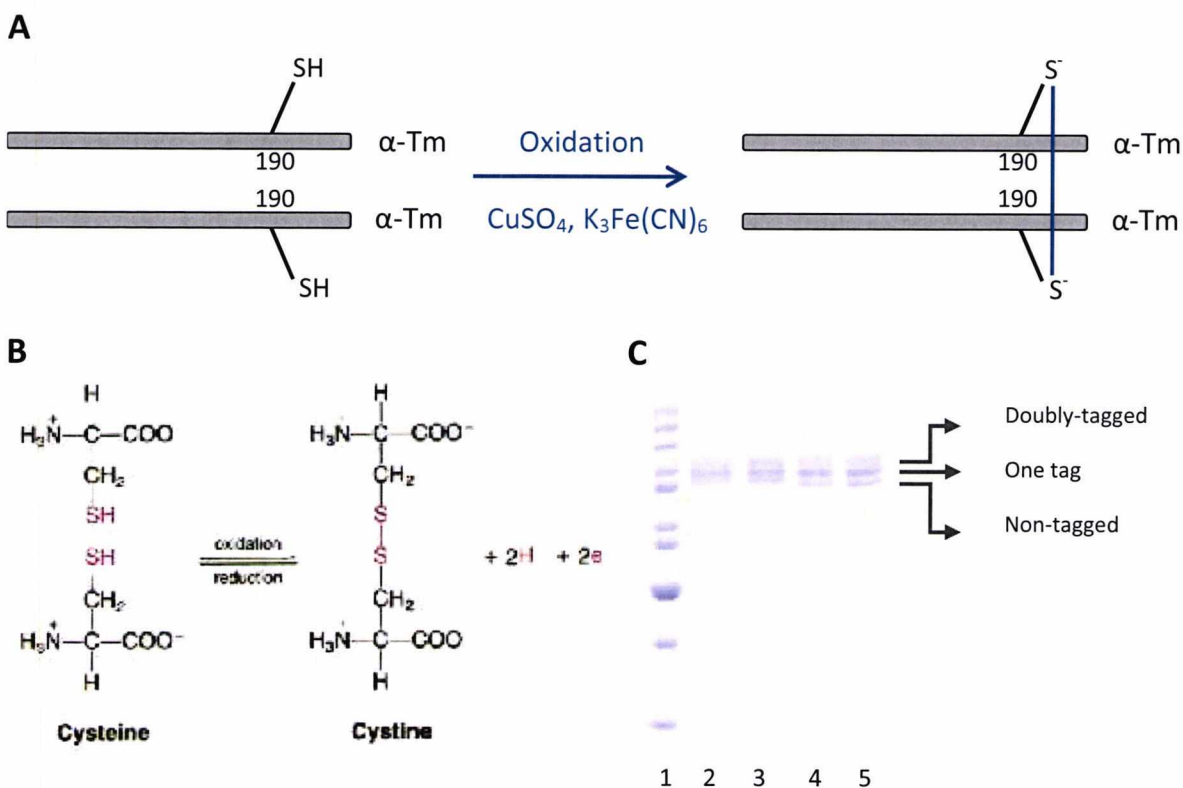
Figure 3.2.3 Schematic representation of Tm dimers chemical cross-linking (A), the reaction scheme (B), and formation of the dimers (C). Tagged and non-tagged Tm constructs were mixed in a 1 : 1 ration heated under reducing conditions, cooled down and chemically cross-linked to form dimers. Tm dimers were then stained with Coomassie blue and run on 10% SDS gel under non-reducing conditions. Lane 1, molecular mass markers; lane 2, His WT-Tm mixed with WT-Tm; lane 3 His WT-Tm mixed with D175N-Tm; lanes 4 and 5, His WT-Tm mixed with E180G-Tm.

Described method for a chemical cross-linking was also used for the evaluation of Tm heterodimers formation when mixed in 1 : 1 ratio (Figure 3.2.3 C). His WT-Tm mixed with WT (lane 2), D175N (lane 3) and E180G (lanes 4 and 5) after cross-linking procedure resulted in a predicted ratio of 1 : 2 : 1 for αα, αα* and α*α*.

The next step was the purification by affinity chromatography. The Strep-tagged proteins were purified using 2.5 ml Strep-Tactin gravity column and His-tagged proteins were purified using 2.5 ml gravity NiNTA column. Both purification methods are similar in methodology which includes the wash, elution and regeneration steps as described in sections 2.2.8.3 and 2.2.8.4 for His- and Strep-tagged Tms, respectively. Individual buffers were used for both affinity columns as they have specific binding competitors. Elution buffer for the Strep-Tactin matrix contained D-desthiobiotin (2.5 mM) and elution buffer for NiNTA matrix contained imidazole (250 mM).

Typical elution profile of the Strep-WT-E180G Tm purification is shown in Figure 3.2.4. Fractions containing heterodimers (lanes 6 – 12) were pooled together and dialysed in high salt buffer overnight. The gel shows that the most of the heterodimers were eluted by wash buffer and 0.1 mM D-desthiobiotin elution step was not required. The flow through and other fractions containing heterodimers as well as homodimers (lanes 3 – 5, and 13 – 15) were pooled together dialysed overnight in wash buffer and purified again due to a high content of heterodimers present in residual sample.
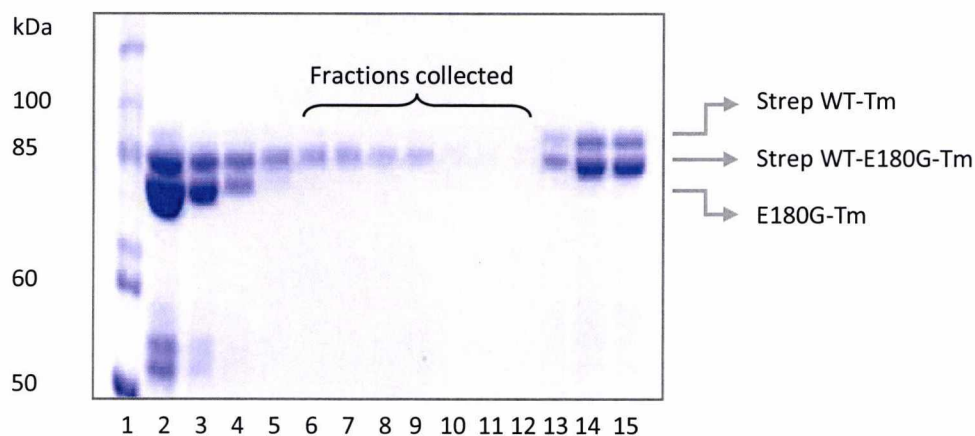
Figure 3.2.4 Elution profile of the Strep WT-E180G-Tm purification by using 2.5 ml Strep-Tactin gravity column. Aliquots from each step were stained with Coomassie blue and run in 10 % SDS-PAGE gel under non-reducing conditions (-BME). Lane 1, molecular mass markers; lane 2, flow

through; lane 3 – 8, wash; lane 9 – 12 elution with buffer containing 0.1 mM D-desthiobiotin; lane 13 – 15 final elution with buffer containing 2.5 mM D-desthiobiotin.

After five to six purification runs (number of purifications was dependent on the level of the heterodimers in the flow through) all samples were pooled together and the final concentration of the purified Tm was then calculated by measuring the absorbance A using a UV spectrophotometer at 280 nm. Formation of Strep WT-E180G-Tm heterodimers and purity of the sample was verified on 10 % SDS-PAGE gel under reducing and non-reducing conditions (Figure 3.2.5). Strep WT-E180G-Tm heterodimer run under reducing conditions, shown in Figure 3.2.5 (lane 2), had expected ratio of 1 : 1 for tagged and non-tagged Tm monomers. Line 1 shows the same sample when cross-linked indicating only minor additional bands. The purity of the heterodimers was good therefore the affinity tag was removed by the proteolytic digestion as the last step of the purification.
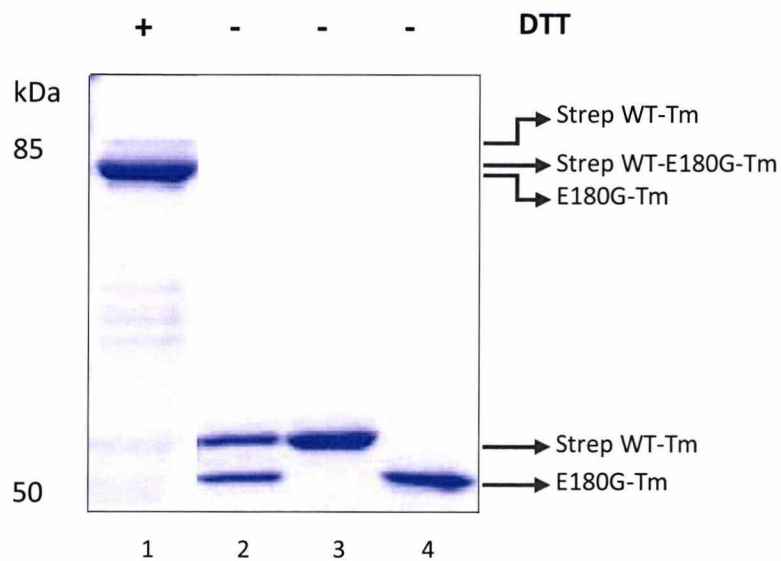
Figure 3.2.5 Verification of Strep WT-E180G-Tm heterodimers formation. Samples were run in 10 % SDS-PAGE gel under reducing (+BME) and non-reducing conditions (-BME). Lane 1, Strep WT-E180G-Tm heterodimers -BME; lane 2, Strep WT-E180G-Tm heterodimers +BME; Lane 3, Strep WT-Tm homodimers +BME; Lane 4, E180G-Tm homodimers +BME.
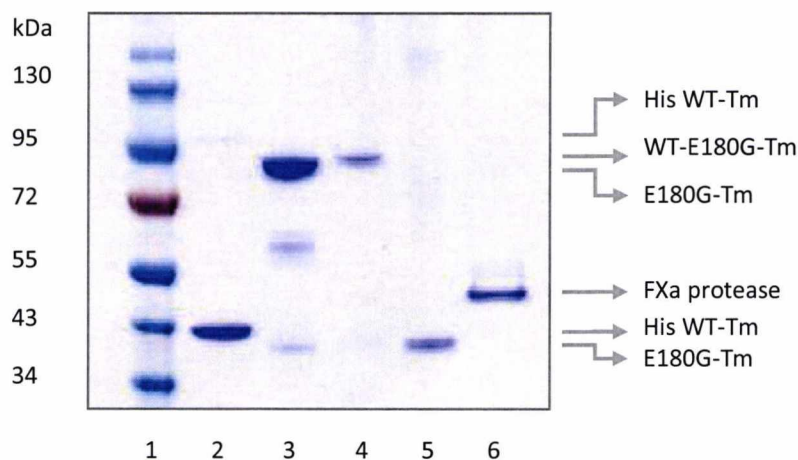
Figure 3.2.6 Affinity tag digestion of His WT-E180G-Tm heterodimers. Samples were run in 4 – 12 % SDS-PAGE gel under reducing (+BME) and non-reducing conditions (-BME). Lane 1, molecular mass markers; lane 2, His WT-Tm homodimers -BME; lane 3, E180G-Tm homodimers -BME; lane 4, WT-E180G-Tm heterodimers –BME (after digestion); lane 5, WT-E180G-Tm heterodimers +BME; lane 6, FXa protease.

The affinity tags (Strep or His) were removed by FXa protease digestion under the same conditions, since both of them contained the identical FXa protease restriction site. Purified heterodimers were incubated with FXa protease (30 units/mg) overnight at room temperature. Digestion of WT-E180G-Tm is shown as an example in Figure 3.2.6. Lanes 2 and 3 show His WT-Tm and E180G-Tm homodimer controls under non-reducing conditions, respectively. The His WT-Tm does not form a cross-link as readily as non-tagged Tm and is shown as a mixture of mostly monomers and some dimers. Lanes 4 and 5 shows WT-E180G-Tm heterodimer after tag digestion under reducing and non-reducing conditions, respectively. Heterodimers under both conditions showed single bands with an apparent molecular mass similar to those of the non-tagged control indicating fully digested and pure heterodimer.

The starting weight of the tagged proteins was 6 mg. The final yield of purified heterodimers was approximately 1 mg of the protein before affinity tag digestion and 600 µg after digestion with final concentration varying from 5 – 10 µM.

3.3 Optimisation of the method

Average yields of the Tm heterodimers, time and material used in the method described previously in section 3.2 above were not efficient. Therefore, changes were made to optimise the process to improve the time of $\alpha\alpha^*$-Tm purification, yield and purity of proteins.

Initially the volume of the Strep-Tactin matrix was increased from 2.5 to 10 ml and connected the column to the fast protein liquid chromatography (FPLC) apparatus (AKTA). We have made these changes as increased volume of the resin should also increase the amount of bound Tm heterodimers (higher yield) and the purification conditions via FPLC are more controlled which could improve efficiency of the binding. Furthermore the ratio of tagged and non-tagged proteins was increased from 3 : 1 to 4 : 1 in order to improve purity of final product. The amount of proteins used was also increased from 18 mg of non-tagged mixed with 6 mg of tagged proteins to 48 mg of non-tagged mixed with 12 mg of tagged Tm.

Strep-tagged Tm dimers were eluted by linear gradient of 0 – 2.5 mM D-desthobiotin. Samples from the fractions with eluted tagged Tm proteins were loaded onto 4 – 12 % SDS-PAGE gel and run under non-reducing conditions. The fractions containing Tm heterodimers were pooled together and the purity was checked on 4 – 12 % SDS-PAGE gel (Figure 3.3.2). Final yield of purified heterodimers was approximately 4 mg of the protein before affinity tag digestion with a final concentration varying from 20 – 48 µM. Amount of the heterodimer was higher as expected, however purity of the protein was lower in comparison to the samples from the gravity column purifications. Elution profile showed in Figure 3.3.1 A that both single and double-tagged Tm dimer were eluted approximately at the same salt concentration (single peak). Furthermore gel electrophoresis of eluted fractions containing protein showed presence of double-tagged dimers in most of the fractions indicating similar affinity of Strep tag for both single and double tagged Tm dimers (Figure 3.3.1 B).

A

B
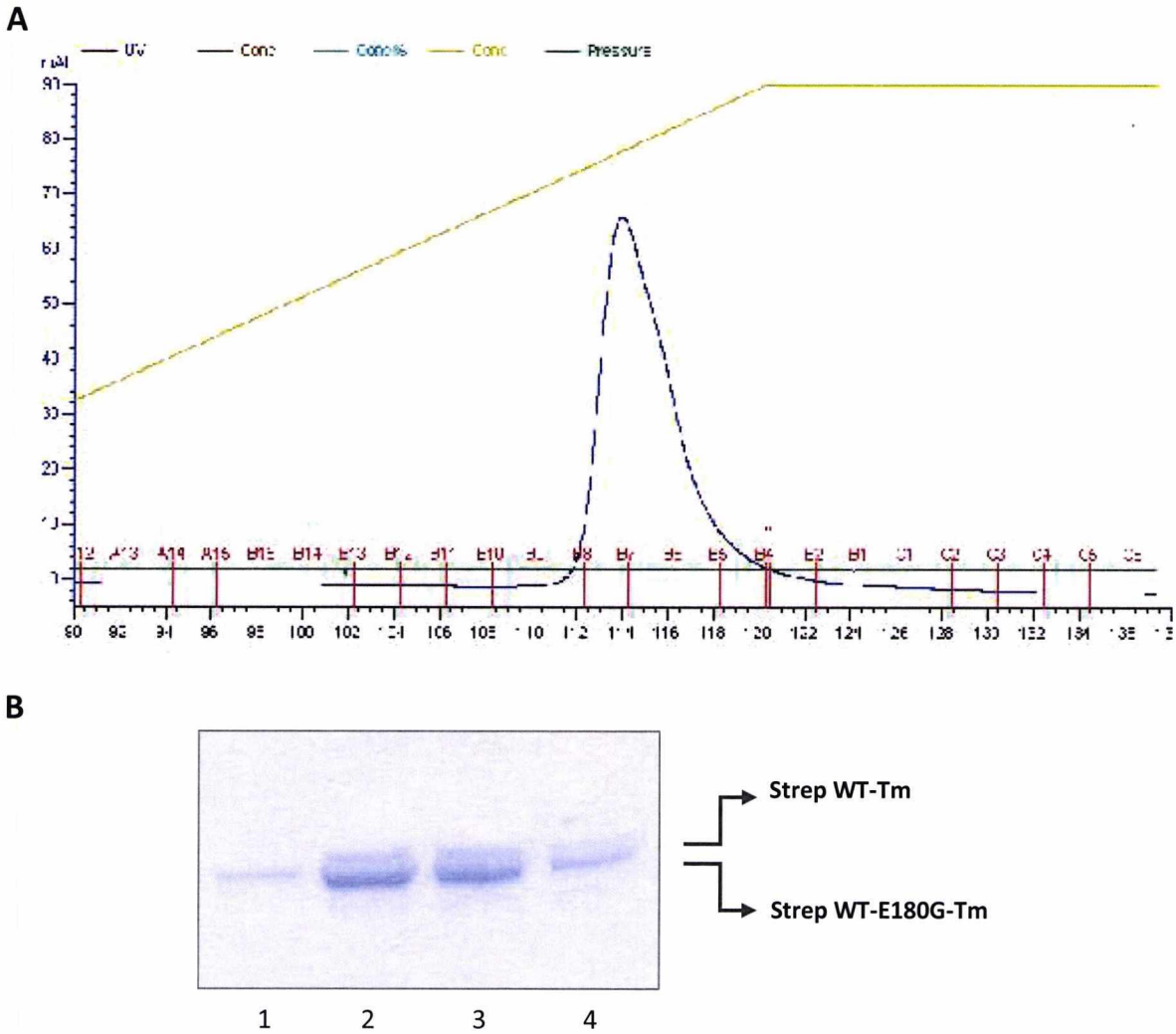
Figure 3.3.1 Elution profile of the Strep WT-E180G-Tm heterodimer. (A) Protein was eluted by linear gradient of 0 – 2.5 mM D-desthobiotin (light green line). Elution of the tagged Tm was continuously monitored by the absorbance at 280 nm (blue line). (B) Fractions of Strep WT-E180G-T-m heterodimer were run on 4 – 12 % SDS-PAGE gel under non-reducing conditions. Lane 1, fraction B9; lane 2, fraction B8; lane 3, fraction B6; lane 4, fraction B5.

At this stage of the project the use of Strep-tagged Tm was completely abandoned due to the low efficiency and purity of the heterodimers produced by this method. For the formation of His-tagged based Tm heterodimers, the NiNTA matrix was replaced by the TALON® Metal Affinity resin (Clontech Laboratories, Inc.) with a final volume of 25 ml. TALON® Metal Affinity resin is the cobalt based affinity matrix which showed higher binding specificity and therefore higher purity in previous experiments with His-tagged proteins. The ratio of tagged and non-tagged proteins remained 1 : 4 although amount of used proteins

was increased to 56 mg of the non-tagged Tm mixed with 14 mg of tagged Tm. Amount of protein was increased as a higher volume of used resin has an increased binding capacity.

Elution of His-tagged dimers was made by linear gradient of 0 – 250 mM imidazole. The monitoring of protein elution at 280 nm by FPLC was hindered by a high concentration of imidazole (from ~30 % of the gradient). The protein content of eluted fractions was therefore monitored by running aliquots from selected fractions on 10 % SDS-PAGE gel (Figure 3.3.2).

1 2 3   4 5 6   7 8 9 10 11 12 13 14 15 16 17 18 19 20 21 22 23 24 25
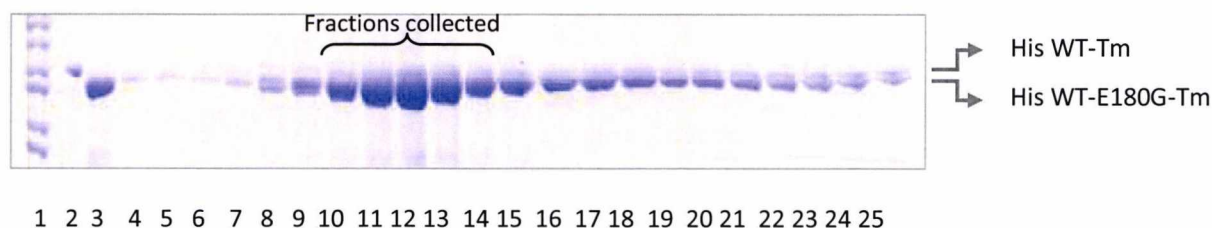
Figure 3.3.2 Elution profile of the His WT-E180G-Tm purification by FPLC using 25 ml TALON® Metal Affinity column. Aliquots from every fourth fraction were stained with Coomassie blue and run in 10 % SDS-PAGE gel under non-reducing conditions (-BME). Lane 1, molecular mass markers; lane 2, His WT-Tm; lane 3 WT-Tm; lanes 4 – 25, eluted Tm dimers; Lanes 10 – 14, collected fractions containing His WT-E180G-Tm heterodimers.

Lanes 2 and 3 in Figure 3.3.2 show His WT-Tm and WT-Tm homodimer controls under non-reducing conditions, respectively. Lanes 4 – 25 show the protein content of elution fractions from low (~20 %) to high (~80 %) concentration of imidazole.

The fractions containing the highest proportion of Tm heterodimers (lanes 10 – 14) were pooled together and treated by FXa-protease to digest the His-tag. Remaining fractions still contained a high proportion of Tm heterodimers, therefore these were subjected to a second purification. Final yield of Tm heterodimers after two rounds of purification after the tag digestion was between usually > 6 mg. The protein purity was routinely checked on 4 -12 % SDS-PAGE gel under reducing and non-reducing conditions. The molecular mass of all purified proteins was determined by mass spectrometry (Bruker Daltonics micrOTOF-Q II) by Kevin Howland. Predicted and measured masses of individual Tm constructs are shown in Table 3.1.

3.3.1 Schematic summary of the results from the Tm heterodimers purification
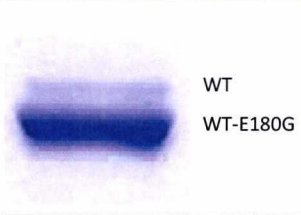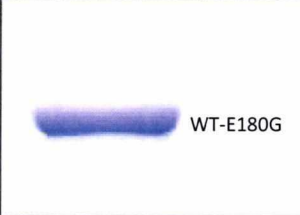
	Gravity column	Strep-Tactin sepharose	TALON®-Co
SDS gel used	10%	4-12 %	4-12 %
Purity check 4 -12 % SDS-PAGE gel Non-reducing	WT WT-E180G E180G	WT WT-E180G	WT-E180G
Starting weight of tagged/non-tagged Tm (mg)	6/18	12/48	14/56
Yield of digested Tm heterodimers (mg)	0.6 mg	2 mg	> 6 mg
Yield of digested Tm heterodimers (%)	10 %	~17 %	~43 %
Final concentration of Tm heterodimers	5 – 10 µM	20 – 45 µM	50 – 100 µM

Figure 3.3.3 Summary of Tm heterodimers purifications using various affinity resins. The purity of Tm heterodimers acquired by Co-TALON purification determined by gel denditometry was >96 %.

Rat skeletal αTm isoforms				
	Monomer mass		Dimer mass	
	Predicted	Measured	Predicted	Measured
WT-Tm	32838.7	32838.2 (-0.5 Da)	65675.4	65675.1 (+0.3 Da)
His WT-Tm	34548.5	34548.4 (-0.1 Da)	69095.0	69097.0 (+2.0 Da)
WT-D175N-Tm	-	-	65674.4	65674.4
D175N-Tm	32837.7	32836.9 (-0.8 Da)	65673.4	65673.4
WT-E180G-Tm	-	-	65603.3	65603.4 (+0.1 Da)
E180G-Tm	32766.6		65531.2	65531.6 (+0.4 Da)

Human skeletal αTm isoforms				
	Predicted		Measured	
	Predicted	Measured	Predicted	Measured
WT-Tm	32866.7	32866.6 (-0.1 Da)	65731.4	65731.6 (-0.2 Da)
His WT-Tm	34576.6	34576.6	69151.2	-
WT-E40K-Tm	~32866.2	32866.1 (-0.1 Da)*	65730.4	65732.7 (+ 2.3 Da)
E40K-Tm	32865.7	32866.3 (+0.6 Da)	65729.4	65729.7 (+0.3 Da)
WT-E54K-Tm	~32866.2	32866.1 (-0.1 Da)*	65730.4	65731.2 (+0.8 Da)
E54K-Tm	32865.7	32865.5 (+0.2 Da)	65729.4	65730.4 (+1.0 Da)
WT-D230N-Tm	~32866.2	32866.0 (-0.2 Da)*	65730.4	65731.6 (+1.2 Da)
D230N-Tm	32865.7	32865.7	65729.4	65730.1 (+0.7 Da)

Table 3.1 Molecular mass of human and rat Tm homo- and heterodimers carrying HCM and DCM mutations. Mass spectroscopy analysis of all constructs showed that measured data were in agreement with estimated values of respective Tm constructs. The difference between predicted and estimated value is indicated in brackets. Note that the rat and human Tm isoforms were used in HCM and DCM constructs, respectively. * indicates the estimated value of the non-cross-linked WT-E40K, WT-E54K and WT-D230N DCM heterodimer samples as they split into the monomers giving the value of the WT and mutant monomers mixture in a ratio of 1 : 1. Predicted value for these samples is an average between the WT and mutant homodimer.

3.4 Discussion

The method for assembly and purification of defined skeletal Tm heterodimers carrying cardiomyopathy mutations in only one chain was optimised. The optimisation resulted in over 10-fold increased amount of the final product with a high purity. The increased yield and purity of proteins were achieved by controlled conditions during the purification process by using FPLC connected to a 25 ml TALON® Metal Affinity column.

The described method was used for the formation of Tm heterodimers carrying HCM and DCM mutations. However, the method can be potentially also used for the formation of Tm heterodimers using other isoforms and such as skeletal and smooth muscle Tm-isoforms, cardiac κ-Tm isoform or cytoskeletal HMW Tm isoforms.

Chapter 4

Characterisation of the striated muscle α-Tm heterodimers carrying one copy of the HCM mutations D175N or E180G

4.1 Introduction

The biochemical and biophysical properties of α-Tm homodimers carrying HCM mutations have been intensively studied and are well established *in vitro* (Bai et al., 2011; Bing et al., 2000; Boussouf et al., 2007; Golitsina et al., 1999; Hilario et al., 2004; Kremneva et al., 2004; Ly and Lehrer, 2012; Mathur et al., 2011). However, affected individuals with heterozygous background are likely to express a mixture of both α*α*-Tm homodimers and αα*-Tm heterodimers (* for mutation). Predicted ratio of Tm dimers in heterozygotes could be 1 : 2 : 1 for αα, αα* and α*α*, respectively, making heterodimers predominant species. Therefore for the characterisation of αα*-Tm heterodimers it is important to understand the consequences of the mutations for cardiac function as the properties of Tm heterodimers may be different of those of either WT or α*α*-Tm homodimers. Our prediction of the ratio between Tm homo and heterodimers *in vivo* is based on the theoretical ratio between two different proteins interacting without binding preferences. The rationale for this prediction was based partially on the results from our *in vitro* experiments where the interactions between WT and the mutant Tm's resulted in a predicted ratio 1 : 2 : 1 for αα, αα* and α*α*, respectively (Figure 3.2.3 C). Furthermore, previous studies which demonstrated 50 % mutant Tm expression *in vivo* (Bottinelli et al.,

1998) and the preferential formation of smooth and striated αβ-Tm heterodimers *in vitro* (Janco et al., 2013; Lehrer and Qian, 1990; Lehrer and Stafford, 1991) supported our predictions.

The two widely studied HCM Tm mutations, D175N and E180G, were selected and used in the following study. Both mutations are located in the highly conserved period 5 of the Tm molecule (Hitchcock-DeGregori et al., 2002). Aspartic acid residue 175 is found within the heptad at position *g* and glutamic acid residue 180 is at position *e* both providing inter- and intra-helical stability for the α-helix as well as the coiled-coil structures. Negatively charged Asp175 can form salt bridge with positively charged Arg178 (i+3) in the same chain however there are repulsive interactions with negatively charged Glu173 at the position *e'* in the opposite chain of the coiled-coil. Negatively charged Glu180 can form salt bridge with positively charged Arg182 at position *g'* in the opposite chain but the intra-helical stability can be decreased by repulsive interactions with negatively charged residues Glu177 (i+3) and Glu184 (i+4). The substitution of the negatively charged residues Asp175 and Glu180 for polar uncharged Asn and Gly, respectively, might cause destabilisation of described interactions within the α-helix and the coiled-coil affecting thermal stability or the binding to the partner proteins, actin and Tn.

Tm heterodimers carrying HCM cardiomyopathy mutations D175N or E180G were formed by the method described in chapter 3 and characterised using various biochemical and biophysical assays. The properties examined were thermal stability, flexibility, actin affinity, Ca^{2+} regulation of myosin subfragment 1 (S1) binding, and Ca^{2+} regulation of myofibril force. Note that the measurements of flexibility and Ca^{2+} regulation of myofibril force were made by collaborating groups lead by Prof William Lehman (USA, Boston), and Prof Corrado Poggesi and Prof Ciara Tesi (Italy, Florence). We provided protein samples for the measurements and the brief overview of the results is included in this chapter.

The results demonstrate that both D175N- and E180G-Tm readily form αα*-Tm heterodimers. WT-D175N-Tm heterodimer did not show any changes in apparent affinity for actin while WT-E180G-Tm heterodimer showed an intermediate decrease between WT- and E180G-Tm homodimers. Thermal stability of the Tm heterodimers using circular dichroism showed no difference between WT-D175N-Tm heterodimer and WT- or D175N-Tm homodimers in both cross-linked and reduced dimers. Thermal stability of the other heterodimer showed an intermediate decrease at lower temperatures (~30 °C) between WT

and E180G-Tm homodimers when cross-linked. The reduction of the WT-E180G-Tm heterodimer resulted in the new thermal transition with significantly decreased stability compared to both homodimers. The calcium activation of the thin filament reconstituted *in vitro* with mutant Tms showed small changes to a lower calcium level required for the activation with measured values ranging between 0.08 and 0.14 pCa units. E180G-Tm homodimers showed the largest change in calcium sensitivity, and this result was confirmed by the measurements of the calcium dependent regulation of the force development in myofibrils. A previous study using an electron microscopy and molecular dynamic simulations showed that D175N- and E180G-Tm homodimers both caused a ~20 % reduction in persistence length of the protein indicating an increase in local and global bending flexibility (Li et al., 2012). The same approach used for the WT-D175N- and WT-E180G-Tm heterodimers showed no difference in the persistence length from their respective homodimers.

Both HCM mutations produced relatively small effects on the measured properties, but noticeably, the heterodimers did not always showed intermediate properties between the WT- and mutant homodimers. Summary and discussion of the results are included at the end of this chapter and in more detail in chapter 6.

4.2 Results

4.2.1 Effect of HCM mutations on thermal stability of tropomyosin homo- and heterodimers

The thermal stability of recombinant rat Tm heterodimers carrying D175N or E180G was measured by circular dichroism (CD) as described in section 2.3.1. The heterodimers were expressed, assembled and purified by the method described in chapter 3 and in Janco, et al., (2012). The secondary structure of the Tm proteins was assayed by CD at wavelengths covering the range from 250 to 190 nm (Figure 4.2.1). The measurements at low temperature (5 °C) showed one positive peak at 190 nm and two negative peaks at 208 and 222 nm, typical for alpha helical proteins. The spectra of the same sample measured at 65 °C showed severely decreased signal indicating unwound Tm molecules. Measurements were

carried out in 10 mM phosphate buffer (0.5836 g of $NaH_2PO_4 \cdot H_2O$ was mixed with 1.5466 g of $Na_2HPO_4 \cdot 7H_2O$ in a final volume of 1 l), 100 mM KCl pH 7 buffer and each measurement was repeated four times. 7 µM of a protein was loaded into a stoppered 1 mm cuvette (Starna Scientific Ltd.) and placed into a Jasco 715-Spectropolarimeter, UK (software: spectra management V1.51.00). Parameters for the spectra scans were: Sensitivity (Standard) 100 mdeg; start 250 nm; end 190 nm; data pitch 0.5 nm; scanning mode continuous; scanning speed 50 nm/min; response 1s; accumulation 4 (repeats). Figure 4.2.1 shows the spectra of the WT-Tm at 5 °C (black line) and 65 °C (red line). The measurement showed that Tm protein is an α-helix (correctly folded) and the highest negative wavelength at 222 nm was used for further experiments assessing the Tm thermal stability by tracking the occurrence of the protein secondary structure unfolding.
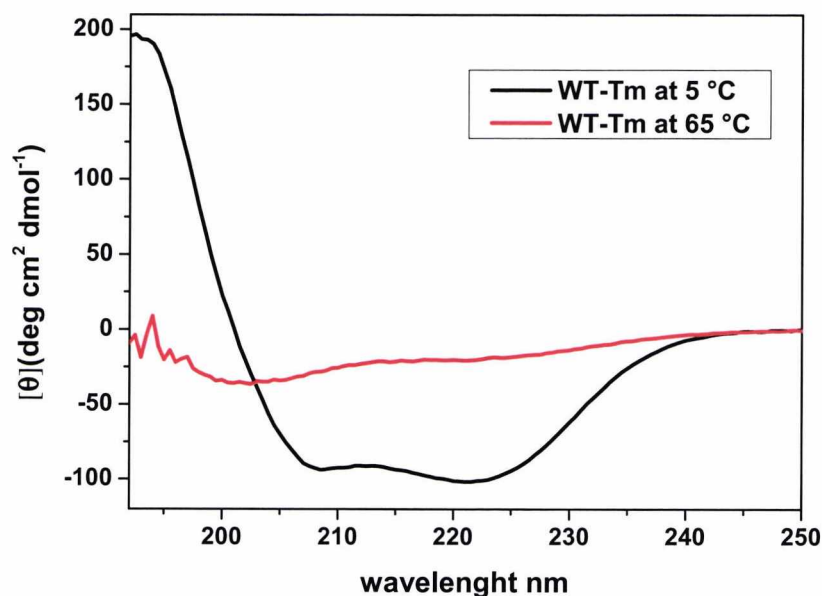
Figure 4.2.1. Circular dichroism spectra of WT-Tm at 5 and 65 °C. Concentration of measured Tm amples was 7 µM. Buffer conditions: 10 mM $KH_2 PO_4$, 100 mM KCl pH 7.

The crosslinked Tm proteins at 7 µM were heated over the range of 5 – 65 °C. The unfolding of cross-linked and reduced proteins was examined by CD at fixed wavelength 222 nm and heating rate 1 °/min. After reaching 65 °C, the unfolded sample was cooled down to 5 °C. During the cooling process Tm molecule refolded into its previous α-helical structure. The reversibility of the unfolding-refolding process was assessed by multiple reheating of the Tm sample (total of seven times) directly after cooling from the previous temperature scan (Figure 4.2.2). The temperature scans were repeated three times without DTT.

After three heating cycles, 1 mM of DTT was added to disrupt the cross-link at cys190. After reduction of the sample (fourth run) the loss of stability was observed at lower temperatures between ~20 – 40 °C. The loss of stability in this region was comparable to the fully reduced proteins in the following cycles (Figure 4.2.2). At higher temperature ranging between 40 – 60 °C (depending on Tm sample) reduced Tm proteins showed typically increased thermal stability between fully reduced isotherms (run 5, 6 and 7) and cross-linked isotherms (runs 1, 2 and 3). Ploted data were normalised (Figure 4.2.2 B) and the melting curves of Tm heterodimers were compared to the WT and mutant homodimers. Raw data showed a small increase of CD signal at 65 ° C when reduced (Figure 4.2.2 A).
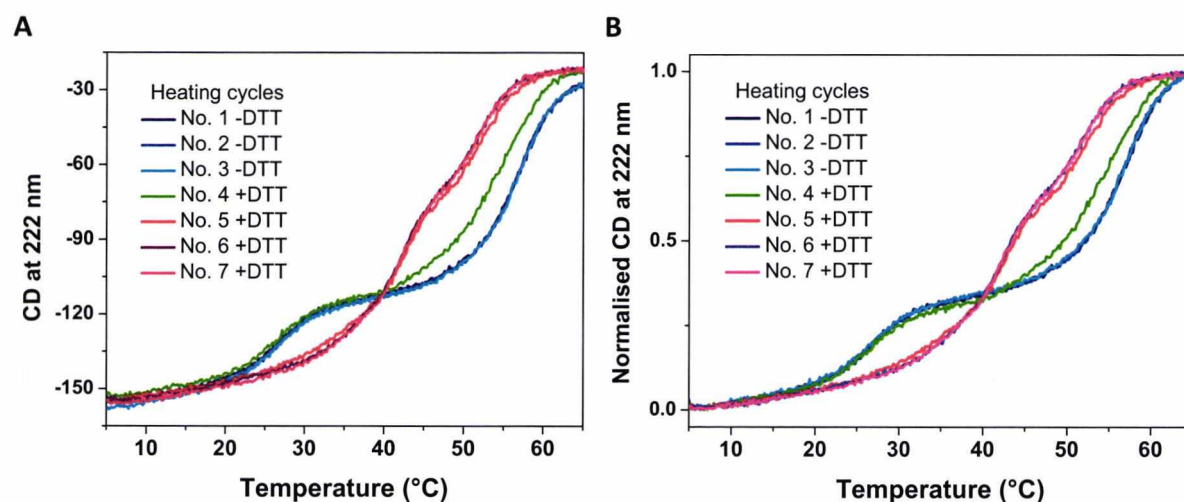
Figure 4.2.2. Reversibility of thermal unfolding of cross-linked, and reduced αTm dimers. (A) Raw data; (B) Normalised data. Seven heating cycles of E180G-Tm homodimer show similar unfolding isotherms when cross-linked (cycle 1, 2, and 3; dark blue, blue, and light blue line respectively) and reduced (cycle 5, 6 and 7; red, purple and magenta line, respectively). Lime green line is the first isotherm after addition of 1 mM DTT (fourth heating cycle) indicating transition between fully cross-linked and fully reduced Tm dimers. Buffer conditions: 0.5 M KCl, 20 mM potassium phosphate buffer, 5 mM MgCl$_2$, pH 7.0.

Figure 4.2.3 shows unfolding isotherms of cross-linked and reduced Tm homo- and heterodimers carrying D175N or E180G mutations. Three thermal transients were typically observed. The first thermal transition of cross-linked Tm proteins occurred at low temperatures ranging between 26 – 36 °C (depending on Tm sample). The major unfolding event was observed at ~57 °C. The first derivative of the data (Figure 4.2.4) resolved a third

smaller domain with a midpoint at ~49 °C. These three unfolding transients will be denoted in following sections as the first, the intermediate and the second unfolding events or thermal transients for clarity. Reduction of Tm decreased the stability of the whole molecule. The first transition occurred at higher temperature ~40 °C and the second unfolding event shifted to ~53 °C while the intermediate transition was unchanged at ~49 °C.

Figure 4.2.3 A shows the unfolding profile of the third heating cycle of the cross-linked WT-Tm homodimer superimposed on the unfolding profile of WT-D175N-Tm heterodimer and D175N-Tm homodimer. The unfolding profiles of these Tm dimers were almost identical and showed the first thermal transition at ~37 °C, the intermediate at ~49 °C and the second unfolding event occurred at ~57 °C.
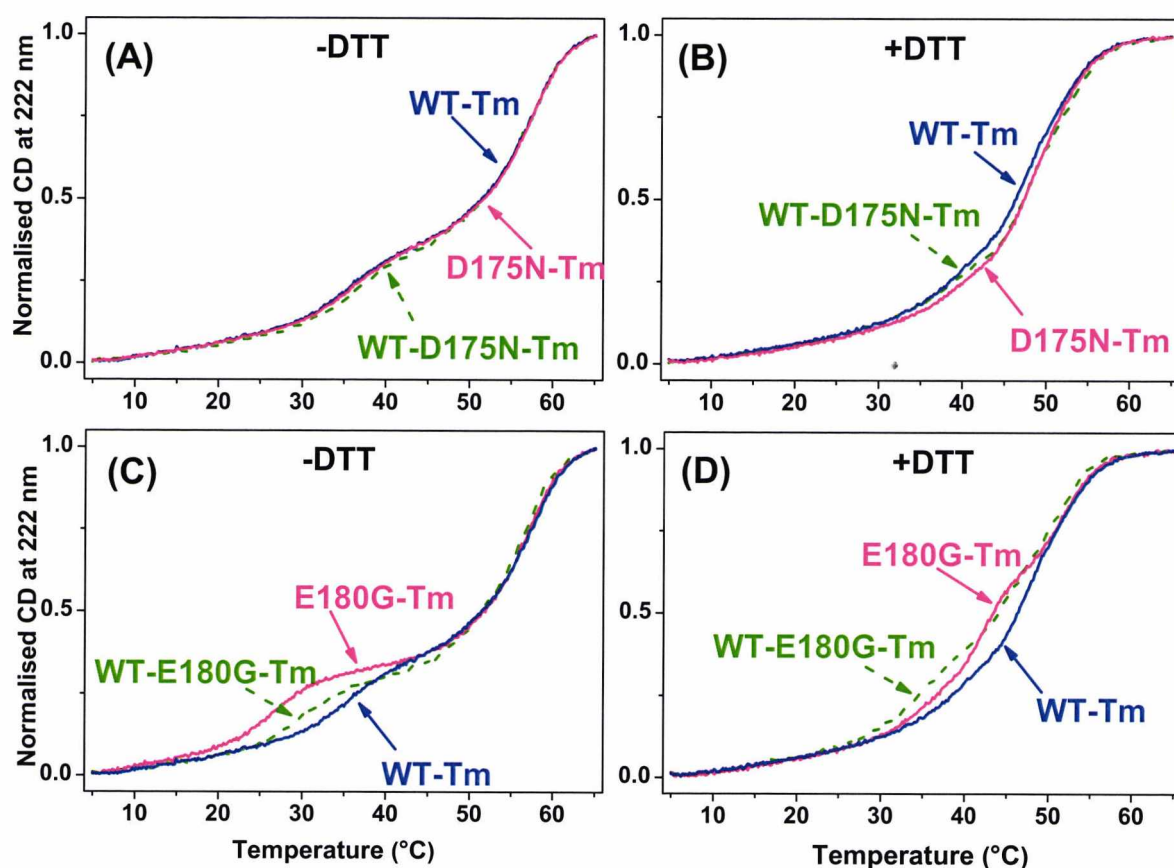
Figure 4.2.3 Thermal unfolding of α-Tm homo and heterodimers carrying D175N or E180G HCM mutations compared to WT-Tm. Normalised unfolding profiles of 7 µM α-WT (blue solid lines); α*α*-Tm homodimers (magenta solid lines) and αα*-Tm heterodimers (lime green dashed lines) of D175N (A & B) and E180G (C & D) in the presence (B & D) or absence (A & C) of 1 mM DTT. Buffer conditions: 0.5 M KCl, 20 mM potassium phosphate buffer, 5 mM MgCl$_2$, pH 7.0.

After reduction of the cross-link (Figure 4.2.3 B) at Cys190 by addition of 1 mM DTT, the WT-Tm showed a reduction in size of the first unfolding event at 37 °C. The intermediate unfolding event at ~49 °C was unchanged. The D175N-Tm homodimer was more stable than WT-Tm by ~1 °C, and the WT-D175N-Tm heterodimer was similar to the WT below 40 °C but closer to the D175N-Tm above 45 °C. The details of the changes occurring to the individual unfolding events are shown more clearly in the first differential of the data (Figure 4.2.4).
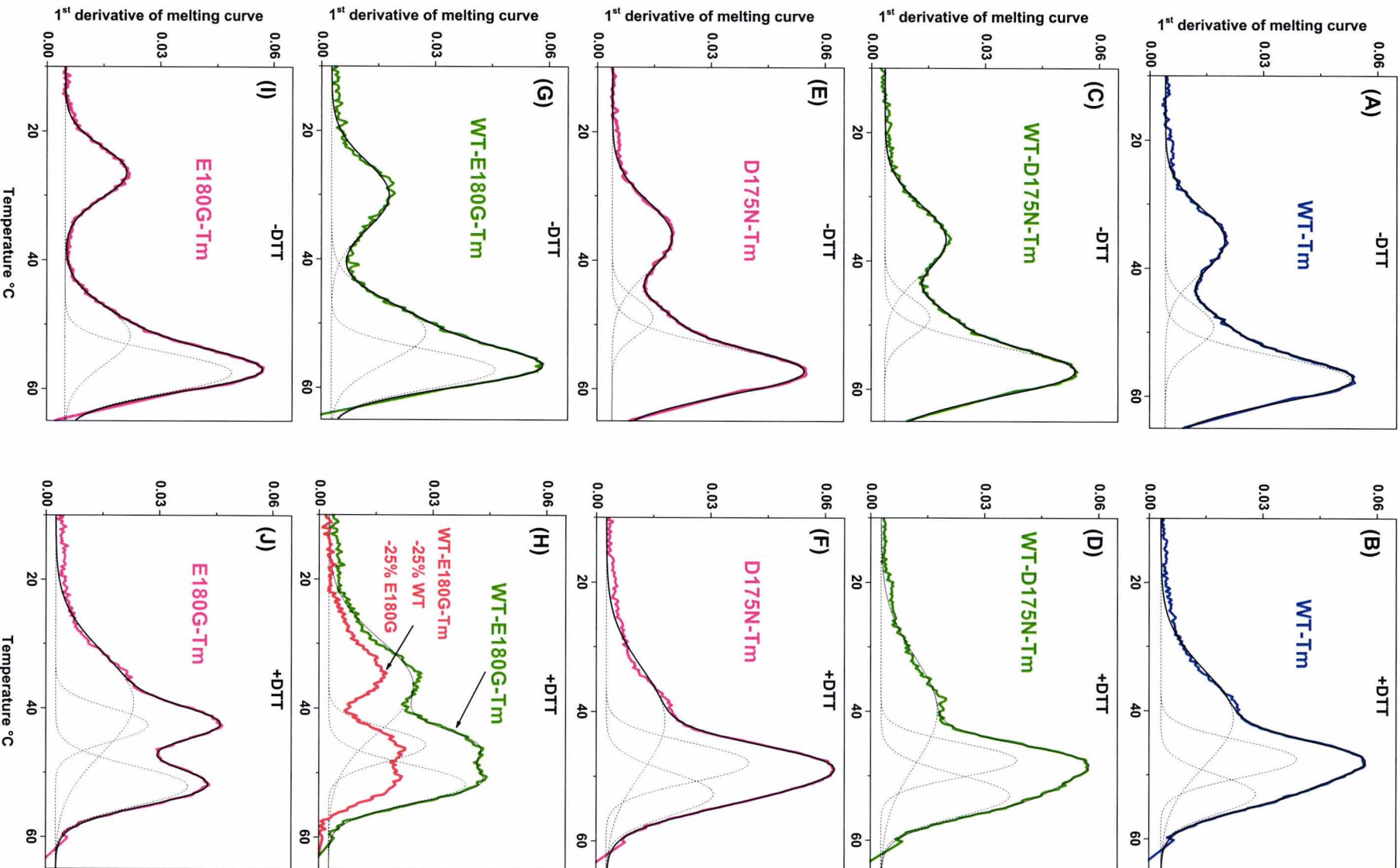
Figure 4.2.4 Thermal unfolding of skeletal α-Tm homo – and heterodimers carrying D175N or E180G HCM mutations. The data from each melting curve shown in Figure 4.2.3 was smoothed (Savitzky-Golay method; 50 points of window), differentiated with the best fit to Gaussian peaks superimposed (dotted line). A summary of the fitted data is shown in Table 4.1.

The data derived from the differentiated curves fitted to multiple Gaussian peaks is shown in Table 4.1 below. These include the fractional peak areas (a measure of the free energy change associated with each unfolding transition), the width of half peaks (measure of unfolding cooperativity) and the midpoints of unfolding transitions.

The unfolding profiles of the third heating cycle of cross-linked E180G-Tm homo- and heterodimers are shown in Figure 4.2.3 C. Thermal stability of the Tms carrying the mutation is significantly decreased at ~30 °C. The decrease in this part of the molecule is proportional to the number of mutations. The first thermal transition occurs at ~30 °C in E180G-Tm homodimer, at ~35 °C in WT-E180G-Tm heterodimer, and at ~40 °C in WT-Tm. Unfolding profiles of all three Tm constructs are identical above 45 °C. Reduction of the cross-link causes decrease of thermal stability in both Tm dimers carrying the mutation over the range of 30 – 50 °C, compared to WT-Tm (Figure 4.2.3 D). The E180G-Tm homodimer showed a new thermal transition at ~ 42 °C, and thermal stability of the WT-E180-Tm heterodimer was significantly decreased at lower temperatures over the range of ~28 – 40 °C, compared with E180G-Tm homodimer. The first differential of the data for the WT-E180G-Tm heterodimers in the presence and absence of 1 mM DTT are shown in figures 4.2.4 G and H, respectively.

It is important to mention that both WT-D175N- and WT-E180G-Tm heterodimers under reducing conditions will reanneal into a mixture of αα-, αα*-, α*α*-Tm dimers (* stands for mutation) in a ratio of 1 : 2 : 1 (Section 3.2; Figure 3.2.3 C). In the case of WT-D175N-Tm, this has little consequence as all dimers have similar unfolding characteristics.

This complicates the interpretation for the WT-E180G-Tm heterodimer as the unfolding profile differs from those of WT and E180G. The unfolding transitions for the WT-E180G-Tm heterodimer were estimated by subtracting 25 % of the expected transitions for WT and E180G homodimers (the expected proportion after reannealing). The error on such a process is large but it indicates the underlying properties and is shown as a thick red line in Figure 4.2.4 H. The substraction of predicted proportion of homodimers does not alter the

positions of the three transitions but does alter their relative proportions where the area of all three transitions is reduced by 55 %. Data shown in Table 4.1 were plotted into bar graphs for clarity and are shown in Figure 4.2.5.

Tm dimers	Peak	Cross-linked Tm (-DTT)			Reduced Tm (+DTT)		
		Fractional Peak area (%)	Width of half peak (°C)	Peak midpoint (°C)	Fractional Peak area (%)	Width of half peak (°C)	Peak midpoint (°C)
WT-Tm	1	26.2 ± 0.5	10.1 ± 0.2	35.7 ± 0.1	44.7 ± 4.2	14.8 ± 0.9	41.2 ± 0.7
	M	14.4 ± 1.5	6.8 ± 0.4	49.1 ± 0.3	31.7 ± 4.7	5.6 ± 0.3	47.5 ± 0.3
	2	59.3 ± 1.3	7.3 ± 0.1	57.4 ± 0.1	23.6 ± 4.2	6.0 ± 0.4	53.1 ± 0.5
WT-D175N-Tm	1	27.3 ± 0.5	10.7 ± 0.2	36.7 ± 0.1	38.0 ± 3.2	16.7 ± 1.0	40.0 ± 0.7
	M	11.2 ± 0.9	6.0 ± 0.3	48.8 ± 0.2	28.4 ± 3.4	5.2 ± 0.2	47.5 ± 0.2
	2	61.5 ± 0.8	7.8 ± 0.1	57.2 ± 0.2	33.6 ± 3.3	6.4 ± 0.3	53.0 ± 0.3
D175N-Tm	1	28.0 ± 0.5	10.8 ± 0.2	36.3 ± 0.1	37.6 ± 4.5	16.1 ± 1.2	41.3 ± 1.0
	M	10.1 ± 0.7	5.7 ± 0.3	48.9 ± 0.1	34.1 ± 11.4	6.0 ± 0.4	47.9 ± 0.6
	2	61.9 ± 0.7	7.5 ± 0.1	57.2 ± 0.04	28.3 ± 11.8	6.6 ± 0.8	52.7 ± 1.1
WT-E180G-Tm	1	24.7 ± 0.7	10.6 ± 0.3	30.1 ± 0.1	47.6 ± 1.9	14.1 ± 0.5	36.4 ± 0.3
	M	35.6 ± 7.5	9.3 ± 1.0	51.3 ± 1.0	19.8 ± 2.7	5.1 ± 0.3	45.7 ± 0.2
	2	39.7 ± 7.2	6.0 ± 0.3	57.1 ± 0.1	32.5 ± 1.9	5.9 ± 0.2	51.7 ± 0.2
E180G-Tm	1	22.9 ± 0.3	7.9 ± 0.1	26.4 ± 0.04	48.3 ± 8.0	15.4 ± 1.2	39.1 ± 1.3
	M	27.7 ± 5.0	9.0 ± 0.7	51.8 ± 0.8	19.2 ± 3.4	5.2 ± 0.3	42.6 ± 0.1
	2	49.4 ± 4.8	6.3 ± 0.1	57.4 ± 0.1	32.6 ± 3.9	6.2 ± 0.3	52.1 ± 0.1

Table 4.1 Thermal unfolding of cross-linked and reduced α-Tm dimers with HCM mutations. Data from the multiple Gaussian fits shown in Figure 4.2.4. The fractional peak areas represent a measure of the free energy change associated with each unfolding transition and are expressed in % of the total. The width of half peaks is a measure of unfolding cooperativity and peak midpoints indicate occurrence of individual thermal transitions, both are given in °C. Three thermal transitions observed in our experiments were denoted in the text as the first (peak 1), the second (peak 2), and the intermediate (peak M). All the data are shown with their respective standard errors and represents an average of at least two measurements (n≥2). All the numerical values of this table are plotted to the bar graphs in Figure 4.2.5.
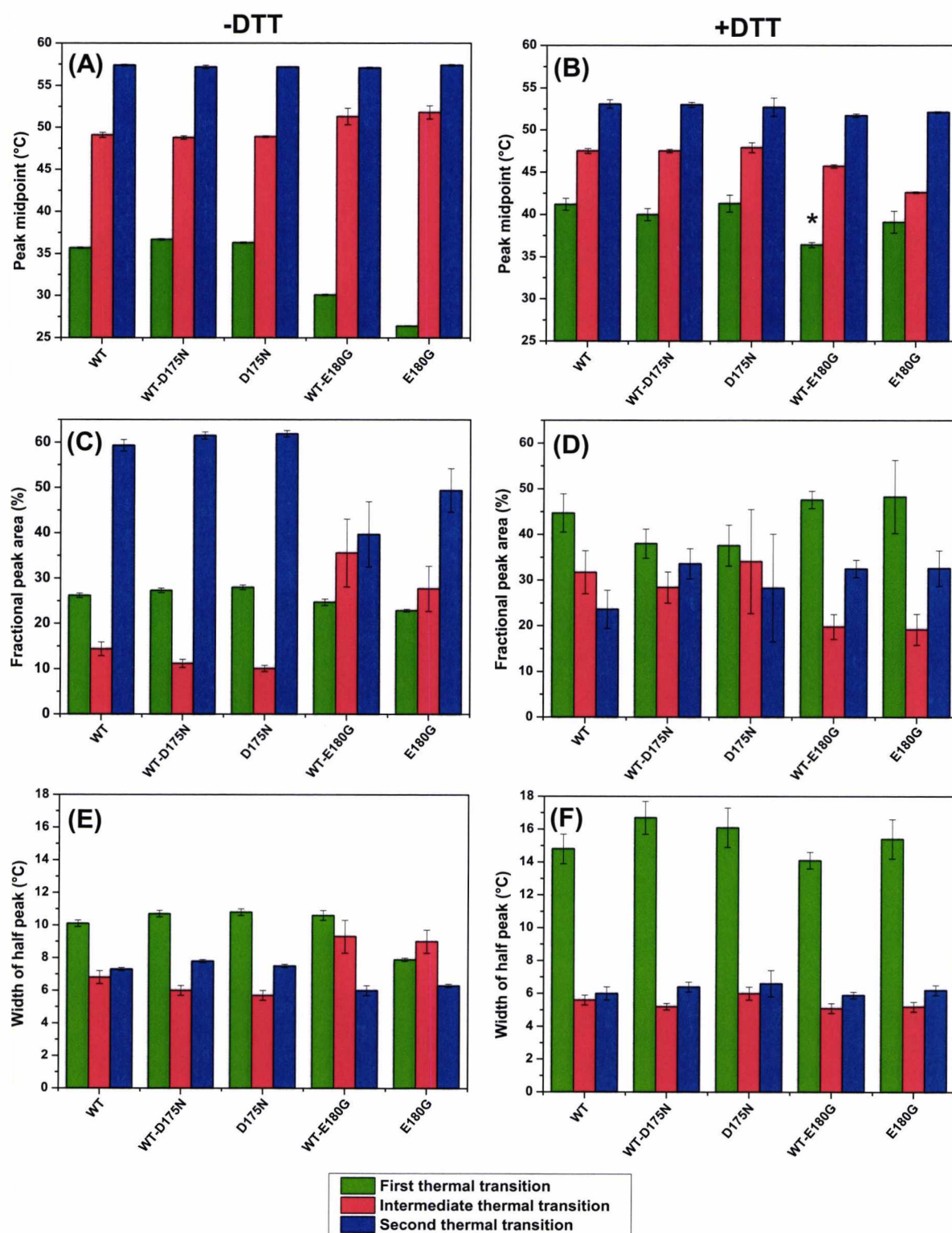
Figure 4.2.5 Thermal unfolding of skeletal αTm homo- and heterodimers carrying HCM mutations D175N or E180G. The graphs are plotted data from Table 4.1. Panels A and B represents fitted peak midpoints (°C) of the three thermal transitions with and without cross-link, respectively. Panels C and D show the fractional peak area (%), and panels E and F show the width of half peak (°C) of the same thermal transitions with or without cross-link, respectively. * indicates possible effect at physiological level.

4.2.2 Actin binding of cross-linked tropomyosin dimers carrying one or two copies of HCM mutation

The binding of recombinant skeletal WT-D175N-Tm and WT-E180G-Tm heterodimers to F-actin were measured using co-sedimentation assays (see chapter 2, section 2.3.2.2). The Tm binds and saturates F-actin filament in a ratio of 7 : 1 (actin : Tm, respectively).

Figure 4.2.6 A shows the SDS-PAGE analysis of the supernatant and pellets of 7 μM actin centrifuged with 0.2 – 2.4 μM WT-D175N-Tm after 1 hour incubation at 20 °C. The gel loaded with fractions containing pellets shows that majority of the actin sediments with a small fraction, probably G actin, remaining in the supernatant. Note that the 10 % gel used in co-sedimentation assays under reducing conditions resolves the WT and D175N Tm monomers. The close similarity of density of the two bands is consistent with pure heterodimer where the ratio of the WT and mutant monomers is 1 : 1.
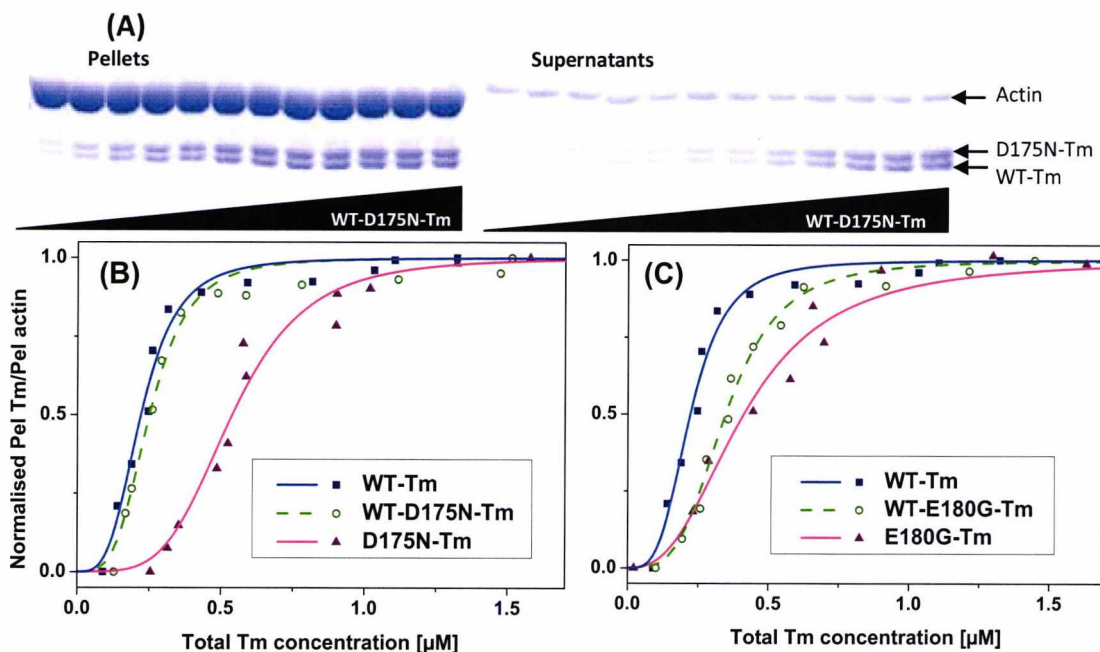
Figure 4.2.6 The affinity of Tm for actin determined by co-sedimentation analysis. Actin (7 μM) incubated with 0.2 - 2.4 μM of Tm dimers at 20°C for 1 hour and then centrifuged at 100,000 rpm. (A) F-actin and Tm fractions from the pellet and supernatant were loaded onto 10 % SDS gels and analysed by densitometry. (B & C) Fractional saturation of actin by Tm plotted as a function of free Tm concentration for (B) WT-Tm (■), WT-D175N-Tm (o) and D175N-Tm (▲) and for (C) WT-Tm (■), WT-E180G-Tm (o) and E180G-Tm (▲) Tm. The best fit to the Hill equation is superimposed on the

plotted data. The actin affinity ($K_{50\%}$) and the Hill coefficient (h) are presented in Table 4.2. Buffer conditions: 100 mM KCl, 20 mM MOPS, 5 mM $MgCl_2$ pH 7.0.

The sigmoid binding curves of WT and D175N Tm constructs to F-actin are shown in Figure 4.2.6 B. Measured data demonstrates the expected polymerising of Tm dimers on the actin surface. Fitting the data to the Hill equation gives an estimate of the Tm affinity ($K_{50\%}$) for F-actin. The apparent affinity ($K_{50\%}$) of WT-D175N-Tm heterodimer for actin (0.23 µM) was indistinguishable from WT-Tm, but tighter in comparison to D175N-Tm homodimer (0.52 µM, p ≤ 0.05). These measurements indicate that the introduction of D175N mutation in only one Tm chain does not have any effect on binding to actin.

Figure 4.2.6 C shows the binding curves of WT and E180G-Tm constructs to F-actin. The affinity of the E180G-Tm homodimer was significantly weaker (0.42 µM, p ≤ 0.05) compared to the WT (0.20 µM) with the heterodimer at an intermediate value (0.27 µM, p ≤ 0.05). The obtained $K_{50\%}$ values for both HCM Tm homodimers are consistent with previously published data (Kremneva et al., 2004). The Hill coefficients showed similar values (2.1 -2.8) for all Tm constructs indicating unchanged apparent cooperativity of HCM mutants to F-actin. The summary of measured data of the actin affinity ($K_{50\%}$) and the Hill coefficient (h) are presented in Table 4.2 below.

Tm dimers	$K_{50\%}$ (µM)	h
WT-Tm	0.20 ± 0.02	2.5 ± 0.8
WT-D175N-Tm	0.23 ± 0.05[†]	2.5 ± 0.5
D175N-Tm	0.52 ± 0.15**	2.8 ± 0.1
WT-E180G-Tm	0.27 ± 0.03*	2.1 ± 0.5
E180G-Tm	0.42 ± 0.12*[$]	2.2 ± 0.4

Table 4.2 The affinity and the binding cooperativity of HCM Tm dimers for F-actin. The actin binding affinity ($K_{50\%}$) and the Hill coefficient (h), both derived for the fit of the Hill equation to data of Figure 4.2.5 B & C. The data represents an average of at least four measurements (n≥4) with given SD values.

* Values differ compared to WT-Tm (*p ≤ 0.05, ** p ≤ 0.01)

$ Values differ compared to WT-E180G-Tm heterodimer p ≤ 0.05

† Values differ compared to WT-D175N-Tm heterodimer p ≤ 0.01

4.2.3 Changes in Ca^{2+} sensitivity of myosin subfragment 1 binding to reconstituted thin filaments caused by HCM mutations on tropomyosin

The calcium dependent occupancy of the blocked state of the thin filament (McKillop and Geeves, 1993) was evaluated by the following stopped flow experiments. All the concentrations used in this section are after mixing unless stated otherwise. Firstly, the activity of reconstituted thin filaments was assayed by mixing 0.25 µM of S1 in the absence and the presence of calcium with a 10-fold excess of pyrene F-actin, WT-Tm and increasing concentrations of hcTn (see chapter2, section 2.3.3.4). The saturation of the thin filament by hcTn was typically reached at ~1 µM with a k_{obs} = 2.0 s^{-1} in the absence of calcium. The same reaction in the presence of calcium increased k_{obs} 3.5-fold to 7.0 s^{-1}, close to the value in the absence of hcTn (8.0 s^{-1}). The proteins with sufficient activity criterion were then used for the formation of the thin filaments reconstituted with pyr-actin, hcTn and αTm carrying a HCM mutation (D175N or E180G) in one or both chains of the Tm dimer. The thin filament proteins were mixed in a ratio of 7 : 2 : 2 for pyrene F-actin, Tm (dimers) and hcTn, respectively. A 10-fold excess of F-actin (2.5 µM) containing corresponding ratios of various Tm constructs and hcTn was rapidly mixed with 0.25 µM of S1 at 20 °C. The set of observed pyrene actin fluorescence transients with each Tm construct in the absence (pCa 8.9) and presence of calcium (pCa 4.6) is shown in Figure 4.2.7. Observed transients were individually fitted to a single exponential and for the WT-Tm the k_{obs} values were 7.68 s^{-1} and k_{obs} = 2.21 s^{-1}, respectively giving the ratio the two values of 3.5 which is in a good agreement with previous measurements for hcTn (Maytum et al., 2003). The decrease in observed rate constant in the absence of calcium (pCa 9.8) has been interpreted as due to a fraction of the unavailable actin sites and the ratio of rate constants in the presence and the absence of calcium $k_{obs}(-Ca^{2+})/k_{obs}(+Ca^{2+})$ = $K_B/(1+K_B)$ where K_B is the equilibrium constant between actin·Tm·Tn complexes in the blocked and closed states. The k_{obs} and K_B values for Tm homo and heterodimers carrying D175n or E180G mutations in the presence and absence of calcium are shown in Table 4.3 below. The values of K_B calculated from the measured data indicate that K_B is independent of the mutations as shown previously for D175N and E180G-Tm homodimers (Boussouf et al., 2007).
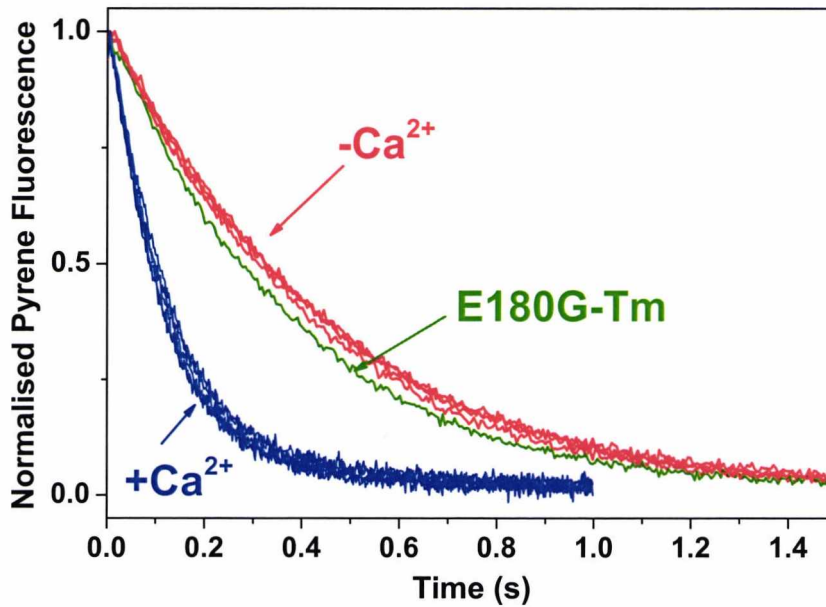
Figure 4.2.7 S1 binding to an excess of reconstituted thin filaments with pyrene-actin·αTm·hcTn in the presence and absence of calcium. Transients of S1 binding to the thin filaments containing WT-, WT-D175N-, D175N-, WT-E180G- and E180G-Tm homo- and heterodimers are shown in the presence (blue lines) or absence (red lines) of calcium. The E180G-Tm (green line) in the presence of Ca^{2+} showed small variation. The best fit single exponential k_{obs} values are shown in Table 4.3. Experimental conditions: 100 mM KCl, 20 mM MOPS, 5 mM $MgCl_2$ pH 7.0 with addition of 2 mM EGTA or 2 mM Ca-EGTA.

The Ca^{2+} sensitivity of the thin filaments containing the various Tm dimers with HCM mutations was measured by stopped flow as described in chapter 2, section 2.3.3.5 and Boussouf et al., (2007). A 10-fold excess of S1 binding to thin filaments was chosen for the experiment due to the limited yields of αα* Tm heterodimers. Thin filament proteins (0.25 μM pyr-actin, 0.1 μM hcTn and 0.1 μM αTm) were pre-incubated for 1 hour at 4 °C and then rapidly mixed with 2.5 μM of S1 over a range of calcium concentrations. Figure 4.2.8 A shows the set of observed sigmoid transients at different calcium concentrations (pCa from 4.6 to 9.8) with thin filaments containing WT-D175N-Tm, as an example. Decrease of pyrene fluorescence signal is caused by S1 binding to the thin filament and the shift between observed sigmoid transients is caused by the presence of calcium at defined concentration (the calculations of pCa concentrations are described in chapter 2, section 2.3.3.5). Observed transients at low Ca^{2+} concentration showed small lag phase caused by Tm molecules occupying actin binding sites.
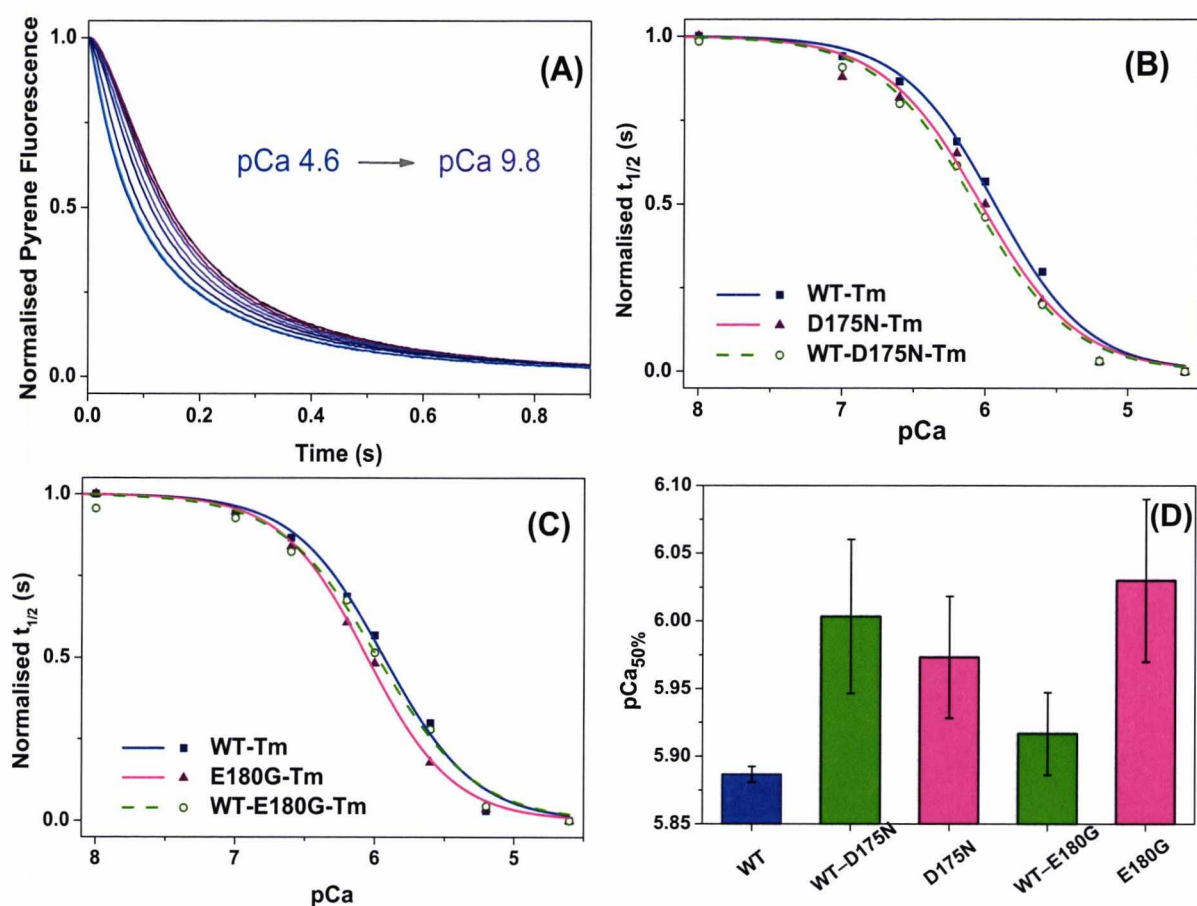
Figure 4.2.8 Dependence of the observed transient of S1 binding to pyrene-actin·sk Tm·hcTn on calcium concentrations. (A) Transients observed for 10-fold excess of S1 rapidly mixed with pre-incubated pyrene-actin αTm·hcTn (0.25 μM ppA, 0.1 μM WT-D175N-Tm and 0.1 μM hcTn) at various calcium concentrations. The fractional half time ($t_{1/2}$) is plotted against pCa concentrations. Data for WT-Tm (■), WT-D175N-Tm (o) and D175N-Tm (▲) are shown in (B) and WT-Tm (■), WT-E180G-Tm (o) and E180G-Tm (▲) are shown in (C). The best fit to the Hill equation is superimposed with midpoints (pCa$_{50\%}$) and Hill coefficients (h) presented in Table 4.3. Each curve in panels A, B and C represent one set of measurements. (D) Comparison of measured values of pCa$_{50\%}$ for the five Tm constructs, including standard deviation. Each column represents an average of three measurements with separate Tm samples (n=3). Experimental conditions: 100 mM KCl, 20 mM MOPS, 5 mM MgCl$_2$, 1 mM DTT pH 7.0 with addition of 2 mM pCa buffers at various calcium concentrations.

The half time of the reaction ($t_{1/2}$) derived from the measured sigmoid transients was plotted against pCa concentration. The data for WT-D175N and WT-E180G-Tm heterodimers with the best fit to the Hill equation superimposed are shown in Figure 4.2.8 B and C, respectively. The figures also show the data for the WT and the mutant homodimers for comparison. The best fit of the Hill model to the data resulted in the sigmoid curve. The

midpoint of the fitted sigmoid curve ($K_{50\%}$) for the mutants compared to the WT is an indication of a change in the calcium sensitivity and the Hill coefficient (h) derived from the Hill fit is a measure of the cooperativity of the system. Measurements for each Tm were repeated three times using two independent samples of Tm combined with two independent samples of hcTn. As the differences between measured values of $K_{50\%}$ for individual Tm constructs are relatively small, a bar graph was used for comparison of the final results (Figure 4.2.8 D). Numerical values of all the mid-points ($pCa_{50\%}$) of the calcium induced change in $t_{1/2}$ and Hill coefficients derived from the fit to the Hill equation are listed in Table 4.3.

Tm dimers	$pCa_{50\%}$	h	k_{obs} (s^{-1})	k_{obs} (s^{-1})	K_B
			$-Ca^{2+}$	$+Ca^{2+}$	
WT-Tm	5.89 ±0.01	1.23 ± 0.03	2.21 ± 0.07	7.68 ± 0.18	0.40
WT-D175N-Tm	6.00 ±0.06*	1.20 ± 0.11	2.31 ± 0.01	8.00 ± 0.14	0.40
D175N-Tm	5.97 ± 0.05*	1.24 ± 0.03	2.41 ± 0.06	8.48 ± 0.07	0.41
WT-E180G-Tm	5.92 ± 0.03	1.20 ± 0.09	2.31 ± 0.04	7.58 ± 0.14	0.47
E180G-Tm	6.03 ± 0.06*†	1.24 ± 0.12	2.71 ± 0.07	8.46 ± 0.16	0.44

Table 4.3 Calcium sensitivity of the thin filaments reconstituted with F-actin, hcTn and αTm carrying HCM mutations. The $pCa_{50\%}$ value is the apparent calcium affinity, and h is the Hill coefficient for calcium switching of the thin filaments, both derived from the best fit of the Hill equation to the data shown in Figure 4.2.7 B and C. All $pCa_{50\%}$ and h values are an average of three measurements using two independent samples of Tm combined with two independent samples of hcTn (n = 3). The k_{obs} values are the observed exponential rate constants of 0.25 µM S1 binding to 10-fold excess thin filaments (2.5 µM ppA, 1 µM hcTn and 1 µM αTm) in the presence and absence of calcium. The values of k_{obs} were derived from observed transients shown in Figure 4.2.6. The k_{obs} rate constants given are an average of two measurements with two independent Tm samples. The K_B is the equilibrium between blocked and closed states of the thin filament. K_B was calculated by using following equation: $k_{obs}(-Ca^{2+})/k_{obs}(+Ca^{2+})=K_B/(1+K_B)$.

* value differs compared to WT-Tm measured value ($p \leq 0.05$).

† value differs compared to WT-E180G-Tm heterodimer ($p \leq 0.05$)

The D175N and E180G-Tm homodimers increased calcium sensitivity of the thin filaments shifting the calcium sensitivity curve to the left (higher $pCa_{50\%}$ value than WT) by 0.086 and 0.143 pCa, respectively. The $pCa_{50\%}$ measurements of WT-D175N heterodimer also exhibit increased calcium sensitivity by 0.116 pCa higher than WT. However, WT-E180G-Tm homodimer did not significantly affect the calcium sensitivity as the measured value of $pCa_{50\%}$ was only 0.03 pCa higher than WT. The Hill coefficients in all HCM mutants did not show any significant changes in comparison to the WT.

Measured data fitted into the Hill plot contain information about estimated calcium sensitivity of the thin filament. However, the more precise description of complex processes occurring during the calcium dependent cooperative binding of S1 to actin filament (see scheme below) requires mathematical models.

$$A.TnI + TnC \xrightleftharpoons{\varepsilon^2\lambda} A + TnC.TnI$$

$$2\tilde{K}_c \Updownarrow \qquad\qquad \Updownarrow 2\hat{K}_g/\varepsilon$$

$$A.TnI + CaTnC \xrightleftharpoons{\varepsilon\lambda} A + CaTnC.TnI$$
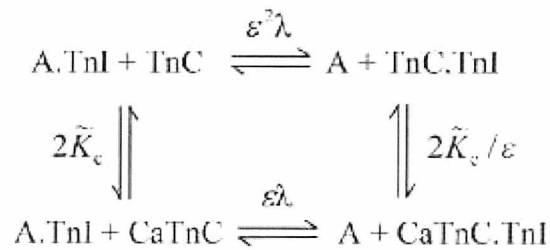
We applied a recently published Smith-Geeves chain model to our measured data (Geeves et al., 2011). Monte carlo simulations using the continuous – flexible regulatory chain model are shown in Figure 4.2.9. We show that the model can fit the measured data with reasonable precision however the fitting was made manually and needs to be refined (work in progress).
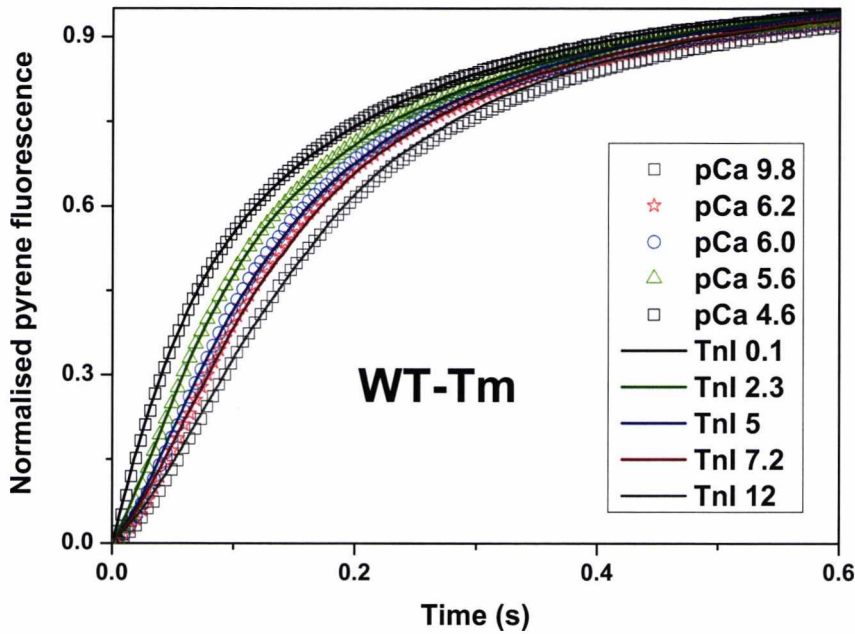
Figure 4.2.9 Monte carlo simulations using the continuous – flexible regulatory chain model (Smith – Geeves). Transients of S1 binding to the thin filaments containing WT-Tm at various calcium concentrations are shown as the data points (geometrical shapes) and the best fit to the model is superimposed to the data (lines).

4.2.4 Functional assay in myofibrils replaced for the endogenous Tm·Tn complex with HCM mutations on tropomyosin

The following experiments for the assessment of the thin filaments calcium sensitivity in rabbit psoas myofibrils containing replaced hcTn·Tm complex were performed by Dr Beatrice Scellini under supervision of Prof Chiara Tesi and Prof Corrado Poggesi, all from University of Florence, Italy. This was the part of collaborative project aiming for the characterisation of WT-D175N and WT-E180G-Tm heterodimers. The experiments with myofibrils were conducted in order to verify our findings from *in vitro* calcium sensitivity measurements and to test the effects of Tm heterodimers in the system closer to *in vivo* conditions. Only the E180G mutation was used in the experiments, based on *in vitro* findings showing the larger effect on calcium sensitivity in E180G-Tm compared to WT-D175N homodimer. The purified Tm constructs including WT, E180G, and WT-E180G-Tm proteins for this project were provided by our lab.

Single myofibrils or bundles of two to three myofibrils were prepared from muscle homogenisation of glycerinated rabbit psoas skeletal muscles, as described previously (Tesi et al., 1999). All solutions were kept at around 0 °C and contained a mixture of protease inhibitors including leupeptin (10 µM), pepstatin (5 µM), phenylmethylsulphonylfluoride (200 µM), E64 (10 µM), NaN$_3$ (500 µM), and DTT (0.5 mM). Endogenous Tm and Tn were replaced in rabbit skeletal muscle myofibrils with hcTn and αTm, as described previously (Scellini et al., 2010; Siththanandan et al., 2009). Tm constructs used for the replacement contained E180G mutation in one or both chains of Tm and the WT-Tm for comparison.

Briefly, myofibrils were washed (5 - 7 times) in a low ionic strength solution (2 mM Tris-HCl pH 8) to remove native Tm and Tn. Extracted myofibrils were then washed in 200 mM ionic strength rigor solution (100 mM KCl, 2 mM MgCl$_2$, 1 mM EGTA, 50 mM Tris·HCl pH 7) and reconstituted with exogenous αTm (5 µM) and hcTn (2 µM) in a 2-steps protocol (0 °C, 2 h incubation per step). Reconstituted myofibrils were washed and stored in 200 mM ionic strength rigor solution at 4 °C, and used within 4 days. At each stage of the protocol, samples were retained from both supernatant and pellet fractions and then used to determine the extent of the Tm-Tn extraction and replacement procedure by 12 % SDS-PAGE analysis (Scellini et al., 2010). SDS-PAGE analyses of samples of myofibrils show that Tm-Tn replacement was about 98 % complete (Figure 4.2.10).
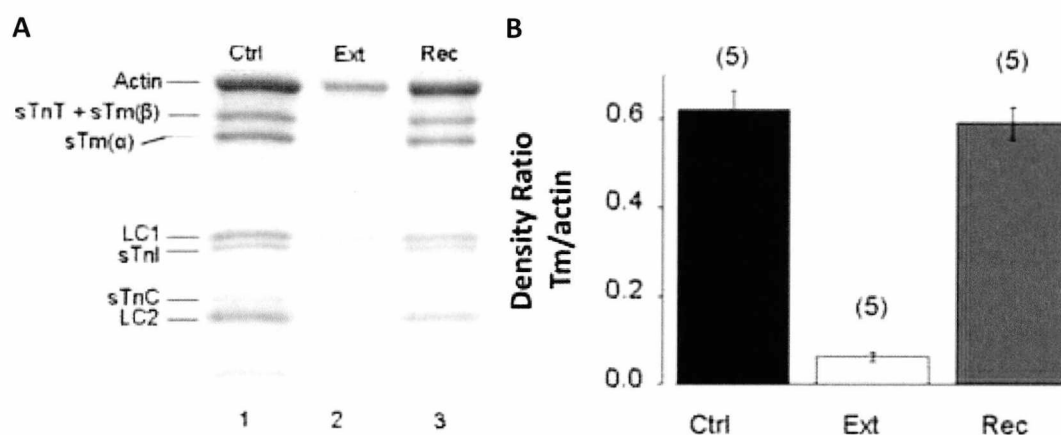
Figure 4.2.10 Extraction and reconstitution of recombinant Tm·Tn complex in rabbit skeletal myofibrils. (A) Analysis of myofilament proteins by SDS-PAGE analysis. Lanes 1 and 2, before and after removal of endogenous Tm·Tn complex, respectively; Lane 3, myofilament proteins after reconstitution. Proteins were stained by Coomassie-blue. (B) Densitometry analysis of the ratio of

the α-Tm to actin band intensities of correspondent gel lines (*Ctrl* control; *Ext* extracted; *Rec* reconstituted). n=5 Image modified from (Scellini et al., 2010).

Force recording was carried out as described previously (de Tombe et al., 2007). Small volume of the myofibril suspension was transferred to a temperature-controlled chamber (15 °C) filled with a relaxing solution (pCa 9.0) on an inverted microscope and mounted horizontally between two glass microtools. One microtool was connected to a length-control motor that could produce rapid (<1 ms) length changes. The second microtool was a calibrated cantilevered force probe (2–6 nm/nN; frequency response 2–5 kHz). Force was measured from the deflection of the image of the force probe projected on a split photodiode. Both the sarcomere length and myofibril diameter were measured from video images (1800X). Myofibrils were activated and relaxed by rapid translation of two continuous streams of relaxing (pCa 9) and activating (pCa 4.6) solutions flowing from a stepper motor controlled double-barrelled glass pipette placed within 0.5 – 1 mm of the preparation.

The maximal activated force (P_0), rate of force development (k_{ACT}), and the rate of force re-development (k_{TR}) following release-restretch protocols (Brenner, 1988) were measured at submaximal calcium concentration (pCa in the range 5.8 - 5.9) and then at saturating calcium concentration (pCa 4.5).

Activating and relaxing solutions were calculated as described previously (Tesi et al., 2002). The solutions were at pH 7 and contained 10 mM total EGTA (CaEGTA : EGTA ratio set to obtain the different pCa used for these experiments), 5 mM MgATP, 1 mM free Mg^{2+}, 10 mM creatine phosphate, 10 mM MOPS, propionate, and sulphate to adjust the final solution to an ionic strength of 200 mM and monovalent cation concentration of 155 mM. The concentration of contaminant inorganic phosphate (Pi) from spontaneous breakdown of MgATP and creatine phosphate was typically ~500 μM.

The presence of E180G mutation in Tm homo- and heterodimers did not show significant effects on the maximally activated force development (P_0) or the kinetics of its development (k_{ACT} and k_{TR}) as shown in Table 4.4. Interestingly, a clear effect was observed with E180G-Tm homodimer when tension development at submaximal calcium (pCa 5.8 - 5.9) was compared to the full activation at pCa 4.5. Myofibrils replaced with WT-E180G-Tm heterodimer did not significantly differ from control WT-Tm while the presence of the

E180G-Tm homodimer significantly increased tension (i.e. thin filament activation) at low calcium concentrations (see Figure 4.2.10 and Table 4.4). The differential effect between Tm mutant homodimers and heterodimers on submaximal calcium activated force was clear even though for the WT-E180G-Tm heterodimers the comparison was made at only one submaximal calcium concentration (pCa 5.85).
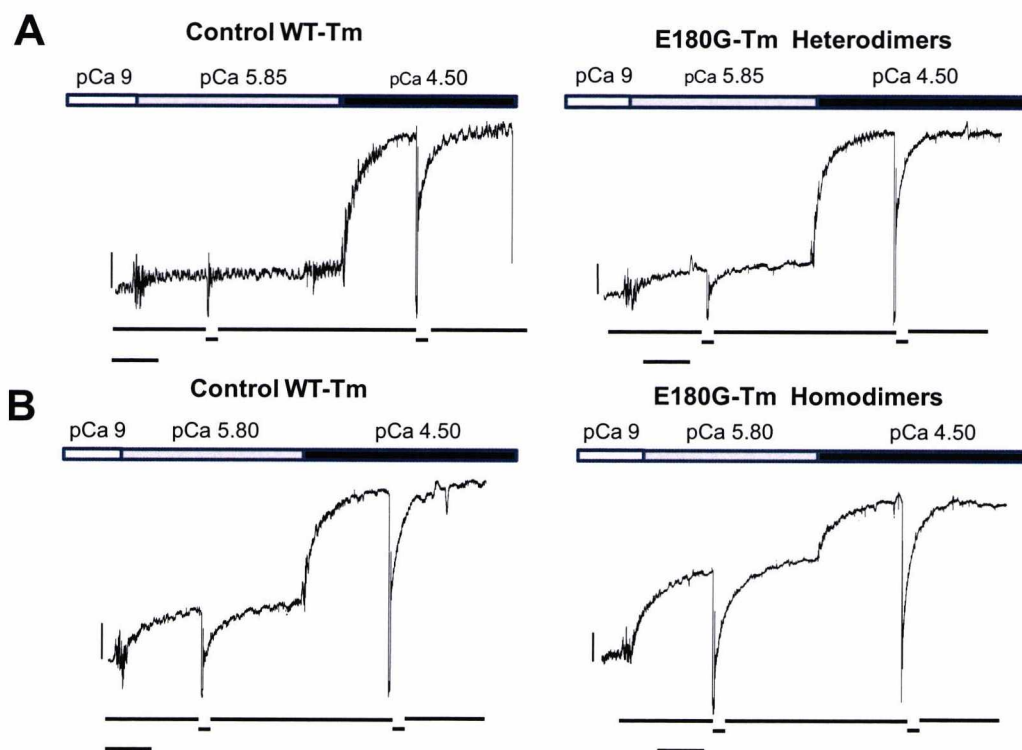
Figure 4.2.11 Force response of rabbit psoas myofibrils replaced for endogenous Tm·Tn complex at submaximal and maximal calcium activation at 15 °C. Myofibrils replaced with WT-E180G-Tm heterodimer (A) and E180G-Tm homodimer (B) carrying E180G mutation (right) or with WT-Tm (left) were activated at submaximal [Ca^{2+}] (pCa 5.85 in A and pCa 5.8 in B) and then subjected to a [Ca^{2+}] jump to full activation at pCa 4.5. Bars above traces correspond to the timing of the solution change. Top traces: force; bottom traces: release-restretch (30 %) of myofibril length. Calibrations are indicated by the horizontal and vertical bars corresponding to 1 s and 100 mN mm^{-2}, respectively.

A left: sarcomere length 2.47 μm, resting tension 102 mN mm^{-2}, Po$_{5.85}$/Po$_{4.50}$= 0.11; A right: sarcomere length 2.45 μm, resting tension 67 mN mm^{-2}, Po$_{5.85}$/Po$_{4.50}$= 0.18

B left: sarcomere length 2.52 μm, resting tension 96 mN mm^{-2}, Po$_{5.80}$/Po$_{4.50}$= 0.31; B right: sarcomere length 2.36 μm, resting tension 87 mN mm^{-2}, Po$_{5.80}$/Po$_{4.50}$= 0.61

(Image from Tesi, personal communication; measured data from Janco, et al., 2012)

Myofibril batch	Sarcomere lenght (nm)	$P_{o\,4.5}$ (mN mm^{-2})	k_{ACT} (s^{-1})	k_{TR} (s^{-1})	$Po_{5.80}/Po_{4.50}$	$Po_{5.85}/Po_{4.50}$	$Po_{5.90}/Po_{4.50}$
E180G-Tm Homodimer							
Mutant Tm	2.24±0.04 (8)	280±33 (9)	5.00± 0.26 (9)	4.60±0.53 (9)	0.50± 0.03 (8) †		0.10±0.03 (7)
Control WT-Tm	2.29±0.04 (8)	286±25 (9)	4.81±0.70 (7)	4.46±0.35 (8)	0.30±0.04 (7)		0.04±0.02 (6)
WT-E180G-Tm Heterodimer							
Mutant Tm	2.41±0.04 (10)	282±32 (10)	5.82±0.42 (8)	5.82±0.32 (10)		0.14±0.01 (8)	
Control WT-Tm	2.42±0.06 (8)	321±32 (9)	5.73±0.55 (9)	5.72±0.43 (6)		0.13±0.01 (6)	

Table 4.4 Mechanical behaviour of skeletal myofibrils replaced with WT, WT-E180G, and E180G-Tm at 15 °C. All values are given as means (± standard error of the mean) and refer to different myofibril batches; number in parentheses is the number of myofibrils. P_0, maximum isometric tension and the index value refers to pCa; k_{ACT}, rate constant of maximally activated tension rise following step-wise pCa decrease (from pCa 9.0 to pCa 4.5) by fast solution switching; k_{TR}, rate constant of tension re-development following release-restretch of maximally activated myofibrils. †$p \leq 0.001$ (Student t test) compared to the same parameter measured in the control preparations. (Measured data from Janco, et al., 2012).

On the other hand, calcium-independent tension which signals presence of some myosin heads able to cycle in the absence of calcium, was not significantly affected by any of E180G-Tm constructs (see Figure 4.2.7; pCa9).

The results showing an increased tension at low calcium concentrations in E180G-Tm homodimer but not in the heterodimer are in agreement with our in solution calcium sensitivity measurements for this Tm mutant. The explanation for the unaffected function of myofibrils containing WT-E180G-Tm might be in preferential binding of the heterodimer to actin and Tn. If the chain containing mutation binds preferentially to actin (measured decrease in affinity, section 4.2.2) then the WT chain binds to the Tn leaving the calcium dependent binding of myosin unaffected.

4.2.5 The flexibility of D175N and E180G-Tm homo- and heterodimers

It has been shown that Tm's global shape and flexibility play an important role in assembly, maintenance and the activation of thin filaments (Li et al., 2010a). Other studies showed that HCM mutations D175N and E180G decrease tropomyosin affinity to F-actin (Boussouf et al., 2007; Janco et al., 2012) and flexibility of Tm molecule (Li et al., 2012) which might affect regulatory motion on F-actin. Our lab was involved in the latter study, where the global and local bending flexibility of Tm homodimers carrying HCM mutations were assessed by electron microscopy and molecular dynamics simulations. The same approach was used for the WT-D175N- and WT-E180G-Tm heterodimers published recently (Janco et al., 2013).

The experimental data of the apparent persistence length as a measure of Tm flexibility presented in this section were performed by Dr Worawit Suphamungmee and Dr Xiouchan Li under supervision of Prof William Lehman, all from Boston University, USA.

Tm dimers	Apparent persistence length PL$_a$ (nm)
WT-Tm	109 ± 19[†]
WT-D175N-Tm	85 ± 9[*]
D175N-Tm	81 ± 8[†]§
WT-E180G-Tm	72 ± 8[*]§
E180G-Tm	82 ± 3[†]§

Table 4.5 The apparent persistence length (PL$_a$) of isolated Tm homo- and heterodimers carrying HCM mutations. PL$_a$ was determined by the tangent correlation method applied to >750 WT-Tm homodimers, >200 D175N- and E180G-Tm homodimers, and ~1000 for mutant heterodimers skeletonized Tm molecules from four preparations. § value differs compared to WT-Tm measured value (p ≤ 0.05). [†] data from Li, et al., 2012; [*] data from Janco, et al., 2013.

2-D images of Tm with length of 40 nm were acquired by electron microscopy, as described previously (Sousa et al., 2010), and used for the calculation of apparent

persistence length PLa. Purified Tm molecules lying on carbon support film were negatively stained for EM imaging. Following drying and adsorbtion of the support film resulted in well-separated single molecules which showed smoothly curved profiles with no obvious kinks or joints. PL_A value derived from EM images was compared to the same mean value obtained by rotary shadowing. Rotary shadowing was performed by following procedure:

Samples diluted to 1.0 μM in 5 mM Tris (pH 7.0), 5 mM KCl, 2 mM $MgCl_2$, 2 mM DTT, and 30% glycerol buffer were sprayed onto freshly cleaved mica. The proteins were left to dry for 10 – 20 min and then placed in an Edward's vacuum evaporator (BOC Edwards, Wilmington, MA) until reached a vacuum lower than 5×10^{-6} Torr. Platinum (9 mg total) was evaporated over a 1 min period from a distance of 9.5 cm at a 9° angle onto the rotating samples. Thin carbon was then deposited over the platinum replica. The carbon-supported platinum replica was floated off the mica onto water and adsorbed onto 400 mesh copper grids. EM was carried out on the shadowed molecules using a Philips CM120 electron microscope (FEI, Hillsboro, OR) at 120 kV, and images were digitised at 28,000× magnification with a 2Kx2K F224HD slow-scan CCD camera (TVIPS, Gauting, Germany).

The recorded images of Tm were then skeletonised after manual selection of 0.5 × 0.5 nm points every 4–5 nm along the centre of the protein's longitudinal axis and the persistence length, ξ, was calculated using the tangent angle correlation method (Li et al., 2010b).

The PLa value for the WT (107 nm) was in a good agreement with previously determined values (Li et al., 2010a; Sousa et al., 2010). Both E180G and D175N-Tm homodimers caused ~20 % decrease in PLa of the protein presumably due to an increased in local and global flexibility (Li et al., 2012). The same approach used for the WT-D175N and WT-E180G-Tm heterodimers showed that similar PLa values to those of their respective homodimers (see Table 4.5). Statistical analysis showed that only WT-E180G Tm heterodimer was significantly different at $p \leq 0.05$. However, considering number of measured WT-Tm molecules (>750), the error for the WT is high and therefore changes in WT-D175N Tm heterodimer PLa may be still significant *in vivo*.

4.3 Discussion

The results of biochemical and biophysical assays used for characterisation of bacterially expressed Tm heterodimers carrying D175N or E180G mutation in one chain of the dimer showed that properties of the heterodimers are not always the mean between the WT-Tm and the mutant homodimers.

Co-sedimentation assays showed ~2.5-fold weaker actin affinity of both D175N and E180G Tm homodimers in comparison to WT ($K_{50\%}$ 0.21 μM), which agrees with previous measurements (Boussouf et al., 2007). An actin affinity of the WT-D175N-Tm heterodimer (0.23 μM) was indistinguishable from the WT while value of the WT-E180G-Tm at 0.27 μM was intermediate between the E180G homodimer and WT. Measured values of actin affinity showed strong interactions between actin and all Tm constructs. However, the differences between the WT-Tm and the HCM mutants are likely to be negligible _in vivo_ due to much higher concentrations of actin and Tm. If all of the homo- and heterodimer tropomyosins were present at similar levels there would be only a very marginal preference for the WT over the mutant proteins.

The thermal unfolding measurements of WT and D175N-Tm homodimers under reducing conditions show two major thermal transitions at 47.5 °C and 53.1 °C and a third smaller transition at 41.2 °C. The data are in agreement with previous measurements for WT-Tm at high salt concentration (Hayley et al., 2011; Kalyva et al., 2012). High salt concentration used in the assays prevents end-to-end polymerisation of Tm which can affect the melting profile of Tm. Similar studies of Tm thermal unfolding at low salt concentration (100 mM KCl) and ~3-fold higher protein concentration using differential scanning calorimetry (DSC) (Kremneva et al., 2004) showed two thermal transitions at 42.7 °C and 50 °C. The differences are probably caused by the different ionic strength of used buffers.

The thermal unfolding of D175N-Tm homodimer was similar to a WT-Tm under reducing and non-reducing conditions, as reported previously (Kremneva et al., 2004). Unsurprisingly the melting profile of the WT-D175N-Tm heterodimer was indistinguishable from WT.

Thermal stability of the E180G Tm homodimer was decreased compared to WT. The cross-linked E180G-Tm homodimer showed thermal transition at ~26 °C well below

127

physiological temperature, while remaining two transitions at higher temperatures are similar to those of WT. When reduced the intermediate thermal event of the mutant homodimer shifts to 42 °C which is 5 °C less then WT. In contrast, the most stable thermal transition at 52.1 °C remains similar to WT and the first thermal event at lower temperatures is only a little less stable than the WT at 39 °C. For the cross-linked WT-E180-Tm heterodimer the least stable thermal transition is intermediate between the mutant homodimer and WT while the thermal events at higher temperatures are similar to the WT. Reduced WT-E180-Tm heterodimer is less stable than the E180G homodimer at physiological temperatures with a mid-point transition close to 36 °C. However the interpretation is more difficult because the protein under these conditions may probably exist as a mixture of homodimers and heterodimers. Therefore the presence of WT-Tm and E180G-Tm homodimers would tend to make this thermal transition appear more stable suggesting that the heterodimer may be significantly less stable than either WT or E180G homodimers and could be partially folded even at normal body temperature. Note however that the binding of Tm to actin increases stability of Tm dimers and once bound would be resistant to unfolding.

It has been established that HCM mutations in thin filament proteins are associated with an increase in calcium sensitivity. Previous work has shown that D175N- and E180G-Tm homodimers increase calcium sensitivity when in a fully assembled actin filament in *in vitro* motility assays (IVM) or experiments using reconstituted fibres (Bai et al., 2011; Bing et al., 2000; Wang et al., 2011) with E180G mutation showing a greater shift than D175N. Our measurements of the apparent calcium affinity for calcium switching of actin Tm-Tn filament for homodimers (Table 4.3) show ΔpCa of +0.08 for D175N and ΔpCa is +0.14 for E180G-Tm homodimer. These values are consistent with previously reported data by Boussouf et al. (2007) using the same method (ΔpCa of +0.08 and ΔpCa of +0.13, respectively) or estimated using IVM by Bing et al. (2000) (ΔpCa of +0.082 and ΔpCa of +0.115, respectively).

Interestingly in the case of the heterodimers the WT-E180G Tm had only a small ΔpCa (+0.03) compared to WT, while the D175N heterodimer had a larger ΔpCa (+0.11) close to that of the homodimer (+0.08). Our data for both homo and heterodimers show the positive

shift in calcium sensitivity expected for HCM mutations. Surprisingly the shift of the WT-E180G-Tm is very small and not significant.

The shifts in calcium sensitivity are small and we tested if the same change could be seen in the sarcomere by replacing the Tm·Tn complex in rabbit psoas myofibrils using hcTn combined with either WT-Tm, WT-E180G-Tm or E180G-Tm dimers. The results (Figure 4.2.11 and Table 4.4) show an increased calcium sensitivity for the E180G-Tm homodimer compared to WT but the heterodimer is unchanged. These measurements are compatible with the solution data using reconstituted thin filaments *in vitro*.

The apparent persistence length calculated from 2-D images acquired by electron microscopy is reduced by ~20 % in both D175N and E180G Tm homodimers. The reduction of the persistence length in Tm dimers is most likely caused by an increase in global and local bending flexibility. The persistence length of both WT-D175N-Tm and WT-E180G-Tm heterodimers is reduced equally as in their respective homodimers (Table 4.5).

Enhanced discussion on the results from this chapter and conclusions based on these results together with the implications for the cardiomyopathy and proposal for the future work are described in the chapter 6.

Chapter 5

Biochemical characterisation of E40K, E54K and D230N DCM heterodimeric mutants of the striated muscle α-Tm

5.1 Introduction

Point mutations in cardiac Tm dimers can cause cardiomyopathy resulting in diverse phenotypes such as hypertrophy or dilation. These two contrasting phenotypes of cardiac remodelling can be caused by the different mutations on the same sarcomeric protein (Seidman and Seidman, 2001). This raises the important question of whether the mutations that generate one phenotype cause the same functional abnormality or there are multiple separate programs that remodel the heart (Robinson et al., 2007; Robinson et al., 2002).

Tm mutations causing both HCM and DCM cardiomyopathies are clustered in discrete regions of the protein indicating strong link between the structure and function. To follow our hypothesis about the predominant presence of Tm αα*-Tm heterodimers in heterozygous tissue and elucidation of their properties, three DCM mutations E40K, E54K and D230N were used in this study. Mutations E40K and E54K are located in period 2 of Tm molecule and both are found at position *e* within the heptad. The 2-Å crystal structure of Tm indicates that Glu40 forms canonical salt linkage with Arg35 and Glu54 is linked by salt bridge to Lys49 at the position *g'* in the opposite chain of the dimer, both stabilising the coil-coil (Brown et al., 2001). Additionally negatively charged Glu40 can form salt bridge with positively charged Lys37 (i+3), and Glu 54 residue can form salt bridge with Lys51 (i+3) in the same chain, both improving intra-helical stability for the α-helix. Substitution of negatively

charged Glu at positions 40 and 54 for positively charged Lys may disrupt the described electrostatic interactions within the dimer and α-helix, presumably affecting the stability of the coiled-coil. The flexibility of Tm and affinity to actin may be also affected as both mutations are positioned between the two alanine clusters at positions 18, 25, 32 and 67, 74, 81 (Brown et al., 2001). Mutation D230N is located in the highly conserved period 7 of Tm molecule at the position *f* within the heptad. Substitution of negatively charged Asp for polar uncharged Asn amino acid residue does not affect stability of Tm coiled-coil as it is on the outer part of the helix. However, Asn substitution might cause destabilisation of Tm intra-chain interaction as native negatively charged Asp may form salt bridges with positively charged Lys-226 (i+4) and Lys-233 (i+3).

The effects of the Tm proteins carrying DCM mutations on the molecular mechanisms of the cardiac contraction have been extensively studied using recombinant (Bai et al., 2012; Borovikov et al., 2011; Chang et al., 2005; Lakdawala et al., 2010; Memo et al., 2013; Mirza et al., 2005; Mirza et al., 2007) or transgenic mice (Rajan et al., 2007) expression systems. The recombinant Tm mutants used in all studies to date were homodimers or mixtures however the predominant species *in vivo* are likely to be heterodimers that can have distinct properties from the homodimers. Here we introduce the first study of defined human cardiac Tm heterodimers carrying DCM mutations in only one chain of the dimer. Biochemical characterisation of Tm dimers carrying E40K, E54K and D230N DCM mutation in one or both chains was made by the assessment of their thermal stability, actin affinity and calcium dependent activation of the thin filament *in vitro*. All three DCM mutant homodimers were recombinantly expressed and purified as described in chapter 2, sections 2.2.8.1 and 2.2.8.2, respectively. Tm heterodimers carrying DCM mutations E40K, E54K and D230N were formed by the method described in chapter 3.

The results showed that thermal stability of all three Tm heterodimer constructs using circular dichroism was decreased at physiological temperatures (~35 °C) under reducing (*in vivo*) conditions. Interestingly, none of the mutant homodimers under the same conditions showed any differences in thermal stability compared to WT up to ~40°C. When cross-linked, E40K and D230N-Tm homo and heterodimers did not show any significant change in thermal stability. Cross-linked WT-E54K-Tm heterodimer was decreased at range of ~35 - 55°C while E54K-Tm homodimer showed an increase at the same temperature range. Apparent actin affinity was significantly decreased (p ≤ 0.05) in E54K-Tm homodimer and

WT-D230N-Tm heterodimer. The calcium activation of the thin filament reconstituted *in vitro* with mutant Tms did not show any significant changes in any protein constructs.

5.2 Results

5.2.1 Alterations in thermal stability of Tm homo- and heterodimers caused by DCM mutations

The thermal stability of recombinantly expressed human Tm heterodimers carrying DCM mutations E40K, E54K and D230N was assessed by CD (for the method, see section 2.3.1). The optimised method for the formation of Tm heterodimers is described in the chapter 3. As Tm is nearly 100 % α-helical protein, the thermal stability was measured at a fixed wavelength of 222 nm detecting the unfolding of secondary structure. Each Tm constructs at 7 µM was continuously (1 °C/min) heated over the range of 5 – 65 °C. Tm dimers, chemically cross-linked at Cys190, repeatedly heated to 65 °C and then cooled down to 5 °C showed similar unfolding profiles indicating reversibility of the thermal unfolding of an α-helical structure in Tm molecules (Figure 5.2.1).

After three heating cycles, 1 mM of DTT was added to disrupt the cross-link. The first thermal isotherm during reduction of the sample (fourth run) showed the loss of stability at lower temperatures between ~25 – 45 °C which was comparable to fully reduced proteins in the following cycles (Figure 5.2.1). At higher temperature ranging between 45 – 60 °C (depending on Tm sample) reduced Tm proteins showed typically an intermediate increase in thermal stability between fully reduced isotherms (run 5, 6 and 7) and cross-linked isotherms (runs 1, 2 and 3). All plotted data were normalised and the melting curves of Tm heterodimers were compared to the WT and mutant homodimers (Figure 5.2.1 B). Note that the normalisation procedure was applied for the precise comparison between the constructs. However, the differences between unfolding profiles of individual Tms before normalisation were small due to the same concentration used for all the samples (Figure 5.2.1.A).
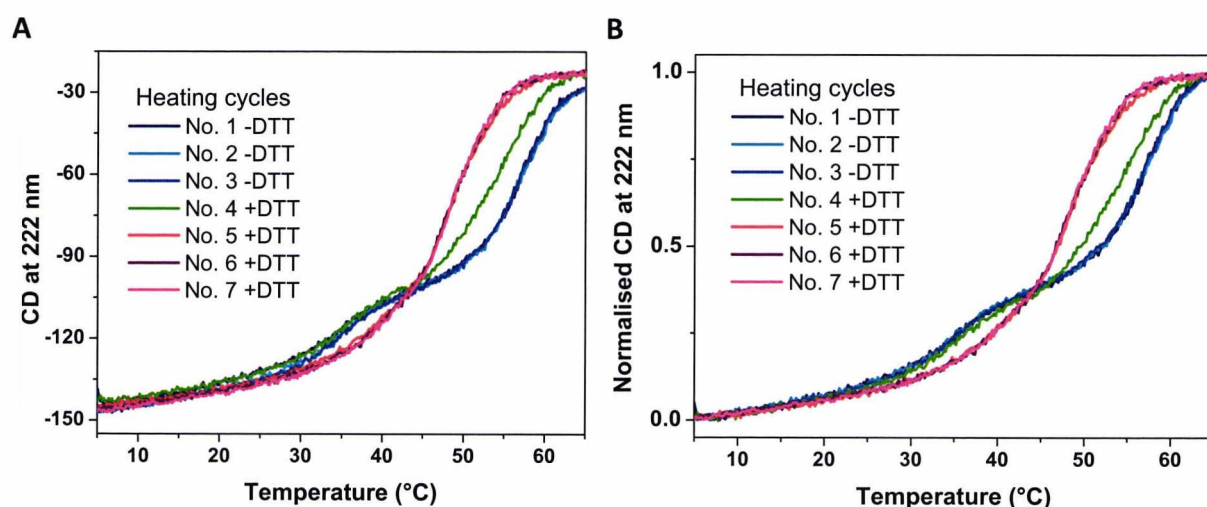
Figure 5.2.1. Reversibility of thermal unfolding of cross-linked, and reduced αTm dimers. (A) Raw data; (B) Normalised data. Seven heating cycles of D230N-Tm homodimer show similar unfolding isotherms when cross-linked (cycle 1, 2, and 3; dark blue, light blue, and blue line respectively) and reduced (cycle 5, 6 and 7; red, purple and magenta line, respectively). Lime green line is the first isotherm after addition of 1 mM DTT (fourth heating cycle) indicating transition between fully cross-linked and fully reduced Tm dimers. Buffer conditions: 0.5 M KCl, 20 mM potassium phosphate buffer, 5 mM MgCl$_2$, pH 7.0.

Figure 5.2.2 shows unfolding isotherms of cross-linked and reduced Tm homo- and heterodimers carrying E40K, E54K or D230N mutations. Similarly as for the HCM Tm constructs described in previous chapter, three thermal transients were typically observed in all Tm's with DCM mutations. These will be denoted in following text as the first (at low temperature), the middle and the second (at high temperature) unfolding events or thermal transients for clarity. The details of the changes occurring to the individual unfolding events are shown more clearly in the first differential of the data fitted into a multiple Gaussian peaks shown in Figure 5.2.3 for E40K-Tm, Figure 5.2.4 for E54K-Tm and Figure 5.2.5 for D230N-Tm homo and heterodimers. The data derived from the fitting includes the midpoints of unfolding transition, the fractional peak areas (a measure of the free energy change associated with each unfolding transition) and the width of half peaks (measure of unfolding cooperativity) (Table 5.1). It should be noted that the differentiation and fitting of the data have some limitations and not always agree with the observed events in the measured data (Figure 5.2.2).
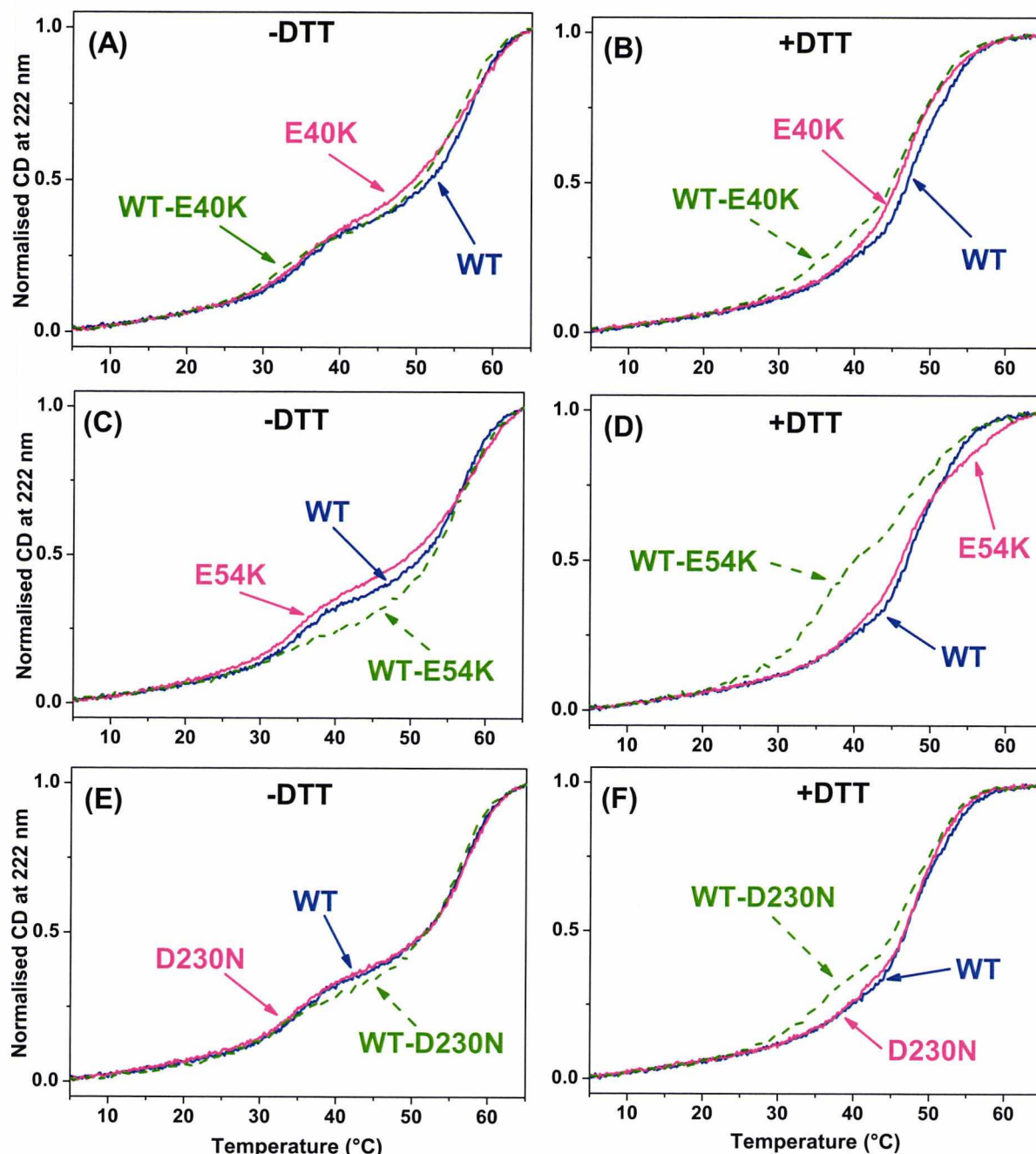
Figure 5.2.2 Thermal unfolding of α-Tm homo and heterodimers carrying E40K, E54K, and D230N mutations compared to WT-Tm. Normalised unfolding profiles of 7 μM α-WT (blue solid lines); α*α*-Tm homodimers (magenta solid lines) and αα*-Tm heterodimers (lime green dashed lines) of E40K (A & B), E54K (C & D) and D230N (E & F) in the absence (A, C, E) and presence (B, D,F) or of 1 mM DTT. Buffer conditions: 0.5 M KCl, 20 mM potassium phosphate buffer, 5 mM MgCl$_2$, pH 7.0.

Figure 5.2.2 A shows the thermal unfolding profiles of the third heating cycle of the cross-linked WT-E40K-Tm heterodimer and E40K-Tm homodimer, compared to those of WT. The first thermal transition of the cross-linked E40K-Tm homodimer occurred at the same

temperature as the WT (~35.3 °C). However, the WT-E40K-Tm heterodimers showed the shift (2.7 °C) in the same thermal transition with decreased stability at 32.6 °C. The middle region in all three Tm constructs (WT, WT-E40K and E40K) was unfolded at higher temperature at ~48 °C and the second unfolding events at the high temperature of ~56.6 °C.

Figure 5.2.2 B shows thermal isotherms of reduced E40K-Tm constructs. The reduction of the WT dimers caused decrease of thermal stability at high temperature (53 °C) by ~4 °C and at ~47 °C (the intermediate transition) by ~1 °C while the first transition at ~ 41 °C showed an increased stability, compared to the cross-linked WT-Tm. The first thermal event (at 41 °C) of E40K-tm homodimer was similar to the WT while the WT-E40K-Tm heterodimer showed a new thermal transition at ~38 °C which was ~2 °C lower compared to those of both WT and E40K-Tm homodimers (Figure 5.2.3 F). The intermediate unfolding event occurred at the similar temperature (~47 °C) in all dimers. The second thermal transition of the E40K-Tm homodimer was similar to the WT (53 °C) and the WT-E40K-Tm heterodimer was shifted by ~1.5 °C lower (peak at 51.4 °C). Notice, that the unfolding profile of E40K-Tm shown in Figure 5.2.2 B indicates slight loss in thermal stability over the range of ~45 - 53 °C, similar to WT-E40K-Tm heterodimer (measured data). However, the first differential of the E40K homodimer data indicates the peak of the second thermal transition at 54.6 °C, which is more stable than the value for the WT. The difference between the measured data and the fitted values is probably caused by two major factors. Firstly, how close are the individual thermal transitions to each other and secondly, how well defined are the peaks?

Additionally, the interpretation of the data for the all DCM mutations carrying heterodimers under reducing conditions can be complicated as the heating process is predicted to cause reannealing of the dimers into a mixture of $\alpha\alpha$-, $\alpha\alpha^*$-, $\alpha^*\alpha^*$-Tm dimers in a ratio of 1 : 2 : 1. The unfolding transitions for the heterodimer can be estimated by subtracting 25 % of the expected transitions for WT and the mutant homodimers (the expected proportion after reannealing). This procedure would be mostly valuable in the cases when the heterodimer thermal transitions occur between the WT and the mutant homodimers. Figure 5.2.3 D shows the data of WT-E40K-Tm heterodimer after the subtraction procedure (red line). The peak proportions were reduced but the definition of the peaks was higher and the positions of the three transitions were relatively unchanged.
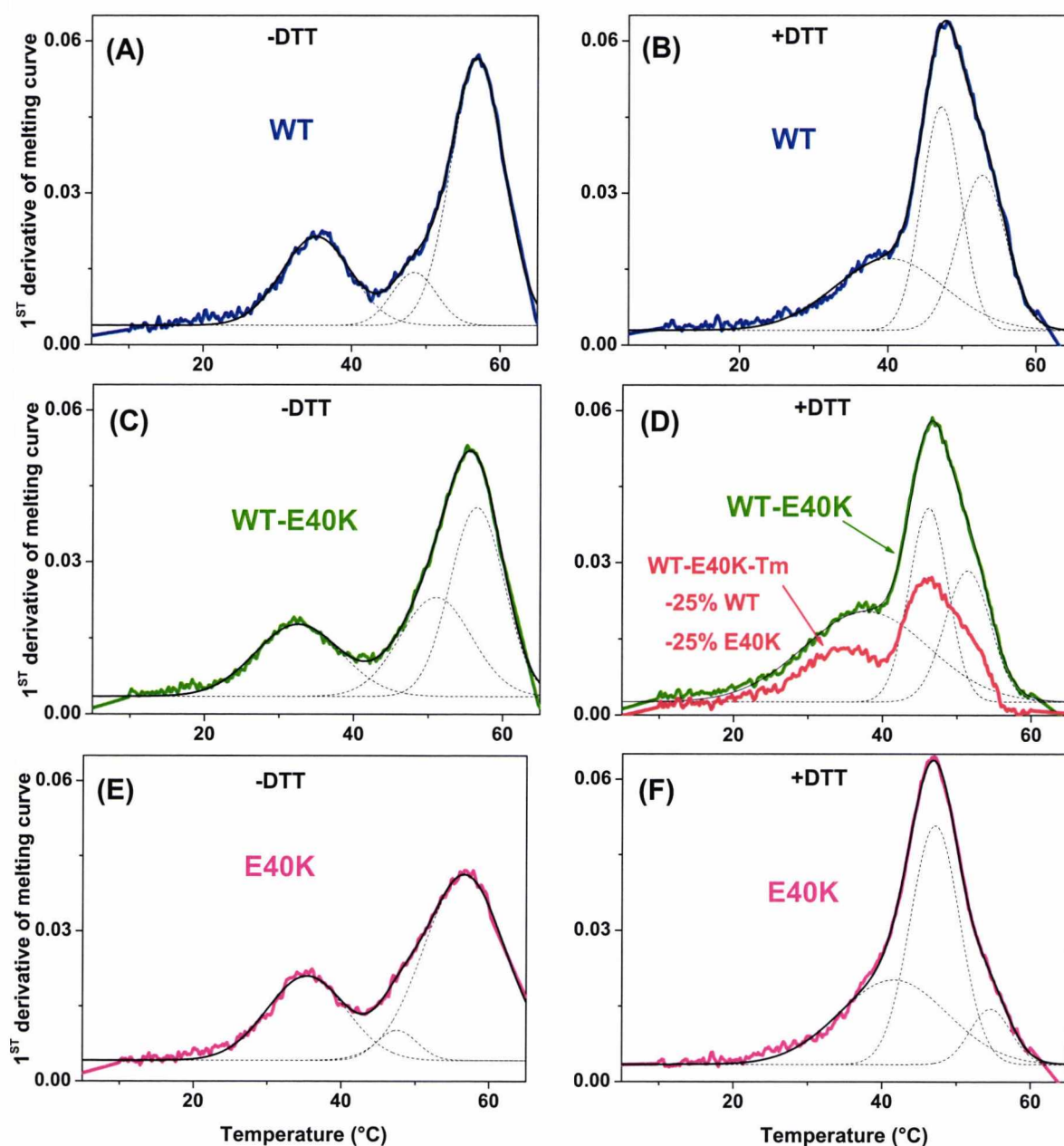
Figure 5.2.3 Thermal unfolding of skeletal α-Tm homo and heterodimers carrying E40K DCM mutations. The data from each melting curve shown in Figure 4.2.2 A and B were smoothed (Savitzky-Golay method; 50 points of window), differentiated with the best fit to Gaussian peaks superimposed (dotted line). Red line in the panel D is an estimation of the WT-E40K-Tm heterodimer unfolding obtained by a subtraction of the 25 % of measured data of both WT and E40K homodimers. A summary of the fitted data is shown in Table 5.1.

Figure 5.2.2 C shows unfolding profiles of the cross-linked E54K-Tm and WT-E54K-Tm constructs, compared to the WT. Each isotherm represents the third heating cycle. The first derivative of the data fitted to a multiple Gaussian peaks are shown in Figure 5.2.4 and the

numerical values derived from the fitting are shown in Table 5.1. The thermal stability of the cross-linked E54K-Tm was slightly reduced at temperatures over the range of 25 – 55 °C but without significant changes of the individual thermal events compared to WT. Interestingly, the WT-E54K-Tm heterodimer showed an increased thermal stability at the temperatures ranging between ~30 – 55 °C. However, the first differential of the heterodimer data at low temperatures (33.7 °C) indicates the loss of the stability compared to WT (35.5 °C). This is caused by the distribution of the thermal transition which was wider and flattened. Width of half peak for the heterodimer was 13.4 °C and fractional peak area was ~18 % while the values of same parameters for the WT were 9.3 °C and ~28 %, respectively. The first thermal transition indicating higher cooperativity with less energy needed for the unfolding of the heterodimer (Figure 5.2.4 C). Thermal events at intermediate (~47 °C) and high (~57 °C) temperatures were relatively unchanged. Addition of 1 mM of DTT to the cross-linked E54K-Tm homodimer caused a small decrease in thermal stability between 40 – 50 °C, while unfolding at higher temperatures (50 – 60 °C) showed significant increase (~5 °C) compared to the WT (see Figures 5.2.2 D for measured CD profile, and 5.2.4 F for the first derivative of the data). The unfolding profile of reduced WT-E54K-Tm heterodimer showed significant loss of stability throughout the most of the heating cycle at temperatures ranging between ~25 – 55 °C. The fitting process of the first derivative of the data (Figure 5.2.4 D) showed typically observed and well defined three unfolding events. The midpoint of the first thermal transition (at 35.5 °C) was 4.7 °C lower than that of WT (40.2 C°) indicating a large loss of thermal stability with the value at the physiological levels. Thermal transitions at the intermediate (46.1 °C) and high (51.5 °C) temperatures showed only 1° C lower midpoints compared to the WT. Interestingly, after the subtraction of 25 % signal of each WT and E54K-Tm homodimers the heterodimer showed only one thermal transition at approximately 35.3 °C (red line in Figure 5.2.4 D). As mentioned previously, the estimation of the properties by using a multiple fitting and the subtraction process will impose a large error on the final result however the single thermal transition at the physiological temperature showed in the WT-E54K-Tm heterodimer may have a significant implications for the muscle contraction in cardiomyopathies.
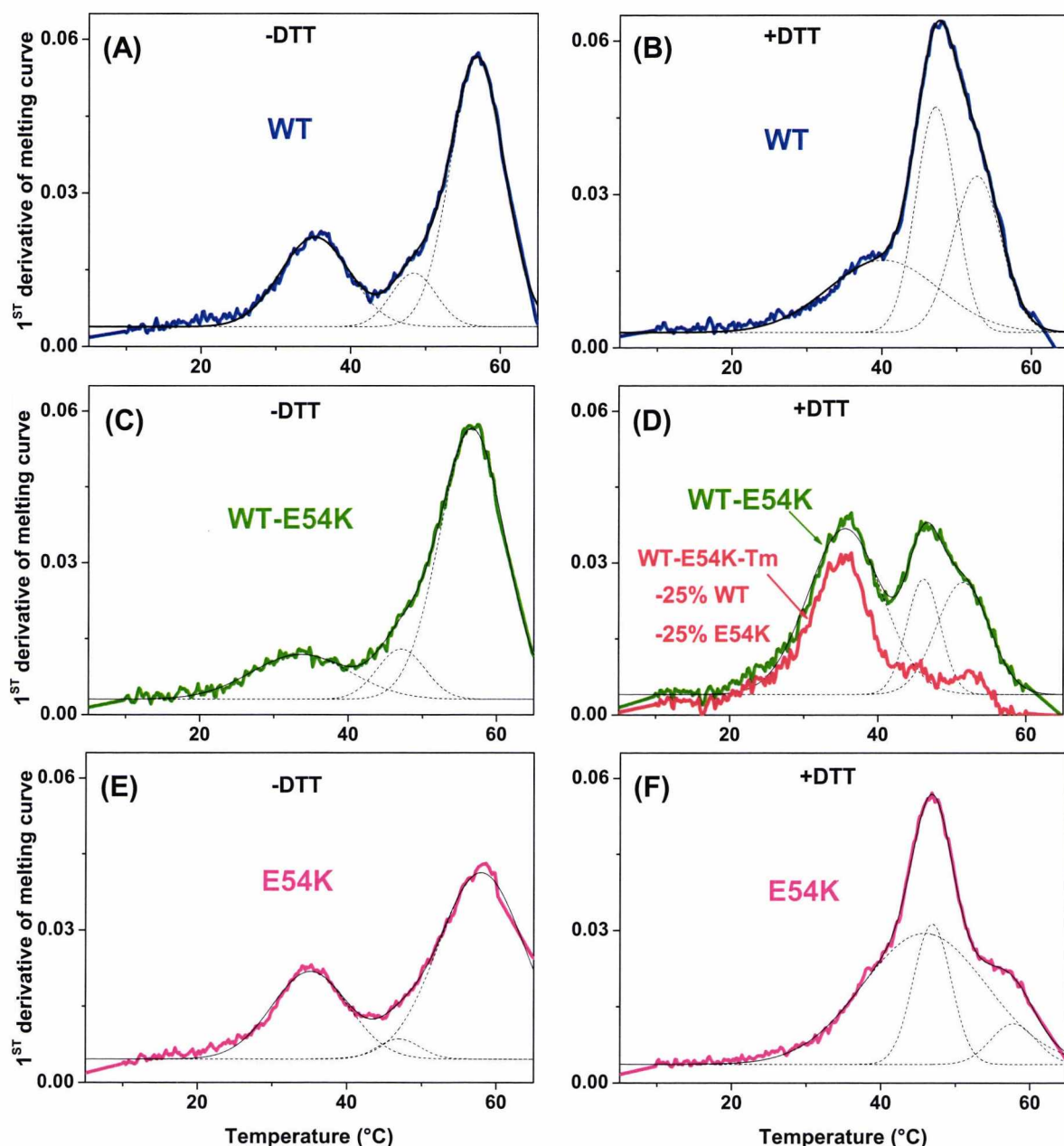
Figure 5.2.4 First derivative of the WT, E54K and WT-E54K-Tm thermal unfolding data measured by CD. The first derivative of the data shown in the Figure 5.2.2 C and D were fitted to multiple Gaussian peaks superimposed (dotted line). Panel D shows an estimation of the WT-E54K-Tm heterodimer unfolding (red line) obtained by a subtraction of the 25 % of measured data of both WT and E54K homodimers. A summary of the fitted data is shown in Table 5.1.

Unfolding profiles of cross-linked D230N-Tm homo and heterodimers are shown in Figure 5.2.2 E. The unfolding profiles of these Tm constructs were almost identical except a small increase of stability over the range of ~37 – 50 °C in the WT-D230N heterodimer.
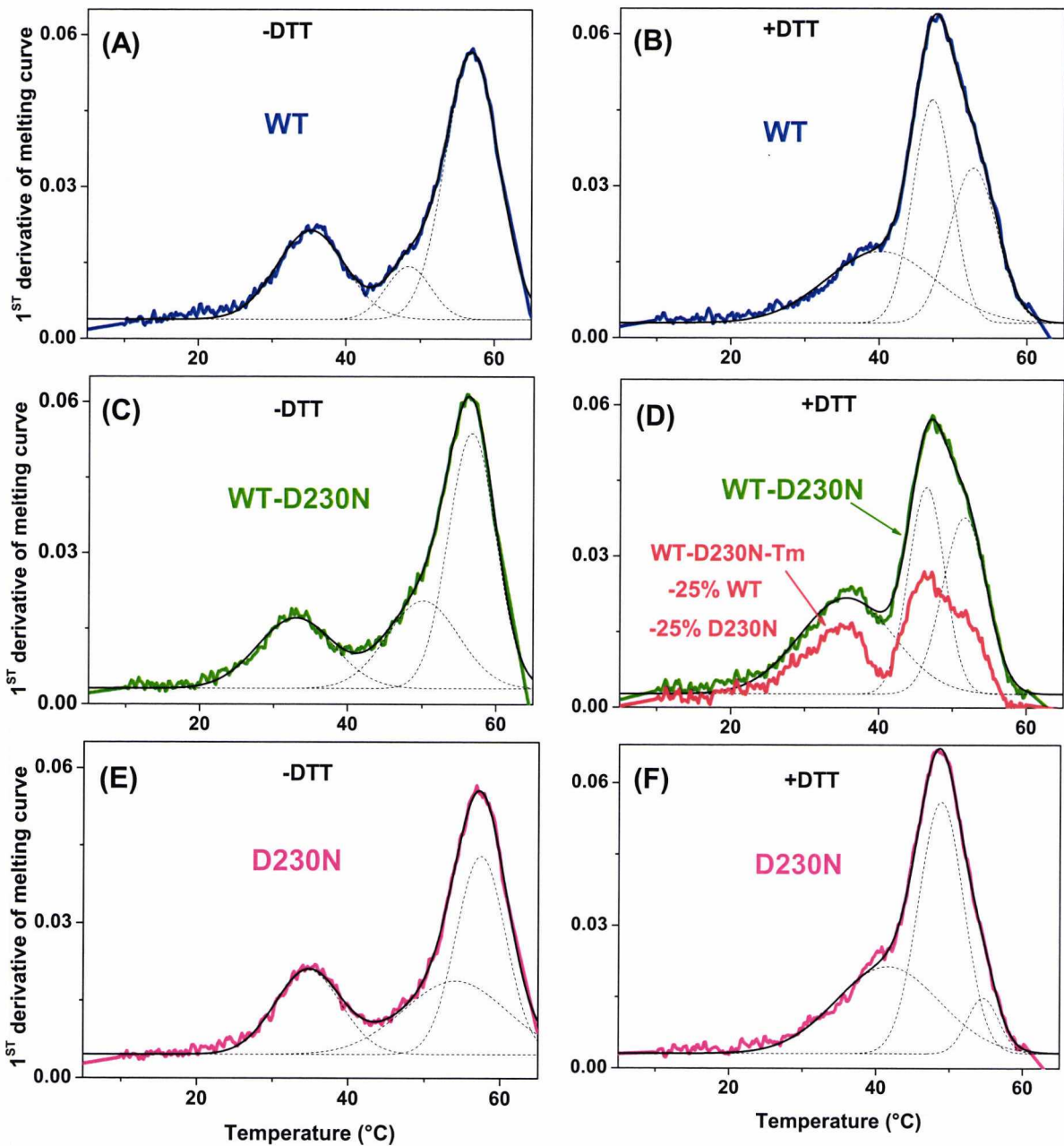
Figure 5.2.5 First derivative of the WT, D230N and WT-D230N-Tm thermal unfolding data. The fitting procedure as for previous DCM constructs. The red line in the Panel D shows an estimation of the WT-D230N-Tm heterodimer unfolding obtained by a subtraction of the 25 % of measured data of both WT and D230N homodimers. A summary of the fitted data is shown in table 5.1.

Figure 5.2.2 F shows the same D230N-Tm dimers after the reduction of the cross-link at Cys190 (seventh heating cycle). Reduced D230N-Tm homodimers did not show any significant changes in comparison to the WT. The heterodimer in contrast showed decreased stability at the temperatures ~30 - 50 °C. The first derivative of the WT-D230N-Tm data (Figure 5.2.5 D) indicates significantly reduced stability (~4.7 °C) of the thermal

transition at 35.6 °C compared to the WT (at 40.2 °C). The position of this thermal transition was not altered after subtraction of 25 % signal of the WT and D230N-Tm homodimers (red line in Figure 5.2.5 D). The thermal event at such a low temperature may have an effect on Tm binding to actin. The intermediate unfolding events at the intermediate (~47 °C) and high (~ 52 °C) remained relatively unchanged. The 1 derivative data were plotted into the bar graphs shown in Figure A 4 (Appendix) for clarity.

Tm dimers	Peak	Cross-linked Tm (-DTT)			Reduced Tm (+DTT)		
		Fractional Peak area (%)	Width of half peak (°C)	Peak midpoint (°C)	Fractional Peak area (%)	Width of half peak (°C)	Peak midpoint (°C)
WT-Tm	1	27.0 ± 0.5	9.3 ± 0.2	35.2 ± 0.1	32.7 ± 3.7	14.8 ± 1.1	40.2 ± 0.9
	M	10.4 ± 0.9	6.0 ± 0.4	48.4 ± 0.2	36.5 ± 4.3	5.3 ± 0.2	47.2 ± 0.2
	2	62.6 ± 0.9	7.2 ± 0.1	56.9 ± 0.1	30.8 ± 3.5	6.4 ± 0.4	52.7 ± 0.4
WT-E40K-Tm	1	26.2 ± 0.8	11.5 ± 0.3	32.6 ± 0.2	45.6 ± 2.1	16.8 ± 0.6	37.8 ± 0.4
	M	30.2 ± 19.5	9.6 ± 2.2	51.0 ± 2.8	30.4 ± 2.9	5.2 ± 0.2	46.2 ± 0.2
	2	43.6 ± 19.1	7.3 ± 0.5	56.5 ± 0.4	24.0 ± 2.7	6.1 ± 0.3	51.4 ± 0.3
E40K-Tm	1	29.0 ± 0.5	10.7 ± 0.2	35.3 ± 0.1	39.3 ± 6.4	14.6 ± 1.2	41.5 ± 1.2
	M	5.3 ± 1.0	5.5 ± 0.5	47.5 ± 0.2	50.9 ± 4.4	6.7 ± 0.2	47.1 ± 0.1
	2	65.7 ± 1.2	11.0 ± 0.2	56.6 ± 0.1	9.8 ± 2.0	5.5 ± 0.4	54.6 ± 0.3
WT-E54K-Tm	1	18.1 ± 0.7	13.4 ± 0.5	33.7 ± 0.2	55.7 ± 0.9	10.0 ± 0.2	35.5 ± 0.1
	M	9.8 ± 0.9	6.4 ± 0.4	47.1 ± 0.1	17.5 ± 3.4	4.5 ± 0.3	46.1 ± 0.2
	2	72.0 ± 0.8	8.8 ± 0.1	56.7 ± 0.1	26.7 ± 3.4	7.1 ± 0.46	51.5 ± 0.5
E54K-Tm	1	28.3 ± 0.6	10.2 ± 0.2	35.1 ± 0.1	69.5 ± 3.7	16.6 ± 0.4	45.8 ± 0.4
	M	3.6 ± 0.9	5.6 ± 0.9	47.0 ± 0.4	22.6 ± 1.4	5.1 ± 0.1	46.8 ± 0.1
	2	68.1 ± 1.2	11.5 ± 0.2	58.0 ± 0.1	7.9 ± 2.1	6.1 ± 0.7	57.8 ± 0.2
WT-D230N-Tm	1	22.7 ± 0.9	10.3 ± 0.4	33.0 ± 0.2	37.3 ± 1.2	12.8 ± 0.4	35.6 ± 0.2
	M	26.3 ± 7.7	9.6 ± 1.6	50.1 ± 1.4	30.7 ± 3.8	4.9 ± 0.2	46.4 ± 0.2
	2	50.9 ± 7.3	6.4 ± 0.2	56.7 ± 0.1	32.0 ± 3.5	6.0 ± 0.3	51.6 ± 0.3
D230N-Tm	1	24.3 ± 0.5	8.7 ± 0.2	34.7 ± 0.1	40.7 ± 4.3	14.1 ± 0.9	41.6 ± 0.8
	M	32.9 ± 2.6	13.6 ± 0.5	54.1 ± 0.5	51.3 ± 3.7	6.2 ± 0.2	48.8 ± 0.1
	2	42.8 ± 2.5	6.5 ± 0.1	57.4 ± 0.1	7.9 ± 1.7	4.3 ± 0.4	54.6 ± 0.3

Table 5.1 Thermal unfolding of cross-linked and reduced α-Tm dimers with DCM mutations. Data from the multiple Gaussian fits shown in Figure 4.1.3. Three thermal transitions observed in our experiments were denoted in the text as the first (peak 1), the second (peak 2), and the intermediate (peak M). All the data are shown with their respective standard errors and represents an average of two measurements (n=2). All the numerical values of this table are plotted to the bar graphs in Figure 5.2.6 for clarity.
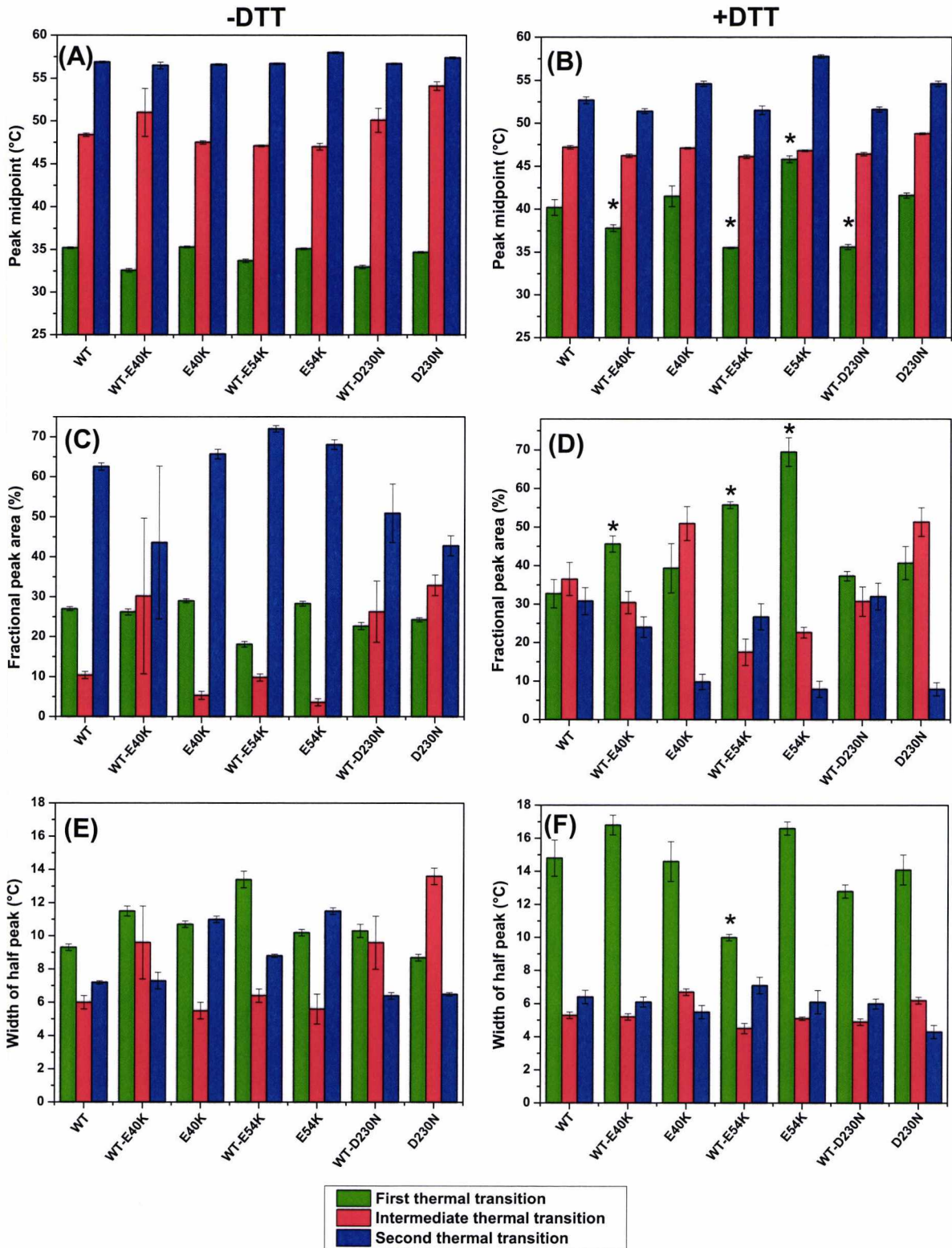
Figure 5.2.6 Thermal unfolding of skeletal αTm homo- and heterodimers carrying DCM mutations E40K, E54K or D230N. The graphs are plotted data from Table 5.1 (Chapter 5). Panels A and B represents fitted peak midpoints (°C) of the three thermal transitions with and without cross-link, respectively. Panels C and D show the fractional peak area (%), and panels E and F show the width of half peak (°C) of the same thermal transitions with or without cross-link, respectively. * indicates possible effect at physiological level.

5.2.2 Actin affinity of tropomyosin dimers carrying one or two copies of DCM mutation

Actin affinity of recombinant skeletal cross-linked WT-E40K, WT-E54K, and D230N-Tm heterodimers to F-actin were measured using co-sedimentation assays (method described in chapter 2, section 2.3.2.2).

An example of 10 % SDS gels loaded with the supernatant and pellet fractions of actin mixed with WT-E40K-Tm heterodimer is shown in Figure 5.2.7 A. Fractions containing 7 μM F-actin mixed with Tm at concentrations 0.2 – 2.4 μM were incubated for 1 hour at 25 °C and then centrifuged. Centrifugation at high speed (100.000 rpm) pelleted most of the actin together with bound Tm. Minor fraction of actin remaining in the supernatant was probably G-actin. All samples were run on the gel under reducing conditions. Interestingly, Tm constructs carrying DCM mutations in only one chain appear on 10 % gel as a single band in contrast to the HCM Tm constructs (two bands). This is due to the small differences in the molecular mass between the WT and the mutant monomers (- 1 Dalton in all DCM mutants compared to the WT).

Figure 5.2.7 B shows the sigmoid binding curves of the WT and E40K-Tm constructs. The Hill equation was fitted to the data to give an estimate of the Tm affinity ($K_{50\%}$) and the apparent cooperativity (h) for F-actin (Table 5.2). The apparent affinity ($K_{50\%}$) of both WT-E40K-Tm heterodimer (0.30 μM) and E40K-Tm homodimer (0.27 μM) for actin were not significantly different (p ≤ 0.05) from the WT-Tm (0.24 μM). Note that each binding curve showed in Figure 5.2.7 (panels B, C and D) was fitted to the data from one individual measurement and does not necessarily represent an average values shown in Table 5.2.

The binding curves of WT and E54K-Tm constructs to F-actin are shown in Figure 5.2.7 C. The binding of the E54K-Tm homodimer was significantly weaker (0.35 μM, p ≤ 0.05) compared to the WT (0.24 μM). Averaged value of $K_{50\%}$ (0.79 μM) for the WT-E54K-Tm heterodimer was the weakest of all constructs. However, large variations between the measurements caused that statistical analysis did not indicate significant difference from the WT (p ≤ 0.05).

Actin binding curves of WT-D230N-Tm heterodimer and D230N-Tm homodimer together with the WT data are shown in Figure 5.2.7 D. Affinity of this mutant homodimer (0.28 μM) to actin was not affected. The introduction of D230N mutation in only one chain
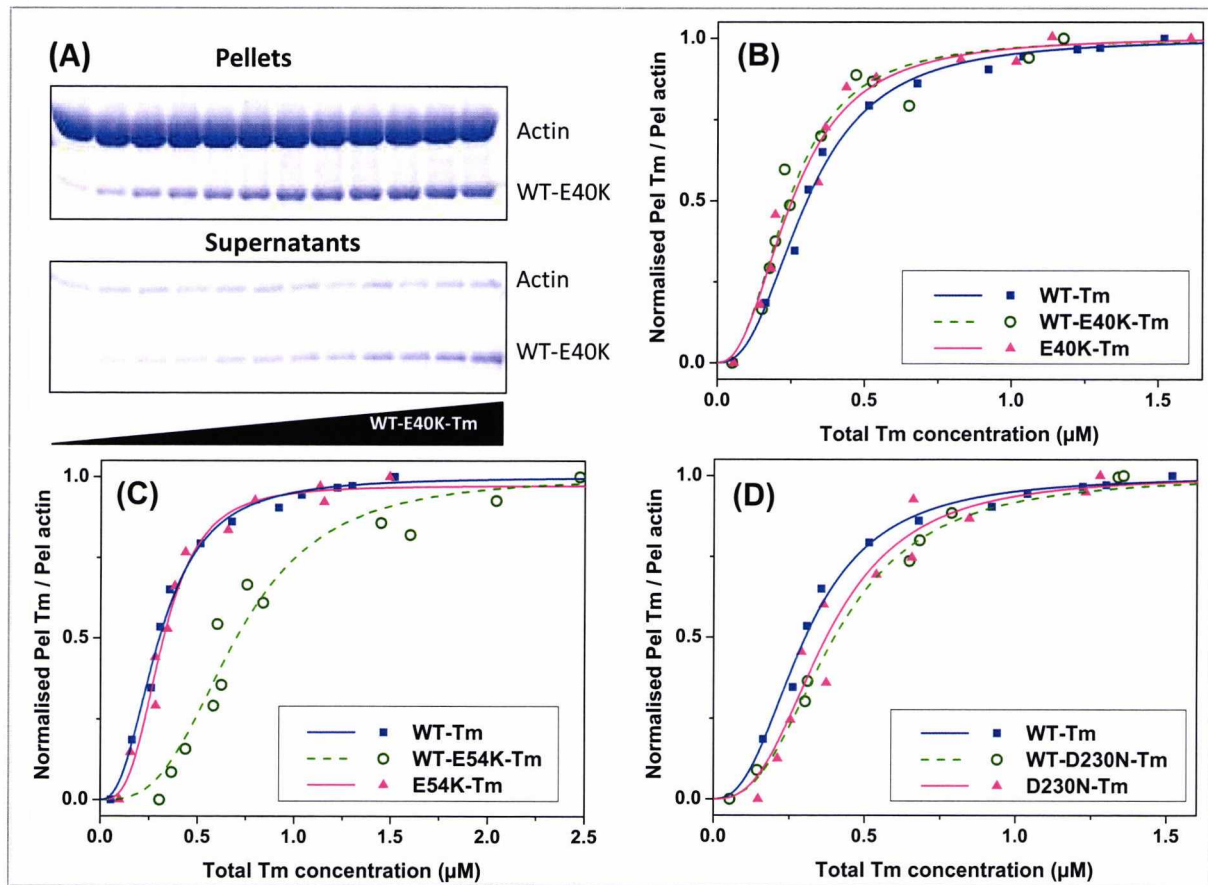
Figure 5.2.7 Actin affinity of Tm carrying DCM mutations. (A) The mixture of F-actin (7 μM) and Tm (0.2 – 2.4 μM) from the pellet and supernatant loaded onto 10 % SDS gel and analysed by densitometry. (B, C and D) Fractional saturation of actin by Tm plotted as a function of free Tm concentration for (B) WT-E40K-Tm (o) and E40K-Tm (▲); for (C) WT-E54K-Tm (o) and E54K-Tm (▲) Tm; and for (D) WT-D230N-Tm (o) and D230N-Tm (▲) Tm. The data of WT-Tm (■) for (B,C & D). The best fit to the Hill equation is superimposed on the data. Each data set is a representation of the one measurement for Tm homo or heterodimer compared to the WT. The actin affinity ($K_{50\%}$) and the Hill coefficient (h) derived from the fitting are listed in Table 5.2. Buffer conditions: 100 mM KCl, 20 mM MOPS, 5 mM $MgCl_2$ pH 7.0.

of Tm dimer caused significant decrease in the affinity to actin (0.46 μM, $p \leq 0.05$). The Hill coefficients in majority of Tm constructs showed similar values (2.0 – 2.9) with exception of the WT-E54K-Tm at low (h =1.3) and the E40K-Tm at high (h = 3.4) values for the apparent cooperativity. It is important to mention that the values of the apparent cooperativity derived from the fits are highly affected by the first points of the measured data. These

points are at very low concentrations (0.2 µM) therefore to reach a high precision of the final values is demanding and the interpretation of the results must be considered carefully.

Tm dimers	$K_{50\%}$ (µM)	h
WT-Tm	0.24 ± 0.03	2.9 ± 2.2
WT-E40K-Tm	0.30 ± 0.08	2.5 ± 1.5
E40K-Tm	0.27 ± 0.05	3.4 ± 1.4
WT-E54K-Tm	0.79 ± 0.35	1.3 ± 0.3
E54K-Tm	0.35 ± 0.04*	2.4 ± 0.7
WT-D230N-Tm	0.46 ± 0.14*	2.0 ± 1.0
D230N-Tm	0.28 ± 0.06	2.6 ± 0.5

Table 5.2 The affinity and the binding cooperativity of HCM Tm dimers for F-actin. The actin binding affinity ($K_{50\%}$) and the Hill coefficient (h), both derived for the fit of the Hill equation to data of Figure 5.2.7 B, C, and D. The data represents an average of at least three measurements ($n \geq 3$) with given SD values.

* Values differ compared to WT-Tm (*$p \leq 0.05$)

5.2.3 Effect of tropomyosin DCM mutations on calcium sensitivity of myosin subfragment 1 binding to a thin filament

The calcium sensitivity of S1 binding to the reconstituted thin filament containing Tm homo and heterodimers carrying DCM mutations was evaluated by the following stopped flow experiments. The concentrations used in this section are after mixing unless stated otherwise. The functional test of the hcTn·Tm complex to regulate binding of S1 to actin was carried out in the presence and absence of calcium (as described in chapter 2, section 2.3.3.4). 0.25 µM of S1 was rapidly mixed with 2.5 µM of ppA (10-fold excess), 1 µM Tm and increasing concentrations of hcTn. Actin was mixed with hcTn concentrations at 0.7, 1.4, 2.1, and 2.8 µM. The saturation was reached at 1.4 µM with a k_{obs} = 1.2 s^{-1} in the absence of calcium. The same reaction after addition of calcium showed an increase in k_{obs} 2-fold to 2.6 s^{-1}. This value was only half of the value in the absence of hcTn (5.3 s^{-1}).

The proteins with sufficient activity (2-fold difference ±calcium) were then used for the formation of the thin filaments reconstituted with pyr-actin, hcTn and αTm carrying a DCM mutation (E40K, E54K, or ED230N) in one or both chains of the Tm dimer.

The calcium sensitivity of the thin filaments containing DCM mutations was measured by stopped flow (for the method see chapter 2, section 2.3.3.5). Similarly as in the previous chapter, a 10-fold excess of S1 binding to thin filaments was chosen for the experiment due to the limited yields of the heterodimers. Thin filament proteins were mixed at the concentration of 2.5, 1, and 1 μM for F-actin, Tm and hcTn, respectively and then pre-incubated for 1 hour at 4 °C. Higher concentration of the proteins ensured efficient reconstitution of the filament with all of its functional components. Samples were then diluted 10-fold to the required concentration (0.25 μM pyr-actin, 0.1 μM hcTn and 0.1 μM αTm) and rapidly mixed with 2.5 μM of S1 over a range of defined calcium concentrations (from pCa 9.8 to pCa 4.6). The set of observed sigmoid transients measured with thin filaments containing E40K-Tm is shown in Figure 5.2.8.
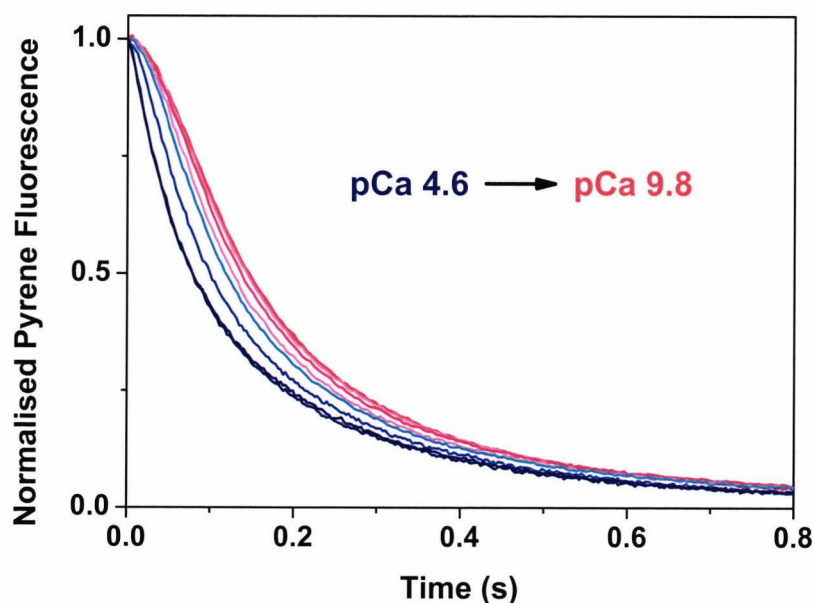
Figure 5.2.8 Observed transients of S1 binding to the thin filaments under various calcium concentrations. Thin filaments were reconstituted with ppA, hcTn and αTm carrying DCM mutations and rapidly mixed with 10-fold excess of S1. Experimental conditions: 100 mM KCl, 20 mM MOPS, 5 mM MgCl₂ pH 7.0 with addition of 2 mM pCa buffers at various calcium concentrations.

The shift between observed sigmoid transients in Figure 5.2.8 is caused by the presence of calcium at defined concentrations. Calcium binds to the N-terminal region of

cTnC and causes a conformational change on cTnI. Tm is shifted further from the actin binding sites enabling cooperative binding of S1. The binding of ATP-as to the pyrene labelled actin decreases the fluorescence signal and higher calcium concentration increases the rate of the reaction.
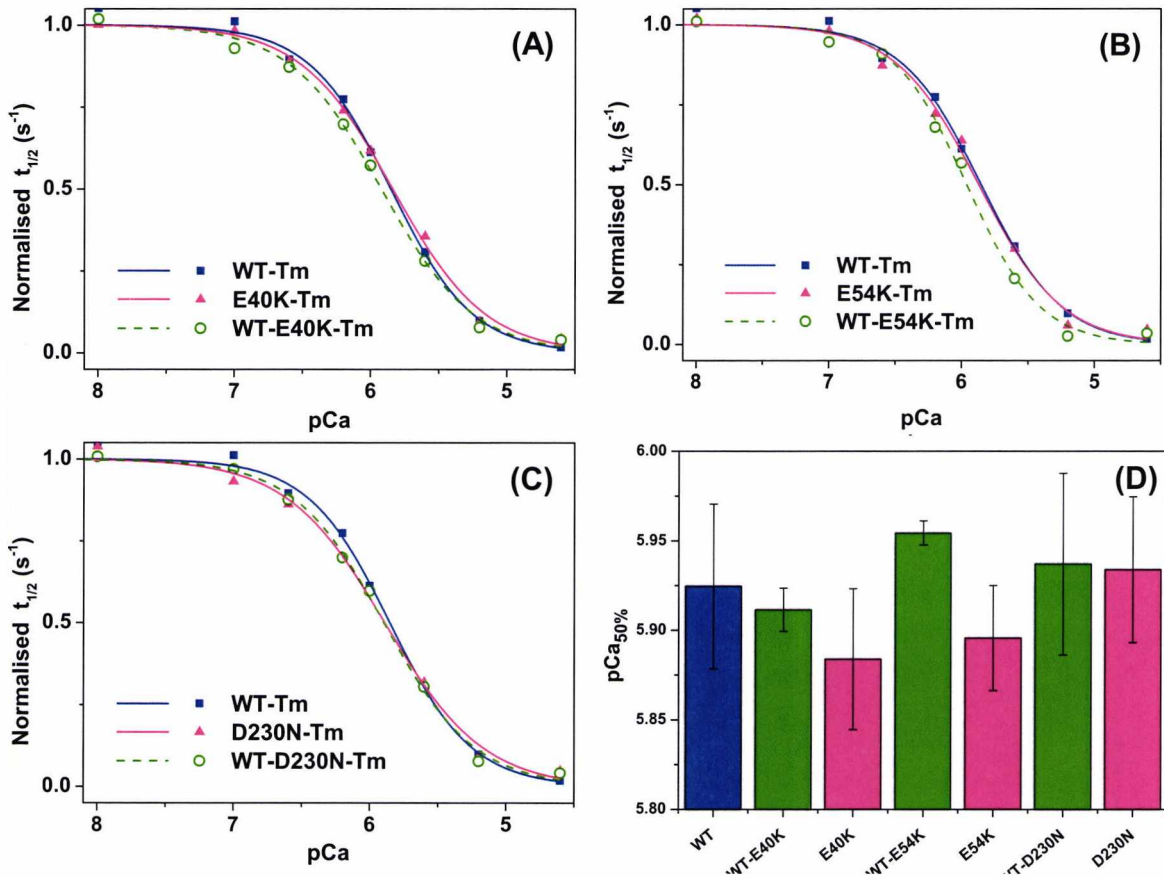
5.2.9 Calcium sensitivity of reconstituted thin filaments binding to S1. The fractional half time ($t_{1/2}$) derived from the observed transients of S1 binding to the thin filaments is plotted against pCa concentrations. Data for WT-Tm (■), WT-E40K-Tm (o) and E40K-Tm (▲) are shown in (A); WT-Tm (■), WT-E54K-Tm (o) and E54K-Tm (▲) are shown in (B); and WT-Tm (■), WT-D230N-Tm (o) and D230N-Tm (▲) are shown in (C).   The best fit to the Hill equation is superimposed with midpoints (pCa$_{50\%}$) and Hill coefficients (h) presented in Table 5.3. Each data set fitted into the individual sigmoid curves showed in the panels A, B and C is a representation of the one measurement. (D) Comparison of all measured values of pCa$_{50\%}$ for the five Tm constructs, including standard deviation. Each column represents an average of three measurements (n=3).

The fractional half times ($t_{1/2}$) derived from the individual observed transients of S1 binding to the thin filaments were plotted against corresponding pCa concentrations. The

data for WT-E40K, WT-E54K-Tm and WT-D230N-Tm heterodimers with the best fit to the Hill equation superimposed are shown in Figure 5.2.9 A, B and C, respectively. The data for the WT and the mutant homodimers are also shown for comparison. Each data set, fitted into the individual sigmoid curves, shown in the panels A, B and C represents one measurement. The calcium sensitivity curves had a typical sigmoid shape. The midpoint of the fitted curve ($K_{50\%}$) and the Hill coefficient (h) for the WT were compared to the same data for the Tm homo and heterodimer constructs.

Tm dimers	$pCa_{50\%}$	h
WT-Tm	5.93 ± 0.05	1.30 ± 0.02
WT-E40K-Tm	5.91 ± 0.01	1.24 ± 0.06
E40K-Tm	5.88 ± 0.04	1.28 ± 0.02
WT-E54K-Tm	5.95 ± 0.01	1.33 ± 0.23
E54K-Tm	5.90 ± 0.03	1.37 ± 0.05
WT-D230N-Tm	5.94 ± 0.05	1.23 ± 0.11
D230N-Tm	5.93 ± 0.04	1.27 ± 0.09

Table 5.3 Calcium sensitivity of the thin filaments reconstituted with F-actin, hcTn and αTm carrying DCM mutations. The $pCa_{50\%}$ value is the apparent calcium affinity, and h is the Hill coefficient for calcium switching of the thin filaments, both derived from the best fit of the Hill equation to the data shown in Figure 5.2.8 A, B and C. All $pCa_{50\%}$ and h values are an average of three measurements (n = 3).

Any change in the $K_{50\%}$ value indicates calcium sensitivity of the system. The fitting procedure yielded also the Hill coefficient (h) which is a measure of the apparent cooperativity of the calcium dependent S1 binding to the thin filament. Each measurement was repeated three times using three independent samples of each Tm construct. A summary of the measured data is shown in Figure 5.2.9 D and the numerical values of $K_{50\%}$ and h derived from the fitting are listed in Table 5.3.

The results showed no significant changes in the calcium sensitivity of thin filaments or cooperativity of the system in any of Tm constructs carrying DCM mutations.

5.3 Discussion

Various biochemical properties of Tm-heterodimers carrying DCM mutations E40K, E54K and D230N in only one chain of the dimer were assessed to elucidate possible differences of these proteins from the WT and double-mutant homodimers. Previous investigations of the effects of DCM mutations on the function of the cardiac muscle have been made mostly with Tm homodimers (Bai et al., 2012; Borovikov et al., 2011; Chang et al., 2005; Mirza et al., 2005; Robinson et al., 2007; Robinson et al., 2002) and some studies have been done with 50 : 50 % mixtures of the WT and mutant protein (Lakdawala et al., 2010; Memo et al., 2013; Mirza et al., 2007). However, the understanding of the delicate interplay between sarcomeric proteins in muscle tissue affected by cardiomyopathy requires characterisation of biophysical and biochemical properties of Tm heterodimers as they are likely predominant species in heterozygous individuals with autosomal dominant DCM. To date, three α-Tm mutations (E40K, E54K and D230N) are known to cause DCM (Lakdawala et al., 2010; Olson et al., 2001). We assembled Tm heterodimers containing only one of each mutation and measured their thermal stability, affinity to actin and calcium dependent activation of reconstituted thin filament *in vitro*.

Results of our study show following findings. Thermal unfolding of the cross-linked WT and D230N-Tm homodimers shows similar unfolding profiles with three thermal transitions. Two major thermal transitions at ~35 °C and at ~57 °C and the third smaller transition at ~48.5 °C. (NB We denoted and refer to the three transitions as the first (at low temperatures), the second (at high temperature), and the intermediate, respectively.) The WT-Tm data are in agreement with previous measurements at high salt concentrations (Hayley et al., 2011; Kalyva et al., 2012). The first and second thermal transitions of the E40K-Tm homodimer occur at the same temperature as the WT and D230N-Tm but the intermediate thermal transition shows ~1 °C decrease in stability. Cross-linked E54K-Tm homodimer shows the same shift (~1 °C) in the intermediate thermal transition as the E40-K homodimer but at the higher temperatures the E54K-Tm gains ~1 °C (Figure 5.2.2 C). The first unfolding event of cross-linked WT-E40K heterodimer occurs at ~2.5 °C lower temperature compared to WT (35.2 °C) while the D230N-Tm construct at the same region is similar to WT. Unfolding isotherms at higher temperatures over 40 °C in WT-E40K indicate

small loss of stability between 45 – 60 °C (Figure 5.2.2 A) and the WT-D230N heterodimer show small gain of stability between ~40 – 50 °C (Figure 5.2.2 E). However, these changes are small and presumably negligible in the physiological conditions. In contrast, thermal stability of the WT-E54-Tm heterodimer is significantly higher by between the range of 35 - 55 °C Figure 5.2.2 C).

Reduction of the cross-link at Cys190 decrease thermal stability of the E40K-Tm homodimer between 40 – 50 °C by ~1.5 °C, compared to reduced WT-Tm. Unfolding profile of reduced D230N-Tm is indistinguishable from WT. Previous CD measurements of E54K-Tm homodimer thermal stability at high salt concentrations (0.5 M NaCl) showed increased thermal stability over the range of 35 – 65 °C (Rajan et al., 2007). However, our measurements for E54K-Tm homodimer show an increased thermal stability only at high temperatures between 50 – 60 °C (Figure 5.2.2 D) with peak of the thermal transition at 57.8 °C (~5.0 °C higher than WT). Stability at temperatures between 40 - 50 °C is increased by ~1°C and the unfolding profile of reduced E54K-Tm homodimer at temperatures under 40 °C matches those of the WT. Interestingly, all reduced Tm heterodimer constructs showed significant decrease of thermal stability compared to both WT and their respective double-mutant homodimers especially at lower temperatures between 30 and 45 °C. Unfolding of reduced WT-E40K and WT-D230N-Tm starts to differ from the WT at ~30 °C and in the case of WT-E54K at ~25 °C. These values are much lower than the physiological temperature (~37 °). Therefore if decrease in thermal stability, caused by DCM mutations, contributes to the cardiac pathology then the heterodimers may have larger impact compared to the mutant homodimers.

Co-sedimentation assays showed ~1.5 and 2-fold weaker affinity to actin of the E54K-Tm homodimer and WT-D230N-Tm heterodimer in comparison to WT ($K_{50\%}$ 0.24 µM), respectively. All the other Tm homo and heterodimer constructs did not show significant difference ($p \leq 0.05$) in actin affinity compared to the WT. Based on the results from thermal stability measurements we predicted that cross-linked WT-E54K-Tm heterodimer might show significant change in actin affinity. Averaged $K_{50\%}$ value for this heterodimer was in fact ~3.3-fold weaker, but a large error in the measured data did not indicate statistically significant difference from the WT value (Figure 5.2.7 and Table 5.2). Additionally the Hill coefficient in all measurements for the WT-E54K-Tm was consistently lower (~2.2-fold) in all measurements indicating loss of cooperativity while all the other Tm constructs were similar

to WT. All Tm constructs bind actin with a tight apparent affinity, and in a muscle fibre where the concentrations of both Tm and actin is much higher, all Tms will bind to actin. Therefore, the measured differences in apparent affinity are probably negligible at physiological level.

Measurements of calcium dependent S1 binding to the reconstituted thin filaments with Tm homo and heterodimers containing selected DCM mutations did not show any significant differences in all samples. Previous measurements of ATP-ase activity with reconstituted thin filaments at 37 °C showed significant decrease in calcium sensitivity for both E40K-Tm (ΔpCa -0.165) and E54K-Tm (ΔpCa -0.476) homodimers (Mirza et al., 2005). Another study of E40K and E54K-Tm isometric tension using the thin filament extraction/reconstitution technique showed no difference in calcium sensitivity at high ionic strength solution (200mM) between either mutant and the WT at 25 °C (Bai et al., 2012). Recent study using quantitative *in vitro* motility assays showed decreased calcium sensitivity in E40K-Tm, increased calcium sensitivity in D230N-Tm while E54KTm was unaffected (Memo et al., 2013). *In vitro* functional studies of calcium dependent myosin S1 binding to reconstituted thin filament containing D230N-Tm showed reduced calcium sensitivity (ΔpCa 0.27), a lower maximum ATPase turnover rate and decreased calcium affinity to the thin filament at 37 °C (Lakdawala et al., 2010). Changes in calcium sensitivity observed in previous studies at 37 °C diminished with lower temperature (25 °C)(Bai et al., 2012). Therefore it is essential that experimental conditions are as close to physiological conditions as possible.

In this chapter we established that some properties of Tm heterodimers are different from WT and their respective mutant homodimers. We also show that DCM mutations cause only small differences. Therefore in order to produce meaningful results it is important to use physiological parameters in the experimental set up if possible. To conclude, our measurements did not show any parameter that changes systematically with DCM mutations in Tm heterodimers which is in agreement with previous studies (Memo et al., 2013; Mirza et al., 2007). Detailed discussion, implications and conclusions on the results from this chapter are described in following chapter 6.

Chapter 6

General Discussion and Conclusions

6.1 General discussion

Hypertrophic (HCM) and dilated (DCM) cardiomyopathy are primarily genetic heart disorders associated with an impaired myocardial function. Characteristic features of HCM are the thickening of the ventricular walls, myocyte disarray and interstitial fibrosis and the key features of DCM are dilation or thinning of the ventricular walls and impaired systolic function. Both HCM and DCM can cause arrhythmias which lead to sudden cardiac death or heart failure. Cardiac dilation and hypertrophy are distinct phenotypes which can be caused by the different mutations on the same sarcomeric protein (Seidman and Seidman, 2001). The important question to address then is whether the mutations that generate one phenotype are caused by the same functional abnormality or there are multiple separate programs that remodel the heart. Presumably heart contractility of affected individuals is abnormal and may be considered as a primary effect.

Additionally, the expression of various Tm isoforms and their ability to form dimers either with the same isoform carrying cardiomyopathy mutation in one or both chains, or with the different isoforms may contribute to the heart function.

Numerous biochemical and biophysical techniques have been used for the characterisation of Tm carrying cardiomyopathy mutations over a broad range of organisation, from single molecule to intact tissue or transgenic animals. In solution studies provide valuable starting point for exploring the downstream consequences of cardiomyopathy mutations on the contractile function. Previously, the properties of Tm carrying DCM or HCM mutations were investigated using only mutant homodimers or

151

mixtures. However, affected heterozygous individuals may express the mutant and WT proteins in a 1 : 1 ratio and so, if there are no preferences in the dimer formation between the mutant and the WT monomers, theoretical ratio of the Tm dimers *in vivo* should be 1 : 2 : 1 for αα, αα* and α*α*, respectively. Heterodimers carrying the mutation in only one chain of Tm dimer can be potentially predominant in the muscle cell. Studies of the expression of Tm carrying cardiomyopathy mutations in cultured cardiac myocytes (Michele et al., 1999) or in human skeletal muscle biopsies (Bottinelli et al., 1998) show expression levels of the mutant Tm at 40 – 50 %. Therefore, there is a high probability of a significant proportions of assembled Tm heterodimers *in situ*, but to date, this has not been investigated in biopsies, cell cultures or transgenic mice. Additionally there are skeletal muscle myopathies associated with the TPM2 and TPM3 genes where the mutations may form αβ*, αγ*, ββ*, γγ* heterodimers in affected tissue (Laing et al., 1995; Lawlor et al., 2010). Little is known about the dimerisation of these isoforms *in vivo* but it is important to address the composition of Tm dimers as it may strongly influence muscle contractile performance (Corbett et al., 2005).

It has been shown that rat HMW Tm isoforms skα-Tm, skβ-Tm and smα-Tm form predominantly heterodimers with Tm-1 (from β gene), Tm-2 and Tm-3 (from α gene) *in vivo* (Gimona et al., 1995). However, the skα-Tm, skβ-Tm and smα-Tm failed to form dimers with LMW cytoskeletal isoforms Tm4 (from γ gene), Tm5a and Tm5b (both from α gene). Additionally the LMW fibroblast isoforms Tm-4 and Tm-5(NM-1) can form homo- and heterodimers with each other but failed to dimerise with HMW isoforms Tm-1, Tm-2 and Tm-3 (Temm-Grove et al., 1996). Expression of multiple isoforms has been shown in the studies of human fibroblasts (Novy et al., 1993) and mammalian vascular smooth muscle cells (Gallant et al., 2011). In the latter at least five LMW and HMW Tm isoforms were observed. Thus the potential to form heterodimers in cells is clearly there. What remains is the direct proof of their presence in tissues and then characterisation of the properties *in vitro* and *in vivo* where our method can be utilized.

Detection of Tm heterodimers in tissue samples might be possible if the dimers can be cross-linked before extraction and further analysis. It is important to mention, that the differences in molecular mass between the WT and all DCM mutations in this study is too small (1 Da) to be detected by SDS-PAGE gels or mass spectroscopy. The mass of the E180G monomer is lower compared to the WT by 72.1 Da but the D175N mutation again differs

just by 1 Da. Isoelectric focusing might be used for detection of Tm heterodimers utilizing different net charges of the dimers (Warren et al., 2008). Whether Tm heterodimers assemble into the thin filaments or alter the calcium activation of muscle contraction will depend on their interactions with the other thin filament components.

Tm can assemble on the surface of actin into polymers via head-to-tail interaction which is a main driver for actin binding. The N-terminal region of Tm can be alternatively spliced by exon 1a for HMW Tms and by exon 1b for LWM. For the C-terminal region there are four alternate exons 9 for TPM 1and TPM3, two exons for TPM2 and one in TPM4. Thus there is range for the alternate N and C-termini to find and preferentially bind to a specific partner. However evidence for or against the specific binding of Tm pairs has not been investigated to date. The potential for formation of co-polymers is present in the case where different Tm-isoforms are expressed with identical N and C-termini. However, the gestalt theory (Holmes and Lehman, 2008) in which the Tm shape is major determinant of actin binding, may allow internal exons – through changes in the shape of Tm, or the precise match with the actin surface of various actin isoforms, to specifically select specific Tm isoform. Similarly, the initiation of actin assembly *in vivo* via actin binding proteins such as formins (Goode and Eck, 2007) may preferentially recruit a specific Tm isoforms. The selection for specific Tm isoforms then may continue via Tm-Tm contacts.

Investigation of the different Tms binding to actin in solution is possible by competition binding experiments or it could be done by measurements of how effective are Tm isoforms at displacing each other from actin filament. The best and most effective method of how establish the extent of Tm isomers co-assembly is via fluorescence labelling of individual isoforms and high resolution single fluorescence methods.

At the beginning of our study, we hypothesised, that Tm heterodimers might have different properties from both WT and $\alpha^*\alpha^*$-Tm homodimers. Non-linear relationship between the functional properties of 1 : 1 WT/mutant Tm homodimer mixture, reported in previous study, suggested that this might be the case (Memo et al., 2013; Mirza et al., 2005).

Prior to the work, a reliable method for the formation and subsequent isolation of defined skeletal Tm heterodimer was not available thus all *in vitro* studies have been made exclusively with Tm homodimer mutants or mixtures of Tm homodimers. Recently such a method was developed for the formation of skeletal $\alpha\beta$-Tm heterodimers (Kalyva et al.,

2012), and here we report an optimisation of the method for α-Tm carrying DCM or HCM mutations. We have shown that bacterially expressed Tm carrying HCM or DCM mutations do not have any preference for the formation of homodimer over heterodimer as a combination of 50 % α*-Tm with 50 % of His α-Tm produced a mixture of dimers close to the predicted ratio of 1 : 2 : 1 (αα, αα*, α*α*) (Section 3.2; Figure 3.2.3 C). The ratio of formed dimers shows that the introduction of the His tag, used in the method for the formation and purification of Tm heterodimers, does not affect dimerisation. Assembled heterodimers were chemically cross-linked at Cys190 in order to ensure stability of the dimers during the purification. Cross-linked dimers were then used in the all assays described in this work except the measurements of calcium sensitivity in DCM constructs (chapter 5, section 5.2.3). It has been shown that in the cases of failing heart the production of reactive oxygen species may be increased (Seddon et al., 2007; Sheeran and Pepe, 2006) and this could lead to oxidation of Tm (Canton et al., 2011). Formation of the cross-link fixes two chains of Tm dimer together which may inflict a strain between the chains. This could explain decreased thermal stability of cross-linked Tm constructs at low temperatures, typically ~25 – 40 °C, (Tables 4.1 and 5.1) compared to reduced Tm dimers. However, Tm is normally reduced *in vivo* (Lehrer et al., 2011) and we are able to make Tm heterodimers without cross-link as the purification did not affect dimer stability. Preliminary measurements of a possible exchange between the chains of reduced Tm homodimers did not show any changes up to 8 days at high salt (500 mM KCl) and 4 °C. Heterodimer samples seem to be stable in laboratory conditions but under the *in vivo* conditions, at higher temperature and protein concentration, the chain exchange may occur.

Because the dimer formation was not affected by the mutations, we considered what other role the side chains of HCM and DCM mutations in the homo and heterodimer might play in the overall function. The surface charge residues of E40K, E54K, D175N, E180G and D230N mutations are in position to alter intra- and inter-chain stability (Li et al., 2012; Olson et al., 2001) or alter the interaction with actin (Lehman et al., 2000) or with cTn and therefore alter calcium sensitivity (primarily HCM mutations positioned in the cTn binding region).

Discussion on the HCM mutants results

Both HCM mutations D175N and E180G reduced the apparent affinity for actin by ~2.5-fold compared to the WT ($K_{50\%}$ = 0.21 µM), as shown previously (Boussouf et al., 2007; Golitsina et al., 1999). Measured values for the WT-D175N-Tm ($K_{50\%}$ = 0.23 µM) heterodimer were similar to the WT while WT-E180G-Tm ($K_{50\%}$ = 0.27 µM) was intermediate between WT- and E180G-Tm homodimers. Both mutations are in very close proximity to each other but while Glu180 at position e can form the salt bridge with Arg182 on the opposite chain (g'), the inter-helical interactions between negatively charged Asp175 at position g and Glu173 (e') are repulsive. Thus the substitution of Glu180 for polar uncharged Gly might cause larger effect by destabilisation of the coiled-coil than the substitution of Asp175 for polar uncharged Asn which should increase the local stability. This assumption is supported by thermal stability measurements using circular dichroism where WT-D175N-Tm heterodimer and D175N-Tm homodimers did not show any difference compared to the WT when cross-linked or reduced (Figure 4.2.3 A and B). Conversely, WT-E180G-Tm heterodimer showed an intermediate decrease in thermal stability at low temperatures (~30 °C) between WT and E180G homodimers when cross-linked (Figure 4.2.3 C). Reduction of the salt bridge at Cys190 resulted in the thermal transition between 30 - 40°C with significantly decreased thermal stability of the WT-E180G-Tm heterodimer at physiological temperature (midpoint of the peak at 36.4 °C). The first derivative of measured data from thermal stability assays were plotted into a bar graphs for clarity (Figure 4.2.5). It has been shown that the binding of Tm to F-actin increases stability of the dimers by ~3 °C (Kremneva et al., 2004) and once bound and polymerised at the actin surface the dimers are resistant to unfolding. Additionally, measurements of the apparent affinity showed strong interactions between all Tm constructs and actin. The differences between the WT and WT-E180G-Tm were statistically significant but *in vivo* might be negligible due to the higher concentration of the proteins present. The co-sedimentation assays binding in the off state were performed at 20 °C but actin affinity at physiological temperatures (~37 °C) may be weakened even more. It also has been shown that affinity of Tm to actin in the off-state may be different compared to affinity for the on-state where S1 is present (Mirza et al., 2007). Additionally, during the vigorous exercise or fewer, temperature can exceed 37 °C and in individuals carrying the E180G mutation may possibly affect normal cardiac function.

The fact that E180G mutation causes more severe HCM than D175N may favour our assumption. The results from thermal stability measurements and co-sedimentation assays indicate that reduced actin affinity of affected HCM Tm constructs could not be caused by partially unfolded Tm dimers as the stability of all proteins at 20 °C was similar to that of WT. It has been postulated that the property essential for Tm binding to actin is the native three-dimensional form of Tm molecule which is pre-shaped to match the actin filament surface (Holmes and Lehman, 2008). This hypothesis has been validated by the electron microscopy studies showing curved or pre-shaped Tm molecules with moderate flexibility ensuring effective binding to actin and the cooperative movement on F-actin (Li et al., 2010; Sousa et al., 2010). Based on these observations, we measured the flexibility of D175N and E180G-Tm homo and heterodimers as the mutations could alter the average Tm curvature and therefore affect proper Tm assembly onto the thin filament and the interactions with Tn leading to an increase calcium sensitivity of the thin filament. The images of our Tm constructs acquired by electron microscopy and analysed by molecular dynamic simulations showed that D175N- and E180G-Tm homodimers both caused a ~20 % reduction in persistence length of the protein indicating an increase in local and global bending flexibility (Table 4.5). The same approach used for the WT-D175N- and WT-E180G-Tm heterodimers showed similar decrease in the persistence length from their respective homodimers. The local charge neutralisation caused by both HCM mutations might affect the orientation of side-chains of neighbouring residues such as E181 which is critical for binding to actin (Li et al., 2011). This perturbation may reduce the steric hindrance of myosin binding to actin and increase calcium sensitivity of the thin filament activation.

Increased calcium sensitivity caused by D175N and E180G-Tm homodimers in a fully assembled actin filament using *in vitro* motility assays or reconstituted muscle fibres has been reported previously (Bai et al., 2011; Bing et al., 2000; Wang et al., 2011). For the investigation of the effects of Tm heterodimers carrying D175N and E180G mutations on calcium sensitivity of the thin filament we used *in vitro* kinetic approach previously described by Boussouf, et al. (2007). Our measurements of the apparent calcium affinity for switching of the reconstituted thin filaments with D175N- (ΔpCa +0.08) and E180G-Tm (ΔpCa +0.14) homodimers are in agreement with previously reported data (0.09 and 0.13, respectively) (Boussouf et al., 2007). Surprisingly, the WT-E180G-Tm heterodimer showed only a small and not significant ΔpCa (+0.03) compared to WT, while the WT-D175N-Tm

ΔpCa (+0.11) was close to the value of D175N homodimer (+0.08). The pCa shifts are small, therefore we tested if the similar changes in calcium sensitivity could be seen in the sarcomere. Mechanical behaviour measurements were carried out only in Tm homo and heterodimer with E180G mutation. Using the extraction-replacement method in isolated rabbit psoas myofibrils (Scellini et al., 2010) we show enhanced tension development (i.e., thin filament activation) in E180G-Tm homodimer at low calcium concentration whereas heterodimer remained unaffected (Table 4.4). These results are in agreement with the data using pure actin·Tm·Tn filaments. The results from actin binding assays and calcium sensitivity measurements in reconstituted thin filaments suggest possible preferential orientation of the WT-D175N and WT-E180G-Tm heterodimers on actin. Our observation suggest that neutral Asn175 residue is positioned on the chain further from actin-Tm binding site and closer to a TnT2 binding site, therefore this heterodimeric variant do not affect actin affinity but can affect calcium sensitivity. In contrast, neutral Gly180 residue is positioned on the chain closer to the actin-Tm binding site and further to the TnT2 binding site causing decreased actin affinity and leaving calcium sensitivity unaffected.

Discussion on the DCM mutants results

Thermal stability measurements of Tm constructs carrying DCM mutations did not show significant changes in cross-linked E40K, E54K, and D230N-Tm homodimers at low temperatures. Cross-linked WT-E40K and WT-D230N-Tm heterodimers (Figure 5.2.2 A and E, respectively) showed a shift of the first thermal transition by ~ 3 °C (at ~32.8 °C). The unfolding profile of the WT-E54K-Tm heterodimer indicated significant increase in thermal stability over the range of 35 – 55 °C (Figure 5.2.2 C). Reduction of the cross-link at Cys-190 did not show any significant differences in thermal stability between WT and all three DCM mutations carrying Tm-homodimers up to 40 °C. Reduced E54K-Tm homodimer (Figure 5.2.2 D) showed 5° C increase in thermal stability at high temperatures (~58 °C) and E40K-Tm homodimer (Figure 5.2.2 B) showed decrease at temperatures between 40 and 55 °C by ~1.5 °C, compared to the WT-Tm. Thermal unfolding profile of reduced D230N-Tm homodimer (Figure 5.2.2 F), similarly as for the cross-linked D230N-Tm homodimer, was indistinguishable from the WT. Measured data of the D230N-Tm indicates that predicted

loss of the intra-helical stability in this mutant (disrupted interactions with Lys-286 and Lys-233) does not have any effect on thermal stability. The changes in thermal stability of E40K and E54K-Tm homodimers underline the importance of individual inter-helical electrostatic interactions (positions *e* and *g*) for the stability of Tm coiled-coil. Reduced WT-E40K-Tm and WT-D230N-Tm heterodimers show decreased thermal stability by ~2.5 °C and ~4.5 °C at low temperatures (30 - 45 °C), respectively (Figure 5.2.2 B and F). The intermediate thermal transitions in both heterodimers occur at ~46.3 °C (decrease by ~1°C) and the second thermal transition occur at ~51.5 °C (decrease by ~1.4 °C), compared to WT. As mentioned previously, the heating procedure of reduced Tm heterodimers will cause reannealing of the protein samples into a mixture of αα-, αα*-, α*α*-Tm dimers in a ratio of 1 : 2 : 1. The estimation of unfolding transitions for the pure Tm heterodimers was made by subtracting 25 % of the expected transitions for WT and the mutant homodimers. The subtraction procedure in both WT-E40K and D230N-Tm heterodimers did not change positions of the individual transitions but reduced their relative proportions. The WT-E54K-Tm heterodimer showed severely reduced thermal stability at the temperatures between ~25 and 55 °C (Figure 5.2.2 D). The first thermal transient at low temperatures is less stable by ~4.7 °C compared to those of WT (40.2 °C). The E54K mutation is close to the E40K, yet the latter shows smaller changes in thermal unfolding of Tm dimer. The differences may be ascribed to the proximity of E40K to the alanine cluster positioned upstream on the chain (residues 18, 22, 25, and 32) while there is a second alanine cluster found downstream (residues 67, 74, 78, and 81) (Brown et al., 2001). The E54K mutation is position between these two alanine clusters possibly affecting both flexible sites and causing enhanced destabilisation compared to E40K mutation. Interestingly, a large loss of stability is underlined by differentiated data for the WT-E54K-Tm heterodimer showing only one thermal transition after above described subtraction procedure (see chapter 5, Figure 5.2.4 D). It is important to mention that the subtraction procedure inflicts a large error on the data and it would be most accurate in cases when measured data of the heterodimer are intermediate between the WT and mutant homodimers. Our measurements under reducing (*in vivo*) conditions demonstrate that all Tm heterodimers carrying DCM mutations are less stable then the pure mutant homodimers at physiological temperatures close to 36 °C. Graphical summary of the first derivative data is shown in Figure 5.2.6.

Co-sedimentation assays show significantly weaker affinity to F-actin for the E54K-Tm homodimer ($K_{50\%}$ 0.35 µM) and WT-D230N-Tm heterodimer ($K_{50\%}$ 0.46 µM) in comparison to the WT ($K_{50\%}$ 0.24 µM). Statistical analysis of D230N-Tm homodimer, E40K DCM homo and heterodimer constructs does not show significant differences in apparent actin affinity from the WT (p ≤ 0.05). The WT-E54K-Tm heterodimer have the weakest measured affinity ($K_{50\%}$ 0.79 µM). However, the large error in the measurements of this heterodimer caused that this value is not significantly different from the WT. The apparent cooperativity of Tm binding to F-actin, defined by the Hill coefficients, show similar values (2.0 – 2.9) in majority of Tm constructs with exception of the WT-E54K-Tm (h = 1.3) and the E40K-Tm (h = 3.4).

We tested calcium sensitivity as an important indicator of cardiomyopathy mutations on the activation of the thin filament using similar approach as for the HCM mutations. However, in solution data of calcium dependent S1 binding to the reconstituted thin filaments do not show significant differences between the WT and DCM constructs. Previous measurements of ATP-ase activity with reconstituted thin filaments at 37 °C reported reduced calcium sensitivity for both E40K-Tm (ΔpCa 0.165) and E54K-Tm (ΔpCa 0.476) homodimers (Mirza et al., 2005). However, recent study of E40K and E54K-Tm mutants using the thin filament extraction/reconstitution technique (measurements were carried out at 25 °C) showed no difference in calcium sensitivity between both mutants and the WT (Bai et al., 2012). *In vitro* functional studies of calcium dependent myosin S1 binding to reconstituted thin filament containing D230N-Tm showed reduced calcium sensitivity (ΔpCa 0.27) at 37 °C (Lakdawala et al., 2010) while recent study showed increased calcium sensitivity (Memo et al., 2013). Considering the experimental conditions in previous studies, the absence of calcium sensitivity shift in any of our DCM constructs may be attributed to the low temperature (20 °) in our set up. The measurements also indicate that considerable variability of the effects of DCM mutations on the calcium sensitivity does not support changes of this property as being important compared to the D175N and E180G-Tm HCM mutations.

Our results show that both HCM and DCM mutations in Tm heterodimer alter various biochemical properties of the molecule (Table 6.1) and in some cases the effect is prevalent compared to the mutant homodimer. Tm heterodimers can therefore play an important role in a functional impairment of the regulation of muscle contraction causing cardiomyopathy specific long term chronic conditions leading to the development of an individual clinical

phenotype. Interestingly, current hypothesis about increased calcium sensitivity responsible for cardiac hypertrophy was confirmed only for the WT-D175N-Tm heterodimer. This observation may suggests other factors contributing to the phenotype development or the effect was not seen due to the experimental conditions set at other then physiological levels (low temperature). The situation in DCM mutations is more complicated as a common molecular phenotype was not yet firmly established. Early studies suggested that decreased calcium sensitivity resulting in a hypocontractile molecular phenotype (the opposite of HCM) may be cause (Olson et al., 2001; Rajan et al., 2007). However, recent studies at higher level of molecular organisation, using transgenic mouse model or proteins from human biopsies, did not confirm this hypothesis (Marston, 2011; Memo et al., 2013). Emerging factor in determination of the phenotype is the phosphorylation status of troponin. However the effect of the phosphorylation was not investigated in our study. We showed that Tm heterodimers carrying DCM mutations have severely reduced thermal stability in comparison to the HCM heterodimers. This may affect polymerisation (population/propagation) on the surface of actin filaments and presumably increase turnover of Tm dimers on the filament which may lead to energy deficiency and remodelling of the heart. Alternatively, our preliminary measurements of actin affinity using non-crosslink DCM heterodimers show similar (WD-D230N-Tm) or even higher (WT-E40K and WT-E54K-Tm) affinity for actin compared to the WT. This might be caused by an increase of the dimer flexibility. However as the WT chain is still present, the increase may "tune" the shape of the heterodimer the way that it matches the surface of actin better than the WT-Tm homodimer. Increased actin affinity of the heterodimers could mean an increased number of the initiation sites in the process of Tm polymerisation on the surface of actin and thus a slower saturation of the actin filament.

6.2 Conclusions

In this thesis we have characterised recombinantly expressed cardiac Tm heterodimers carrying HCM or DCM mutations in one chain of the dimer using various biochemical and biophysical methods *in vitro*. We established that the properties of Tm

heterodimers cannot be predicted from the interpolation of the WT and mutant homodimer data. We examined properties of the Tm homo and heterodimers including thermal stability, flexibility, actin affinity, calcium regulation of S1 biding, and calcium regulation of myofibril force. Our measurements show that the properties of the heterodimer may be similar to those of the WT (thermal stability of reduced WT-D175N; actin affinity of WT-E40K, and WT-D175N; ΔpCa of WT-E40K, WT-E54K, WT-E180G, WT-D230N) or the mutant homodimer (ΔpCa of WT-D175N, PL$_a$ of WT-D175N and WT-E180G), intermediate between two (actin affinity of WT-E180G), or different from both (discussed below). The measured data of calcium sensitivity and actin affinity in HCM Tm heterodimers suggested possible preferential binding to the partner proteins, actin and cTn. All chosen cardiomyopathy mutation, widely distributed within the Tm molecule (exons 2, 5 and 7), showed the strong link between the structure and function of Tm. Interestingly, in many cases (thermal stability of reduced WT-E40K, WT-E54K, WT-E180G, and WT-D230N; actin affinity of WT-E40, WT-E54K, and WT-D230N; ΔpCa of D175N) Tm heterodimers showed stronger effects than mutant homodimers. This observation may redefine our knowledge about the effect of Tm cardiomyopathy mutation on muscle contraction as Tm heterodimers are potentially predominant species in affected muscle cell. Summary of our results is provided in Table 6.1.

Results of this study provide insight into the molecular mechanism of functional impairment and consequent modification of myocardial phenotype in the presence of HCM or DCM mutations in Tm.

6.3 Future work

The work presented in this thesis could be enhanced by additional experiments in the future. It would be interesting to carry out co-sedimentation experiments and calcium sensitivity assays at physiological temperature 37 °C without the cross-link at Cys190. Increase of the temperature might show extended effects of Tm mutations on assessed properties closer to the *in vivo* scenario. Note that in the case of co-sedimentation assays at 37 °C a possible exchange of the chains between the non-cross-linked dimers must be

considered due to the length of the assay (~3 hours). As discussed previously, it has been shown that DCM mutations in Tm at physiological temperatures decrease calcium sensitivity for activation of the thin filament. However, recent study reported uncoupling of the effects caused by DCM mutations in Tm from TnI phosphorylation (Memo et al., 2013). Assessment of this findings using our experimental set up and DCM Tm heterodimers would be surely valuable addition to the topic as well as the evaluation of the flexibility in the Tm heterodimers carrying DCM mutations by electron microscopy or atomic force microscopy.

Another proposition for the future experiments would be to measure thermal stability at physiological salt concentration (~150 mM) in the presence and absence of actin. These measurements should be carried out by using differential scanning calorimetry as shown previously (Kremneva et al., 2004). This method is based on the changes in amount of heat required to increase the temperature of the sample compared to reference as a function of temperature. Therefore it is suitable for the measurements of the mixed samples (Tm and actin) unlike the circular dichroism method (used in this study for pure Tm) measuring the protein unfolding by monitoring of the secondary structure.

Based on the measured data of calcium sensitivity and actin affinity in WT-D175N and WT-E180G-Tm heterodimers, we suggested possible preferential binding of Tm heterodimers to F-actin and cTn. Further establishment of our predictions would require more experiments such as Tn binding to Tm-F-actin complex, thin filament activation or activated force development in WT-D175N heterodimer, EM or atomic force microscopy structural studies as well as use of other HCM or DCM mutations.

The most important question to address and experimentally confirm is the existence of Tm heterodimers carrying cardiomyopathy mutations *in vivo*. This might be quite challenging as the differences in molecular mass between $\alpha\alpha$-, $\alpha\alpha^*$- and $\alpha^*\alpha^*$-Tm dimers are very small. Firstly the dimers must be cross-linked before the extraction from the tissue and then samples could be differentiated by 2D electrophoresis gels.

Tm dimer	Thermal stability		Actin affinity	Flexibility	Calcium sensitivity	
	Cross-linked	Reduced			Reconstituted thin filament	Muscle fibrils
HCM constructs						
WT-D175N	≈	≈	≈	↑	↑	
D175N	≈	≈	↓	↑	↑	
WT-E180G	↓ (30 – 50 °C)	↓ (30 – 50 °C)	↓	↑	≈	≈
E180G	↓ (25 – 37 °C)	↓ (35 – 50 °C)	↓	↑	↑	↑
DCM constructs						
WT-E40K	↓ (50 – 60 °C)	↓ (30 – 55 °C)	≈		≈	
E40K	↓ (43 – 55 °C)	↓ (40 – 55 °C)	≈		≈	
WT-E54K	↑ (35 – 55 °C)	↓ (25 – 55 °C)	↓		≈	
E54K	↓ (35 – 55 °C)	↑ (50 – 60 °C)	↓		≈	
WT-D230N	≈	↓ (30 – 50 °C)	↓		≈	
D230N	≈	≈	≈		≈	

Table 7.1 Summary of the effects of HCM and DCM mutations on biochemical and biophysical properties of Tm. ↓ represents decrease; ↑ increase; ≈ indicates the same value as the WT.

Appendix
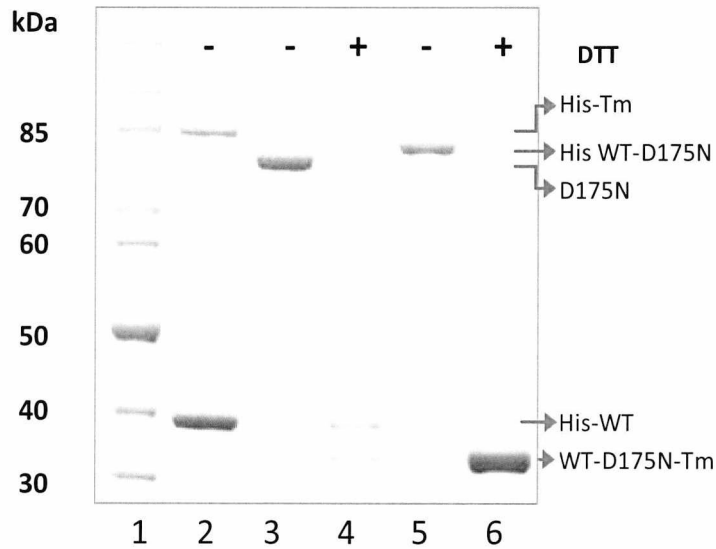
Figure A 1 Purity check of WT-D175N-Tm heterodimers: lane 1,molecular mass markers; lane 2, mixture of His-Tm dimers and monomers; lane 3, D175N-Tm dimers; lanes 4 and 5, His WT-D175N-Tm heterodimer under reducing and non-reducing conditions, respectively; lane 6, WT-D175N-Tm heterodimer after removal of the His tag under reducing conditions. Samples were run on 4 – 12 % SDS gel.
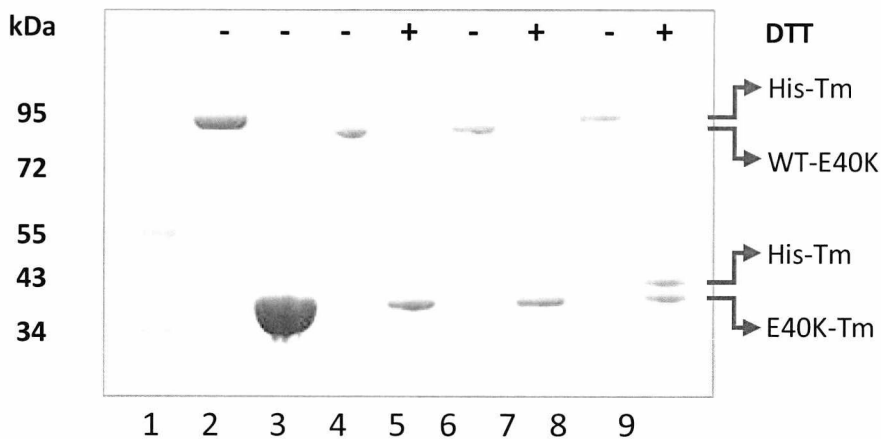
Figure A 2 Purity check of WT-E40K-Tm heterodimers: lane 1,molecular mass markers; lane 2, mixture of His-Tm dimers and monomers; lane 3, E40K-Tm dimers and monomers; lanes 4 and 5, WT-E40K-Tm (sample 1) heterodimer after removal of the His tag under non-reducing and reducing conditions, respectively; lanes 6 and 7, WT-E40K-Tm (sample 2) heterodimer after removal of the His tag under non-reducing and reducing conditions, respectively; lanes 8 and 9, His WT-E40K-Tm (sample 2) heterodimer before digestion under non-reducing and reducing conditions, respectively. Samples were run on 4 – 12 % SDS gel.

164

References

Ackermann M.A., Kontrogianni-Konstantopoulos A. (2011) Myosin binding protein-C: a regulator of actomyosin interaction in striated muscle. J Biomed Biotechnol 2011:636403. DOI: 10.1155/2011/636403.

Al-Sarayreh S.A. (2011) Effect of hypertrophic and dilated cardiomyopathies associated mutations in troponin I on cardiac thin filament dynamics., Ph.D. Dissertation, University of Leicester, Leicester, U.K.

al-Hillawi E., Bhandari D.G., Trayer H.R., Trayer I.P. (1995) The effects of phosphorylation of cardiac troponin-I on its interactions with actin and cardiac troponin-C. Eur J Biochem 228:962-70.

Ammann P., Pfisterer M., Fehr T., Rickli H. (2004) Raised cardiac troponins. BMJ 328:1028-9. DOI: 10.1136/bmj.328.7447.1028.

Antman E.M., Tanasijevic M.J., Thompson B., Schactman M., McCabe C.H., Cannon C.P., Fischer G.A., Fung A.Y., Thompson C., Wybenga D., Braunwald E. (1996) Cardiac-specific troponin I levels to predict the risk of mortality in patients with acute coronary syndromes. N Engl J Med 335:1342-9. DOI: 10.1056/NEJM199610313351802.

Araya E., Berthier C., Kim E., Yeung T., Wang X., Helfman D.M. (2002) Regulation of coiled-coil assembly in tropomyosins. J Struct Biol 137:176-83. DOI: 10.1006/jsbi.2002.4463.

Ashrafian H., Redwood C., Blair E., Watkins H. (2003) Hypertrophic cardiomyopathy:a paradigm for myocardial energy depletion. Trends Genet 19:263-8. DOI: 10.1016/S0168-9525(03)00081-7.

Bai F., Groth H.L., Kawai M. (2012) DCM-Related Tropomyosin Mutants E40K/E54K Over-Inhibit the Actomyosin Interaction and Lead to a Decrease in the Number of Cycling Cross-Bridges. PLoS One 7:e47471. DOI: 10.1371/journal.pone.0047471.

Bai F., Weis A., Takeda A.K., Chase P.B., Kawai M. (2011) Enhanced active cross-bridges during diastole: molecular pathogenesis of tropomyosin's HCM mutations. Biophys J 100:1014-23. DOI: 10.1016/j.bpj.2011.01.001.

Bailey K. (1946) Tropomyosin: a new asymmetric protein component of muscle. Nature 157:368.

Barefield D., Sadayappan S. (2010) Phosphorylation and function of cardiac myosin binding protein-C in health and disease. J Mol Cell Cardiol 48:866-75. DOI: 10.1016/j.yjmcc.2009.11.014.

Bing W., Knott A., Redwood C., Esposito G., Purcell I., Watkins H., Marston S. (2000) Effect of hypertrophic cardiomyopathy mutations in human cardiac muscle alpha -tropomyosin (Asp175Asn and Glu180Gly) on the regulatory properties of human cardiac troponin determined by in vitro motility assay. J Mol Cell Cardiol 32:1489-98. DOI: 10.1006/jmcc.2000.1182.

Borovikov Y.S., Avrova S.V., Karpicheva O.E., Robinson P., Redwood C.S. (2011) The effect of the dilated cardiomyopathy-causing Glu40Lys TPM1 mutation on actin-myosin interactions during the ATPase cycle. Biochem Biophys Res Commun 411:496-500. DOI: 10.1016/j.bbrc.2011.06.138.

Bottinelli R., Coviello D.A., Redwood C.S., Pellegrino M.A., Maron B.J., Spirito P., Watkins H., Reggiani C. (1998) A mutant tropomyosin that causes hypertrophic cardiomyopathy is expressed in vivo and associated with an increased calcium sensitivity. Circ Res 82:106-15.

Boussouf S.E., Maytum R., Jaquet K., Geeves M.A. (2007) Role of tropomyosin isoforms in the calcium sensitivity of striated muscle thin filaments. J Muscle Res Cell Motil 28:49-58. DOI: 10.1007/s10974-007-9103-z.

Brenner B. (1988) Effect of Ca2+ on cross-bridge turnover kinetics in skinned single rabbit psoas fibers: implications for regulation of muscle contraction. Proc Natl Acad Sci U S A 85:3265-9.

Bronson D.D., Schachat F.H. (1982) Heterogeneity of contractile proteins. Differences in tropomyosin in fast, mixed, and slow skeletal muscles of the rabbit. J Biol Chem 257:3937-44.

Brown H.R., Schachat F.H. (1985) Renaturation of skeletal muscle tropomyosin: implications for in vivo assembly. Proc Natl Acad Sci U S A 82:2359-63.

Brown J.H. (2006) Breaking symmetry in protein dimers: designs and functions. Protein Sci 15:1-13. DOI: 10.1110/ps.051658406.

Brown J.H. (2010) How sequence directs bending in tropomyosin and other two-stranded alpha-helical coiled coils. Protein Sci 19:1366-75. DOI: 10.1002/pro.415.

Brown J.H., Cohen C. (2005) Regulation of muscle contraction by tropomyosin and troponin: how structure illuminates function. Adv Protein Chem 71:121-59. DOI: 10.1016/S0065-3233(04)71004-9.

Brown J.H., Kim K.H., Jun G., Greenfield N.J., Dominguez R., Volkmann N., Hitchcock-DeGregori S.E., Cohen C. (2001) Deciphering the design of the tropomyosin molecule. Proc Natl Acad Sci U S A 98:8496-501. DOI: 10.1073/pnas.131219198.

Brown J.H., Zhou Z., Reshetnikova L., Robinson H., Yammani R.D., Tobacman L.S., Cohen C. (2005) Structure of the mid-region of tropomyosin: bending and binding sites for actin. Proc Natl Acad Sci U S A 102:18878-83. DOI: 10.1073/pnas.0509269102.

Canton M., Menazza S., Sheeran F.L., Polverino de Laureto P., Di Lisa F., Pepe S. (2011) Oxidation of myofibrillar proteins in human heart failure. J Am Coll Cardiol 57:300-9. DOI: 10.1016/j.jacc.2010.06.058.

Chang A.N., Harada K., Ackerman M.J., Potter J.D. (2005) Functional consequences of hypertrophic and dilated cardiomyopathy-causing mutations in alpha-tropomyosin. J Biol Chem 280:34343-34349. DOI: 10.1074/jbc.M505014200.

Chandra M., Dong W.J., Pan B.S., Cheung H.C., Solaro R.J. (1997) Effects of protein kinase A phosphorylation on signaling between cardiac troponin I and the N-terminal domain of cardiac troponin C. Biochemistry 36:13305-11. DOI: 10.1021/bi9710129.

Chesarone M.A., Goode B.L. (2009) Actin nucleation and elongation factors: mechanisms and interplay. Curr Opin Cell Biol 21:28-37. DOI: 10.1016/j.ceb.2008.12.001.

Chong P.C., Hodges R.S. (1982) Photochemical cross-linking between rabbit skeletal troponin and alpha-tropomyosin. Attachment of the photoaffinity probe N-(4-azidobenzoyl-[2-3H]glycyl)-S-(2-thiopyridyl)-cysteine to cysteine 190 of alpha-tropomyosin. J Biol Chem 257:9152-60.

Clark K.A., McElhinny A.S., Beckerle M.C., Gregorio C.C. (2002) Striated muscle cytoarchitecture: an intricate web of form and function. Annu Rev Cell Dev Biol 18:637-706. DOI: 10.1146/annurev.cellbio.18.012502.105840.

Clayton L., Johnson M.H. (1998) Tropomyosin in preimplantation mouse development: identification, expression, and organization during cell division and polarization. Exp Cell Res 238:450-64. DOI: 10.1006/excr.1997.3854.

Clos J., Brandau S. (1994) pJC20 and pJC40--two high-copy-number vectors for T7 RNA polymerase-dependent expression of recombinant genes in Escherichia coli. Protein Expr Purif 5:133-7. DOI: 10.1006/prep.1994.1020.

Cooper J.A. (1987) Effects of cytochalasin and phalloidin on actin. J Cell Biol 105:1473-8.

Corbett M.A., Akkari P.A., Domazetovska A., Cooper S.T., North K.N., Laing N.G., Gunning P.W., Hardeman E.C. (2005) An alphaTropomyosin mutation alters dimer preference in nemaline myopathy. Ann Neurol 57:42-9. DOI: 10.1002/ana.20305.

Craig R., Lehman W. (2001) Crossbridge and tropomyosin positions observed in native, interacting thick and thin filaments. J Mol Biol 311:1027-36. DOI: 10.1006/jmbi.2001.4897.

Crick F.H.C. (1953) The Packing of a-Helices: Simple Coiled-Coils. Acta Crystallogr 6:689-697.

Criddle A.H., Geeves M.A., Jeffries T. (1985) The use of actin labelled with N-(1-pyrenyl)iodoacetamide to study the interaction of actin with myosin subfragments and troponin/tropomyosin. Biochem J 232:343-9.

Crilley J.G., Boehm E.A., Blair E., Rajagopalan B., Blamire A.M., Styles P., McKenna W.J., Ostman-Smith I., Clarke K., Watkins H. (2003) Hypertrophic cardiomyopathy due to sarcomeric gene mutations is characterized by impaired energy metabolism irrespective of the degree of hypertrophy. J Am Coll Cardiol 41:1776-82.

de Tombe P.P., Belus A., Piroddi N., Scellini B., Walker J.S., Martin A.F., Tesi C., Poggesi C. (2007) Myofilament calcium sensitivity does not affect cross-bridge activation-relaxation kinetics. Am J Physiol Regul Integr Comp Physiol 292:R1129-36. DOI: 10.1152/ajpregu.00630.2006.

dos Remedios C.G., Chhabra D., Kekic M., Dedova I.V., Tsubakihara M., Berry D.A., Nosworthy N.J. (2003) Actin binding proteins: regulation of cytoskeletal microfilaments. Physiol Rev 83:433-73. DOI: 10.1152/physrev.00026.2002.

Drees B., Brown C., Barrell B.G., Bretscher A. (1995) Tropomyosin is essential in yeast, yet the TPM1 and TPM2 products perform distinct functions. J Cell Biol 128:383-92.

Egelman E.H. (1985) The structure of F-actin. J Muscle Res Cell Motil 6:129-51.

Eyre H., Akkari P.A., Wilton S.D., Callen D.C., Baker E., Laing N.G. (1995) Assignment of the human skeletal muscle alpha-tropomyosin gene (TPM1) to band 15q22 by fluorescence in situ hybridization. Cytogenet Cell Genet 69:15-7.

Fatigati V., Murphy R.A. (1984) Actin and tropomyosin variants in smooth muscles. Dependence on tissue type. J Biol Chem 259:14383-8.

Fatkin D., Graham R.M. (2002) Molecular mechanisms of inherited cardiomyopathies. Physiol Rev 82:945-80. DOI: 10.1152/physrev.00012.2002.

Fettiplace R., Hackney C.M. (2006) The sensory and motor roles of auditory hair cells. Nat Rev Neurosci 7:19-29. DOI: 10.1038/nrn1828.

Filatov V.L., Katrukha A.G., Bulargina T.V., Gusev N.B. (1999) Troponin: structure, properties, and mechanism of functioning. Biochemistry (Mosc) 64:969-85.

Fisher C.L., Pei G.K. (1997) Modification of a PCR-based site-directed mutagenesis method. Biotechniques 23:570-1, 574.

Flicker P.F., Phillips G.N., Jr., Cohen C. (1982) Troponin and its interactions with tropomyosin. An electron microscope study. J Mol Biol 162:495-501.

Frye J., Klenchin V.A., Rayment I. (2010) Structure of the tropomyosin overlap complex from chicken smooth muscle: insight into the diversity of N-terminal recognition. Biochemistry 49:4908-20. DOI: 10.1021/bi100349a.

Galinska-Rakoczy A., Engel P., Xu C., Jung H., Craig R., Tobacman L.S., Lehman W. (2008) Structural basis for the regulation of muscle contraction by troponin and tropomyosin. J Mol Biol 379:929-35. DOI: 10.1016/j.jmb.2008.04.062.

Galkin V.E., Orlova A., Schroder G.F., Egelman E.H. (2010) Structural polymorphism in F-actin. Nat Struct Mol Biol 17:1318-23. DOI: 10.1038/nsmb.1930.

Gallant C., Appel S., Graceffa P., Leavis P., Lin J.J., Gunning P.W., Schevzov G., Chaponnier C., DeGnore J., Lehman W., Morgan K.G. (2011) Tropomyosin variants describe distinct functional subcellular domains in differentiated vascular smooth muscle cells. Am J Physiol Cell Physiol 300:C1356-65. DOI: 10.1152/ajpcell.00450.2010.

Geeves M.A., Holmes K.C. (1999) Structural mechanism of muscle contraction. Annu Rev Biochem 68:687-728. DOI: 10.1146/annurev.biochem.68.1.687.

Geeves M.A., Holmes K.C. (2005) The molecular mechanism of muscle contraction. Adv Protein Chem 71:161-93. DOI: 10.1016/S0065-3233(04)71005-0.

Geeves M., Griffiths H., Mijailovich S., Smith D. (2011) Cooperative [Ca(2)+]-dependent regulation of the rate of myosin binding to actin: solution data and the tropomyosin chain model. Biophys J 100:2679-87. DOI: 10.1016/j.bpj.2011.04.020.

Geeves M.A., Lehrer S.S. (1994) Dynamics of the muscle thin filament regulatory switch: the size of the cooperative unit. Biophys J 67:273-82. DOI: 10.1016/S0006-3495(94)80478-3.

Gimona M. (2008) Dimerization of tropomyosins. Adv Exp Med Biol 644:73-84.

Gimona M., Watakabe A., Helfman D.M. (1995) Specificity of dimer formation in tropomyosins: influence of alternatively spliced exons on homodimer and heterodimer assembly. Proc Natl Acad Sci U S A 92:9776-80.

Goode B.L., Eck M.J. (2007) Mechanism and function of formins in the control of actin assembly. Annu Rev Biochem 76:593-627. DOI: 10.1146/annurev.biochem.75.103004.142647.

Gooding C., Smith C.W. (2008) Tropomyosin exons as models for alternative splicing. Adv Exp Med Biol 644:27-42.

Gordon A.M., Homsher E., Regnier M. (2000) Regulation of contraction in striated muscle. Physiol Rev 80:853-924.

Gordon A.M., Regnier M., Homsher E. (2001) Skeletal and cardiac muscle contractile activation: tropomyosin "rocks and rolls". News Physiol Sci 16:49-55.

Golitsina N., An Y., Greenfield N.J., Thierfelder L., Iizuka K., Seidman J.G., Seidman C.E., Lehrer S.S., Hitchcock-DeGregori S.E. (1999) Effects of two familial hypertrophic cardiomyopathy-causing mutations on alpha-tropomyosin structure and function. Biochemistry 38:3850. DOI: 10.1021/bi9950701.

Greenfield N.J., Huang Y.J., Swapna G.V., Bhattacharya A., Rapp B., Singh A., Montelione G.T., Hitchcock-DeGregori S.E. (2006) Solution NMR structure of the junction between tropomyosin molecules: implications for actin binding and regulation. J Mol Biol 364:80-96. DOI: 10.1016/j.jmb.2006.08.033.

Greenfield N.J., Palm T., Hitchcock-DeGregori S.E. (2002) Structure and interactions of the carboxyl terminus of striated muscle alpha-tropomyosin: it is important to be flexible. Biophys J 83:2754-66. DOI: 10.1016/S0006-3495(02)75285-5.

Gregory S.G., Barlow K.F., McLay K.E., Kaul R., Swarbreck D., Dunham A., Scott C.E., Howe K.L., Woodfine K., Spencer C.C., Jones M.C., Gillson C., Searle S., Zhou Y., Kokocinski F., McDonald L., Evans R., Phillips K., Atkinson A., Cooper R., Jones C., Hall R.E., Andrews T.D., Lloyd C., Ainscough R., Almeida J.P., Ambrose K.D., Anderson F., Andrew R.W., Ashwell R.I., Aubin K., Babbage A.K., Bagguley C.L., Bailey J., Beasley H., Bethel G., Bird C.P., Bray-Allen S., Brown J.Y., Brown A.J., Buckley D., Burton J., Bye J., Carder C., Chapman J.C., Clark S.Y., Clarke G., Clee C., Cobley V., Collier R.E., Corby N., Coville G.J., Davies J., Deadman R., Dunn M., Earthrowl M., Ellington A.G., Errington H., Frankish A., Frankland J., French L., Garner P., Garnett J., Gay L., Ghori M.R., Gibson R., Gilby L.M., Gillett W., Glithero R.J., Grafham D.V.,

Griffiths C., Griffiths-Jones S., Grocock R., Hammond S., Harrison E.S., Hart E., Haugen E., Heath P.D., Holmes S., Holt K., Howden P.J., Hunt A.R., Hunt S.E., Hunter G., Isherwood J., James R., Johnson C., Johnson D., Joy A., Kay M., Kershaw J.K., Kibukawa M., Kimberley A.M., King A., Knights A.J., Lad H., Laird G., Lawlor S., Leongamornlert D.A., Lloyd D.M., *et al.* (2006) The DNA sequence and biological annotation of human chromosome 1. Nature 441:315-21. DOI: 10.1038/nature04727.

Gunning P., O'Neill G., Hardeman E. (2008) Tropomyosin-based regulation of the actin cytoskeleton in time and space. Physiol Rev 88:1-35. DOI: 10.1152/physrev.00001.2007.

Gunning P.W., Schevzov G., Kee A.J., Hardeman E.C. (2005) Tropomyosin isoforms: divining rods for actin cytoskeleton function. Trends Cell Biol 15:333-41. DOI: 10.1016/j.tcb.2005.04.007.

Guo B., Guilford W.H. (2006) Mechanics of actomyosin bonds in different nucleotide states are tuned to muscle contraction. Proc Natl Acad Sci U S A 103:9844-9. DOI: 10.1073/pnas.0601255103.

Had L., Faivre-Sarrailh C., Legrand C., Rabie A. (1993) The expression of tropomyosin genes in pure cultures of rat neurons, astrocytes and oligodendrocytes is highly cell-type specific and strongly regulated during development. Brain Res Mol Brain Res 18:77-86.

Hancock C.R., Brault J.J., Terjung R.L. (2006) Protecting the cellular energy state during contractions: role of AMP deaminase. J Physiol Pharmacol 57 Suppl 10:17-29.

Hanson J., Lowy J. (1964) The Structure of Actin Filaments and the Origin of the Axial Periodicity in the I-Substance of Vertebrate Striated Muscle. Proc R Soc Lond B Biol Sci 160:449-60.

Hayley M., Chevaldina T., Heeley D.H. (2011) Cold adaptation of tropomyosin. Biochemistry 50:6559-66. DOI: 10.1021/bi200327g.

Hilario E., da Silva S.L., Ramos C.H., Bertolini M.C. (2004) Effects of cardiomyopathic mutations on the biochemical and biophysical properties of the human alpha-tropomyosin. Eur J Biochem 271:4132-40. DOI: 10.1111/j.1432-1033.2004.04351.x.

Hitchcock-DeGregori S.E. (2008) Tropomyosin: function follows structure. Adv Exp Med Biol 644:60-72.

Hitchcock-DeGregori S.E., Song Y., Greenfield N.J. (2002) Functions of tropomyosin's periodic repeats. Biochemistry 41:15036-44.

Hodges R.S., Mills J., McReynolds S., Kirwan J.P., Tripet B., Osguthorpe D. (2009) Identification of a unique "stability control region" that controls protein stability of tropomyosin: A two-stranded alpha-helical coiled-coil. J Mol Biol 392:747-62. DOI: 10.1016/j.jmb.2009.07.039.

Holmes K.C., Angert I., Kull F.J., Jahn W., Schroder R.R. (2003) Electron cryo-microscopy shows how strong binding of myosin to actin releases nucleotide. Nature 425:423-7. DOI: 10.1038/nature02005.

Holmes K.C., Geeves M.A. (2000) The structural basis of muscle contraction. Philos Trans R Soc Lond B Biol Sci 355:419-31. DOI: 10.1098/rstb.2000.0583.

Holmes K.C., Lehman W. (2008) Gestalt-binding of tropomyosin to actin filaments. J Muscle Res Cell Motil 29:213-9. DOI: 10.1007/s10974-008-9157-6.

Holmes K.C., Popp D., Gebhard W., Kabsch W. (1990) Atomic model of the actin filament. Nature 347:44-9. DOI: 10.1038/347044a0.

Hunt C.C., Eyre H.J., Akkari P.A., Meredith C., Dorosz S.M., Wilton S.D., Callen D.F., Laing N.G., Baker E. (1995) Assignment of the human beta tropomyosin gene (TPM2) to band 9p13 by fluorescence in situ hybridisation. Cytogenet Cell Genet 71:94-5.

Huxley A.F., Niedergerke R. (1954) Structural changes in muscle during contraction; interference microscopy of living muscle fibres. Nature 173:971-3.

Huxley H., Hanson J. (1954) Changes in the cross-striations of muscle during contraction and stretch and their structural interpretation. Nature 173:973-6.

Huxley H.E. (1972) Structural changes in actin and myosin-containing filaments during contraction. Cold Spring Harbor Symp Quant Biol 37:361-376.

Ishii Y., Lehrer S.S. (1990) Excimer fluorescence of pyrenyliodoacetamide-labeled tropomyosin: a probe of the state of tropomyosin in reconstituted muscle thin filaments. Biochemistry 29:1160-6.

Janco M., Kalyva A., Scellini B., Piroddi N., Tesi C., Poggesi C., Geeves M.A. (2012) alpha-Tropomyosin with a D175N or E180G Mutation in Only One Chain Differs from Tropomyosin with Mutations in Both Chains. Biochemistry. DOI: 10.1021/bi301323n.

Janco M., Suphamungmee W., Li X., Lehman W., Lehrer S.S., Geeves M.A. (2013) Polymorphism in tropomyosin structure and function. J Muscle Res Cell Motil. DOI: 10.1007/s10974-013-9353-x.

Jin J.P., Chong S.M. (2010) Localization of the two tropomyosin-binding sites of troponin T. Arch Biochem Biophys 500:144-50. DOI: 10.1016/j.abb.2010.06.001.

Kalyva A., Schmidtmann A., Geeves M.A. (2012) In Vitro formation and characterization of the skeletal muscle alpha*beta Tropomyosin heterodimers. Biochemistry. DOI: 10.1021/bi300340r.

Kamisago M., Sharma S.D., DePalma S.R., Solomon S., Sharma P., McDonough B., Smoot L., Mullen M.P., Woolf P.K., Wigle E.D., Seidman J.G., Seidman C.E. (2000) Mutations in sarcomere protein genes as a cause of dilated cardiomyopathy. N Engl J Med 343:1688-96. DOI: 10.1056/NEJM200012073432304.

Kammerer R.A., Schulthess T., Landwehr R., Lustig A., Engel J., Aebi U., Steinmetz M.O. (1998) An autonomous folding unit mediates the assembly of two-stranded coiled coils. Proc Natl Acad Sci U S A 95:13419-24.

Kirwan J.P., Hodges R.S. (2010) Critical interactions in the stability control region of tropomyosin. J Struct Biol 170:294-306. DOI: 10.1016/j.jsb.2010.01.020.

Kontrogianni-Konstantopoulos A., Ackermann M.A., Bowman A.L., Yap S.V., Bloch R.J. (2009) Muscle giants: molecular scaffolds in sarcomerogenesis. Physiol Rev 89:1217-67. DOI: 10.1152/physrev.00017.2009.

Kontrogianni-Konstantopoulos A., Catino D.H., Strong J.C., Sutter S., Borisov A.B., Pumplin D.W., Russell M.W., Bloch R.J. (2006) Obscurin modulates the assembly and organization of sarcomeres and the sarcoplasmic reticulum. FASEB J 20:2102-11. DOI: 10.1096/fj.06-5761com.

Kopylova G.V., Shchepkin D.V., Nikitina L.V. (2013) Study of Regulatory Effect of Tropomyosin on Actin–Myosin Interaction in Skeletal Muscle by in vitro Motility Assay. Biochemistry (Moscow) 78:348-356. DOI: 10.1134/S0006297913030073.

Kremneva E., Boussouf S., Nikolaeva O., Maytum R., Geeves M.A., Levitsky D.I. (2004) Effects of two familial hypertrophic cardiomyopathy mutations in alpha-tropomyosin, Asp175Asn and Glu180Gly, on the thermal unfolding of actin-bound tropomyosin. Biophys J 87:3922-33. DOI: 10.1529/biophysj.104.048793.

Kubota H., Mikhailenko S.V., Okabe H., Taguchi H., Ishiwata S. (2009) D-loop of actin differently regulates the motor function of myosins II and V. J Biol Chem 284:35251-8. DOI: 10.1074/jbc.M109.013565.

Kulkarni P.A., Sano M., Schneider M.D. (2004) Phosphorylation of RNA polymerase II in cardiac hypertrophy: cell enlargement signals converge on cyclin T/Cdk9. Recent Prog Horm Res 59:125-39.

Kurzawa S.E., Geeves M.A. (1996) A novel stopped-flow method for measuring the affinity of actin for myosin head fragments using microgram quantities of protein. J Muscle Res Cell Motil 17:669-76.

Lakdawala N.K., Dellefave L., Redwood C.S., Sparks E., Cirino A.L., Depalma S., Colan S.D., Funke B., Zimmerman R.S., Robinson P., Watkins H., Seidman C.E., Seidman J.G., McNally E.M., Ho C.Y. (2010) Familial dilated cardiomyopathy caused by an alpha-tropomyosin mutation: the distinctive natural history of sarcomeric dilated cardiomyopathy. J Am Coll Cardiol 55:320-9. DOI: 10.1016/j.jacc.2009.11.017.

Laing N.G., Dye D.E., Wallgren-Pettersson C., Richard G., Monnier N., Lillis S., Winder T.L., Lochmuller H., Graziano C., Mitrani-Rosenbaum S., Twomey D., Sparrow J.C., Beggs A.H., Nowak K.J. (2009) Mutations and polymorphisms of the skeletal muscle alpha-actin gene (ACTA1). Hum Mutat 30:1267-77. DOI: 10.1002/humu.21059.

Laing N.G., Wilton S.D., Akkari P.A., Dorosz S., Boundy K., Kneebone C., Blumbergs P., White S., Watkins H., Love D.R., et al. (1995) A mutation in the alpha tropomyosin gene TPM3 associated with autosomal dominant nemaline myopathy. Nat Genet 9:75-9. DOI: 10.1038/ng0195-75.

Lawlor M.W., Dechene E.T., Roumm E., Geggel A.S., Moghadaszadeh B., Beggs A.H. (2010) Mutations of tropomyosin 3 (TPM3) are common and associated with type 1 myofiber hypotrophy in congenital fiber type disproportion. Hum Mutat 31:176-83. DOI: 10.1002/humu.21157.

Layland J., Solaro R.J., Shah A.M. (2005) Regulation of cardiac contractile function by troponin I phosphorylation. Cardiovasc Res 66:12-21. DOI: 10.1016/j.cardiores.2004.12.022.

Lazarides E. (1975) Tropomyosin antibody: the specific localization of tropomyosin in nonmuscle cells. J Cell Biol 65:549-61.

Leger J., Bouveret P., Schwartz K., Swynghedauw B. (1976) A comparative study of skeletal and cardiac tropomyosins: subunits, thiol group content and biological activities. Pflugers Arch 362:271-7.

Lehman W., Craig R. (2008) Tropomyosin and the steric mechanism of muscle regulation. Adv Exp Med Biol 644:95-109.

Lehman W., Hatch V., Korman V., Rosol M., Thomas L., Maytum R., Geeves M.A., Van Eyk J.E., Tobacman L.S., Craig R. (2000) Tropomyosin and actin isoforms modulate the localization of tropomyosin strands on actin filaments. J Mol Biol 302:593-606. DOI: 10.1006/jmbi.2000.4080.

Lehrer S.S., Ly S., Fuchs F. (2011) Tropomyosin is in a reduced state in rabbit psoas muscle. J Muscle Res Cell Motil 32:19-21. DOI: 10.1007/s10974-011-9249-6.

Lehrer S.S., Geeves M.A. (1998) The muscle thin filament as a classical cooperative/allosteric regulatory system. J Mol Biol 277:1081-9. DOI: 10.1006/jmbi.1998.1654.

Li M.X., Gagne S.M., Tsuda S., Kay C.M., Smillie L.B., Sykes B.D. (1995) Calcium binding to the regulatory N-domain of skeletal muscle troponin C occurs in a stepwise manner. Biochemistry 34:8330-40.

Li X.E., Holmes K.C., Lehman W., Jung H., Fischer S. (2010a) The shape and flexibility of tropomyosin coiled coils: implications for actin filament assembly and regulation. J Mol Biol 395:327-39. DOI: 10.1016/j.jmb.2009.10.060.

Li X.E., Suphamungmee W., Janco M., Geeves M.A., Marston S.B., Fischer S., Lehman W. (2012) The flexibility of two tropomyosin mutants, D175N and E180G, that cause

hypertrophic cardiomyopathy. Biochem Biophys Res Commun 424:493-6. DOI: 10.1016/j.bbrc.2012.06.141.

Li X.E., Lehman W., Fischer S. (2010b) The relationship between curvature, flexibility and persistence length in the tropomyosin coiled-coil. J Struct Biol 170:313-8. DOI: 10.1016/j.jsb.2010.01.016.

Li X.E., Tobacman L.S., Mun J.Y., Craig R., Fischer S., Lehman W. (2011) Tropomyosin position on F-actin revealed by EM reconstruction and computational chemistry. Biophys J 100:1005-13. DOI: 10.1016/j.bpj.2010.12.3697.

Lin J.J., Eppinga R.D., Warren K.S., McCrae K.R. (2008) Human tropomyosin isoforms in the regulation of cytoskeleton functions. Adv Exp Med Biol 644:201-22.

Ly S., Lehrer S.S. (2012) Long-range effects of familial hypertrophic cardiomyopathy mutations E180G and D175N on the properties of tropomyosin. Biochemistry 51:6413-6420. DOI: 10.1021/bi3006835.

Lorenz M., Poole K.J.V., Popp D., Rosenbaum G., Holmes K.C. (1995) An Atomic Model of the Unregulated Thin Filament Obtained by X-ray Fiber Diffraction on Oriented Actin-Tropomyosin Gels. Journal of Molecular Biology 246:108-119.

Madej T., Addess K.J., Fong J.H., Geer L.Y., Geer R.C., Lanczycki C.J., Liu C., Lu S., Marchler-Bauer A., Panchenko A.R., Chen J., Thiessen P.A., Wang Y., Zhang D., Bryant S.H. (2012) MMDB: 3D structures and macromolecular interactions. Nucleic Acids Res 40:D461-4. DOI: 10.1093/nar/gkr1162.

Margossian S.S., Lowey S. (1982) Preparation of myosin and its subfragments from rabbit skeletal muscle. Methods Enzymol 85 Pt B:55-71.

Maron B.J., Gardin J.M., Flack J.M., Gidding S.S., Kurosaki T.T., Bild D.E. (1995) Prevalence of hypertrophic cardiomyopathy in a general population of young adults. Echocardiographic

analysis of 4111 subjects in the CARDIA Study. Coronary Artery Risk Development in (Young) Adults. Circulation 92:785-9.

Marston S., Copeland O., Gehmlich K., Schlossarek S., Carrier L. (2012) How do MYBPC3 mutations cause hypertrophic cardiomyopathy? J Muscle Res Cell Motil 33:75-80. DOI: 10.1007/s10974-011-9268-3.

Marston S.B., Copeland O., Messer A.E., Macnamara E., Nowak K., Zampronio C.G., Ward D.G. (2013) Tropomyosin isoform expression and phosphorylation in the human heart in health and disease. J Muscle Res Cell Motil. DOI: 10.1007/s10974-013-9347-8.

Marston S., El-Mezgueldi M. (2008) Role of tropomyosin in the regulation of contraction in smooth muscle. Adv Exp Med Biol 644:110-23.

Marston S.B. (2011) How do mutations in contractile proteins cause the primary familial cardiomyopathies? J Cardiovasc Transl Res 4:245-55. DOI: 10.1007/s12265-011-9266-2.

Mathur M.C., Chase P.B., Chalovich J.M. (2011) Several cardiomyopathy causing mutations on tropomyosin either destabilize the active state of actomyosin or alter the binding properties of tropomyosin. Biochem Biophys Res Commun 406:74-8. DOI: 10.1016/j.bbrc.2011.01.112.

Maytum R., Westerdorf B., Jaquet K., Geeves M.A. (2003) Differential regulation of the actomyosin interaction by skeletal and cardiac troponin isoforms. J Biol Chem 278:6696-6701. DOI: 10.1074/jbc.M210690200.

McConnell B.K., Jones K.A., Fatkin D., Arroyo L.H., Lee R.T., Aristizabal O., Turnbull D.H., Georgakopoulos D., Kass D., Bond M., Niimura H., Schoen F.J., Conner D., Fischman D.A., Seidman C.E., Seidman J.G. (1999) Dilated cardiomyopathy in homozygous myosin-binding protein-C mutant mice. J Clin Invest 104:1771.

McElhinny A.S., Schwach C., Valichnac M., Mount-Patrick S., Gregorio C.C. (2005) Nebulin regulates the assembly and lengths of the thin filaments in striated muscle. J Cell Biol 170:947-57. DOI: 10.1083/jcb.200502158.

McKillop D.F., Geeves M.A. (1993) Regulation of the interaction between actin and myosin subfragment 1: evidence for three states of the thin filament. Biophys J 65:693-701. DOI: 10.1016/S0006-3495(93)81110-X.

McLachlan A.D., Stewart M. (1975) Tropomyosin coiled-coil interactions: evidence for an unstaggered structure. J Mol Biol 98:293-304.

McLachlan A.D., Stewart M. (1976) The 14-fold periodicity in alpha-tropomyosin and the interaction with actin. J Mol Biol 103:271-98.

McLachlan A.D., Stewart M., Smillie L.B. (1975) Sequence repeats in alpha-tropomyosin. J Mol Biol 98:281-91.

Memo M., Leung M.C., Ward D.G., Dos Remedios C., Morimoto S., Zhang L., Ravenscroft G., McNamara E., Nowak K.J., Marston S.B., Messer A.E. (2013) Familial dilated cardiomyopathy mutations uncouple troponin I phosphorylation from changes in myofibrillar Ca2+ sensitivity. Cardiovasc Res 99:65-73. DOI: 10.1093/cvr/cvt071.

Metzger J.M., Westfall M.V. (2004) Covalent and noncovalent modification of thin filament action: the essential role of troponin in cardiac muscle regulation. Circ Res 94:146-58. DOI: 10.1161/01.RES.0000110083.17024.60.

Michele D.E., Albayya F.P., Metzger J.M. (1999) Direct, convergent hypersensitivity of calcium-activated force generation produced by hypertrophic cardiomyopathy mutant alpha-tropomyosins in adult cardiac myocytes. Nat Med 5:1413-7. DOI: 10.1038/70990.

Minakata S., Maeda K., Oda N., Wakabayashi K., Nitanai Y., Maeda Y. (2008) Two-crystal structures of tropomyosin C-terminal fragment 176-273: exposure of the hydrophobic core

to the solvent destabilizes the tropomyosin molecule. Biophys J 95:710-9. DOI: 10.1529/biophysj.107.126144.

Mirza M., Marston S., Willott R., Ashley C., Mogensen J., McKenna W., Robinson P., Redwood C., Watkins H. (2005) Dilated cardiomyopathy mutations in three thin filament regulatory proteins result in a common functional phenotype. J Biol Chem 280:28498-506. DOI: 10.1074/jbc.M412281200.

Monteiro P.B., Lataro R.C., Ferro J.A., Reinach Fde C. (1994) Functional alpha-tropomyosin produced in Escherichia coli. A dipeptide extension can substitute the amino-terminal acetyl group. J Biol Chem 269:10461-6.

Murakami K., Stewart M., Nozawa K., Tomii K., Kudou N., Igarashi N., Shirakihara Y., Wakatsuki S., Yasunaga T., Wakabayashi T. (2008) Structural basis for tropomyosin overlap in thin (actin) filaments and the generation of a molecular swivel by troponin-T. Proc Natl Acad Sci U S A 105:7200-5. DOI: 10.1073/pnas.0801950105.

Muthuchamy M., Pajak L., Howles P., Doetschman T., Wieczorek D.F. (1993) Developmental analysis of tropomyosin gene expression in embryonic stem cells and mouse embryos. Mol Cell Biol 13:3311-23.

Nakajima-Taniguchi C., Matsui H., Nagata S., Kishimoto T., Yamauchi-Takihara K. (1995) Novel missense mutation in alpha-tropomyosin gene found in Japanese patients with hypertrophic cardiomyopathy. J Mol Cell Cardiol 27:2053-8. DOI: 0022-2828(95)90026-8 [pii].

Narita A., Yasunaga T., Ishikawa T., Mayanagi K., Wakabayashi T. (2001) Ca(2+)-induced switching of troponin and tropomyosin on actin filaments as revealed by electron cryo-microscopy. J Mol Biol 308:241-61. DOI: 10.1006/jmbi.2001.4598.

Nitanai Y., Minakata S., Maeda K., Oda N., Maeda Y. (2007) Crystal structures of tropomyosin: flexible coiled-coil. Adv Exp Med Biol 592:137-51. DOI: 10.1007/978-4-431-38453-3_13.

Novy R.E., Lin J.L., Lin C.S., Lin J.J. (1993) Human fibroblast tropomyosin isoforms: characterization of cDNA clones and analysis of tropomyosin isoform expression in human tissues and in normal and transformed cells. Cell Motil Cytoskeleton 25:267-81. DOI: 10.1002/cm.970250307.

Oda T., Iwasa M., Aihara T., Maeda Y., Narita A. (2009) The nature of the globular- to fibrous-actin transition. Nature 457:441-5. DOI: 10.1038/nature07685.

Odronitz F., Kollmar M. (2007) Drawing the tree of eukaryotic life based on the analysis of 2,269 manually annotated myosins from 328 species. Genome Biol 8:R196. DOI: 10.1186/gb-2007-8-9-r196.

Ookubo N., Ueno H., Ooi T. (1975) Similarities and differences of the alpha and beta components of tropomyosin. J Biochem 78:739-47.

Olson T.M., Kishimoto N.Y., Whitby F.G., Michels V.V. (2001) Mutations that alter the surface charge of alpha-tropomyosin are associated with dilated cardiomyopathy. J Mol Cell Cardiol 33:723-32. DOI: 10.1006/jmcc.2000.1339.

Palm T., Graboski S., Hitchcock-DeGregori S.E., Greenfield N.J. (2001) Disease-causing mutations in cardiac troponin T: identification of a critical tropomyosin-binding region. Biophys J 81:2827-37. DOI: 10.1016/S0006-3495(01)75924-3.

Parry D.A. (1975) Analysis of the primary sequence of alpha-tropomyosin from rabbit skeletal muscle. J Mol Biol 98:519-35.

Parry D.A., Squire J.M. (1973) Structural role of tropomyosin in muscle regulation: analysis of the x-ray diffraction patterns from relaxed and contracting muscles. J Mol Biol 75:33-55.

Peng Y., Chen X., Zhang H., Xu Q., Hacker T.A., Ge Y. (2013a) Top-down targeted proteomics for deep sequencing of tropomyosin isoforms. J Proteome Res 12:187-98. DOI: 10.1021/pr301054n.

Peng Y., Yu D., Gregorich Z., Chen X., Beyer A.M., Gutterman D.D., Ge Y. (2013b) In-depth proteomic analysis of human tropomyosin by top-down mass spectrometry. J Muscle Res Cell Motil. DOI: 10.1007/s10974-013-9352-y.

Perrin B.J., Ervasti J.M. (2010) The actin gene family: function follows isoform. Cytoskeleton (Hoboken) 67:630-4. DOI: 10.1002/cm.20475.

Phillips G.N., Jr. (1986) Construction of an atomic model for tropomyosin and implications for interactions with actin. J Mol Biol 192:128-31.

Pirani A., Xu C., Hatch V., Craig R., Tobacman L.S., Lehman W. (2005) Single particle analysis of relaxed and activated muscle thin filaments. J Mol Biol 346:761-72. DOI: 10.1016/j.jmb.2004.12.013.

Poole K.J., Lorenz M., Evans G., Rosenbaum G., Pirani A., Craig R., Tobacman L.S., Lehman W., Holmes K.C. (2006) A comparison of muscle thin filament models obtained from electron microscopy reconstructions and low-angle X-ray fibre diagrams from non-overlap muscle. J Struct Biol 155:273-84. DOI: S1047-8477(06)00108-0 [pii]

Potter J.D., Gergely J. (1975) The calcium and magnesium binding sites on troponin and their role in the regulation of myofibrillar adenosine triphosphatase. J Biol Chem 250:4628-33.

Purcell I.F., Bing W., Marston S.B. (1999) Functional analysis of human cardiac troponin by the in vitro motility assay: comparison of adult, foetal and failing hearts. Cardiovasc Res 43:884-91.

Rajan S., Ahmed R.P., Jagatheesan G., Petrashevskaya N., Boivin G.P., Urboniene D., Arteaga G.M., Wolska B.M., Solaro R.J., Liggett S.B., Wieczorek D.F. (2007) Dilated cardiomyopathy mutant tropomyosin mice develop cardiac dysfunction with significantly decreased fractional shortening and myofilament calcium sensitivity. Circ Res 101:205-14. DOI: 10.1161/CIRCRESAHA.107.148379.

Rajan S., Jagatheesan G., Karam C.N., Alves M.L., Bodi I., Schwartz A., Bulcao C.F., D'Souza K.M., Akhter S.A., Boivin G.P., Dube D.K., Petrashevskaya N., Herr A.B., Hullin R., Liggett S.B., Wolska B.M., Solaro R.J., Wieczorek D.F. (2010) Molecular and functional characterization of a novel cardiac-specific human tropomyosin isoform. Circulation 121:410-8. DOI: 10.1161/CIRCULATIONAHA.109.889725.

Ray K.P., England P.J. (1976) Phosphorylation of the inhibitory subunit of troponin and its effect on the calcium dependence of cardiac myofibril adenosine triphosphatase. FEBS Lett 70:11-6.

Rayment I., Rypniewski W.R., Schmidt-Base K., Smith R., Tomchick D.R., Benning M.M., Winkelmann D.A., Wesenberg G., Holden H.M. (1993) Three-dimensional structure of myosin subfragment-1: a molecular motor. Science 261:50-8.

Reiffert S.U., Jaquet K., Heilmeyer L.M., Jr., Herberg F.W. (1998) Stepwise subunit interaction changes by mono- and bisphosphorylation of cardiac troponin I. Biochemistry 37:13516-25. DOI: 10.1021/bi980280j.

Robertson S.P., Johnson J.D., Holroyde M.J., Kranias E.G., Potter J.D., Solaro R.J. (1982) The effect of troponin I phosphorylation on the Ca2+-binding properties of the Ca2+-regulatory site of bovine cardiac troponin. J Biol Chem 257:260-3.

Robinson P., Griffiths P.J., Watkins H., Redwood C.S. (2007) Dilated and hypertrophic cardiomyopathy mutations in troponin and alpha-tropomyosin have opposing effects on the calcium affinity of cardiac thin filaments. Circ Res 101:1266-73. DOI: 10.1161/CIRCRESAHA.107.156380.

Robinson P., Mirza M., Knott A., Abdulrazzak H., Willott R., Marston S., Watkins H., Redwood C. (2002) Alterations in thin filament regulation induced by a human cardiac troponin T mutant that causes dilated cardiomyopathy are distinct from those induced by troponin T mutants that cause hypertrophic cardiomyopathy. J Biol Chem 277:40710-6. DOI: 10.1074/jbc.M203446200.

Ross J.L., Ali M.Y., Warshaw D.M. (2008) Cargo transport: molecular motors navigate a complex cytoskeleton. Curr Opin Cell Biol 20:41-7. DOI: 10.1016/j.ceb.2007.11.006.

Seddon M., Looi Y.H., Shah A.M. (2007) Oxidative stress and redox signalling in cardiac hypertrophy and heart failure. Heart 93:903-7. DOI: 10.1136/hrt.2005.068270.

Seidman J.G., Seidman C. (2001) The genetic basis for cardiomyopathy: from mutation identification to mechanistic paradigms. Cell 104:557-67.

Scellini B., Piroddi N., Poggesi C., Tesi C. (2010) Extraction and replacement of the tropomyosin-troponin complex in isolated myofibrils. Adv Exp Med Biol 682:163-74. DOI: 10.1007/978-1-4419-6366-6_9.

Schaertl S., Lehrer S.S., Geeves M.A. (1995) Separation and characterization of the two functional regions of troponin involved in muscle thin filament regulation. Biochemistry 34:15890-4.

Schevzov G., O'Neill G. (2008) Tropomyosin gene expression in vivo and in vitro. Adv Exp Med Biol 644:43-59.

Schevzov G., Whittaker S.P., Fath T., Lin J.J., Gunning P.W. (2011) Tropomyosin isoforms and reagents. Bioarchitecture 1:135-164. DOI: 10.4161/bioa.1.4.17897.

Schoenenberger C.A., Mannherz H.G., Jockusch B.M. (2011) Actin: from structural plasticity to functional diversity. Eur J Cell Biol 90:797-804. DOI: 10.1016/j.ejcb.2011.05.002.

Seidman J.G., Seidman C. (2001) The genetic basis for cardiomyopathy: from mutation identification to mechanistic paradigms. Cell 104:557-67.

Sheeran F.L., Pepe S. (2006) Energy deficiency in the failing heart: linking increased reactive oxygen species and disruption of oxidative phosphorylation rate. Biochim Biophys Acta 1757:543-52. DOI: 10.1016/j.bbabio.2006.03.008.

Singh A., Hitchcock-DeGregori S.E. (2003) Local destabilization of the tropomyosin coiled coil gives the molecular flexibility required for actin binding. Biochemistry 42:14114-21. DOI: 10.1021/bi0348462.

Singh A., Hitchcock-DeGregori S.E. (2006) Dual requirement for flexibility and specificity for binding of the coiled-coil tropomyosin to its target, actin. Structure 14:43-50. DOI: 10.1016/j.str.2005.09.016.

Singh A., Hitchcock-DeGregori S.E. (2007) Tropomyosin's periods are quasi-equivalent for actin binding but have specific regulatory functions. Biochemistry 46:14917-27. DOI: 10.1021/bi701570b [doi].

Singh A., Hitchcock-Degregori S.E. (2009) A peek into tropomyosin binding and unfolding on the actin filament. PLoS One 4:e6336. DOI: 10.1371/journal.pone.0006336.

Siththanandan V.B., Tobacman L.S., Van Gorder N., Homsher E. (2009) Mechanical and kinetic effects of shortened tropomyosin reconstituted into myofibrils. Pflugers Arch 458:761-76. DOI: 10.1007/s00424-009-0653-3.

Sodek J., Hodges R.S., Smillie L.B., Jurasek L. (1972) Amino-acid sequence of rabbit skeletal tropomyosin and its coiled-coil structure. Proc Natl Acad Sci U S A 69:3800-4.

Sousa D., Cammarato A., Jang K., Graceffa P., Tobacman L.S., Li X.E., Lehman W. (2010) Electron microscopy and persistence length analysis of semi-rigid smooth muscle tropomyosin strands. Biophys J 99:862-8. DOI: 10.1016/j.bpj.2010.05.004.

Spudich J.A., Watt S. (1971) The regulation of rabbit skeletal muscle contraction. I. Biochemical studies of the interaction of the tropomyosin-troponin complex with actin and the proteolytic fragments of myosin. J Biol Chem 246:4866-71.

Steinmetz M.O., Jelesarov I., Matousek W.M., Honnappa S., Jahnke W., Missimer J.H., Frank S., Alexandrescu A.T., Kammerer R.A. (2007) Molecular basis of coiled-coil formation. Proc Natl Acad Sci U S A 104:7062-7. DOI: 10.1073/pnas.0700321104.

Steinmetz M.O., Stock A., Schulthess T., Landwehr R., Lustig A., Faix J., Gerisch G., Aebi U., Kammerer R.A. (1998) A distinct 14 residue site triggers coiled-coil formation in cortexillin I. EMBO J 17:1883-91. DOI: 10.1093/emboj/17.7.1883.

Stewart M. (2001) Structural basis for bending tropomyosin around actin in muscle thin filaments. Proc Natl Acad Sci U S A 98:8165-6. DOI: 10.1073/pnas.151265198.

Warren C.M., Arteaga G.M., Rajan S., Ahmed R.P., Wieczorek D.F., Solaro R.J. (2008) Use of 2-D DIGE analysis reveals altered phosphorylation in a tropomyosin mutant (Glu54Lys) linked to dilated cardiomyopathy. Proteomics 8:100-5. DOI: 10.1002/pmic.200700772.

Sweeney H.L., Houdusse A. (2010) Structural and functional insights into the Myosin motor mechanism. Annu Rev Biophys 39:539-57. DOI: 10.1146/annurev.biophys.050708.133751.

Swenson C.A., Stellwagen N.C. (1989) Flexibility of smooth and skeletal tropomyosins. Biopolymers 28:955-63. DOI: 10.1002/bip.360280504.

Takeda S., Yamashita A., Maeda K., Maeda Y. (2003) Structure of the core domain of human cardiac troponin in the Ca(2+)-saturated form. Nature 424:35-41. DOI: 10.1038/nature01780.

Temm-Grove C.J., Guo W., Helfman D.M. (1996) Low molecular weight rat fibroblast tropomyosin 5 (TM-5): cDNA cloning, actin-binding, localization, and coiled-coil interactions.

Cell Motil Cytoskeleton 33:223-40. DOI: 10.1002/(SICI)1097-0169(1996)33:3<223::AID-CM6>3.0.CO;2-B.

Tesi C., Colomo F., Nencini S., Piroddi N., Poggesi C. (1999) Modulation by substrate concentration of maximal shortening velocity and isometric force in single myofibrils from frog and rabbit fast skeletal muscle. J Physiol 516 (Pt 3):847-53.

Tesi C., Piroddi N., Colomo F., Poggesi C. (2002) Relaxation kinetics following sudden Ca(2+) reduction in single myofibrils from skeletal muscle. Biophys J 83:2142-51. DOI: 10.1016/S0006-3495(02)73974-X.

Thierfelder L., Watkins H., MacRae C., Lamas R., McKenna W., Vosberg H.P., Seidman J.G., Seidman C.E. (1994) Alpha-tropomyosin and cardiac troponin T mutations cause familial hypertrophic cardiomyopathy: a disease of the sarcomere. Cell 77:701-12. DOI: 0092-8674(94)90054-X [pii].

Tobacman L.S. (1996) Thin filament-mediated regulation of cardiac contraction. Annu Rev Physiol 58:447-81. DOI: 10.1146/annurev.ph.58.030196.002311.

Tsai S.H., Chu S.J., Hsu C.W., Cheng S.M., Yang S.P. (2008) Use and interpretation of cardiac troponins in the ED. Am J Emerg Med 26:331-41. DOI: 10.1016/j.ajem.2007.05.031.

Tskhovrebova L., Trinick J., Sleep J.A., Simmons R.M. (1997) Elasticity and unfolding of single molecules of the giant muscle protein titin. Nature 387:308-12. DOI: 10.1038/387308a0.

Vibert P., Craig R., Lehman W. (1997) Steric-model for activation of muscle thin filaments. J Mol Biol 266:8-14. DOI: 10.1006/jmbi.1996.0800.

Vrhovski B., Theze N., Thiebaud P. (2008) Structure and evolution of tropomyosin genes. Adv Exp Med Biol 644:6-26.

Wang F., Brunet N.M., Grubich J.R., Bienkiewicz E.A., Asbury T.M., Compton L.A., Mihajlovic G., Miller V.F., Chase P.B. (2011) Facilitated cross-bridge interactions with thin filaments by familial hypertrophic cardiomyopathy mutations in alpha-tropomyosin. J Biomed Biotechnol 2011:435271. DOI: 10.1155/2011/435271.

Wang C.L., Coluccio L.M. (2010) New insights into the regulation of the actin cytoskeleton by tropomyosin. Int Rev Cell Mol Biol 281:91-128. DOI: 10.1016/S1937-6448(10)81003-2.

Ward D.G., Ashton P.R., Trayer H.R., Trayer I.P. (2001) Additional PKA phosphorylation sites in human cardiac troponin I. Eur J Biochem 268:179-85.

Wegner A. (1980) The interaction of alpha, alpha- and alpha , beta-tropomyosin with actin filaments. FEBS Lett 119:245-8.

Whitby F.G., Phillips G.N., Jr. (2000) Crystal structure of tropomyosin at 7 Angstroms resolution. Proteins 38:49-59.

White S.P., Cohen C., Phillips G.N., Jr. (1987) Structure of co-crystals of tropomyosin and troponin. Nature 325:826-8. DOI: 10.1038/325826a0.

Wilton S.D., Lim L., Dorosz S.D., Gunn H.C., Eyre H.J., Callen D.F., Laing N.G. (1996) Assignment of the human alpha-tropomyosin gene TPM4 to band 19p13.1 by fluorescence in situ hybridization. Cytogenet Cell Genet 72:294-6.

Wolgemuth C.W., Sun S.X. (2006) Elasticity of alpha-helical coiled coils. Phys Rev Lett 97:248101.

Wolska B.M., Wieczorek D.M. (2003) The role of tropomyosin in the regulation of myocardial contraction and relaxation. Pflugers Arch 446:1-8. DOI: 10.1007/s00424-002-0900-3.

Xie L., Miyazaki J., Hirabayashi T. (1991) Identification and distribution of tropomyosin isoforms in chicken digestive canal. J Biochem 109:872-8.

Yamauchi-Takihara K., Nakajima-Taniguchi C., Matsui H., Fujio Y., Kunisada K., Nagata S., Kishimoto T. (1996) Clinical implications of hypertrophic cardiomyopathy associated with mutations in the alpha-tropomyosin gene. Heart 76:63-5.